Title
Simulating Bioclogging Effects on Dynamic Permeability, Infiltration, and Subsurface Geochemistry

Author
Newcomer, Michelle Elizabeth

Publication Date
2016

Peer reviewed|Thesis/dissertation

Simulating Bioclogging Effects on Dynamic Permeability, Infiltration, and Subsurface Geochemistry

by

Michelle Elizabeth Newcomer

A dissertation submitted in partial satisfaction of the
requirements for the degree of
Doctor of Philosophy

in

Engineering- Civil & Environmental Engineering

in the

Graduate Division

of the

University of California, Berkeley

Committee in charge:

Professor Yoram Rubin, Chair
Assistant Professor Sally Thompson
Adjunct Professor Susan Hubbard
Professor Mary Power

Spring 2016

Simulating Bioclogging Effects on Dynamic Permeability, Infiltration, and Subsurface Geochemistry

Abstract

Simulating Bioclogging Effects on Dynamic Permeability, Infiltration, and Subsurface Geochemistry

by

Michelle Elizabeth Newcomer

Doctor of Philosophy in Engineering- Civil & Environmental Engineering

University of California, Berkeley

Professor Yoram Rubin, Chair

Bioclogging in rivers can detrimentally impact aquifer recharge. This is particularly so in dry regions, where losing rivers are common, and where disconnection between surface water and groundwater (leading to the development of an unsaturated zone) can occur. Reduction in riverbed permeability due to biomass growth is a time-variable parameter that is often neglected, yet permeability reduction from bioclogging can introduce order of magnitude changes in seepage fluxes from rivers over short (i.e., monthly) timescales. To address the combined effects of bioclogging and disconnection on infiltration, I developed numerical representations of bioclogging processes within 1D, 2D, and 3D variably-saturated flow models representing losing-connected and losing-disconnected rivers subject to Mediterranean climatic effects on riverbed sediments. I tested bioclogging formulations using a synthetic and field case study informed with biological data obtained from the Russian River, California, U.S.A. My findings show that modeled biomass growth reduced seepage for losing-connected and losing-disconnected rivers. However, for rivers undergoing disconnection, infiltration declines occurred only after the system was fully disconnected. Before full disconnection, biologically-induced permeability declines were not significant enough to offset the infiltration gains introduced by disconnection. The two effects combine to lead to a characteristic infiltration curve where peak infiltration magnitude and timing is controlled by permeability declines relative to hydraulic gradient gains. Biomass growth was found to hasten the onset of full disconnection; a condition I term effective disconnection. Biomass growth leading to sediment pore-space clogging and consumption of river Carbon and Nitrogen reveal fundamental controls on bioclogging and river nutrient cycling based on riverine sediment conditions. These results show that river infiltration can respond dynamically to bioclogging and subsequent permeability declines that are highly dependent on river connection status.

-Scott Belsky

When 99% of people doubt your idea, you're either gravely wrong or about to make history.

Contents

List of Figures

List of Tables

Acknowledgments

I want to thank the many people that supported me through this journey. First I am grateful for the indispensable guidance from my adviser Yoram Rubin. I am very thankful for the independence I was given to pursue my research interests, as well as the helpful critiques during our weekly group research seminars. I am especially thankful for the connections Yoram gave me with key collaborators across the Berkeley network, Lawrence Berkeley National Lab, and UFZ Helmholtz Center in Leipzig, Germany. I am also very thankful for the guidance and mentorship from Susan Hubbard. I am appreciative of Susan's constructive advice, helping me navigate my research and my future career. Susan's scientific guidance and advice have helped me to effectively communicate my research findings, as well being someone to look up to as a role model. I am grateful to my dissertation committee members, Sally Thompson and Mary Power, who helpfully critiqued the progress of my research during the qualifying exam, and during the writing phase of my dissertation. A special thanks to my other qualifying exam member, Mark Stacey, who thoughtfully pointed out some theoretical aspects I was not yet considering when trying to mathematically describe conductivity as a dynamic parameter. In hindsight, my qualifying exam was quite a fortunate opportunity to get constructive advice on my research from some of the best thinkers in this field.

I would also like to thank my colleagues from UFZ Helmholtz Center in Germany: Jan Fleckenstein, Uli Maier, Christian Schmidt, and Martin Thullner for helping me develop a sound research plan with the best numerical tools available. A huge thank you to my fellow PhD students within the CEE department, especially Heather Savoy, Brad Harken, Karina Cucchi, Nigel Chen, and to other collaborators Changhong Wang, and Carlos Murillo for the time spent discussing ideas and derivations on our sticky white board. Finally, I am very appreciative of the support from my family and friends. Without their support, this experience would have never been possible.

Chapter 1

Introduction to Groundwater-Surface Water Exchange

Quantifying the exchange of water at the sediment-water interface in fluvial settings is driven by the need for better understanding of hydrological and ecological processes as well as for determining better, more sustainable groundwater pumping regimes for nearby filtration facilities [*Brunner et al.*, 2009a, 2011; *Rosenberry and Pitlick*, 2009]. Infiltration to the groundwater is controlled by the hydraulic connection status of a surface water body, such as a perennial river. Connected, disconnected, and transitional systems can form from physical changes in the water table depth, air-entry pressure, river width and stage, aquifer thickness, permeability of the aquifer and streambed sediments, and nearby pumping rates [*Su et al.*, 2007; *Brunner et al.*, 2009b, 2011]. Dynamic riverbed permeability, in many cases, is hypothesized to occur through sedimentation [*Hubbs*, 2006; *Buss et al.*, 2009; *Zhang et al.*, 2011], and more recently has been shown to occur from biomass growth in the sediment pore space [*Thullner et al.*, 2002a; *Brovelli et al.*, 2009; *Treese et al.*, 2009; *Thullner*, 2010]. Understanding the spatial and temporal nature of dynamic permeability is necessary to quantify the influence of heterogeneous geological media on flow, to properly characterize the flow domain structure, and to accurately predict the timing and extent of development of an unsaturated zone at an appropriate level of detail for delivering estimates of sustainable riverbank pumping rates [*Giambastiani et al.*, 2012].

Riverbank filtration (RBF) pumping facilities often rely on effective infiltration from nearby rivers, which simultaneously improves the quality of recharged water through a variety of physiochemical and biological processes [*Zhang et al.*, 2011]. RBF facilities can provide an additional sustainable source of water to surrounding communities if the system is managed properly, and can make use of surface water supplies that would otherwise flow downstream and discharge into the ocean [*Su et al.*, 2007; *Zhang et al.*, 2011; *Jaramillo*, 2012]. Many RBF facilities also use inflatable dams to increase the river stage and hydraulic

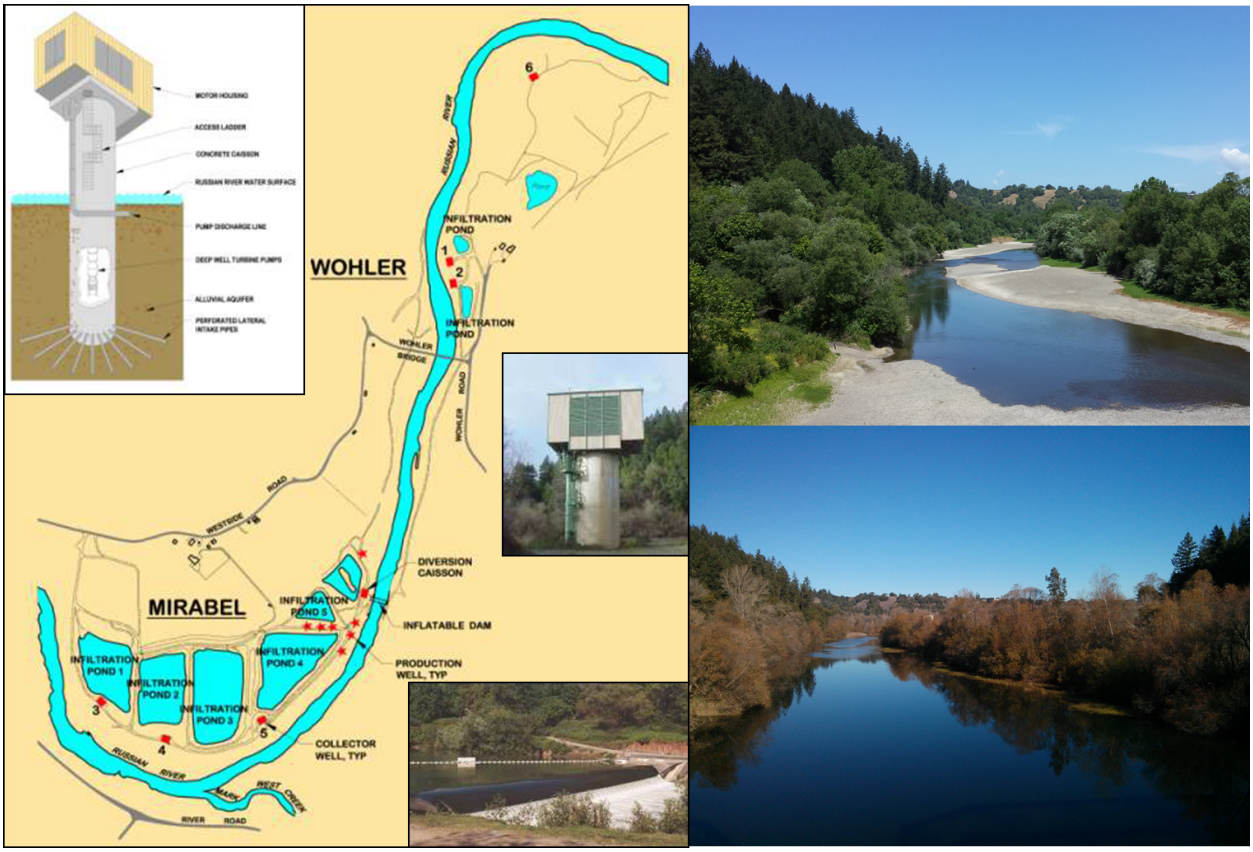

Figure 1.1: Russian River in Sonoma County CA. The collector well is shown in the inset and the site map on the left. Two images of the site when the inflatable dam is down (top) and raised (bottom) show river capacity and width during different seasons.

head thus supplementing the pumping rate during dry periods or emergencies [*Su et al.*, 2007; *Zhang et al.*, 2011; *Ulrich et al.*, 2015]. Inflatable dams have unintended consequences and can induce a negative feedback cycle consisting of increased sedimentation, decreased permeability, decreased seepage, development of an unsaturation zone, reduction in pumping capacity, which causes water managers to require the dam to be raised further [*Zhang et al.*, 2011; *Ulrich et al.*, 2015]. Periods of scour during high flow periods can mitigate these feedback effects and is hypothesized to return permeability values to pre-dam inflation conditions A collector well in Sonoma County, CA is shown in Figure 1.1 with a graphic of the well-construction.

While it is difficult to capture the small-scale spatial and temporal heterogeneity of sediment parameters such as riverbed permeability, extensive field monitoring and sophisticated

inverse modeling efforts cannot yet predict the transient nature of this boundary condition alone. Thus it is necessary for field sites to couple limited field data with statistical models of dynamic and heterogeneous permeability to better predict timing and extent of unsaturated zone formation, timing of complete de-saturation, and to understand the heterogeneous cross-sectional structure of the unsaturated zone. Development of a dynamic permeability function (spatial and temporal) as well as understanding the biological control on seepage can prove to be a procedure that is relevant for the understanding of riverbed and aquifer architecture effects on groundwater pumping availability. Similarly, this will provide a better understanding of the feasibility of using a statistical approach to model heterogeneity for input to groundwater models of any riverbank filtration facility and may provide a method for developing an artificial yet statistically significant boundary condition with the use of limited but costly field measurements. For this study I define the dynamic permeability as the spatially and temporally variable permeability that is hypothesized to change the sediment properties include hydraulic conductivity (K_{sc}) and porosity (ϕ) and introduce dynamic feedbacks into infiltration and nutrient fluxes [*Genereux et al.*, 2008].

1.1 Infiltration Coupled with Dynamic Permeability

Essential for water resources management is an ability to accurately predict infiltration from rivers, recharge of water to groundwater aquifers, flux of water to supply wells, and residence times of contaminants. Infiltration rates are also an integral component to the alluvial aquifer water balance, and accurate estimates of infiltration are necessary for closing the water balance gap and predicting river discharge [*Crosbie et al.*, 2014]. Accurate prediction of infiltration is dependent on the characterization of riverbed sediment properties. One such property is the riverbed permeability. Although dynamic riverbed permeability is a widely recognized phenomenon, most surface-groundwater simulations assume that it is constant over time and space. In addition to consideration of dynamic permeability, accurate prediction of seepage from a losing river depends on the status of river-aquifer connection (Figure 1.2). Studies that assume a river and aquifer remain connected (i.e. entirely saturated or at steady-state) risk order of magnitude errors in the infiltration estimates, directly affecting model certainty [*Brunner et al.*, 2009b; *Lamontagne et al.*, 2013].

Although several studies have documented changes of riverbed permeability and river-aquifer connections [*Treese et al.*, 2009; *Hatch et al.*, 2010; *Lamontagne et al.*, 2011], their coupled influence on infiltration dynamics has not been quantified. Disconnection in rivers occurs when a lowering of the groundwater table no longer affects the infiltration rate [*Brunner et al.*, 2009a]. Disconnection leads to the development of an unsaturated zone beneath the river, which coincides with the onset of maximum seepage [*Brunner et al.*, 2009a, b, 2011]. When a river becomes disconnected, the infiltration rate thereafter is primarily a function

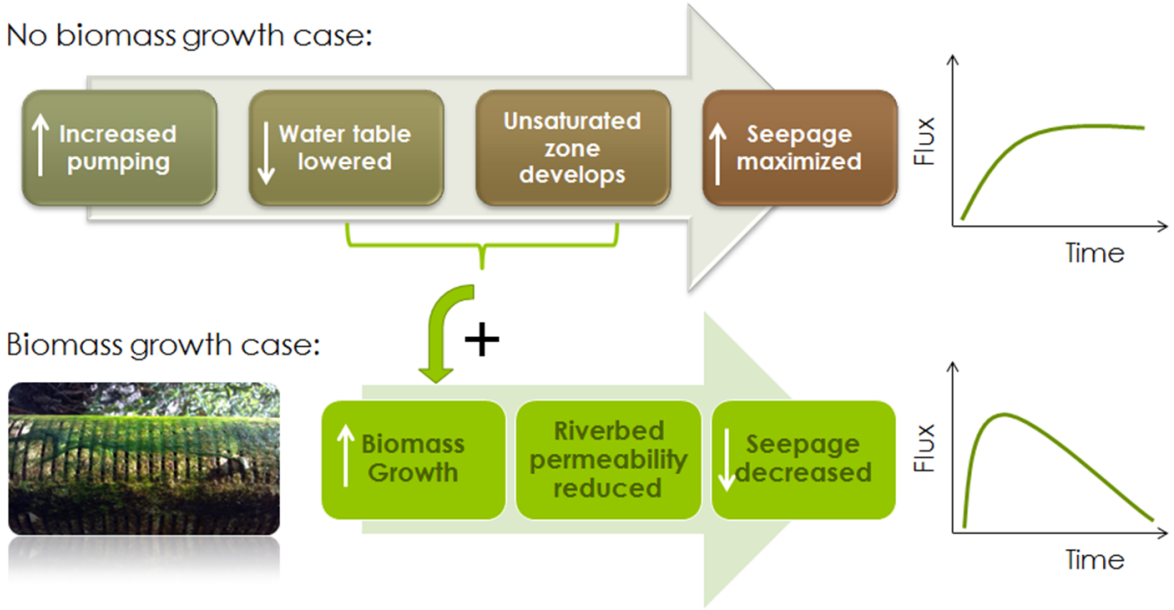

Figure 1.2: Conceptual model of the chain of events between the case where biomass does not grow and when biomass grows in a scenario where the river and aquifer originally undergo disconnection.

of the hydraulic conductivity. Changes in permeability, such as from bioclogging, can therefore change the peak flux predicted by the process of disconnection when a river is either losing-connected or losing-disconnected (Figure 1.3) [*Schubert*, 2006].

Connection regimes can vary worldwide depending on local groundwater and climatic conditions. Arid, semi-arid, and Mediterranean climatic regions typically have losing rivers, or even losing-disconnected rivers if pumping is nearby [*Su et al.*, 2007; *Treese et al.*, 2009; *Lamontagne et al.*, 2013; *McCallum et al.*, 2013]. Temperate regions can have both gaining and losing rivers that remain fully connected even with pumping nearby [*Schubert*, 2002, 2006]. The relationship between seepage and bioclogging may differ widely in gaining versus losing streams, and connected versus disconnected states. These differences could be due to many coupled factors including: 1) disconnection versus connection, 2) spatially heterogeneous variations in hydraulic conductivity, 3) context-dependent parameters for biomass growth, 4) climatic forcing such as drought, and 5) feedbacks between nutrient fluxes and infiltration strength (Figure 1.3) [*Hatch et al.*, 2010].

While the mathematical relationship between bioclogging and hydraulic conductivity is well-established at the pore-scale [*Thullner et al.*, 2002b, a, 2004; *Brovelli et al.*, 2009], applicability of these models and parameters at the field-scale is not yet tested. Parameters for

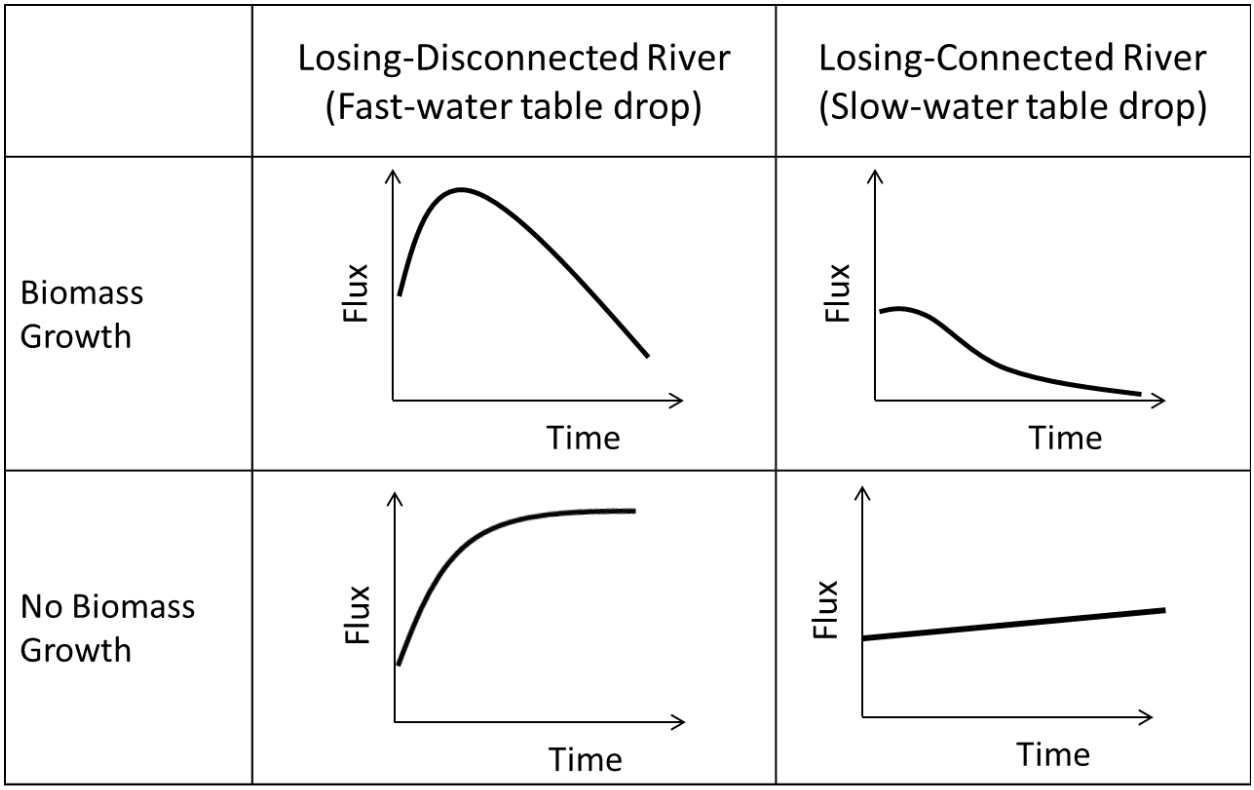

Figure 1.3: Point scale infiltration rates hypothesized for the various connection and bioclogging regimes. The field scale rate is hypothesized to be a combination of all the point scale fluxes.

biomass growth derived from ideal laboratory conditions are typically used in pore-scale numerical models and may not be suitable for larger scale models representing field conditions. Biomass models from laboratory data may not describe the true nature of biomass growth in the field because of the heterogeneous nature of the environment. Water depth, topography, sunlight, pebble size, temperature, and water velocities all influence the growth of periphyton (surficial algae), which is the carbon source for biomass growth in the pore-space. Furthermore, the relation between bioclogging and seepage decline has only been assessed for laboratory scale systems, which are typically fully saturated. Laboratory-scale models do not account for the effects of pumping and unsaturated zone growth. These limitations necessitate a better understanding of how dynamic permeability alters seepage trends under the framework of a large-scale disconnecting river system [*Su et al.*, 2007; *Zhang et al.*, 2011].

The effect of bioclogging on losing and gaining rivers, connected and disconnected sys-

tems, and the influence of climatic variability has not been analyzed sufficiently in the literature, justifying a clear focus on this topic. Capabilities to predict infiltration fluxes in a system demonstrating coupled effects of bioclogging and disconnection are not available and this remains an imperative area of research. This predictive ability is necessary for managing pumping in drought prone areas, especially over long time-frames, such as seasons, when feedback effects become important [*Treese et al.*, 2009; *Hatch et al.*, 2010].

1.2 Study Area

Located along the Russian River in Sonoma County, CA, the Wohler Riverbank Filtration (RBF) site provides drinking water to 600,000 people annually from six collector wells and infiltration galleries along the river (Figure 1.4). Taking advantage of natural filtration processes, these RBF systems are used around the world as an inexpensive, reliable way to treat surface water for public uses [*Tufenkji et al.*, 2002]. Shale bedrock of the Franciscan Complex underlies the unconsolidated alluvial river valley. Sands and gravels underlie sporadic lenses of clay and silt in the alluvial aquifer. Previous studies specific to the Wohler site have found infiltration rates between 0.4-1 m day^{-1} [*Harding Lawson Associates*, 1988].

Riverbank filtration at the Wohler site in Sonoma County is managed by the Sonoma County Water Agency whose aim is to provide a sustainable water supply. River water used to substitute a portion of the groundwater supply with surface water infiltrated through the hyporheic zone to provide an additional method of filtration to the water [*Hatch*, 2007; *Su et al.*, 2007]. Issues and data/knowledge gaps related to the Wohler site include understanding the nature of seepage changes [*Hatch*, 2007; *Ulrich et al.*, 2015], the nature of transient permeability (spatial, temporal, and source-sedimentary or biological) [*Faybishenko*, 1999; *Ulrich et al.*, 2015], processes related to the development of an unsaturated zone beneath the river [*Su et al.*, 2007], and processes of the connected/disconnected river status [*Brunner et al.*, 2009a; *Lamontagne et al.*, 2013], all of which affect the sustainable pumping at the RBF facility.

RBF facilities rely on maintaining constant pumping rates for their constituents needs and also for stabilizing an important agricultural economy. Determining an accurate pumping value that will allow continuous pumping for the duration of one summer, and for ensuring the sustainability of this pumping method is challenging. Thus the conjunctive and sustainable use of this system requires modeling efforts to aid in developing prediction tools for addressing the system needs. RBF is a cost-effective pre-treatment technology, and the designation as groundwater of this source instead of surface water also provides an incentive to use this technology instead of more traditional water treatment programs that necessitate the use of chemical additions. Water pumped by the RBF collector wells is naturally filtered and impurities are removed as it travels through sands and gravels, allowing water to comply

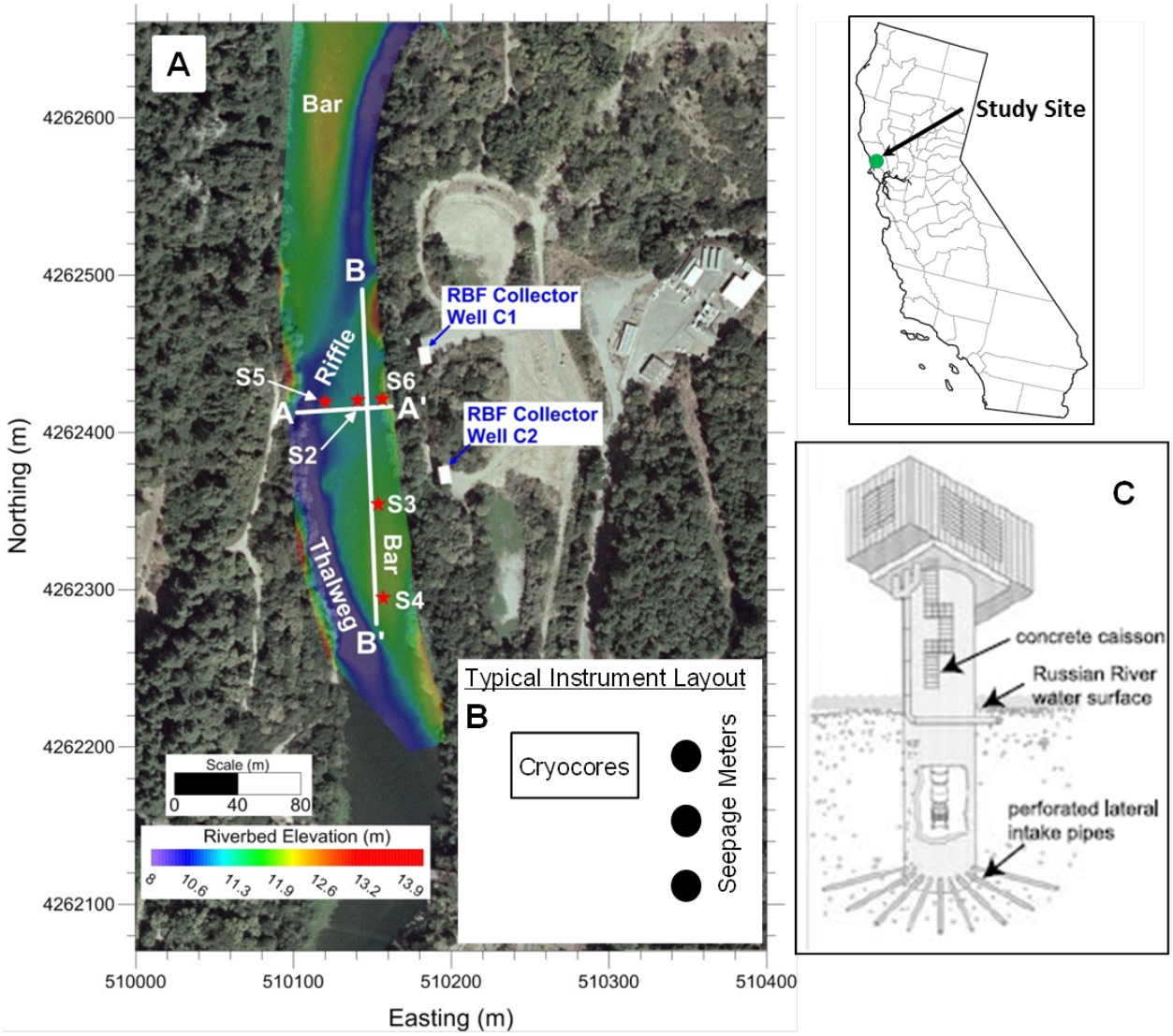

Figure 1.4: Location map of the Wohler site and distribution of the measurement locations. Map used with permission from *Ulrich et al.* [2015].

with State and Federal drinking water standards naturally. This natural process allows the water to be classified as groundwater and is exempt from costly regulations applied to surface water [*Sonoma County Water Agency*, 2012].

The coupling between bioclogging-induced riverbed dynamic permeability and disconnection processes could have significant ramifications for practical management of water

resources. In particular, riverbank filtration systems consist of high capacity pumping wells that are located adjacent to or beneath rivers. Taking advantage of natural filtration processes, these systems are used around the world as an inexpensive, reliable way to treat surface water for public uses [*Tufenkji et al.*, 2002]. The groundwater-surface water interface as a conduit to the wells provides valuable ecological services including natural attenuation of contaminants [*Buss et al.*, 2009]. In some cases, riverbed permeability can be much lower than the adjacent aquifer, and permeability dynamics are related to larger scale catchment hydrological processes such as catchment runoff, dam releases, bedform creation, and climate factors such as precipitation that increases discharge and scours bed sediments [*Schubert*, 2002; *Buss et al.*, 2009]. Physical, mechanical, chemical, and biological clogging are all processes reported to occur during riverbank filtration [*Jaramillo*, 2012]. Well production has been documented to be dependent on river water depth, previous pumping rates, sediment deposition, biological clogging, and aquifer/riverbed permeability anisotropy [*Zhang et al.*, 2011].

River discharge at the site is often spatially and temporally variable due to seasonal and natural climate variability effects, such as from the El Niño Southern Oscillation (ENSO). It is currently unknown how dynamic feedbacks between surface water discharge, ecological changes, and feedbacks with subsurface microbes may change overall infiltration rates and volumes. For example, one hypothesis is that decreased bioclogging during drought years may increase the overall recharge rate, and lead to greater differences in river discharge ($\uparrow \Delta Q$) between upstream and downstream stations. Conversely, increased bioclogging during flood years may decrease the overall recharge rate and lead to smaller differences in river discharge between locations ($\downarrow \Delta Q$) (Figure 1.5). These combined dynamic factors have overall cumulative effects on infiltration at the Wohler RBF site and present complicated balances to maintain flow and nutrients for conjunctive ecosystem and human use.

1.3 Factors Affecting Seepage

Seepage rates at the site change dramatically in response to pumping and previous studies have found large spatial variability in seepage rates and directions of movement [*Hatch*, 2007]. Additionally, in many cases, it has been found that the seepage direction does not agree with the hydraulic head gradient, indicating the presence of geomorphic features (shoals, pits, dunes, preferential pathways, spatial heterogeneity) that dramatically impact the flux in the hyporheic zone [*Gasperikova et al.*, 2008; *Rosenberry and Pitlick*, 2009]. When analyzing the factors that govern sustainable pumping rates, *Zhang et al.* [2011] determined from a modeling analysis that seepage is proportional to pumping, however strongly limited by riverbed permeability which they determined was the dominant factor affecting seepage [*Zhang et al.*, 2011]. Hyporheic zone fluxes are generally measured on a scale allowing for determination

of the direction of movement into and out of the sediments at the interface. Larger scale hyporheic zone fluxes that occur in response to the connection status of a river (connected, transitional, and disconnected) can be determined from larger scale responses such as the development of an unsaturated zone in response to stream stage, stream width, streambed hydraulic conductivity and thickness, and aquifer hydraulic conductivity, transmissivity, and specific yield[Shanafield et al., 2012]. Seepage generally increases during growing disconnection if the stream stage is raised, however reaching asymptotic levels after a period of time [*Zhang et al.*, 2011; *Shanafield et al.*, 2012a].

Dynamic permeability (a measure of riverbed clogging) was modeled using inversion techniques by *Zhang et al.* [2011] at the Wohler site using river stage, pumping rate, and temperature. The ratio between riverbed permeability and aquifer permeability was determined to be the driving mechanism of unsaturated zone formation [*Zhang et al.*, 2011]. However, during one period of calibration, modeled permeability increased during a time period of hypothesized low permeability (low permeability is hypothesized during the summer when the dam is inflated and sediments are hypothesized to deposit thereby reducing permeability), and the authors reasoned that this was due to the temperature dependence of hydraulic conductivity and not from scour [*Su et al.*, 2007; *Zhang et al.*, 2011]. The effect of heterogeneous streambed permeability can have a significant effect on the development of the unsaturated zone and on the spatial distribution of water content beneath the streambed, and a general effect of this was shown by *Su et al.* [2004] however not extensively examined [*Su et al.*, 2007].

Temperature plays a key role in the estimation of permeability. In the Summer of 2007, *Zhang et al.* [2011] found that large pumping rates induced greater infiltration rates beneath the river. Also, during this time period, the dam was inflated thus increasing the hydraulic head. Gas saturation profiles indicated the development of an unsaturated zone, however an inverse model predicted increased permeability (possibly test for by pass flow) during this time period which was contrary to the original hypothesis (dam inflation causes sediment deposition and decreased permeability). The increase in permeability may be speculated by the temperature dependence of hydraulic conductivity. Hydraulic conductivity (K) is a function of viscosity and relative permeability effects, however viscosity variations between 10°C and 20°C are not variable enough to explain the large permeability changes found during the experimental run. Hydraulic conductivity values are influenced by the temperature dependence of relative permeability as demonstrated by isothermal water retention curves given built by *Constantz* [1991]. The temperature dependence of hydraulic conductivity may explain the unexpected change in riverbed permeability modeled by *Zhang et al.* [2011][*Constantz*, 1982, 1991; *She and Sleep*, 1998; *Tong et al.*, 2011; *Zhang et al.*, 2011], however these effects need to be more extensively examined and may not completely explain why modeled permeability values do not agree with the hypothesized processes at the site. *Genereux et al.* [2008] compensated hydraulic conductivity values in a streambed for temperature and

found that temperature variations in the stream were not a significant factor in driving the observed temporal and spatial variability of K measurements [*Genereux et al.*, 2008].

1.4 Rivers Can Undergo Disconnection

Rivers can have functionally different flow regimes coupled to the underlying aquifer relative to hyporheic flows. In many arid, semi-arid, and Mediterranean climatic around the world, rivers typically feed groundwater, and have losing-connected or losing-disconnected conditions with the underlying aquifer [*Su et al.*, 2007; *Treese et al.*, 2009; *Lamontagne et al.*, 2013; *McCallum et al.*, 2013]. Disconnected rivers typically have a large unsaturated zone beneath the river and infiltration fluxes downward are fully maximized in this state [*Brunner et al.*, 2009b]. Gaining rivers are typically found in temperate regions that remain fully connected even during pumping [*Schubert*, 2002, 2006]. When fluxes from gaining or losing conditions are large, hyporheic fluxes can becomes negligible contributors to overall transformations relative to the large scale flow patterns [*Cardenas*, 2009]. Transient connection regimes (i.e. those that shift from gaining $\rightarrow$ losing $\rightarrow$ gaining) may dominate patterns and processes of biogeochemical cycling especially during low base flow conditions [*Cardenas*, 2009]. Infiltration patters along river networks can be a function of both the connection status and bioclogging regime, and can vary spatially along the downstream corridor, and the direction of flow, and subsequent transient changes should always be a primary factor of consideration [*Ivkovic*, 2009; *Lamontagne et al.*, 2012], and can vary from gaining to losing over small (i.e. 1-2m scales) [*Brookfield and Sudicky*, 2012]. Assumptions of saturated conditions with constant parameters are typical for river-aquifer studies leading to errors in projected infiltration rates and estimates of nutrient cycling [*Brunner et al.*, 2009a; *Lamontagne et al.*, 2011].

Development of an unsaturated zone reduces the aquifer hydraulic conductivity, limits water production, and increases aeration which impacts the biogeochemical processes and water quality entering the collector wells [*Zhang et al.*, 2011]. *Zhang et al.* [2011] hypothesized that riverbed permeability may directly affect the development of an unsaturated zone under 2 scenarios: 1) the riverbed permeability is less than the aquifer permeability, and 2) the pumping rate is greater than the recharge rate [*Zhang et al.*, 2011]. Unsaturated zone development is influenced by the ratio of riverbed permeability to aquifer permeability, pumping, and regional flowthe first two have already been extensively studied. In many cases, streambed volumetric flux is not reaching the collector wells, indicating the important role of the regional groundwater system [*Su et al.*, 2007]. *Su et al.* [2007] simulated the development of the unsaturated zone beneath the Wohler site using the TOUGH2 numerical model, however this model was not calibrated to temperature and pressure point measurements [*Su et al.*, 2007]. These simulations were also conducted using constant effective permeability

and pumping values.

1.5 Climate Considerations

Floods and droughts are important agents of natural disturbance, and dominate connection regimes in rivers. The type of climate regime found in a location can be a strong predictor of the gaining or losing conditions of rivers [*Su et al.*, 2007; *Treese et al.*, 2009; *Lamontagne et al.*, 2013; *McCallum et al.*, 2013]. Relationships between seepage and bioclogging may also differ widely in gaining versus losing streams, connected versus disconnected states [*Newcomer et al.*, 2016], and type of climate dominating river flow. These factors can drastically change the growth of an unsaturated zone, spatially focused reduction in hydraulic conductivity from bioclogging, and feedbacks between nutrient fluxes and infiltration direction [*Hatch et al.*, 2010]. The role of climate variability introduced from the El Niño Southern Oscillation (ENSO) is one such process. Climate variability from ENSO is related to changes in the strength of the Walker Circulation in the Pacific Ocean [*NOAA CPC*, 2015]. Warm phases (El Niño -EN) are related to warmer sea-surface temperature and lower pressure anomalies in the Eastern Pacific (near Ecuador and Peru) which reduce the strength of the Walker Circulation and enhance the strength of convective cells across latitudes. Warm phases typically produce greater than average precipitation in California. Opposite effects and reduced precipitation typically occur during cold periods (La Niña -LN) [*NOAA CPC*, 2015]. ENSO and other climatic perturbations, even one scouring bankfull discharge event, may have large regional effects on the dynamics of benthic ecosystems such as algae growth and bioclogging [*Power*, 1992; *Piggott et al.*, 2015].

Many studies have closely established the significance of the ENSO signal in precipitation, snowfall accumulation, and streamflow in other regions [*Cayan et al.*, 1999]. Differences in the ENSO signal between California Coastal rivers versus rivers draining the Sierra Nevada were also noted [*Cayan et al.*, 1999] finding an amplified effect on streamflow compared with precipitation because of snowmelt lags in the Sierras. Additionally, with projected snow-to-rain transitions for the Western United States, likely impacts include a shift in the exceedance probability and return time of extreme flows [*Klos et al.*, 2014]. California rivers typically show reduced signals of ENSO however, although this can depend on latitude. Discharge between moderate LN and EN years is shown in Figure 1.5 and associated statistics of bankfull discharge return intervals. The return interval of annual peak flows for the Russian River between EN and LN years is not discernable, and shows overlapping confidence intervals indicating no significant differences (Figure 1.5).

Effects of ENSO on California sediment transport, however, can range over 5 orders of magnitude in phase with climate fluctuations despite flow management amongst most rivers [*Inman and Jenkins*, 1999; *Andrews and Antweiler*, 2012]. ENSO was found to be

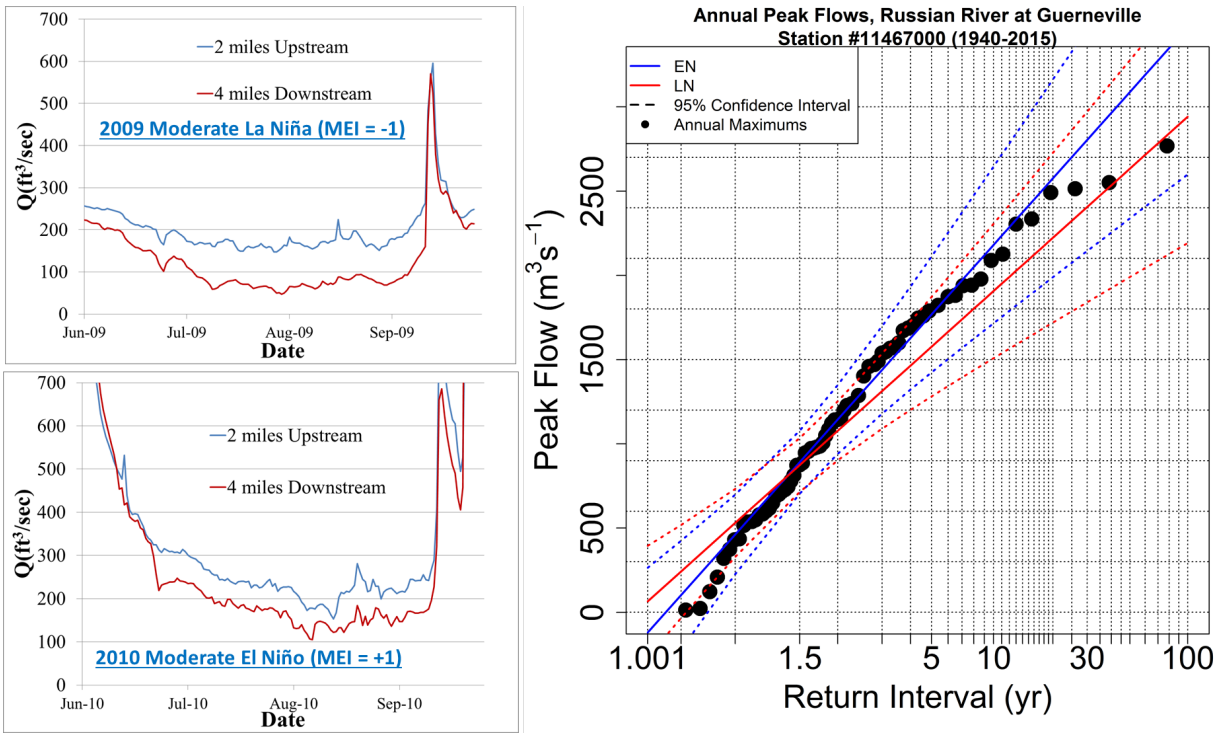

Figure 1.5: Differences in discharge between drought and flood years. When the Multivariate ENSO Index (MEI) is consistently negative, climate conditions for California are categorized as drought. When the MEI is consistently positive, California is in a wet/flood year. Return intervals for EN versus LN years are shown based on annual peak flows.

a dominant factor in sand suspended sediment discharge and 10x more sediment discharge between EN versus LN years in the Salinas River, CA [*Gray et al.*, 2015]. Episodic sediment flux and deposition events related to ENSO in other locations around the world point to the influence that large scale climate perturbations can have on local scale geomorphologic features [*Aalto et al.*, 2003; *Kondrashov*, 2005], as well as cascading effects on food-webs that feed subsurface micro-organisms [*Power*, 1992; *Power et al.*, 2008, 2009].

1.6 Spatial Heterogeneity

Spatial and temporal heterogeneity of hydraulic conductivity (K) are important variables that strongly influence hyporheic exchange. Spatial variability of heterogeneous streambed sediments is widely studied and quantified, however the dynamic attributes of streambed K as a function of space and time has not yet been explicitly examined and merits additional

study [*Cardenas et al.*, 2004; *Genereux et al.*, 2008; *Boano et al.*, 2010; *Giambastiani et al.*, 2012]. *Genereux et al.* [2008] measured streambed hydraulic conductivity spatially along a river reach and sampled the same location bi-monthly [*Genereux et al.*, 2008]. While finding clear trends in the spatial structure (higher K in the middle of the stream, lower K along the banks, higher K downstream of a dam, and lower K upstream), they were not able to definitively determine the temporal trends nor the reasons for the trends, reasoning that more analysis is needed to determine the processes responsible for temporal variations to better explain and predict observed field changes [*Genereux et al.*, 2008].

Many studies in hyporheic zone literature focus on micro-scale, patch-scale, topography driven, and morphology driven fluxes (all synonymous to bed-form driven flow) as a function of bed-form scale heterogeneity in the streambed [*Cardenas et al.*, 2004; *Salehin et al.*, 2004; *Hester and Doyle*, 2008; *Sawyer and Cardenas*, 2009; *Stewardson et al.*, 2011; *Zlotnik et al.*, 2011]. Bed-form scale heterogeneity includes bed-form geomorphology such as dunes, ripples, pools, riffles, cross-bedded sediment, and usually assumes sediment homogeneity at these larger scales. These studies only assess fluxes occurring over short paths of approximately 1 cm to 10 m horizontally within the top 1m of the riverbed. Patch-scale fluxes return water to the river downstream, and often neglect deeper, larger scale fluxes through the hyporheic zone to the aquifer [*Stewardson et al.*, 2011]. To simulate bed-form heterogeneity, a common technique is to undulate the riverbed head boundary condition using a sinusoidal function. *Cardenas et al.* [2004] found that for homogeneous and heterogeneous streambed sediments under a sinusoid head boundary condition, sediment heterogeneity increased the flux across the streambed sediments [*Cardenas et al.*, 2004]. The induced head gradients were applied under the assumption that bed forms can dominate hyporheic flux on under certain circumstances, and that the bed form amplitude and frequency relative to heterogeneity are inversely proportional in dominance depending on river stage and stream curvature [*Cardenas et al.*, 2004]. Evolution of the surface-subsurface exchange (within the top 1m only) in response to streamflow variability was analyzed by *Boano et al.* [2010], and their findings indicate that the exchange flux shows a non-linear relationship with streamflow and that this relationship is also dependent on the bed-forms developed from previous years [*Boano et al.*, 2010]. Bed-form heterogeneity induced flux processes at scales of 1m are common in hyporheic zone literature and it is important that this is recognized as a distinct scale from that of the larger scale processes affecting flux into the aquifer.

Larger scale heterogeneity includes thalwegs, meanders, macropores, banks, riverbed permeability heterogeneity and aquifer permeability heterogeneity [*Ryan and Boufadel*, 2006; *Genereux et al.*, 2008; *Kalbus et al.*, 2009; *Shanafield et al.*, 2012b; *Ulrich et al.*, 2015]. Larger scale fluxes, such as those from the stream to an aquifer, require a different lens through which heterogeneity is observed. When analyzing hyporheic flow from a stream to an aquifer occurring between 1-20m, streambed hydraulic conductivity is important and is thought to be the dominant process relative to the bed-forms at this scale [*Cardenas et al.*, 2004; *Salehin*

et al., 2004; *Ryan and Boufadel*, 2006]. Competing influences to hyporheic exchange between bed-form and sediment dynamics requires analyses that isolate each effect, however this is difficult as the observed effects depend on the relative positions of the bed-forms and sediment heterogeneities to each other. While keeping the bed-form effect constant, *Cardenas et al.* [2004] show that hyporheic flux increases when heterogeneous sediment is introduced. However, they also conclude that the effects of sediment heterogeneity also depend on the location relative to the bed-forms [*Cardenas et al.*, 2004]. What these previous studies indicate is that the project scope should determine the necessary scale of observation. Thus, for a project scope analyzing riverbed flux to an aquifer, an appropriate observation scale would include models and data that look at mean properties over slightly larger scales (1-10m) than those required for micro-scale hyporheic zone flux analysis (1-10cm). *Cardenas et al.* [2004] only consider fluxes in the upper 1-m zone and do not consider discharge to the groundwater. While *Cardenas et al.* [2004] assess the impact of heterogeneous sediments on upper 1-m fluxes and residence time distributions of particles, they do not consider the groundwater component [*Cardenas et al.*, 2004]. Fluxes across the streambed into the aquifer are larger scale fluxes that may be dependent on hydrofacies scale and sub-hydrofacies scale fluxes. *Frei et al.* [2009] assess the hydrofacies scale and sub-hydrofacies scale heterogeneities [*Frei et al.*, 2009]. While both hydrofacies scale and sub-hydrofacies scale heterogeneities affect the distribution and rates of seepage, sub-hydrofacies scale heterogeneities have the potential to significantly affect the volumes of seepage compared with hydrofacies scale heterogeneity.

Small scale heterogeneity is important for quantifying patterns and dynamics of river-aquifer exchange to better support environmental management decisions. Watershed-scale (10^4 m), river scale (10^3 m), reach scale (10^2 m), and bedform scale (10^{-1} m) studies all present different methods for quantifying heterogeneity and fluxes. Additionaly geologic heterogeneity scales are typically defined at the hydrofacies scale (10^2-10^3 m) which are defined as lithological units formed under a specific depositional environment, and the sub-hydrofacies scale (10^{-1}-10^1 m) which are defined by hydraulic conductivity differences within a distinct lithological unit [*Fleckenstein et al.*, 2006; *Frei et al.*, 2009; *Kalbus et al.*, 2009; *Irvine et al.*, 2012]. Studies at the watershed and river scale typically assume geologic homogeneity at the sub-hydrofacies scale for the purpose of answering questions about long-term fluxes. Recent studies assessing fluxes at the reach scale have begun addressing geologic heterogeneity at the hydrofacies and sub-hydrofacies scale to better address questions about patterns and volumes of exchange as a function of hydraulic conductivity variability [*Fleckenstein et al.*, 2006; *Frei et al.*, 2009]. Aquifer heterogeneity and preferential flow are larger scale processes that influence flux to the water table. Macropores, for example, can extend the riverbed, unsaturated zone, and the saturated zone and increase flux rates orders of magnitude. Generally, hyporheic zone studies assume a homogeneous sediment matrix and K value which ignore the presence of large macropores, mainly because of the difficulty of quantifying such features.

1.7 Research Questions and Hypotheses

Overarching dissertation hypothesis: Evidence from field data show that dynamic permeability of riverbed sediments (the change in hydraulic conductivity over time from sediment, biomass, detritus, etc.) is occurring at different temporal and spatial scales. How does dynamic permeability affect infiltration in losing and gaining rivers, especially when they are controlled by top-down drivers including climate perturbations on sediments and disconnection from pumping? What is the overall cumulative effect of the combination of these dynamic processes on overall flow and transport in large scale vertical hyporheic flows and smaller scale lateral flows? How do the small-scale feedback mechanisms imposed by bioclogging feedback into numerical simulations of flow and nutrient transformations such as subsurface gas production? I break these questions down into three dissertation chapters.

First, I developed a temporally dynamic permeability function using field data and microbial clogging models coupled with numerical models of flow to assess the effects of dynamic permeability on infiltration. Permeability decreases dramatically during the summer months when the dam is inflated, temperatures are high, and when biomass grows and feedback mechanisms contribute to the development of the unsaturation zone. I show, for the first time, the coupling of transient permeability and disconnection on the infiltration rate in losing rivers.

Second, microbial biomass growth was implemented as a novel feedback mechanism within the numerical code MIN3P. This feedback effect allows testing of the cumulative effects of biomass growth on total nutrient transformation leading to carbon and nitrate consumption, microbial byproducts, bioclogging, flow, and transport given different initial starting conditions of sediments. My results show that initial conditions of sediment parameters and governing properties of top-down controls strongly regulate subsurface carbon and nitrogen consumption through aerobic respiration and anaerobic denitrification. This has major implications for how rivers are understood in the context of their ability to act as sources and sinks in carbon and nitrogen budgets.

Third, I use algal and grain-size distribution field data from the Wohler site to model scenarios of horizontal and vertical hyporheic flow given additional redox processes that include Iron and Sulfate reduction. I include predictions of dissolved oxygen and primary productivity as an imposed model boundary condition to apply a top-down control from climate, sediments and benthic ecology on subsurface microbial transformations. These results show that surface benthic ecology has a strong control on subsurface microbial C and N processing through pulses of nutrients to the subsurface.

1.8 Conclusions

Better understanding of the mechanisms controlling the impacts of riverbed bioclogging can not only provide quantitative protocols for managing pumping, but can also inform assessments and models of surface water-groundwater interactions and the role of biological factors in managing RBF systems. The purpose of my dissertation is to analyze how dynamic permeability from bioclogging can affect the vadose zone flow dynamics, and see how this correlates to the connection status of the river and measures of drought. Major research results from my dissertation show that comparing and simulating the combined effects of biomass and disconnection on seepage is required for accurately predicting infiltration rates. Bioclogging ultimately shapes the magnitude of the infiltration flux, however the process of disconnection shapes the timing of peak flux and of unsaturated zone growth. Dynamic permeability feedbacks on nutrient and infiltration fluxes have shown measureable impacts on ecosystem services such as carbon and nitrate transformation in the hyporheic zone. Recognition of the feedbacks relating to point scale and field scale fluxes and volumes, and of the feedbacks between topographical patterns and heterogeneous biomass can lead to better estimates of local water volumes and pumping capacities, especially when these systems are used as municipal and public water supply sources. Predicting how droughts and floods change the conditions that allow rivers and aquifer to be connected is important for better managing flow in rivers to meet downstream discharge requirements. Additionally, predicting recharge as a function of changes occurring on the surface can allow water managers to more strategically bank and pump water to make better use of supplies when they are available.

Bibliography

Aalto, R., L. Maurice-Bourgoin, T. Dunne, D. R. Montgomery, C. A. Nittrouer, and J.-L. Guyot (2003), Episodic sediment accumulation on Amazonian flood plains influenced by El Nio/Southern Oscillation, *Nature*, *425*(6957), 493–497, doi:10.1038/nature02002.

Andrews, E. D., and R. C. Antweiler (2012), Sediment Fluxes from California Coastal Rivers: The Influences of Climate, Geology, and Topography, *The Journal of Geology*, *120*(4), 349–366, doi:10.1086/665733.

Boano, F., R. Revelli, and L. Ridolfi (2010), Effect of streamflow stochasticity on bedform-driven hyporheic exchange, *Advances in Water Resources*, *33*(11), 1367–1374, doi:10.1016/j.advwatres.2010.03.005.

Brookfield, A. E., and E. A. Sudicky (2012), Implications of Hyporheic Flow on Temperature-Based Estimates of Groundwater/Surface Water Interactions, *Journal of Hydrologic Engineering*, p. 121018101344009, doi:10.1061/(ASCE)HE.1943-5584.0000726.

Brovelli, A., F. Malaguerra, and D. Barry (2009), Bioclogging in porous media: Model development and sensitivity to initial conditions, *Environmental Modelling & Software*, *24*(5), 611–626, doi:10.1016/j.envsoft.2008.10.001.

Brunner, P., P. G. Cook, and C. T. Simmons (2009a), Hydrogeologic controls on disconnection between surface water and groundwater, *Water Resources Research*, *45*(1), 1–13, doi:10.1029/2008WR006953.

Brunner, P., C. T. Simmons, and P. G. Cook (2009b), Spatial and temporal aspects of the transition from connection to disconnection between rivers, lakes and groundwater, *Journal of Hydrology*, *376*(12), 159–169, doi:10.1016/j.jhydrol.2009.07.023.

Brunner, P., P. G. Cook, and C. T. Simmons (2011), Disconnected Surface Water and Groundwater: From Theory to Practice, *Ground Water*, *49*(4), 460–467, doi:10.1111/j.1745-6584.2010.00752.x.

Buss, S., Z. Cai, B. Cardenas, J. Fleckenstein, D. Hannah, K. Heppell, P. Hulme, T. Ibrahim, D. Kaeser, S. Krause, D. Lawler, D. Lerner, J. Mant, I. Malcolm, G. H. Old, G. Parkin, R. Pickup, G. Pinay, J. Porter, G. Rhodes, A. Ritchie, J. Riley, A. Robertson, D. Sear, B. Shields, J. Smith, J. Tellam, and P. Wood (2009), *The Hyporheic Handbook: A Handbook on the groundwater-surface water interface and hyporheic zone for environmental managers*, National Environment Research Council Centre for Ecology & Hydrology, Environment Agency, Bristol, United Kingdom.

Cardenas, M. B. (2009), Stream-aquifer interactions and hyporheic exchange in gaining and losing sinuous streams, *Water Resources Research*, *45*(6), n/a–n/a, doi:10.1029/2008WR007651.

Cardenas, M. B., J. L. Wilson, and V. A. Zlotnik (2004), Impact of heterogeneity, bed forms, and stream curvature on subchannel hyporheic exchange, *Water Resources Research*, *40*(8), 1–13, doi:10.1029/2004WR003008.

Cayan, D. R., K. T. Redmond, and L. G. Riddle (1999), ENSO and Hydrologic Extremes in the Western United States, *Journal of Climate*, *12*(9), 2881–2893, doi:10.1175/1520-0442(1999)012⟨2881:EAHEIT⟩2.0.CO;2.

Constantz, J. (1982), Temperature dependence of unsaturated hydraulic conductivity of two soils, *Soil Science Society of America Journal*, *46*(3), 466–470.

Constantz, J. (1991), Comparison of Isothermal and Isobaric Water Retention Paths in Nonswelling Porous Materials, *Water Resources Research*, *27*(12), 3165–3170, doi:10.1029/91WR02194.

Crosbie, R. S., A. R. Taylor, A. C. Davis, S. Lamontagne, and T. Munday (2014), Evaluation of infiltration from losing-disconnected rivers using a geophysical characterisation of the riverbed and a simplified infiltration model, *Journal of Hydrology*, *508*, 102–113, doi:10.1016/j.jhydrol.2013.07.045.

Faybishenko, B. (1999), Short-term and long-term vadose zone monitoring: Current technologies, development, and applications, *Tech. Rep. LBNL Report 43408*, Lawrence Berkeley National Laboratory, Berkeley, CA.

Fleckenstein, J. H., R. G. Niswonger, and G. E. Fogg (2006), River-Aquifer Interactions, Geologic Heterogeneity, and Low-Flow Management, *Ground Water*, *44*(6), 837–852, doi:10.1111/j.1745-6584.2006.00190.x.

Frei, S., J. Fleckenstein, S. Kollet, and R. Maxwell (2009), Patterns and dynamics of river-aquifer exchange with variably-saturated flow using a fully-coupled model, *Journal of Hydrology*, *375*(34), 383–393, doi:10.1016/j.jhydrol.2009.06.038.

Gasperikova, E., Y. Zhang, and S. Hubbard (2008), Using Self Potential and Multiphase Flow Modeling to Optimize Groundwater Pumping, *EOS Transactions American Geophysical Union Abstract #H42D-02*, *89*(53).

Genereux, D. P., S. Leahy, H. Mitasova, C. D. Kennedy, and D. R. Corbett (2008), Spatial and temporal variability of streambed hydraulic conductivity in West Bear Creek, North Carolina, USA, *Journal of Hydrology*, *358*(34), 332–353, doi:10.1016/j.jhydrol.2008.06.017.

Giambastiani, B. M. S., A. M. McCallum, M. S. Andersen, B. F. J. Kelly, and R. I. Acworth (2012), Understanding groundwater processes by representing aquifer heterogeneity in the Maules Creek Catchment, Namoi Valley (New South Wales, Australia), *Hydrogeology Journal*, *20*(6), 1027–1044, doi:10.1007/s10040-012-0866-y.

Gray, A. B., G. B. Pasternack, E. B. Watson, J. A. Warrick, and M. A. Goi (2015), Effects of antecedent hydrologic conditions, time dependence, and climate cycles on the suspended sediment load of the Salinas River, California, *Journal of Hydrology*, *525*, 632–649, doi: 10.1016/j.jhydrol.2015.04.025.

Harding Lawson Associates (1988), Hydrogeologic Investigation Wohler Aquifer Study. Sonoma County, California, *Tech. Rep. HLA Job No. 1916,005.02*, Sonoma County, CA.

Hatch, C. E. (2007), Spatial and temporal dynamic of surface water-groundwater interactions using time-series analysis of streambed thermal records in coastal streams, Ph.D. thesis, University of California, Santa Cruz, Department of Earth Sciences.

Hatch, C. E., A. T. Fisher, C. R. Ruehl, and G. Stemler (2010), Spatial and temporal variations in streambed hydraulic conductivity quantified with time-series thermal methods, *Journal of Hydrology*, *389*(34), 276–288, doi:10.1016/j.jhydrol.2010.05.046.

Hester, E. T., and M. W. Doyle (2008), In-stream geomorphic structures as drivers of hyporheic exchange, *Water Resources Research*, *44*(3), n/a–n/a, doi:10.1029/2006WR005810.

Hubbs, S. A. (2006), Evaluating Streambed Forces Impacting the Capacity of Riverbed Filtration Systems, in *Riverbank Filtration Hydrology*, edited by S. A. Hubbs, no. 60 in Nato Science Series: IV: Earth and Environmental Sciences, pp. 21–42, Springer Netherlands.

Inman, D. L., and S. A. Jenkins (1999), Climate Change and the Episodicity of Sediment Flux of Small California Rivers, *The Journal of Geology*, *107*(3), 251–270, doi:10.1086/314346.

Irvine, D. J., P. Brunner, H.-J. H. Franssen, and C. T. Simmons (2012), Heterogeneous or homogeneous? Implications of simplifying heterogeneous streambeds in models of losing streams, *Journal of Hydrology*, *424425*, 16–23, doi:10.1016/j.jhydrol.2011.11.051.

Ivkovic, K. M. (2009), A topdown approach to characterise aquiferriver interaction processes, *Journal of Hydrology*, *365*(3-4), 145–155, doi:10.1016/j.jhydrol.2008.11.021.

Jaramillo, M. (2012), Riverbank Filtration: An Efficient and Economical Drinking-Water Treatment Technology, *DYNA*, *79*(171), 148–157.

Kalbus, E., C. Schmidt, J. W. Molson, F. Reinstorf, and M. Schirmer (2009), Influence of aquifer and streambed heterogeneity on the distribution of groundwater discharge, *Hydrology and Earth System Sciences*, *13*(1), 69–77, doi:10.5194/hess-13-69-2009.

Klos, P. Z., T. E. Link, and J. T. Abatzoglou (2014), Extent of the rain-snow transition zone in the western U.S. under historic and projected climate, *Geophysical Research Letters*, *41*(13), 2014GL060,500, doi:10.1002/2014GL060500.

Kondrashov, D. (2005), Oscillatory modes of extended Nile River records (A.D. 6221922), *Geophysical Research Letters*, *32*(10), doi:10.1029/2004GL022156.

Lamontagne, S., A. Taylor, R. Crosbie, and P. G. Cook (2011), Interconnection of Surface and Groundwater Systems-River Losses from Losing/Disconnected Streams. Billabong Creek Site Report, in *Water for a Healthy Country Flagship Report series ISSN: 1835-095X*, p. 37, NSW Office of Water, Australia.

Lamontagne, S., R. Crosbie, A. Davis, T. Munday, A. Taylor, and K. Cahill (2012), Hydrogeophysics project: Reach-scale infiltration flux in losing-disconnected rivers, in *Water for a Healthy Country Flagship Report series ISSN: 1835 - 095X*, p. 56, NSW Office of Water, Australia.

Lamontagne, S., A. R. Taylor, P. G. Cook, R. S. Crosbie, R. Brownbill, R. M. Williams, and P. Brunner (2013), Field assessment of surface water - groundwater connectivity in a semi-arid river basin (Murray-Darling, Australia), *Hydrological Processes*, pp. 1561–1672, doi:10.1002/hyp.9691.

McCallum, A. M., M. S. Andersen, B. M. S. Giambastiani, B. F. J. Kelly, and R. Ian Acworth (2013), Riveraquifer interactions in a semi-arid environment stressed by groundwater abstraction, *Hydrological Processes*, *27*(7), 1072–1085, doi:10.1002/hyp.9229.

Newcomer, M. E., S. S. Hubbard, J. H. Fleckenstein, U. Maier, C. Schmidt, M. Thullner, C. Ulrich, N. Flipo, and Y. Rubin (2016), Simulating bioclogging effects on dynamic riverbed permeability and infiltration, *Water Resources Research*, pp. n/a–n/a, doi:10.1002/2015WR018351.

NOAA CPC (2015), El Nio Southern Oscillation.

Piggott, J. J., R. K. Salis, G. Lear, C. R. Townsend, and C. D. Matthaei (2015), Climate warming and agricultural stressors interact to determine stream periphyton community composition, *Global Change Biology*, *21*(1), 206–222, doi:10.1111/gcb.12661.

Power, M., R. Lowe, P. Furey, J. Welter, M. Limm, J. Finlay, C. Bode, S. Chang, M. Goodrich, and J. Sculley (2009), Algal mats and insect emergence in rivers under Mediterranean climates: towards photogrammetric surveillance, *Freshwater Biology*, *54*(10), 2101–2115, doi:10.1111/j.1365-2427.2008.02163.x.

Power, M. E. (1992), Hydrologic and trophic controls of seasonal algal blooms in northern California rivers, *Archiv fr Hydrobiologie*, *125*(4), 385–410.

Power, M. E., M. S. Parker, and W. E. Dietrich (2008), Seasonal reassembly of a river food web: floods, droughts, and impacts of fish, *Ecological Monographs*, *78*(2), 263–282, doi:10.1890/06-0902.1.

Rosenberry, D. O., and J. Pitlick (2009), Local-scale variability of seepage and hydraulic conductivity in a shallow gravel-bed river, *Hydrological Processes*, *23*(23), 3306–3318, doi:10.1002/hyp.7433.

Ryan, R. J., and M. C. Boufadel (2006), Evaluation of streambed hydraulic conductivity heterogeneity in an urban watershed, *Stochastic Environmental Research and Risk Assessment*, *21*(4), 309–316, doi:10.1007/s00477-006-0066-1.

Salehin, M., A. I. Packman, and M. Paradis (2004), Hyporheic exchange with heterogeneous streambeds: Laboratory experiments and modeling, *Water Resources Research*, *40*(11), n/a–n/a, doi:10.1029/2003WR002567.

Sawyer, A. H., and M. B. Cardenas (2009), Hyporheic flow and residence time distributions in heterogeneous cross-bedded sediment, *Water Resources Research*, *45*(8), 1–12, doi:10.1029/2008WR007632.

Schubert, J. (2002), Hydraulic aspects of riverbank filtrationfield studies, *Journal of Hydrology*, *266*(34), 145–161, doi:10.1016/S0022-1694(02)00159-2.

Schubert, J. (2006), Experience with Riverbed Clogging Along the Rhine River, in *Riverbank Filtration Hydrology*, edited by S. A. Hubbs, no. 60 in Nato Science Series: IV: Earth and Environmental Sciences, pp. 221–242, Springer Netherlands.

Shanafield, M., C. L. Shope, and W. A. McKay (2012a), Comparison of heat tracer models in the estimation of upward flux through streambed sediments, *Hydrology and Earth System Sciences Discussions*, *9*(4), 4305–4332, doi:10.5194/hessd-9-4305-2012.

Shanafield, M., P. G. Cook, P. Brunner, J. McCallum, and C. T. Simmons (2012b), Aquifer response to surface water transience in disconnected streams, *Water Resources Research*, *48*(11), 1–8, doi:10.1029/2012WR012103.

She, H. Y., and B. E. Sleep (1998), The effect of temperature on capillary pressure-saturation relationships for air-water and perchloroethylene-water systems, *Water Resources Research*, *34*(10), 2587–2597, doi:10.1029/98WR01199.

Sonoma County Water Agency (2012), Radial Collector Well Water Quality Studies-Agreements: County of Sonoma, Agenda Item, Summary Report, *Tech. rep.*, Sonoma County Water Agency, Sonoma County, CA.

Stewardson, M., S. Grant, and I. Marusic (2011), Modelling hyporheic exchange: From the boundary layer to the basin, in *Sustaining our Future: Understanding and Living with Uncertainty*, Perth, Australia.

Su, G. W., J. Jasperse, D. Seymour, and J. Constantz (2004), Estimation of Hydraulic Conductivity in an Alluvial System Using Temperatures, *Ground Water*, *42*(6), 890–901, doi:10.1111/j.1745-6584.2004.t01-7-.x.

Su, G. W., J. Jasperse, D. Seymour, J. Constantz, and Q. Zhou (2007), Analysis of pumping-induced unsaturated regions beneath a perennial river, *Water Resources Research*, *43*(8), doi:10.1029/2006WR005389.

Thullner, M. (2010), Comparison of bioclogging effects in saturated porous media within one- and two-dimensional flow systems, *Ecological Engineering*, *36*(2), 176–196, doi:10.1016/j.ecoleng.2008.12.037.

Thullner, M., L. Mauclaire, M. H. Schroth, W. Kinzelbach, and J. Zeyer (2002a), Interaction between water flow and spatial distribution of microbial growth in a two-dimensional flow field in saturated porous media, *Journal of Contaminant Hydrology*, *58*(34), 169–189, doi:10.1016/S0169-7722(02)00033-5.

Thullner, M., J. Zeyer, and W. Kinzelbach (2002b), Influence of Microbial Growth on Hydraulic Properties of Pore Networks, *Transport in Porous Media*, *49*(1), 99–122, doi:10.1023/A:1016030112089.

Thullner, M., M. H. Schroth, J. Zeyer, and W. Kinzelbach (2004), Modeling of a microbial growth experiment with bioclogging in a two-dimensional saturated porous media flow field, *Journal of Contaminant Hydrology*, *70*(12), 37–62, doi:10.1016/j.jconhyd.2003.08.008.

Tong, F., L. Jing, and T. Bin (2011), A Water Retention Curve Model for the Simulation of Coupled Thermo-Hydro-Mechanical Processes in Geological Porous Media, *Transport in Porous Media*, *91*(2), 509–530, doi:10.1007/s11242-011-9857-z.

Treese, S., T. Meixner, and J. F. Hogan (2009), Clogging of an Effluent Dominated Semi-arid River: A Conceptual Model of Stream-Aquifer Interactions, *JAWRA Journal of the American Water Resources Association*, *45*(4), 1047–1062, doi:10.1111/j.1752-1688.2009.00346.x.

Tufenkji, N., J. N. Ryan, and M. Elimelech (2002), The Promise of Bank Filtration, *Environmental Science & Technology*, *36*(21), 422A–428A, doi:10.1021/es022441j.

Ulrich, C., S. Hubbard, J. Florsheim, D. O. Rosenberry, S. Borglin, M. Trotta, and D. Seymour (2015), Riverbed Clogging associated with a California Riverbank Filtration System: An assessment of mechanisms and monitoring approaches, *Journal of Hydrology*, *529*(3), 1740–1753, doi:10.1016/j.jhydrol.2015.08.012.

Zhang, Y., S. Hubbard, and S. Finsterle (2011), Factors governing sustainable groundwater pumping near a river, *Ground Water*, *49*(3), 432–444.

Zlotnik, V. A., M. B. Cardenas, and D. Toundykov (2011), Effects of Multiscale Anisotropy on Basin and Hyporheic Groundwater Flow, *Ground Water*, *49*(4), 576–583, doi:10.1111/j.1745-6584.2010.00775.x.

Chapter 2

Simulating Bioclogging Effects on Dynamic Riverbed Permeability and Infiltration

Abstract: Bioclogging in rivers can detrimentally impact aquifer recharge. This is particularly so in dry regions, where losing rivers are common, and where disconnection between surface water and groundwater (leading to the development of an unsaturated zone) can occur. Reduction in riverbed permeability due to biomass growth is a time-variable parameter that is often neglected, yet permeability reduction from bioclogging can introduce order of magnitude changes in seepage fluxes from rivers over short (i.e., monthly) timescales. To address the combined effects of bioclogging and disconnection on infiltration, we developed numerical representations of bioclogging processes within a one-dimensional, variably-saturated flow model representing losing-connected and losing-disconnected rivers. We tested these formulations using a synthetic case study informed with biological data obtained from the Russian River, California, U.S.A. Our findings show that modeled biomass growth reduced seepage for losing-connected and losing-disconnected rivers. However, for rivers undergoing disconnection, infiltration declines occurred only after the system was fully disconnected. Before full disconnection, biologically-induced permeability declines were not significant enough to offset the infiltration gains introduced by disconnection. The two effects combine to lead to a characteristic infiltration curve where peak infiltration magnitude and timing is controlled by permeability declines relative to hydraulic gradient gains. Biomass growth was found to hasten the onset of full disconnection; a condition we term effective disconnection. Our results show that river infiltration can respond dynamically to bioclogging and subsequent permeability declines that are highly dependent on river connection status.[1]

[1]This chapter was recently published in Water Resources Research [*Newcomer et al.*, 2016]: Newcomer, M. E., Hubbard, S. S., Fleckenstein, J. H., Maier, U., Schmidt, C., Thullner, M., Ulrich, C., Flipo, N. and

2.1 Introduction

The ability to accurately predict infiltration from rivers and recharge of water to nearby groundwater aquifers is essential to water resources management [*Crosbie et al.*, 2014; *Harvey and Gooseff*, 2015]. Riverbank Filtration (RBF) systems (Figure 2.1 on page 26), typically used for the production of drinking water, make use of high infiltration capacities in addition to passive filtration benefits provided by river systems [*Jaramillo*, 2012; *McCallum et al.*, 2013]. Accurate management of RBF pumping strategies requires information about infiltration dynamics, which depend on characterization of sediment properties and their temporal variability, such as streambed permeability. Although field measurements indicate that riverbed permeability is often dynamic, due to processes such as subsurface bioclogging and sedimentation [*Annan*, 2001; *Blaschke et al.*, 2003; *Doppler et al.*, 2007; *Genereux et al.*, 2008; *Hatch et al.*, 2010; *Engeler et al.*, 2011; *Zhang et al.*, 2011; *Kurtz et al.*, 2012; *Taylor et al.*, 2013], most surface-groundwater numerical models assume that it is constant over time [*Doppler et al.*, 2007; *Flipo et al.*, 2014]. Ignoring these dynamic processes in predictive numerical models could have significant ramifications for practical management of water resources, especially in drought-prone regions where losing rivers are common.

Subsurface bioclogging can affect pore scale sediment permeability and porosity through river system ecological processes and surface-groundwater interactions*Battin and Sengschmitt* [1999]. Biofilms are aggregates of microbial biomass that consist of bacterial cells and exopolymeric saccharides (EPS) produced by these cells [*Wingender et al.*, 1999; *Or et al.*, 2007]. These aggregates can occupy pore throats and pore spaces, thereby decreasing hydraulic conductivity by orders of magnitude through physical clogging [*Baveye et al.*, 1998; *Rockhold*, 2002; *Thullner*, 2010]. Although many models represent microbial growth and decay as a function of nutrient substrates [*Molz et al.*, 1986; *Murphy and Ginn*, 2000; *Thullner et al.*, 2007], most model approaches describing bioclogging are pore-scale models (e.g. *Suchomel et al.* [1998]; *Kim et al.* [2000]; *Dupin et al.* [2001]; *Thullner et al.* [2002a]; *Thullner and Baveye* [2008]; *Ezeuko et al.* [2011]; *Rosenzweig et al.* [2014]). Few of these incorporate scaled-up representations of bioclogging processes [*Kildsgaard and Engesgaard*, 2001; *Thullner et al.*, 2004; *Brovelli et al.*, 2009; *Soleimani et al.*, 2009; *Sams et al.*, 2016] that are required to simulate bioclogging influences on river system behavior.

Accurate prediction of infiltration from a losing river depends on the status of river-aquifer connection as well as dynamic streambed permeability. Rivers can be hydraulically connected to an aquifer (with no unsaturated zone beneath the riverbed, low hydraulic gradients, and minimal vertical seepage), or they can be hydraulically disconnected (with a fully-developed unsaturated zone, unit-gradient (UG) flow, and maximum seepage) [*Fox*

Rubin, Y. (2016), Simulating bioclogging effects on dynamic riverbed permeability and infiltration. Water Resour. Res.. Accepted Author Manuscript. doi:10.1002/2015WR018351

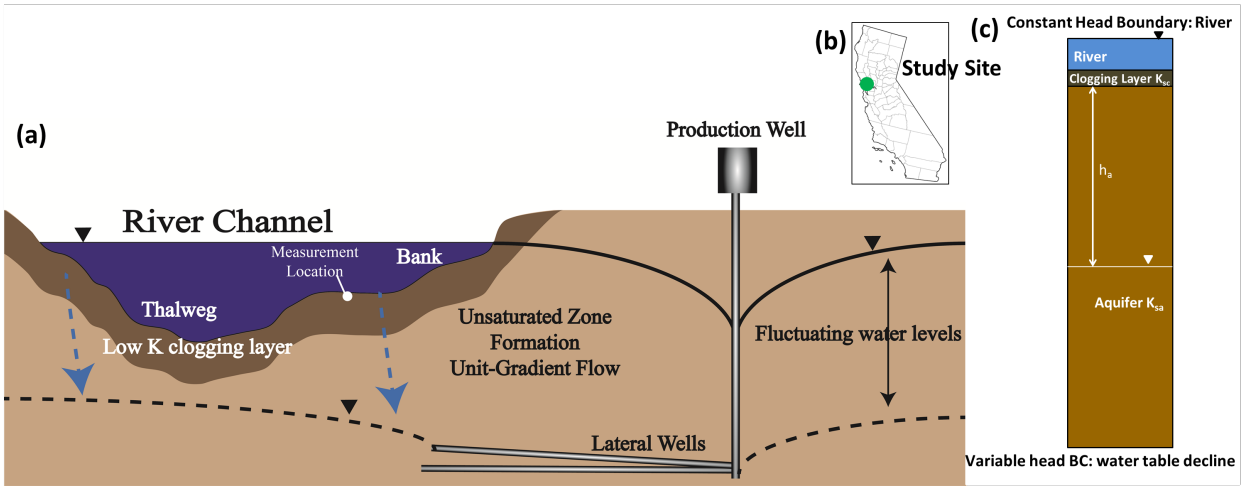

Figure 2.1: (a) Conceptual, two-dimensional diagram of a river and key aspects that govern infiltration, based on the Wohler RBF site in CA. The figure illustrates aspects such as riverbed clogging layer (low conductivity layer), aquifer layer, fluctuating water table, unsaturated zone formation (disconnection), location of unit-gradient (UG) flow, RBF well location, and lateral pumping wells. (b) Location map of the Wohler RBF site in California, whose data inspired this study (Lat: 38.5, Long: -122.9). (c) One-dimensional profile of the layered sediments at a general location within the river cross section where the flow path is dominantly vertical and where disconnection occurs. Note: This figure is not to scale. Lateral wells are located sufficiently below the river that all flow paths are dominantly vertical from the river, even those in the unsaturated zone.

and Durnford, 2003; *Brunner et al.*, 2009a; *Rivire et al.*, 2014]. The process of disconnection begins when groundwater levels drop, such as from pumping or long periods of drought (Figure 2.1 on page 26). When rivers are fully disconnected, further groundwater level drops no longer affect the infiltration rate. Although several studies have documented dynamics in riverbed permeability and river-aquifer connection separately [*Treese et al.*, 2009; *Hatch et al.*, 2010; *Lamontagne et al.*, 2011], their coupled influence on infiltration has not been fully evaluated. Confounding indications from field measurements, which show seepage increases concurrent with riverbed permeability declines, motivate the development of models that can account for transient river-aquifer connection [*Hatch et al.*, 2010; *Zhang et al.*, 2011; *Ulrich et al.*, 2015].

In this study, we assess the controlling mechanisms of infiltration in a losing river under conditions of subsurface bioclogging using a synthetic case study inspired by field data from the Russian River near Wohler, California, U.S.A. We use a generic one-dimensional profile

to demonstrate bioclogging effects on long-term infiltration trends to emphasize the applicability of this approach to other rivers where bioclogging and disconnection may dominate. We evaluate the effects of bioclogging on infiltration trends, timing of peak infiltration, and the evolution of unsaturated zone profiles from losing-connected to losing-disconnected river conditions. Our main goal is to isolate two important monthly/seasonal scale processes that, when combined, can reproduce observed temporal trends. To our knowledge, bioclogging and assessment of temporally dynamic parameters on infiltration in field scenarios have not been analyzed sufficiently in the literature, which motivates this study. This predictive ability is critical for optimal management of pumping in drought-prone areas, especially over long time frames where feedback effects may become important [*Treese et al.*, 2009; *Hatch et al.*, 2010]. This work aims to bridge the gap between hydrological and eco-hydrological views of the stream-aquifer interface by incorporating pore-scale representations of bioclogging processes into local-scale models of river system infiltration to account for temporal variability found in natural settings.

2.2 Wohler Study Site, Previous Modeling, and Data Sets Used

Located along the Russian River in Sonoma County, CA, USA, the Sonoma County Water Agency (SCWA) Wohler site provides drinking water to 600,000 people annually. To provide this water, collector wells located on the riverbank use lateral wellbores that extend at depth toward the river to pump water that has infiltrated from the river downward through sediments (Figure 2.1 on page 26). The total production capacity of the SCWA RBF facility is estimated to be 350,000 m^3 per day (92 million gallons per day). Prior studies have estimated riverbed infiltration rates ranging between 0.11 m/day at various locations along the Russian River [*Harding Lawson Associates*, 1988]. During peak demand months, SCWA raises an inflatable dam on the Russian River downstream of the Wohler site to increase infiltration. On-off pumping cycles, as well as the rate of daily pumping, can change the water table position on a daily and sub-daily timescale. Pumping over the entire summer season leads to a large, regional water table drop. A conceptual one-dimensional and two-dimensional schematic of the river system, including the river, the riverbed clogging layer, and the fluctuating groundwater level, is shown in Figure 2.1 on page 26. The clogging layer represents a sediment boundary where an inverted water table (i.e., a saturated zone overlies an unsaturated zone) can potentially form [*Dillon and Liggett*, 1983; *Peterson*, 1989; *Xie et al.*, 2013; *Rivire et al.*, 2014].

Both numerical and experimental studies have been performed at the Wohler Site to aid RBF operations. Experimental studies along the Russian River and Pajaro River (150 km

south of the Russian River) have documented that infiltration did not simply decline with riverbed permeability: in some cases, measured flux was found to increase when permeability decreased [*Su et al.*, 2007; *Hatch et al.*, 2010; *Ulrich et al.*, 2015]. Numerical, two-dimensional simulations and inversions for riverbed permeability at the Wohler site indicated a strong, dynamic component that had not previously been accounted for in models of infiltration [*Su et al.*, 2007; *Zhang et al.*, 2011]. These models did not account for bioclogging-induced permeability effects, or for simultaneous river disconnection.

Motivated by these simulation results, extensive field campaigns were conducted in 2012 to investigate spatio-temporal controls on riverbed clogging processes [*Ulrich et al.*, 2015]. Here, we use three of the data sets collected during those campaigns to inform and compare with model results: (1) grain size distributions (GSD) from 38 sediment samples used for estimating porosity from five riverbed sites, (2) subsurface biomass from cryocores analyzed using the phospholipid fatty acid technique at three of the five sites [*White and Ringelberg*, 1998] (Figure 2.2 on page 29), and (3) spatially averaged seepage from seepage meters collected at four of the sites (Figure 2.2 on page 29). Large variability in the seepage data indicates that infiltration in different parts of the river may be subject to spatially variable disconnection or clogging at different times. Riverbed sediments were collected to a depth of 0.2 m during spring, summer, and fall of 2012. Cryocoring techniques were used to preserve the structural and biological integrity of the riverbed sediment samples during transport to the laboratory. All samples were collected along the bank of the river cross section. Data were collected during five months, May through November, which represent the time period (160 days) when bioclogging is most relevant. An important finding of the *Ulrich et al.* [2015] study was that biotic processes play a much larger role in riverbed clogging at the Wohler site relative to abiotic processes (e.g., sedimentation and erosion; see*Blaschke et al.* [2003]). We focus on riverbed clogging by biofilms because of the potential for significant decreases in permeability over relatively short time periods (i.e., one summer season).

Analysis of the data described above, as well as other Wohler data sets, revealed key spatial and temporal characteristics of the study site [*Ulrich et al.*, 2015]. Riverbed sediments contained gravels and cobbles with a sandy-silt matrix. Bacterial, fungal, algal, and general plant biomass cells per gram of sediment ranged from 10^4 cells/gram-dry-weight in the spring to 10^7 cells/gram-dry-weight in the late summer. Biomass concentrations are similar to those reported in *Gupta and Swartzendruber* [1962] and *Seki et al.* [2006]. Another important finding from *Ulrich et al.* [2015] was the development of a laterally extensive unsaturated zone mid-way through the summer, shown using time-lapse Electrical Resistivity Tomography (ERT) images. Average seepage values from multiple sites (represented by white dots in Figure 2.1 on page 26), from the end of May until November 2012 (160 days), show that the seepage increased midway through the summer, then decreased to almost zero by the end of the summer (Figure 2.2 on page 29). This seepage trend is consistent with the hypothesis that the system initially experiences disconnection (predicting seepage increases), followed

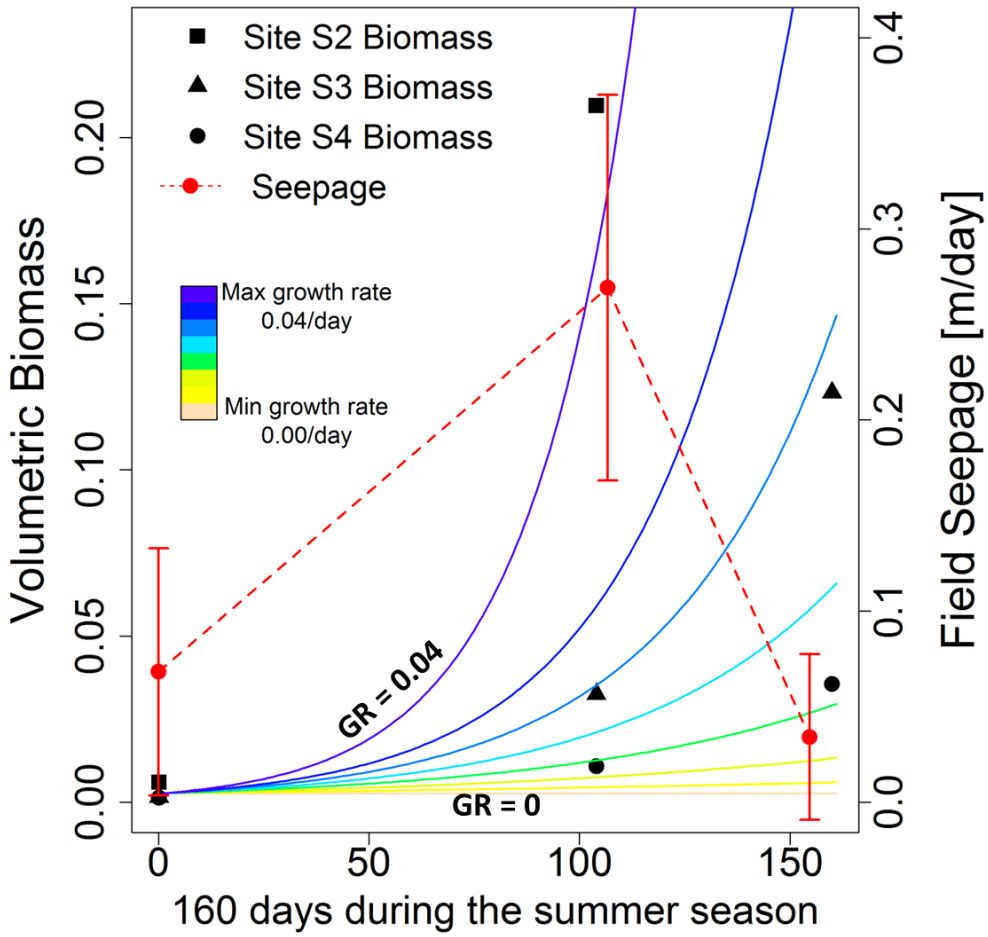

Figure 2.2: Field values of seepage measured and averaged across multiple locations. The red dashed line connects seepage measurements made during three field campaigns; error bars show the large variability between sites. Field values of volumetric biomass are shown at three locations. Predicted exponential biomass growth curves range across many growth rates. Volumetric biomass is the ratio of the biomass volume relative to the volume of the sediment sample. Different curves over the range of biomass growth rates (GR) are shown. For the color versions of these figures, the reader is referred to the electronic version of this article. Seepage data can be found in the supporting information file for this article online.

by bioclogging limitations thereafter. To our knowledge, this is the first observation of disconnection in a real river. Additional details about the data sets are provided in *Ulrich et al.* [2015].

2.3 Methods

Biomass Growth and Volume Fraction

Continuous biomass growth curves (Figure 2.2 on page 29) were calculated using a first-order exponential model fitted to the biomass field data obtained from the top of the field core (μg g^{-1} dry weight). Decay, sorption, and grazer consumption were ignored; therefore this represents a very simplified growth model. The first-order exponential model of biomass growth is given by:

$$\frac{dX}{dt} = \mu X \tag{2.1}$$

X is the mass (dry weight) of biomass per unit mass of solids (μg g^{-1}), and μ is the specific growth rate with units of day^{-1}. A range of effective biomass growth rates fit to the field data were used (μ = 0.005-0.04 day^{-1}). An initial value of biomass (A0) was set at 0.4 μg g^{-1}. Growth rates found in the literature can range by many orders of magnitude and are typically used with Monod kinetic reactions [*Murphy and Ginn*, 2000; *Brun and Engesgaard*, 2002; *Thullner et al.*, 2007]. For our simulations, we did not use Monod kinetics because of the lack of nutrient data, and because our aim was to constrain the model with true biomass field data.

Each biomass growth model was converted to a time-series of relative porosity using Equations 2.2-2.5. A porosity associated with each grain-size distribution was calculated using Equations 2.2 and 2.3. The original porosity (n_0) was obtained from the field-sampled grain size distributions, where d10 represents the grain size (mm) at which 10% of the data fall below, and similarly for d60 [*Barahona-Palomo et al.*, 2011]:

$$n_0 = 0.255(1 + 0.83^U) \tag{2.2}$$

$$U = \frac{d_{10}}{d_{60}} \tag{2.3}$$

From the 38 grain size distributions, the mean porosity was 0.276 and standard deviation was 0.017.

Biomass volumetric fraction (n_{bio}) was calculated with Equation 2.4:

$$n_{bio} = \frac{X_s \rho_b}{\rho_s} \tag{2.4}$$

In this equation, X_s is the mass (dry weight) of the biomass per unit mass of solids (μg g^{-1}), the bulk density of the porous medium is given by ρ_b, and the density of the average biomass is given by ρ_s which represents a sum of all the microorganisms, bacteria, algae, fungi, EPS, etc. Units for ρ_b and ρ_s are given in kg m^{-3}. Bulk density of the riverbed sediments (ρ_b) and density of the biomass (ρ_s) were unknown, and thus were selected from the range of values published in the literature (ρ_b=1600 [kg m^{-3}] is a typical value for sands, and ρ_b=0.25-2.5 [kg m^{-3}] dry mass/wet volume) [*Coughlan et al.*, 2002; *Thullner et al.*, 2004; *Rockhold et al.*, 2005; *Brown and Wherrett*, 2014; *Rosenzweig et al.*, 2014]. Biomass volume fraction times-series for each growth rate are shown in Figure 2.2 on page 29.

Relative porosity (n_r), shown by Equation 2.5, expresses the new porosity given biomass growth relative to the original porosity, and is given by the ratio of the updated porosity ($n_{new} = n_0$-n_{bio}) to the original porosity (n_0).

$$n_r = \frac{n_0 - n_{bio}}{n_0} = \frac{n_{new}}{n_0} \tag{2.5}$$

Dynamic Permeability Functions

To link biomass growth models over time (cf. Figure 2.2 on page 29) to a clogging potential represented by a hydraulic conductivity drop, we used the Colonies and Biofilm constitutive models [*Thullner et al.*, 2002b, a] shown in Equations 2.6 and 2.8 with previously published parameters from pore-network simulations (Table 2.1) [*Thullner et al.*, 2002a]. We use both Colonies and Biofilm models because they have been tested against experimental data and show acceptable performance [*Thullner*, 2010], and because there is no general agreement in the literature which model is most adequate. These two models represent a reasonable range of the degree of bioclogging a system may experience.

The Colonies model, conceptualized as aggregates of biomass within the pore-space, is given as:

$$K_r(n_r) = a\left(\frac{n_r - n_r^0}{1 - n_r^0}\right)^3 + (1-a)\left(\frac{n_r - n_r^0}{1 - n_r^0}\right)^2 \tag{2.6}$$

In Equation 2.6, parameters include n_r^0 and a. Values for n_r^0 range from 0 to 1, and represent the value of the relative porosity at which the relative saturated hydraulic conductivity asymptotically approaches a minimum. The parameter a represents a functional weight of the conductivity decline. Relative porosity (n_r) from Equation 2.5 is an input to Equation 2.6. $K_r(n_r)$ is the relative saturated hydraulic conductivity given by the ratio

	Biofilm		Colonies
K_{min}	$n_r{}^0$	a	$n_r{}^0$
0.008	0.3	-1.8	0.8

Table 2.1: Parameter set for the Biofilm and Colonies models [*Thullner et al.*, 2002b]

of the updated saturated hydraulic conductivity ($K_{sc,new}$) of the riverbed sediment clogging layer, to the original saturated hydraulic conductivity (K_{sc}) of that same layer:

$$K_r(n_r) = \frac{K_{sc,new}}{K_{sc}} \tag{2.7}$$

The Biofilm model, conceptualized as a film enveloping each sediment grain, is given as:

$$K_r(n_r) = \left[\left(\frac{n_r - n_r^0}{1 - n_r^0}\right)^{1.8} + K_{min}\right] \frac{1}{1 + K_{min}} \tag{2.8}$$

In the Biofilm model, K_r, n_r, and $n_r{}^0$ are the same as the Colonies model, and K_{min} is a parameter describing the residual relative conductivity of a fully clogged medium. The Biofilm and Colonies models are shown in Figure 2.3a on page 33, which shows the degree of clogging and conductivity decline for each.

Dynamic permeability functions representing changes over time in hydraulic conductivity from biomass growth (solutions to Equations 2.6 and 2.8) are shown as continuous functions over time in Figure Figure 2.3b on page 33, and are represented by the relative hydraulic conductivity $K_r(n_r)$. Marginal probability density functions (pdfs) of $K_r(n_r)$ by season are shown in Figure Figure 2.3c on page 33. Once $K_r(n_r)$ was found, Equation 2.6 could be rearranged to solve for $K_{sc,new}$, given an initial condition for K_{sc}. All permeability models shown in Figure Figure 2.3b on page 33 were supplied as inputs to the HYDRUS-1D numerical code as daily updates of the clogging layer conductivity and porosity ($K_{sc,new}$ and n_{new}).

Numerically Linking the Bioclogging Models and HYDRUS-1D

Inspired by the Wohler CA field infiltration data, we implemented two main processes within the modeling framework to test our hypothesis that disconnection and bioclogging co-occur to produce the long-term infiltration trend (Figure 2.2 on page 29): (1) time-dependent parameters calculated from the field bioclogging data, and (2) a time-dependent, lower head boundary condition to induce disconnection (representing the effects of pumping).

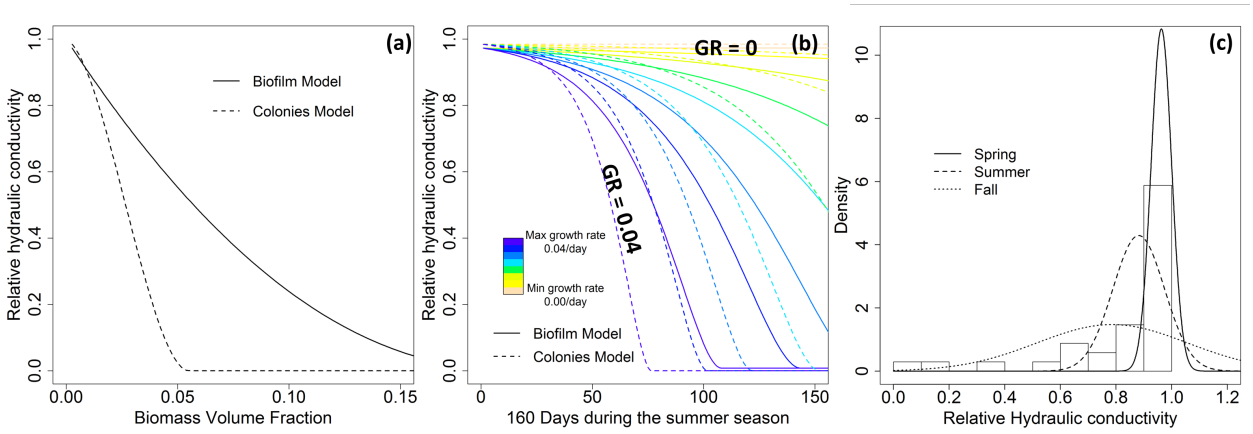

Figure 2.3: (a) Biofilm constitutive model (solid line) and Colonies constitutive model (dashed line) link a biomass volume fraction to a hydraulic conductivity decrease. (b) Dynamic permeability functions are shown over time. Different curves over the range of biomass growth rates (GR) are shown. (c) Fitted marginal probability density functions (pdfs) of the relative hydraulic conductivity estimates from the field biomass data for each season. For interpretation of the color in all figure legends, the reader is referred to the web version of this article.

Time-dependent parameters: We generated time series of parameters n_{new} and $K_{sc,new}$ from the field data according to Equations 2.5 - 2.8. A time series of decreases in hydraulic conductivity due to bioclogging are shown in Figure 2.3b on page 33. We generated these time series using the bioclogging field data (Figure 2.2 on page 29), the sediment GSD for the initial porosity values (n_0, Equation 2.2), the biological growth models (fast or slow growth rates) (Figure 2.2 on page 29, Equation 2.1), and the clogging constitutive models (Biofilm and Colonies) described by Equations 2.6-2.8 and shown in Figure 2.3a on page 33. These time series were used as time-dependent parameterization for the riverbed clogging layer (Figure 2.1 on page 26), and updated within the HYDRUS-1D numerical models using a daily update scheme described below.

Time-dependent lower head boundary: We examined two types of rivers showing the end-members of the disconnection spectrum: (1) a river undergoing disconnection from fast water table declines, and (2) a river remaining connected from slow water table declines. Water table decline rates imposed in the HYDRUS-1D model are ideal, linear representations of pumping effects on local water levels over the course of the summer months. Local observation wells show much variability in water levels from on-off pumping cycles. Our goal was not to simulate the random water table fluctuations from high-frequency pumping cycles, but instead to represent the overall summer water table decline trend. Fast water

table declines can be conceptualized as the highest pumping rates, and slow water table declines can be conceptualized as low/moderate pumping rates. Four different rates of water table decline between the two end-members defined above were used: 0.03, 0.06, 0.15, and 0.59 cm day^{-1}. From each water table decline rate, we generated a time series of daily head values to update the lower boundary condition of the numerical model (Figure 2.1c on page 26). Fast water table drops allowed the system to disconnect quickly, and showed greater change in storage (unsaturated zone development) before significant bioclogging occurred, while slow water table drops allowed the system to remain connected during bioclogging.

HYDRUS-1D: Modeling consisted of a series of two autonomous models that were loosely-coupled: HYDRUS-1D transient simulations, and our time-dependent bioclogging parameterization [*Simunek et al.*, 2008; *PC-Progress*, 2011]. Since HYDRUS-1D does not have bioclogging capabilities, we used a loosely-coupled modeling approach to synchronize our bioclogging data at each time step within HYDRUS-1D. Loosely-coupled approaches allow the exchange of sequenced output data from autonomous models, and may address some of the reported difficulties (see *Alarcon et al.* [2014] for a detailed description) of representing pore-scale processes in fully-coupled, local-to-continuum-scale flow models [*Tang et al.*, 2015].

The lower pressure head, porosity, and saturated hydraulic conductivity ($K_{sc,new}$) were updated daily within the numerical model during the 160-day simulation period. We updated the lower pressure head at the bottom boundary to represent a water table decline from pumping. All transient parameters were applied to the model as daily averages. Each daily simulation was updated with new parameters at the beginning of the new day. Initial conditions with the previous days steady state pressure heads were imposed on the next simulation, and approximated the new steady state after a few hours. Model test runs using 0.5 day conductivity update time steps produced identical fluxes over the simulation period, confirming insensitivity to the time steps at which the conductivity was updated. This approach is justified because conductivity changes from bioclogging occur gradually each day over the entire summer season.

Synthetic Domain: The synthetic one-dimensional domain consists of two sediment layers representing the riverbed clogging layer (0.1 m) and the aquifer layer (0.9 m) (Figure 2.1c on page 26), initialized with hydraulic conductivity values characteristic of typical values for loam and sand, respectively (Table 2.2), and represents a generic location within the river-aquifer cross-section (Figure 1a). The inclusion of temporal variations in riverbed hydraulic conductivity is an extension of the model described by Brunner et al., [2009a], which is a well-established reference case in the literature (Figure 2.1c on page 26). Depth of ponded water (d) was 0.2 m. The domain was discretized with a grid spacing of 0.001 m, with initial pressure head conditions linearly varying between 0.2 m (top) and 0.95 m (bottom) representing completely connected, and losing initial conditions. This choice of initially losing conditions arbitrarily starts our model at values of infiltration larger than 0. The field

Layer	Depth	θr	θs	α	n	l	K_s
	(m)	(-)	(-)	(m^{-1})	(-)	(m^{-1})	(m day^{-1})
Clogging Layer	0-0.1	0.078	0.27	3.6	1.56	0.5	0.205
Aquifer	0.1-1	0.045	0.43	14.5	2.68	0.5	20-100

Table 2.2: van Genuchten parameters supplied as initial values to the layers in the synthetic HYDRUS-1D model [*van Genuchten*, 1980]. Parameters for the residual water content (θr), the saturated water content (θs), a measure of the inverse air-entry suction (α), a measure of the porosity distribution (n), a constant parameter (l), and saturated hydraulic conductivity (Ks) can be found from the Rosetta database [*Schaap et al.*, 2001]

data of seepage (Figure 2.2 on page 29) shows some starting infiltration values around 0. We believe this is because in winter and early spring groundwater may discharge into the river. We start our models with fully losing conditions rather than gaining to save model run time. The van Genuchten parameters used in the van Genuchten-Mualem water retention functions in HYDRUS-1D are provided in Table 2.2 [*van Genuchten*, 1980]. A total of 192 simulations were run representing different combinations of growth rate parameters (μ = 0.005-0.04 day^{-1}), rate of water table drop to represent fast or slow pumping (0.030.59 cm day^{-1}), aquifer conductivity (20-100 m day^{-1}), and constitutive model (Biofilm or Colonies).

Using a one-dimensional simplification of a two-dimensional groundwater-surface water conceptual model and a sufficiently small capillary zone, *Brunner et al.* [2009b] presented a theoretical development to approximate the context for the occurrence of disconnection:

$$\frac{K_{sc}}{K_{sa}} = \frac{h_c}{d + h_c} \tag{2.9}$$

Here K_{sc} is the saturated hydraulic conductivity of the riverbed clogging layer [L T^{-1}], K_{sa} is the saturated hydraulic conductivity of the aquifer [L T^{-1}], h_c is the thickness of the clogging layer [L], and d is the depth of ponded water [L] [*Brunner et al.*, 2009a, 2011]. *Brunner et al.* [2009b] approximated local unit-gradient (UG) conditions at the time of maximum infiltration between the clogging layer and the water table represented by a pressure head = 0, leading to an approximation of the total head as $dH/dz_a \approx 1$, where H is total head [L] and z_a is elevation [L]. The approximation of UG conditions does not allow for non-linear effects of dH/dz_a in the capillary zone, which leads to the criterion presented in Equation 2.9. Equation 2.8 represents whether the given one-dimensional flow geometry has potential to disconnect. The initial value of hc/(d+hc) for our domain is 0.33, and Equation 2.9 is fulfilled by our choice of initial K_{sc} and K_{sa} values.

The rates of the water table drop were classified as losing-connected, losing-transitional,

or losing-disconnected, based on the behavior of the no-biomass-growth case according to the following classification scheme and total head gradient through the aquifer (dH/dz_a) measured between the base of the clogging layer and the groundwater level represented by a pressure head = 0 m. These definitions are rather loose constraints, as there is no exact cutoff between them:

- Losing-connected: when the baseline no-growth case fails to reach the maximum flux after the 160-day simulation, and remains sensitive to increases in the total head gradient. The column remains saturated for the baseline no-growth case ($dH/dz_a \ll 1$).
- Losing-transitional: when the baseline no-growth case approaches the maximum flux, but remains sensitive to increases in the total head gradient. The column shows a small, unsaturated zone developing, where pressures are below zero but not yet surpassing air-entry ($0 < dH/dz_a < 1$).
- Losing-disconnected: when the baseline no-growth case reaches a maximum flux, is insensitive to changes in the total head gradient, and shows localized UG conditions (measured between the base of the clogging layer and the groundwater level represented by a pressure head = 0 m). Losing-disconnected cases experience connected conditions first, transition, and finally disconnection ($dH/dz_a \rightarrow 1$).

From each 160-day simulation representing five months of summer conditions when bioclogging is most relevant, we extracted the following variables of interest: peak flux, daily clogging layer conductivities ($K_{sc,new}$), daily unsaturated aquifer conductivities at a point below the clogging layer (K_{ua}), the updated clogging layer saturated thickness ($h_{c,new}$) with pressure head $\geq$ 0m, and dH/dz_a from the base of the clogging layer to the water table. We chose this measurement strategy for dH/dz_a for two reasons: (1) measuring the hydraulic gradient in the unsaturated zone between the base of the clogging layer and the top of the capillary zone, for example, can show localized UG conditions well before maximum flux is reached, and (2) the total head gradient is not uniform throughout the one-dimensional domain. An elongated capillary zone has a total head gradient much smaller than that in the unsaturated zone where UG conditions are found. Combined with conductivities below air-entry, the capillary zone has the potential to be the flux-limiting zone. Our method provides a depth-integrated assessment of dH/dz_a values at the time of peak flux without assuming UG conditions *a priori*.

Effective Disconnection and Peak Flux

Disconnection and UG conditions may not always coincide with maximum seepage. Maximum infiltration has been shown to sometimes occur in the transition period leading up to

full disconnection [*Brunner et al.*, 2009a; *Rivire et al.*, 2014]. We chose peak flux as the key variable of interest, because it represents the point at which the system transitions from flow defined by the time-dependency of the hydraulic gradient to flow defined by the time-dependency of hydraulic conductivity, as pointed out previously by *Rivire et al.* [2014]. We propose the term effective disconnection, hereafter D-$_{\mathrm{Eff}}$, to define these conditions occurring at peak flux, and to guide our interpretation of peak flux relative to the measurement of $\mathrm{dH/dz_a}$. Effective disconnection is not characterized by the existence of UG conditions, but by the occurrence of peak flow. Additionally, we do not assume *a priori* that max flux may only occur for $\mathrm{dH/dz_a}$ values of 1; therefore, D-$_{\mathrm{Eff}}$ helps to define the occurrence of max fluxes at many values of $\mathrm{dH/dz_a}$ that occur during non-UG flow conditions. This implies that UG conditions are only required as an indicator of disconnection in the absence of biomass growth. Since we also measure changes in $\mathrm{h_{c,new}}$ over time, we explore how the criterion in Equation 2.9 evolves from a static criterion to a dynamic one relative to changes in $\mathrm{K_{sc}}$ as the system desaturates.

Limitations to the One-dimensional Approach

The one-dimensional modeling approach presents conceptual limitations to our river-aquifer flow system. A one-dimensional approach cannot capture complex spatial variability from river geometry or a two-dimensional groundwater mound. Larger scale features may govern flow paths and lead to situations where the river is connected in some areas (thalweg), and disconnected in others (bank), leading to preferential flow paths. A two-dimensional or three-dimensional model would be needed for these joint, spatio-temporal processes. Given that the flow direction is predominantly vertical, and since bioclogging can occur in many locations with a high nutrient flux, the overall trend of disconnection and bioclogging experienced by a point on the bank may be similar to other points in the near vicinity along the bank, or in other predominantly losing rivers. Additionally, our model does not account for other processes that would be required to replicate spatial and temporal variability of infiltration at all sites at daily timescales within the river, such as sediment deposition events, erosion/scour, mechanical clogging by the algal mat, transient river flow regimes, as well as temperature effects that influence water viscosity and biological growth rates. While our approach is not able to simulate total flow volumes to the RBF wells and joint spatial-temporal variability, it is sufficient to demonstrate our hypothesis along a vertical flow path at monthly to seasonal timescales.

2.4 Results

Biological Effects on Seepage

Seepage curves from the one-dimensional synthetic case study are shown across a range of water decline rates, considering conditions of a losing-connected river (Figure 2.4a on page 39), a losing-transitional river (Figure 2.4b on page 39), and a losing-disconnected river (Figure 2.4c,d on page 39), all coupled with permeability dynamics from biomass (represented as $K_{sc,new}$ values in the modeling framework). The models illustrate that seepage follows the characteristic disconnection curve sequence (top solid green line for growth rate = 0, no-growth baseline case), and represents the synthetic case where no biomass grows and full disconnection is reached (Figure 2.4c,d on page 39). In all cases with biomass growth, seepage deviates substantially from the no-growth baseline scenario, and flux values never reach the same magnitude as the no-biomass-growth case. Figure 2.4 on page 39 shows infiltration for both the Biofilm and Colonies models. Since results do not significantly vary between constitutive models, we only present results for the Colonies model in subsequent figures.

Peak fluxes depend on whether the river is losing-connected, losing-transitional, or losing-disconnected. For cases with slow water table drops (representing weak losing-connected conditions from slow pumping in Figure 2.4a on page 39), peak fluxes only exist at or near the beginning of the simulation. In the case of the highest biomass growth rate (GR) (0.04 day^{-1}), and the slowest water table drop (Figure 2.4a, grey curve), flux goes into decline and never reaches a peak. Losing-disconnected cases occur with the fastest water table drops (highest pumping, Figure 2.4c, Figure 2.4d). As permeability declines (and biomass grows) simultaneously with lowering water tables, seepage does not immediately decline, but continues to increase. Seepage increases during the connected stage (where $dH/dz_a \ll 1$, but rising fast), and continues to increase until peak flux and D_{Eff} is reached. Peak fluxes (black solid dots in all figures) are higher, occur earlier on in the fast water table decline cases, and show that water tables can drop a greater distance vertically before reaching peak flux compared to the losing-connected and losing-transitional cases. Even with the presence of biomass growth, seepage increases in strongly-losing rivers as a consequence of increasing total head gradients from the water table drop and from the decline in the pressure head at the base of the clogging layer.

Infiltration fluxes are compared as a function of the water table drop in Figure 2.5 for a range of water table decline rates for the moderate GR of 0.02 day^{-1}, and an aquifer conductivity value of 100 m day^{-1}. Slow water table drops represent cases that are classified as losing-connected, because under no-biomass-growth scenarios they never produce an unsaturated zone. A river that is weakly losing, and remains losing-connected for the entirety of the simulation (Figure 2.5, green curves), will only show maximum seepage at the onset of the

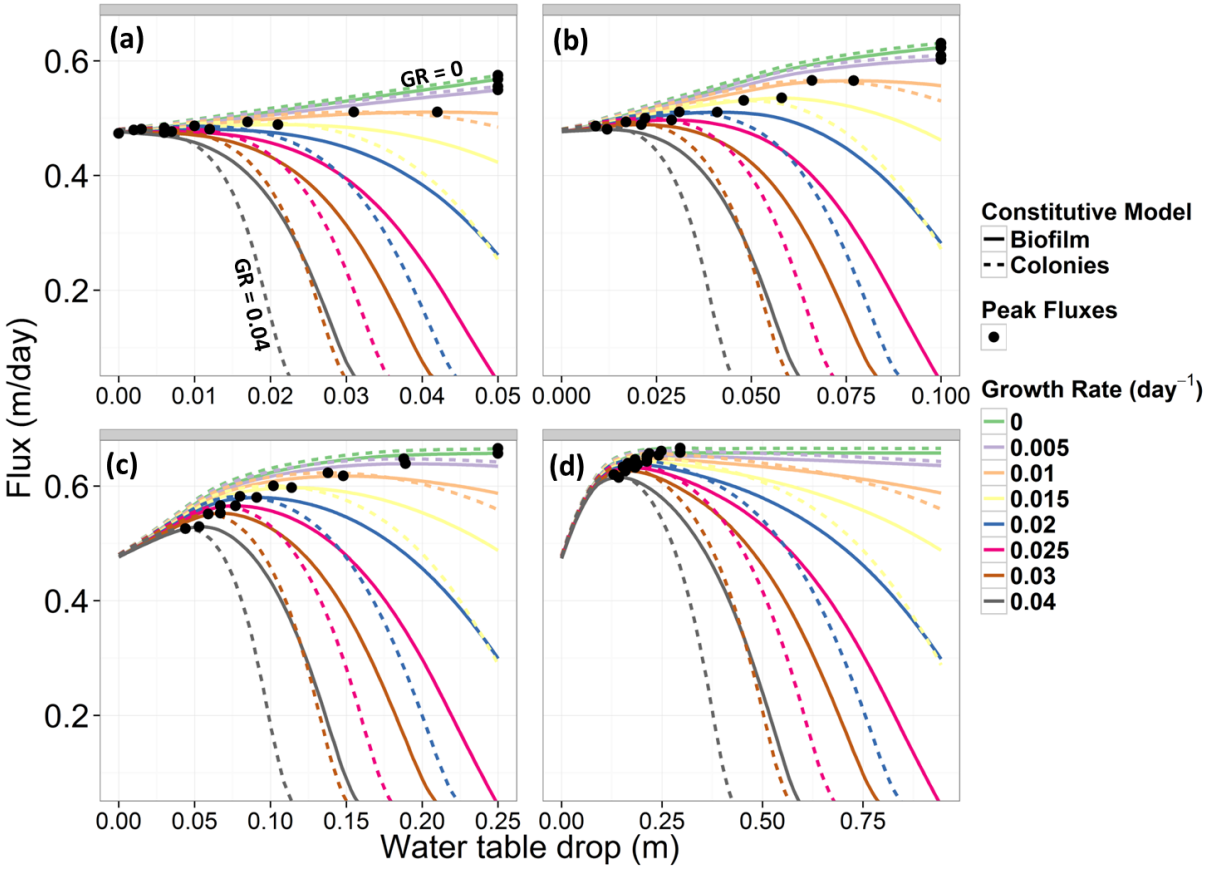

Figure 2.4: Seepage curves are shown as a function of the water table drop for a range of biomass growth rates (GR) and a range of water table decline rates. (a) Losing-connected: 0.0313 cm day^{-1}. (b) Losing transitional: 0.0625 cm day^{-1}. (c) Losing-disconnected: 0.1563 cm day^{-1}. (d) Losing-disconnected: 0.5900 cm day^{-1}. The amount of time represented is the same for each simulation (160 days). Note the different scales for the x-axis, which represent overall differences in the total water table drop over the 160-day simulation. The continuum of GR is the same for all panels. For interpretation of the color in all figure legends, the reader is referred to the web version of this article.

simulation if biomass grows fast and the gradient is not sufficient to pull flow. Peak flux is rarely achieved in losing-connected cases, because higher rates of water table drop are needed to overcome and outpace conductivity declines such that infiltration can be maintained or increased. Compared with a losing-disconnected river (Figure 2.5, yellow curve), the fast water table drop can help keep infiltration rates high at the beginning when biomass has

not yet reached a volume sufficient for fully clogging the pore-space. Modeled fluxes follow a similar trend to those measured in the field, providing assurance that the two hypothesized processes are well represented (Figure 2.2, red line).

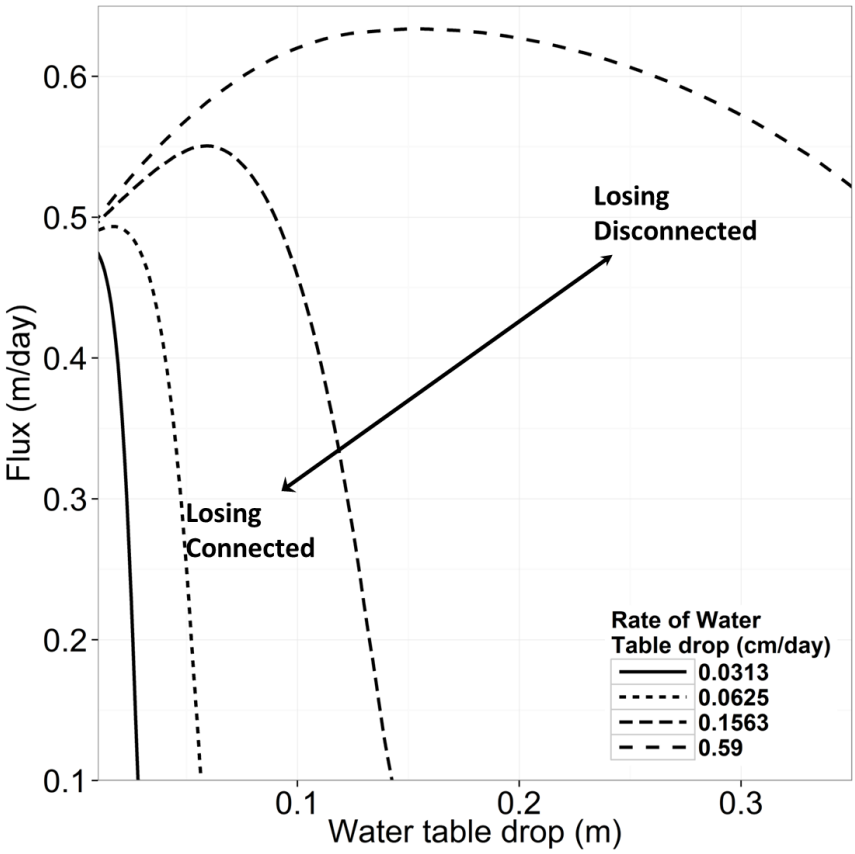

Figure 2.5: Infiltration fluxes with the Colonies model are shown as a function of the water table drop for a range of water table decline rates, for the moderate growth rate of 0.02 day^{-1}, and an aquifer conductivity value of 100 m day^{-1}. Slow water table drops represent cases that are losing-connected; fast water table drops represent losing-disconnected cases.

Biological Effects on Pressure Head Profiles

Pressure head profile snapshots with depth under losing-connected and losing-disconnected conditions are shown in Figure 2.6 for day 90 (mid-way through the summer; Figure 2.6a, c), and the day of peak flux (day of peak flux varies by simulation; Figure 2.6b, d). Peak

flux is typically reached midway through each simulation (between day 20 and 50). Unsaturated zone conditions present at the time of peak flux vary across the simulations. When comparing snapshots for the day of peak flux (Figure 2.6b, d), peak flux occurs without the presence of an unsaturated zone for the losing-connected case (Figure 2.6b), in contrast to the losing-disconnected case (Figure 2.6d), which shows peak flux occurring with the downward shift of the capillary zone. In the losing-disconnected case (Figure 2.6d) for a GR = 0, the zone where unit-gradient (UG) conditions are found and the zone where non-UG conditions are found is highlighted and demonstrate that our measurement strategy for dH/dz_a captures the linear and non-linear conditions for dH/dz_a. While peak fluxes for biomass GR = 0 may coincide with localized UG conditions, depth-integrated dH/dz_a is not 1. Furthermore, for larger biomass GR, peak flux actually occurs with smaller capillary zones and non-UG conditions in the majority of the vertical domain.

For both cases of losing-connected and losing-disconnected rivers, peak flows are achieved when both pressure reduction from biomass growth (Figure 2.6c, d) and the rate of change of the hydraulic gradient are not enough to outpace the rate of change of conductivity. These two simultaneous and opposing processes dominate infiltration at different times, and only when the magnitude of one (clogging) outpaces the other (increases in gradient), does peak flux occur which we define as the point of effective disconnection, D_{Eff} . In all scenarios, peak flux occurs when D_{Eff} is reached with $dH/dz_a < 1$.

When comparing unsaturated zone conditions on the same day (Day 90; Figure 2.6a, c), it is clear that biomass growth affects unsaturated zone conditions by reducing (more negative) the pressure at the bottom of the clogging layer, and extending the length of the capillary zone in the aquifer and clogging layer (Figure 2.6c). For the losing-disconnected case (2.6c), higher rates of biomass growth show noticeable drops in pressure beneath the clogging layer, leading to longer and more tension-dominated capillary zones compared with low biomass growth rates and losing-connected conditions. UG conditions above the capillary zone are visible in Day 90 for all GR. Yet dH/dz_a conditions vary because of capillary zone length (Figure 2.6c). The inverted water table is also noticeable in these simulations leading to a smaller extent of saturation ($h_{c,new}$) within the clogging layer.

Figure 2.7 shows pressure heads measured at the base of the clogging layer (elevation = 0.9 m), conductivity as a function of bioclogging, and total head gradients (dH/dz_a) measured between the base of the clogging layer and the water table represented by a pressure head equal to 0 m. The point in time at which peak flux occurs is shown by the black dots (same peak fluxes from Figure 2.4), and represents D_{Eff}. As dH/dz_a increases, the pressure head approaches a minimum (Figure 2.7a). Large biomass GR shift dH/dz_a towards smaller values of the water table drop at the time of D_{Eff} , and hence hasten the onset of D_{Eff} (Figure 2.7c). This is consistent with Figure 2.6d, where the length of the unsaturated zone is smaller at the onset of D_{Eff} for higher biomass GR. Take note of the green curve in Figure 2.7c, which is the case with no biomass growth. For this case, peak flux occurs when

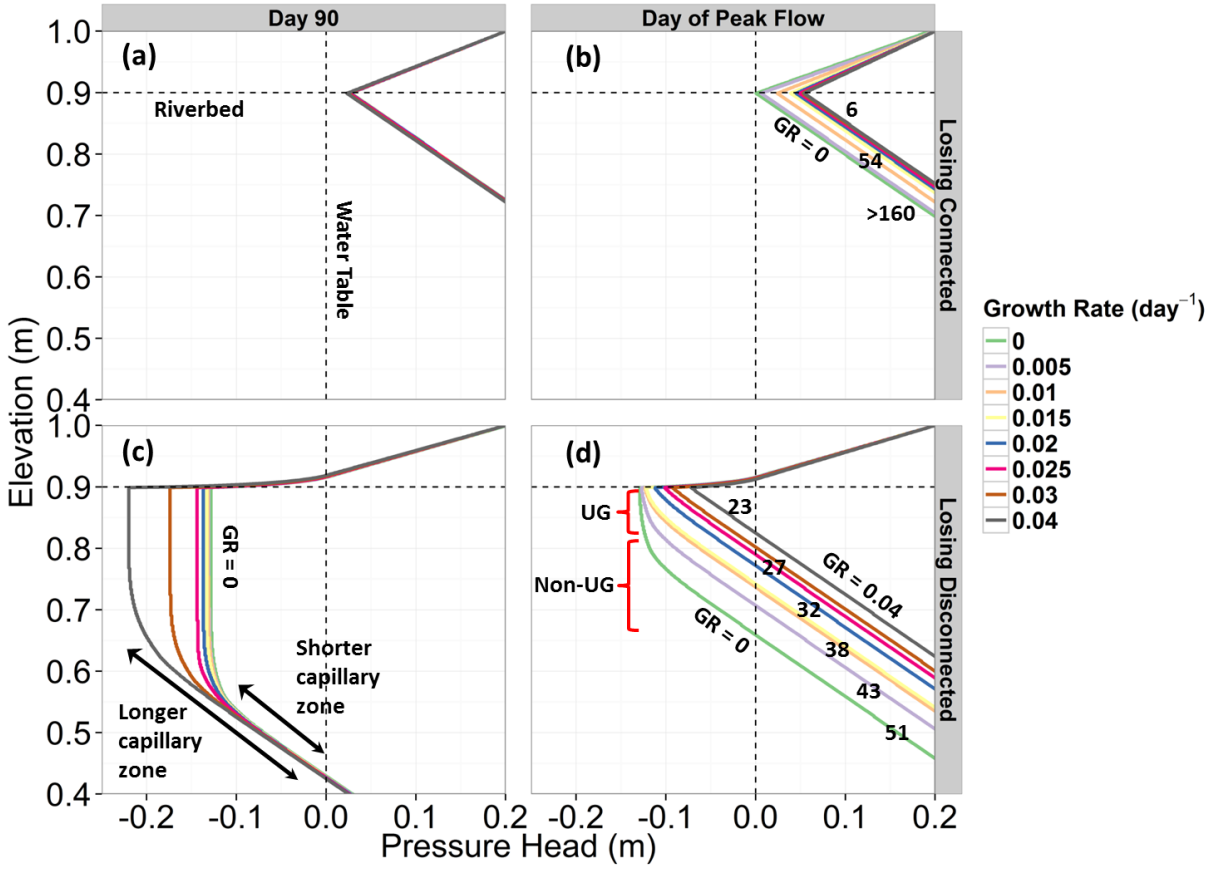

Figure 2.6: Pressure head profiles with depth for losing-connected and losing-disconnected conditions. Different snapshots in time are shown representing day 90 (mid-way through the summer; (a) and (c)), and snapshots on the day of the simulation when peak flux occurred ((b) and (d)). A few time stamps for peak fluxes are shown on top of each line. For the losing-disconnected case, on day 90 the water table is found at 0.42 m elevation, which represents a total water table drop of 0.53 m from the starting position of 0.95 m. Unit-gradient (UG) and non-UG zones are pointed out for GR = 0.

dH/dz_a 0.5. Our measurement strategy that follows the water table was chosen to account for the effects of the transition phase and the lengthened capillary zone (Figure 2.6c). If the measurement of dH/dz_a was taken at two static points, one at the base of the clogging layer and another at a point 10 cm below the clogging layer, dH/dz_a would be 1 much earlier. However, this would overlook the effects of a growing capillary zone on flow through the entire 1 m domain (See Figure 2.6d for the localized zone of UG conditions at peak flux for

the GR=0 case only).

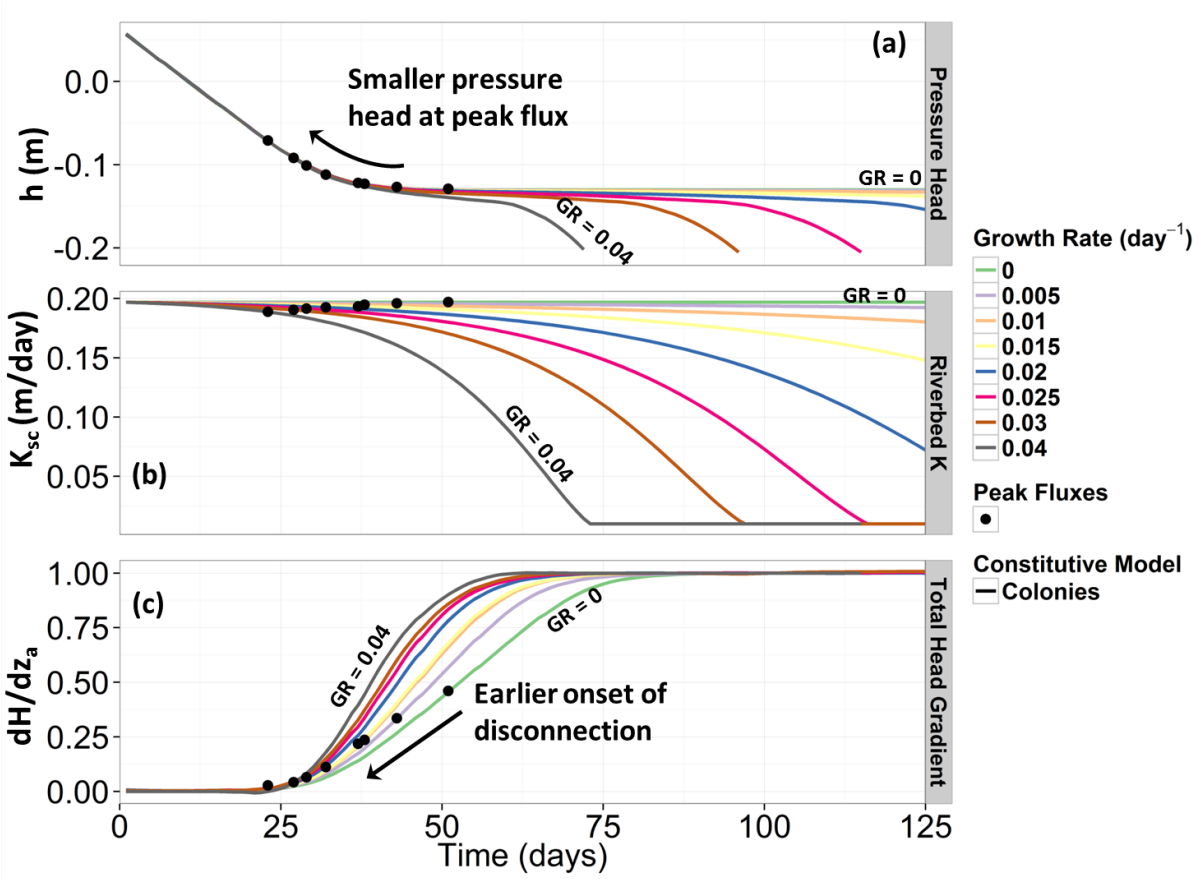

Figure 2.7: (a) Pressure heads measured at the base of the clogging layer. (b) Conductivity declines in the riverbed layer from bioclogging. (c) dH/dz_a shown as functions of time for different values of the biomass growth rate and the Colonies model. As the total head gradient increases, the pressure head approaches a minimum. The point in time at which peak flux occurs is shown by the black dots.

An Effective Disconnection Criterion

Using the extracted variables of interest during peak flux ($K_{sc,new}$, K_{ua}, dH/dz_a,$h_{c,new}$, with peak flux represented as the dots in Figure 2.4), we deduce two different states of the system depending on the biomass GR. A visualization of these two states is shown in Figure 2.8. We plotted the ratio of the updated conductivities ($K_{sc,new}$ / K_{ua}) against dH/dz_a, and

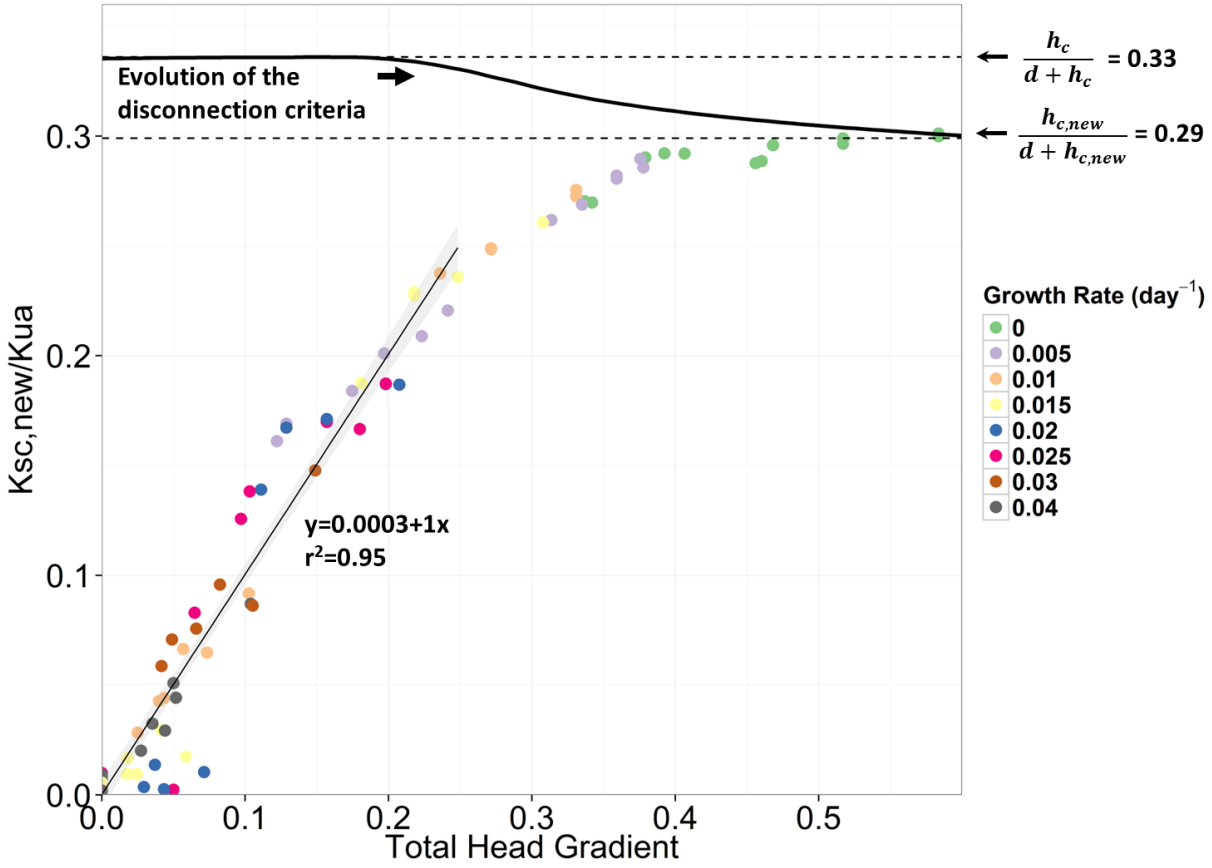

Figure 2.8: Ratio $K_{sc,new}$ / K_{ua} plotted against dH/dz_a across the range of biomass growth rates, and rates of water table drop, measured at the time of peak flux. The dashed lines in Figure 2.8 represent the bounds of the disconnection criterion (Equation 2.9). The solid black line is the evolution of the criterion as the water table declines and an inverted water table forms in the clogging layer beginning at 0.33 and evolving to 0.29. The bounds represents cases with low biomass growth rates, and shows the asymptote of $K_{sc,new}$ / K_{ua} as it approaches the updated disconnection criterion. The linear model represents cases with fast biomass growth rates, and shows the linear one-to-one relation between $K_{sc,new}$ / K_{ua} and dH/dz_a at the point of peak flux. Green dots show the baseline no-growth case. The green dots should be overlapping, and exactly equal. However, in many scenarios the simulation finished before full disconnection was reached (for example, in the losing-connected cases), and thus shows lower total head gradient for the peak, marking the end of the simulation.

the disconnection criterion from Equation 2.9 against dH/dz_a. For large rates of biomass growth (Figure 2.4, linear model), peak flux occurs when:

$$\frac{K_{sc,new}}{K_{ua}} = \frac{dH}{dz_a} \tag{2.10}$$

This criterion shown by the fitted model in Figure 2.8 defines the point when effective disconnection occurs and displays a significant modification to the static disconnection criteria defined in Equation 2.9. For small rates of biomass growth, peak flux occurs at larger values of dH/dz_a (Figure 2.8, asymptote) coincident with larger capillary zones and an inverted water table in the clogging layer (represented by changes in $h_{c,new}$). In the cases where no biomass grows, peak flux occurs when $K_{sc,new}$ / K_{ua} reaches the inflection point of the dH/dz_acurve (Figure 2.8b). Specifically, peak flux for low/no biomass growth cases approximates a dynamic disconnection criterion:

$$\frac{K_{sc,new}}{K_{ua}} = \frac{h_{c,new}}{d + h_{c,new}} \tag{2.11}$$

The two states shown in Figure 2.8 represent a distinction between cases when D_{Eff} occurs before the unsaturated zone and inverted water table develop (high rates of biomass growthfast permeability declines), and cases after these features develop (low rates of biomass growthslow permeability declines). In all cases, peak flux occurs at the point of D_{Eff} between fully connected and disconnected flow and when dH/dza < 1. As the GR approaches 0, the pressure profiles exhibit localized UG conditions and get closer to the dynamic criteria from Equation 2.9. Some of the points for GR=0 do not fall on the evolving criteria line because of very slow pumping rates reaching 160 days without significant unsaturated zone growth.

For large biomass GR, peak fluxes occur when $K_{sc,new}$ / K_{ua} is approximately dH/dz_a (Equation 2.10). Peak fluxes tend to occur earlier, typically while the system is still completely saturated (Figure 2.6b, d). In the high GR cases, the ratio $K_{sc,new}$ / K_{ua} diverges from the disconnection criterion because peak flux occurs with small values of dH/dz_a . In these cases the unsaturated zone and inverted water table are not fully developed, as the capillary zone is still in contact with the clogging layer. Large biomass growth rates change the ratio of $K_{sc,new}$ / K_{ua} faster than changes to dH/dz_a , because K_{ua} is still relatively large compared with $K_{sc,new}$. When these two ratios are equal, peak flux is reached.

For small biomass GR, peak flux does not occur until a capillary zone, an unsaturated zone, and an inverted water table are almost fully developed (Figure 2.8, Evolution of the disconnection criteria). In the cases where no biomass grows, as the unsaturated zone develops, peak flux occurs when $K_{sc,new}$ / K_{ua} converges to the updated, dynamic disconnection criterion (Equation 2.10). Biomass produces negligible pressure declines at the base of the clogging layer and $K_{sc,new}$does not decline fast enough, thus allowing dH/dz_a to be larger at the onset of peak flux.

2.5 Discussion

Bioclogging Effects on Seepage

The synthetic case study demonstrated that dynamic permeability and connection status must be accounted for to accurately simulate infiltration trends. Biomass growth reduced seepage by reducing the hydraulic conductivity; however the importance of this depends on whether the baseline case for the river is losing-connected or losing-disconnected, and the strength of losing conditions. For strongly losing rivers (Figure 2.4c, d), seepage continued to grow even while K_{sc} declined and showed peak flux once D_{Eff} was reached. It is during these early stages that field observations may show simultaneous seepage increases and hydraulic conductivity decreases, which can typically confound system interpretation and model development. Increasing the rate of the water table drop (such as through higher pumping rates) will result in greater infiltration rates, but consequently a larger unsaturated zone during peak seepage (Figure 2.6b, d), and quicker declines post-disconnection. In weak losing-connected reaches, where hydraulic gradients remain small (Figure 2.4a, Figure 2.5, Figure 2.6b), the pressure decline from biomass growth, as well as the limited dH/dz_a increases, is not large enough to overcome the conductivity decline, resulting only in seepage decreases. With no biomass growth, weak losing rivers are only able to show slight infiltration increases. Figure 2.9 shows a generalized schematic of the nature of these dual processes and the overall effects on infiltration.

In a river undergoing disconnection, this behavior indicates that infiltration is highly sensitive to riverbed permeability changes only after D_{Eff} is reached. For strongly losing rivers and high rates of biomass growth, D_{Eff} occurs much earlier than UG conditions (Figure 2.7b). In a river remaining connected, the behavior of the peak flux and the apparent insensitivity to water table declines while still fully saturated indicate that D_{Eff}occurs without the presence of an unsaturated zone. In the case of losing-connected rivers that experience clogging, that insensitivity occurs earlier than in losing-disconnected rivers. In terms of practical RBF management, increasing pumping early in the summer before conditions become favorable for biomass growth may lead to disconnection, and thus increased total production volumes compared to maintaining the river at losing-connected conditions. Such strategies could also be beneficial for optimizing other water management practices, such as bank storage and managed aquifer recharge.

Several processes that may influence infiltration were not considered in this study. In our simulations, we did not introduce feedback effects from declining infiltration and nutrient fluxes on biomass growth, because the goal of our simulations was only to test field observed biomass growth as a constraint on infiltration trends. When a river is undergoing disconnection, infiltration can change the nutrient flux entering the riverbed, which can potentially drive or inhibit biomass growth. Where pumping drives bioclogging through

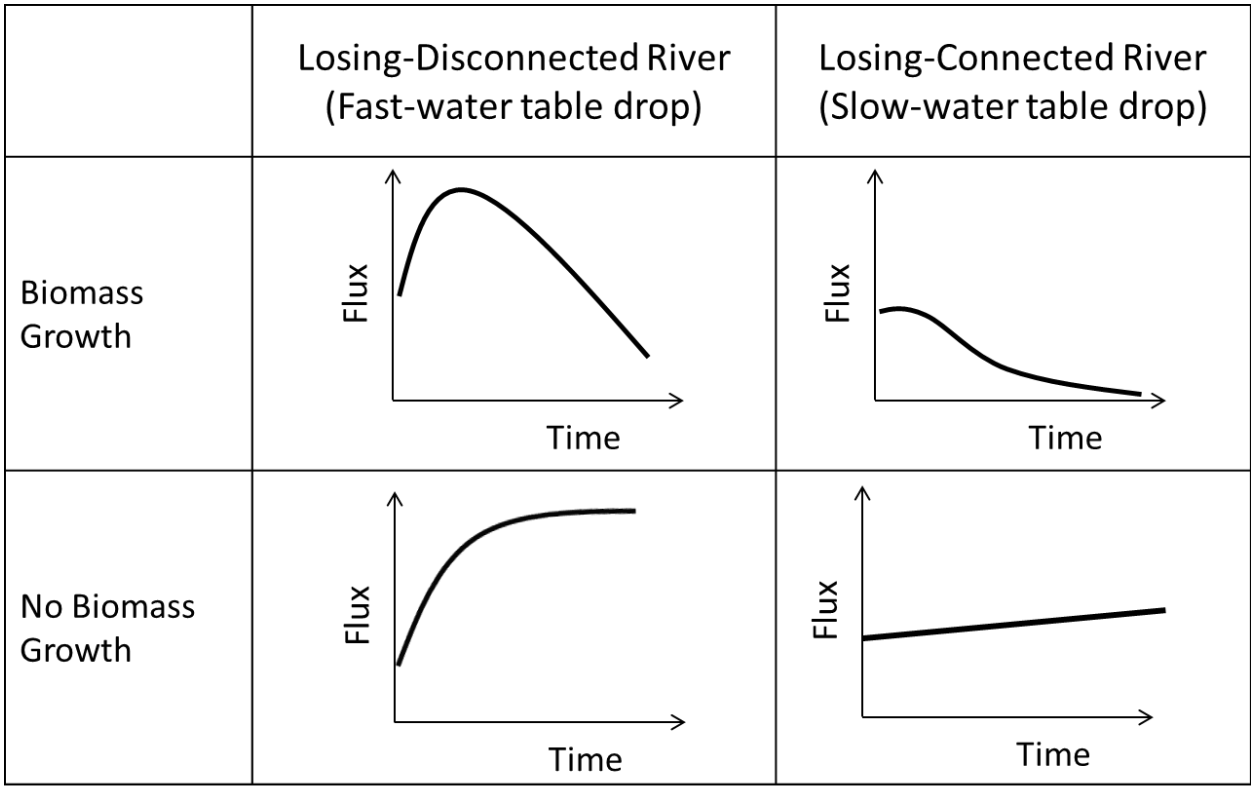

Figure 2.9: Generalized trends for infiltration in a losing river when experiencing biomass growth, as well as strong or weak losing conditions.

increased fluxes, feedback effects between clogging and pumping would need consideration. It is unknown how cycling pumping will change overall microbial growth. We also did not test the effects of water table fluctuations and/or effects of accelerating water table declines on infiltration. Other processes not considered here, but potentially relevant for site specific infiltration prediction at daily time scales, include: scouring and sediment disturbance events (which have been shown to increase infiltration by a factor of 7 [*Rosenberry et al.*, 2010], transient river flow boundaries, mechanical clogging from algal growth, grazer-algal food chain dynamics [*Power et al.*, 2008], preferential flow paths, river geometry, and parameter sensitivity to temperature. All of these processes might also contribute to the dynamics of the infiltration rates. However, our results show that even in the absence of these processes, seasonal changes of infiltration rates can be explained through observations of bioclogging and disconnection.

Importance of the Transition Phase

The transition phase represents the time where dH/dz_a is changing fast, and flow becomes dominated by conductivity declines. This phase was shown to occur differently based on biomass growth conditions. We found peak fluxes occurred during the transition phase precisely when reaching D_{Eff}.

When there is a permeability and porosity reduction from biomass growth, physically the pore space is reduced, and pressure head values decline (become more negative) (Figure 2.6c and 2.7a). The drop in the pore space pressure at the clogging layer-aquifer interface increases the hydraulic gradient while simultaneously reducing K_{ua}. These processes act in opposition until the D_{Eff}, when peak flux occurs, at which time the conductivity drops become the dominating process. For fast biomass growth rates, the resulting $K_{sc,new}$ / K_{ua} ratio occurs when total head gradients are $\ll 1$ and biomass growth works to hasten the onset of D_{Eff}(Figure 2.7b).

In the literature, full disconnection is approximated as either $dH/dz_a \cong 1$, or when total head gradients no longer affect the infiltration rate [*Brunner et al.*, 2011]. In this work we measured dH/dz_a between a point directly below the clogging layer and the water table. Using this depth-integrated approach, we found that effective disconnection occurred for the no-biomass growth case when $dH/dz_a \cong 0.5$, which is the inflection point of the dH/dz_a curve, and during the transition phase (Figure 2.7c, green curve). This is in line with previous interpretations of peak flux representing a shift from changes in flow dominated by gradient to changes in flow dominated by conductivity declines [*Rivire et al.*, 2014]. With biomass growth, this point of effective disconnection occurs much earlier in time (Figure 2.7c), and precisely occurs at the time when head changes become negligible compared to conductivity changes (Figure 2.7).

The transition phase is important because it pinpoints the time when water managers should monitor water tables and pumping to account for bioclogging impacts. After the transition phase, any increase in pumping will have negligible effects on infiltration from the river. In most cases, the portion of water infiltrated by the additional pumping will increasingly draw from the alluvial aquifer, or additional sections of the river such as the thalweg undergoing disconnection from the larger radial extent of the cone of depression. Only when water tables are already low will the impact of biomass and disconnection negatively affect pumping.

Predicting Peak Flux from Effective Disconnection

In all cases of biomass growth, simulated flux does not begin to decline until D_{Eff} is reached. In the losing-connected case, D_{Eff} occurs without the existence of an unsaturated zone (below air-entry). In some of the losing-connected cases, flux increases due to gains

in the hydraulic gradient. However, the flow becomes effectively disconnected, in the sense that water tables declines can no longer drive flow. In fact, even in the fully connected cases where no unsaturated zone develops, permeability declines are much more dominant in determining the magnitude of flux, because they are orders of magnitude greater than water table declines. In all simulations, peak fluxes and D_{Eff} are occurring before $dH/dz_a = 1$. This result is in agreement with *Brunner et al.* [2010] and *Rivire et al.* [2014], who showed peak fluxes occurred during the transition phase rather than during disconnection. Our follow the water table measurement strategy for dH/dz_a shows that D_{Eff} occurs for two different states of the system, depending on whether biomass GR are large or small relative to water table drop rates. D_{Eff} can be used to predict when peak fluxes occur given measurements of subsurface conditions of dH/dz_a. Since pressure conditions below the riverbed are mostly unknown and without direct measurements, water managers may find it beneficial to install piezometers directly below the riverbed to monitor the extent of disconnection, and decide to bank more water as subsurface storage before infiltration rates decline.

2.6 Summary and Conclusions

In this study, we systematically investigated (1) how permeability dynamics induced through bioclogging affect the exchange of flows between a river and its underlying aquifer as a function of the connection status of the river, (2) established a D_{Eff} criterion for predicting when peak fluxes occur relative to pressure head and total head gradient conditions in the subsurface, and (3) developed simple numerical capabilities that permit exploration and predictive understanding of coupled field-scale processes. We tested the net effect of two opposing phenomena: (1) the drop of water table leading to increased fluxes, and (2) bioclogging leading to decreased fluxes. For each case, we considered different rates of changes, and examined how net fluxes depend on combinations of the differing rates of change, and on the existence and timing of peak flux.

Our study highlights that consideration of riverbed dynamic permeability coupled with the connection status of the river is required for accurate prediction of infiltration dynamics. We found that bioclogging ultimately controls the magnitude of the infiltration flux. However, the process of disconnection relative to permeability changes governs the timing of peak flux (Figure 2.7) and unsaturated zone growth (Figure 2.6). Characteristic seepage curves of coupled biomass growth, combined with scenarios of losing-connected and losing-disconnected rivers, highlight a dynamic, dual influence on infiltration (Figure 2.9).

Our research provides an explanation of the processes occurring in natural rivers that can explain field measurements that show simultaneous permeability declines and seepage increases. Diverging trends in temporally dynamic permeability and seepage can indicate a river is undergoing disconnection simultaneously with biomass growth, and this research

explains the nature of their dual influence. In this work we also explored the criteria for D_{Eff} as a predictor of peak fluxes, which always occurred during the transition phase when head changes became negligible compared to conductivity changes. Our work presents the idea of effective disconnection to account for unsaturated zone growth and dynamic permeability.

Better understanding the mechanisms controlling riverbed clogging and its impacts on groundwater-surface water interactions can provide quantitative protocols for managing pumping. These prediction methods can also inform assessments of biological factors in managing RBF systems. Future work needs to incorporate streambed morphology and texture, feedbacks between infiltration and bioclogging which can limit and enhance biological growth, and nutrient limitations on growth, and account for infiltration differences in gaining and losing rivers showing various degrees of dynamic permeability. At even larger scales (e.g., catchment-scales), it is not yet understood how biomass growth in the entire river corridor may affect regional water balances, hyporheic flows, and river discharge, especially in drought-prone climates. Recognition of the feedbacks of bioclogging at different geomorphological and hydrological scales can lead to better estimates of local water volumes and pumping capacities, especially when these systems are used as municipal and public water supply sources.

2.7 Acknowledgments

This research was supported by the Jane Lewis Fellowship from the University of California, Berkeley, the Sonoma County Water Agency (SCWA), the Roy G. Post Foundation Scholarship, the U.S. Department of Energy, Office of Science, Office of Biological and Environmental Research under Award Number DE-AC02-05CH11231, and the UFZ-Helmholtz Centre for Environmental Research, Leipzig, Germany. We thank Marcus Trotta, Donald Seymour, John Mendoza, and Jay Jasperse of SCWA for their useful suggestions. We would also like to acknowledge the efforts of Markus Neubauer, Gerrit Laube, Falk Heβe, Changhong Wang, Brad Harken, Heather Savoy, Karina Cucchi, and Jon Sege for their helpful comments and ideas. Supplementary data can be found in the online version of this article.

Bibliography

Alarcon, V. J., D. Johnson, W. H. McAnally, J. v. d. Zwaag, D. Irby, and J. Cartwright (2014), Nested Hydrodynamic Modeling of a Coastal River Applying Dynamic-Coupling, *Water Resources Management*, *28*(10), 3227–3240, doi:10.1007/s11269-014-0671-6.

Annan, J. D. (2001), Modelling under uncertainty: Monte Carlo methods for temporally varying parameters, *Ecological Modelling*, *136*(23), 297–302, doi:10.1016/S0304-3800(00)00413-0.

Barahona-Palomo, M., M. Riva, X. Sanchez-Vila, E. Vazquez-Sune, and A. Guadagnini (2011), Quantitative comparison of impeller-flowmeter and particle-size-distribution techniques for the characterization of hydraulic conductivity variability, *Hydrogeology Journal*, *19*(3), 603–612, doi:10.1007/s10040-011-0706-5.

Battin, T., and D. Sengschmitt (1999), Linking Sediment Biofilms, Hydrodynamics, and River Bed Clogging: Evidence from a Large River, *Microbial Ecology*, *37*(3), 185–196, doi:10.1007/s002489900142.

Baveye, P., P. Vandevivere, B. L. Hoyle, P. C. DeLeo, and D. S. de Lozada (1998), Environmental Impact and Mechanisms of the Biological Clogging of Saturated Soils and Aquifer Materials, *Critical Reviews in Environmental Science and Technology*, *28*(2), 123–191, doi:10.1080/10643389891254197.

Blaschke, A. P., K.-H. Steiner, R. Schmalfuss, D. Gutknecht, and D. Sengschmitt (2003), Clogging Processes in Hyporheic Interstices of an Impounded River, the Danube at Vienna, Austria, *International Review of Hydrobiology*, *88*(3-4), 397–413, doi:10.1002/iroh.200390034.

Brovelli, A., F. Malaguerra, and D. Barry (2009), Bioclogging in porous media: Model development and sensitivity to initial conditions, *Environmental Modelling & Software*, *24*(5), 611–626, doi:10.1016/j.envsoft.2008.10.001.

Brown, K., and A. Wherrett (2014), Fact Sheets Bulk Density-Measurement.

Brun, A., and P. Engesgaard (2002), Modelling of transport and biogeochemical processes in pollution plumes: literature review and model development, *Journal of Hydrology*, *256*(3-4), 211–227, doi:10.1016/S0022-1694(01)00547-9.

Brunner, P., P. G. Cook, and C. T. Simmons (2009a), Hydrogeologic controls on disconnection between surface water and groundwater, *Water Resources Research*, *45*(1), 1–13, doi:10.1029/2008WR006953.

Brunner, P., C. T. Simmons, and P. G. Cook (2009b), Spatial and temporal aspects of the transition from connection to disconnection between rivers, lakes and groundwater, *Journal of Hydrology*, *376*(12), 159–169, doi:10.1016/j.jhydrol.2009.07.023.

Brunner, P., C. T. Simmons, P. G. Cook, and R. Therrien (2010), Modeling Surface Water-Groundwater Interaction with MODFLOW: Some Considerations, *Ground Water*, *48*(2), 174–180, doi:10.1111/j.1745-6584.2009.00644.x.

Brunner, P., P. G. Cook, and C. T. Simmons (2011), Disconnected Surface Water and Groundwater: From Theory to Practice, *Ground Water*, *49*(4), 460–467, doi:10.1111/j.1745-6584.2010.00752.x.

Coughlan, K., H. Cresswell, and N. McKenzie (2002), *Soil Physical Measurement and Interpretation for Land Evaluation*, no. Australian Soil and Land Survey Handbooks Series 5 in CSIRO Land and Water, CSIRO Publishing.

Crosbie, R. S., A. R. Taylor, A. C. Davis, S. Lamontagne, and T. Munday (2014), Evaluation of infiltration from losing-disconnected rivers using a geophysical characterisation of the riverbed and a simplified infiltration model, *Journal of Hydrology*, *508*, 102–113, doi:10.1016/j.jhydrol.2013.07.045.

Dillon, P. J., and J. A. Liggett (1983), An ephemeral stream-aquifer interaction model, *Water Resources Research*, *19*(3), 621–626, doi:10.1029/WR019i003p00621.

Doppler, T., H.-J. H. Franssen, H.-P. Kaiser, U. Kuhlman, and F. Stauffer (2007), Field evidence of a dynamic leakage coefficient for modelling riveraquifer interactions, *Journal of Hydrology*, *347*(12), 177–187, doi:10.1016/j.jhydrol.2007.09.017.

Dupin, H. J., P. K. Kitanidis, and P. L. McCarty (2001), Pore-scale modeling of biological clogging due to aggregate expansion: A material mechanics approach, *Water Resources Research*, *37*(12), 2965–2979, doi:10.1029/2001WR000306.

Engeler, I., H. Hendricks Franssen, R. Mller, and F. Stauffer (2011), The importance of coupled modelling of variably saturated groundwater flow-heat transport for assessing

riveraquifer interactions, *Journal of Hydrology*, *397*(34), 295–305, doi:10.1016/j.jhydrol.2010.12.007.

Ezeuko, C., A. Sen, A. Grigoryan, and I. Gates (2011), Pore-network modeling of biofilm evolution in porous media, *Biotechnology and Bioengineering*, *108*(10), 2413–2423, doi:10.1002/bit.23183.

Flipo, N., A. Mouhri, B. Labarthe, and S. Biancamaria (2014), Continental hydrosystem modelling: the concept of nested streamaquifer interfaces, *Hydrology and Earth System Sciences Discussions*, *11*(1), 451–500, doi:10.5194/hessd-11-451-2014.

Fox, G. A., and D. S. Durnford (2003), Unsaturated hyporheic zone flow in stream/aquifer conjunctive systems, *Advances in Water Resources*, *26*(9), 989–1000, doi:10.1016/S0309-1708(03)00087-3.

Genereux, D. P., S. Leahy, H. Mitasova, C. D. Kennedy, and D. R. Corbett (2008), Spatial and temporal variability of streambed hydraulic conductivity in West Bear Creek, North Carolina, USA, *Journal of Hydrology*, *358*(34), 332–353, doi:10.1016/j.jhydrol.2008.06.017.

Gupta, R. P., and D. Swartzendruber (1962), Flow-Associated Reduction in the Hydraulic Conductivity of Quartz Sand, *Soil Science Society of America Journal*, *26*(1), 6, doi:10.2136/sssaj1962.03615995002600010003x.

Harding Lawson Associates (1988), Hydrogeologic Investigation Wohler Aquifer Study. Sonoma County, California, *Tech. Rep. HLA Job No. 1916,005.02*, Sonoma County, CA.

Harvey, J., and M. Gooseff (2015), River corridor science: Hydrologic exchange and ecological consequences from bedforms to basins, *Water Resources Research*, *51*(9), 6893–6922, doi:10.1002/2015WR017617.

Hatch, C. E., A. T. Fisher, C. R. Ruehl, and G. Stemler (2010), Spatial and temporal variations in streambed hydraulic conductivity quantified with time-series thermal methods, *Journal of Hydrology*, *389*(34), 276–288, doi:10.1016/j.jhydrol.2010.05.046.

Jaramillo, M. (2012), Riverbank Filtration: An Efficient and Economical Drinking-Water Treatment Technology, *DYNA*, *79*(171), 148–157.

Kildsgaard, J., and P. Engesgaard (2001), Numerical analysis of biological clogging in two-dimensional sand box experiments, *Journal of Contaminant Hydrology*, *50*(3-4), 261–285, doi:10.1016/S0169-7722(01)00109-7.

Kim, D.-S., S. Thomas, and H. S. Fogler (2000), Effects of pH and Trace Minerals on Long-Term Starvation of Leuconostoc mesenteroides, *Applied and Environmental Microbiology*, *66*(3), 976–981, doi:10.1128/AEM.66.3.976-981.2000.

Kurtz, W., H.-J. Hendricks Franssen, and H. Vereecken (2012), Identification of time-variant river bed properties with the ensemble Kalman filter, *Water Resources Research*, *48*(10), n/a–n/a, doi:10.1029/2011WR011743.

Lamontagne, S., A. Taylor, R. Crosbie, and P. G. Cook (2011), Interconnection of Surface and Groundwater Systems-River Losses from Losing/Disconnected Streams. Billabong Creek Site Report, in *Water for a Healthy Country Flagship Report series ISSN: 1835-095X*, p. 37, NSW Office of Water, Australia.

McCallum, A. M., M. S. Andersen, B. M. S. Giambastiani, B. F. J. Kelly, and R. Ian Acworth (2013), Riveraquifer interactions in a semi-arid environment stressed by groundwater abstraction, *Hydrological Processes*, *27*(7), 1072–1085, doi:10.1002/hyp.9229.

Molz, F. J., M. A. Widdowson, and L. D. Benefield (1986), Simulation of Microbial Growth Dynamics Coupled to Nutrient and Oxygen Transport in Porous Media, *Water Resources Research*, *22*(8), 1207–1216, doi:10.1029/WR022i008p01207.

Murphy, E. M., and T. R. Ginn (2000), Modeling microbial processes in porous media, *Hydrogeology Journal*, *8*(1), 142–158.

Newcomer, M. E., S. S. Hubbard, J. H. Fleckenstein, U. Maier, C. Schmidt, M. Thullner, C. Ulrich, N. Flipo, and Y. Rubin (2016), Simulating bioclogging effects on dynamic riverbed permeability and infiltration, *Water Resources Research*, pp. n/a–n/a, doi:10.1002/2015WR018351.

Or, D., S. Phutane, and A. Dechesne (2007), Extracellular Polymeric Substances Affecting Pore-Scale Hydrologic Conditions for Bacterial Activity in Unsaturated Soils, *Vadose Zone Journal*, *6*(2), 298–305, doi:10.2136/vzj2006.0080.

PC-Progress (2011), PC-PROGRESS - Homepage.

Peterson, D. M. (1989), Modeling the Effects of Variably Saturated Flow on Stream Losses, *Tech. rep.*, Harding Lawson Associates, Novato, CA.

Power, M. E., M. S. Parker, and W. E. Dietrich (2008), Seasonal reassembly of a river food web: floods, droughts, and impacts of fish, *Ecological Monographs*, *78*(2), 263–282, doi:10.1890/06-0902.1.

Rivire, A., J. Gonalvs, A. Jost, and M. Font (2014), Experimental and numerical assessment of transient streamaquifer exchange during disconnection, *Journal of Hydrology*, *517*, 574–583, doi:10.1016/j.jhydrol.2014.05.040.

Rockhold, M. L. (2002), Interactions between Microbial Dynamics and Transport Processes in Soils, Ph.D. thesis, Oregon State University, Oregon.

Rockhold, M. L., R. R. Yarwood, M. R. Niemet, P. J. Bottomley, and J. S. Selker (2005), Experimental Observations and Numerical Modeling of Coupled Microbial and Transport Processes in Variably Saturated Sand, *Vadose Zone Journal*, *4*(2), 407, doi:10.2136/vzj2004.0087.

Rosenberry, D. O., L. Toran, and J. E. Nyquist (2010), Effect of surficial disturbance on exchange between groundwater and surface water in nearshore margins, *Water Resources Research*, *46*(6), n/a–n/a, doi:10.1029/2009WR008755.

Rosenzweig, R., A. Furman, C. Dosoretz, and U. Shavit (2014), Modeling biofilm dynamics and hydraulic properties in variably saturated soils using a channel network model, *Water Resources Research*, *50*(7), 5678–5697, doi:10.1002/2013WR015211.

Sams, R., J. Garca, P. Molle, and N. Forquet (2016), Modelling bioclogging in variably saturated porous media and the interactions between surface/subsurface flows: Application to Constructed Wetlands, *Journal of Environmental Management*, *165*, 271–279, doi:10.1016/j.jenvman.2015.09.045.

Schaap, M. G., F. J. Leij, and M. T. van Genuchten (2001), Rosetta: A computer program for estimating soil hydraulic parameters with hierarchical pedotransfer functions, *Journal of Hydrology*, *251*(34), 163–176, doi:10.1016/S0022-1694(01)00466-8.

Seki, K., M. Thullner, J. Hanada, and T. Miyazaki (2006), Moderate Bioclogging Leading to Preferential Flow Paths in Biobarriers, *Ground Water Monitoring & Remediation*, *26*(3), 68–76, doi:10.1111/j.1745-6592.2006.00086.x.

Simunek, J., M. T. van Genuchten, and M. Sejna (2008), Development and Applications of the HYDRUS and STANMOD Software Packages and Related Codes, *Vadose Zone Journal*, *7*(2), 587–600, doi:10.2136/vzj2007.0077.

Soleimani, S., P. J. Van Geel, O. B. Isgor, and M. B. Mostafa (2009), Modeling of biological clogging in unsaturated porous media, *Journal of Contaminant Hydrology*, *106*(12), 39–50, doi:10.1016/j.jconhyd.2008.12.007.

Su, G. W., J. Jasperse, D. Seymour, J. Constantz, and Q. Zhou (2007), Analysis of pumping-induced unsaturated regions beneath a perennial river, *Water Resources Research*, *43*(8), doi:10.1029/2006WR005389.

Suchomel, B. J., B. M. Chen, and M. B. Allen III (1998), Network Model of Flow, Transport and Biofilm Effects in Porous Media, *Transport in Porous Media*, *30*(1), 1–23, doi:10.1023/A:1006560705680.

Tang, Y., A. J. Valocchi, and C. J. Werth (2015), A hybrid pore-scale and continuum-scale model for solute diffusion, reaction, and biofilm development in porous media, *Water Resources Research*, *51*(3), 1846–1859, doi:10.1002/2014WR016322.

Taylor, R. G., B. Scanlon, P. Dll, M. Rodell, R. van Beek, Y. Wada, L. Longuevergne, M. Leblanc, J. S. Famiglietti, M. Edmunds, L. Konikow, T. R. Green, J. Chen, M. Taniguchi, M. F. P. Bierkens, A. MacDonald, Y. Fan, R. M. Maxwell, Y. Yechieli, J. J. Gurdak, D. M. Allen, M. Shamsudduha, K. Hiscock, P. J.-F. Yeh, I. Holman, and H. Treidel (2013), Ground water and climate change, *Nature Climate Change*, *3*(4), 322–329, doi:10.1038/nclimate1744.

Thullner, M. (2010), Comparison of bioclogging effects in saturated porous media within one- and two-dimensional flow systems, *Ecological Engineering*, *36*(2), 176–196, doi:10.1016/j.ecoleng.2008.12.037.

Thullner, M., and P. Baveye (2008), Computational pore network modeling of the influence of biofilm permeability on bioclogging in porous media, *Biotechnology and Bioengineering*, *99*(6), 1337–1351, doi:10.1002/bit.21708.

Thullner, M., L. Mauclaire, M. H. Schroth, W. Kinzelbach, and J. Zeyer (2002a), Interaction between water flow and spatial distribution of microbial growth in a two-dimensional flow field in saturated porous media, *Journal of Contaminant Hydrology*, *58*(34), 169–189, doi:10.1016/S0169-7722(02)00033-5.

Thullner, M., J. Zeyer, and W. Kinzelbach (2002b), Influence of Microbial Growth on Hydraulic Properties of Pore Networks, *Transport in Porous Media*, *49*(1), 99–122, doi:10.1023/A:1016030112089.

Thullner, M., M. H. Schroth, J. Zeyer, and W. Kinzelbach (2004), Modeling of a microbial growth experiment with bioclogging in a two-dimensional saturated porous media flow field, *Journal of Contaminant Hydrology*, *70*(12), 37–62, doi:10.1016/j.jconhyd.2003.08.008.

Thullner, M., P. Regnier, and P. Van Cappellen (2007), Modeling Microbially Induced Carbon Degradation in Redox-Stratified Subsurface Environments: Concepts and Open Questions, *Geomicrobiology Journal*, *24*(3-4), 139–155, doi:10.1080/01490450701459275.

Treese, S., T. Meixner, and J. F. Hogan (2009), Clogging of an Effluent Dominated Semiarid River: A Conceptual Model of Stream-Aquifer Interactions, *JAWRA Journal of the American Water Resources Association*, *45*(4), 1047–1062, doi:10.1111/j.1752-1688.2009.00346.x.

Ulrich, C., S. Hubbard, J. Florsheim, D. O. Rosenberry, S. Borglin, M. Trotta, and D. Seymour (2015), Riverbed Clogging associated with a California Riverbank Filtration System: An assessment of mechanisms and monitoring approaches, *Journal of Hydrology*, *529*(3), 1740–1753, doi:10.1016/j.jhydrol.2015.08.012.

van Genuchten, M. T. (1980), A Closed-form Equation for Predicting the Hydraulic Conductivity of Unsaturated Soils, *Soil Science Society of America Journal*, *44*(5), 892, doi:10.2136/sssaj1980.03615995004400050002x.

White, D. C., and D. B. Ringelberg (1998), Signature Lipid Biomarker Analysis, in *Techniques in Microbial Ecology*, edited by R. S. Burlage, pp. 255–289, Oxford University Press, New York, NY.

Wingender, J., T. R. Neu, and H.-C. Flemming (1999), What are Bacterial Extracellular Polymeric Substances?, in *Microbial Extracellular Polymeric Substances*, edited by J. Wingender, T. R. Neu, and H.-C. Flemming, p. 258, Springer-Verlag, Berlin Heidelberg.

Xie, Y., P. G. Cook, P. Brunner, D. J. Irvine, and C. T. Simmons (2013), When Can Inverted Water Tables Occur Beneath Streams?, *Groundwater*, *52*(5), 769–774, doi:10.1111/gwat.12109.

Zhang, Y., S. Hubbard, and S. Finsterle (2011), Factors governing sustainable groundwater pumping near a river, *Ground Water*, *49*(3), 432–444.

Chapter 3

Hyporheic Zone Contributions to River Nutrient Cycling and Net Primary Productivity

Abstract: In California and other regions with Mediterranean climates, losing rivers, which act as a source of recharge to groundwater, are common. Fluxes of water from the river into the subsurface can generate dynamic responses in the hyporheic zone that affect porosity and permeability, cycling of nutrients, and microbial aerobic/anaerobic growth that regulate the removal of Carbon and Nitrogen from natural systems. Permeability decline from hyporheic zone bioclogging is a feedback mechanism that begins from hyporheic rivergroundwater fluxes that stimulate microbial growth, decrease permeability, and thereby reduce the initial hyporheic rivergroundwater flux. Evolution of bioclogging within hyporheic zones depends on initial conditions of the riverbed sediment porosity and permeability which is associated with antecedent winter flow conditions in Mediterranean climates. Variability from wet-year and dry-year end members in these climates can influence the initial grain size distribution and sorting demonstrating a large scale climate-control on end-of-wet-season riverbed characteristics. Depending on the initial state of the hyporheic characteristics, the mechanisms responsible for Carbon and Nitrogen removal during the following year may be enhanced or suppressed given conditions of median grain size and sorting. Resulting effects on biogeochemical fluxes and biogenic gas emissions are then a unique function of the physical, hydraulic, and biological factors that contribute to the initial and final state of microbial growth during the dry season. In this study, I hypothesize that hyporheic contributions to river net primary productivity and denitrification are governed by these joint factors. To address this, I simulated biological growth, parameter and carbon dynamics, and hyporheic biogenic gas production using 1D and 2D MIN3P numerical models, allowing a range of initial grain size distributions to represent wet season control of riverbed scour. I introduced

stochastic water level fluctuations to exert dynamic climate and human based controls on summer dry-season infiltration. Over a three year numerical simulation, I quantified microbial growth, total carbon and infiltration fluxes, and total CO_2 and N_2 production which represent the effectiveness of C and N transformations. Our results showed that infiltration declines due to bioclogging were greatest in higher permeability sediments (which are typically deposited following wet winters with greater bankfull discharge). In these higher permeability sediments, cumulative C and N transformations and infiltration volumes were higher than in low permeability sediments (which are typically associated with drier winters with less overall scour). Lower permeability sediments contributed to lower rates and cumulative fluxes of C and N from lower clogging. The initial sediment grain size distribution exerted strong control on the location of bioclogging and gas production, especially when an unsaturated zone developed. Our results demonstrate a flow and nutrient transport feedback mechanism where bioclogging, and C and N cycling become limited by wet-season controlled initial sediment conditions. These results provide a new understanding of nutrient cycling and bioclogging in losing rivers governing hyporheic C and N budgets and cumulative transformations across watersheds.

3.1 Introduction

Hyporheic zones in rivers worldwide play an important role in nutrient cycling and in the exchange of water, energy and nutrient fluxes between surface and ground waters. Top-down climatic drivers governing riverbed characteristics such as geomorphology, extreme flows, sediments, and benthic ecology, stimulate and constrain subsurface biogeochemical transformations. Rivers perform a multitude of ecosystem services, including denitrification [*Gomez-Velez et al.*, 2015; *Harvey et al.*, 2013; *Harvey and Gooseff*, 2015], providing hotspots for global Carbon (C) and Nitrogen (N) degradation and emissions [*Battin et al.*, 2016; *Gomez-Velez et al.*, 2015; *Hotchkiss et al.*, 2015; *Peyrard et al.*, 2011], and include a significant component of landscape biological productivity and respiration [*Findlay*, 1995; *Rode et al.*, 2015]. Despite the importance of rivers for these ecosystem services, tremendous variation in factors as fundamental as denitrification rate and net ecosystem exchange exists between rivers [] [Ranalli and Macalady, 2010]. The causes of such variation remain poorly understood and are hypothesized to function dynamically across landscapes, climates, and scales within a watershed with impacts on watershed cumulative flow and chemistry [*Harvey and Gooseff*, 2015].

Despite their small areal extent, rivers are increasingly recognized as major sources of biogenic gases to the atmosphere [*Hotchkiss et al.*, 2015]. The significance of CO_2 production due to microbial activity in the hyporheic zone for the overall carbon balance of rivers is poorly quantified, and is typically estimated as the residual of in-stream metabolism [*Hall*

et al., 2015; *Hotchkiss et al.*, 2015]. Carbon dioxide is produced within the hyporheic zone due to aerobic respiration (AR) and anaerobic denitrification (DN), both of which rely on dissolved organic carbon (DOC) as a substrate for growth [*Baker et al.*, 1999]. The rate of biogenic gas release associated with river systems is strongly tied to the physical characteristics of the hyporheic interface that regulates the exchange of water (and associated solutes) between the rivers water column and underlying sediments [*Rode et al.*, 2015]. Conditions favoring either AR or DN (or both) are associated with sufficient flow delivering substrates, and subsurface redox conditions that consume O_2 significantly to allow DN to begin. Residence time distributions (RTDs) and reaction rates (RR) quantified by the Dahmköhler number represent these competing timescales of reactions versus flows in sediments where AR and DN occur [*Harvey et al.*, 2013]. Microbial micro-niches along hyporheic flow paths that facilitate AR and DN occupy a significant volume of space within the sediment, yet their physical effect on flow paths and nutrient delivery remains an unquantified, bottom-up feedback that changes the RTD and RR within the sediments. Much controversy currently exists about where and when DN occurs, and why upstream vs. downstream areas may better facilitate this reaction [*Ranalli and Macalady*, 2010]. Most conceptual and numerical models neglect this important pore-scale feedback, and filling this gap could provide useful information for better and more accurate C and N budgets, and may help explain different transformation-potentials between rivers.

One potential driver of significant differences in measured rates of riverine nutrient processing and carbon exchange between rivers may be associated with the significance of the hyporheic zone as the region in which biogeochemical processing occurs. The hyporheic zone lies at the intersection of surface and groundwater domains and functions as a filtering compartment between these zones. Processes in the hyporheic zone are influenced by the transport of water and dissolved or entrained particulate matter between these zones. In particular, rates of DN and AR in the hyporheic zone depend on the provision of suitable substrates for heterotrophic bacteria, primarily DOC, and the development of relatively aerobic or anoxic conditions that favor AR or DN respectively, primarily controlled by the relative rates of supply and consumption of oxygen (O_2) (we assume the N supply is not limiting because the DN reaction rate is much smaller than AR and thus controlled by leftover DOC).

These physical characteristics are not constant in time, but instead vary dynamically as a function of microbial growth within riverbed sediments [*Newcomer et al.*, 2016]. These microbes subsist upon carbon and micronutrient substrates transported to them by infiltrating water, generating biogenic gases as a byproduct of their growth. As microbial populations increase, biofilms and cellular matter associated with their growth fill sediment pore spaces, reducing riverbed porosity, and thereby also infiltration and the rate of substrate provision. This dynamic dependence of porosity upon biomass, and of biomass growth rates on porosity generates a complex, self-limiting feedback cycle [*Nogaro et al.*, 2010]. The impact of this feedback cycle on seasonal rates of biogenic gas production and microbial growth, however,

is likely to vary with the conditions of the riverbed at the beginning of the growing season, which, in Mediterranean climates, corresponds with the dry, low-flow summer period. Consequently flow variability during the wet season, which sets the initial condition of the riverbed sediments, may determine the functioning of the hyporheic zone in losing rivers, as a site of nutrient processing and biogenic gas generation, during summer. California, and many other seasonally dry climates [*Vico et al.*, 2015], are characterized by tremendous variability in wet season conditions, meaning that a wide suite of potential summer behaviors are plausible.

These dynamics highlight the significance of water transport through the hyporheic zone and the growth rates of microbiota within the hyporheic zone in controlling denitrification and overall respiration, but they neglect several critical features, including flow transitions, sediment/microbial feedbacks, ecological production of substrates, and anthropogenic disturbances. Typical modeling approaches also neglect river-aquifer conditions that govern infiltration rates, river discharge controls on initial riverbed sediment characteristics after the wet-season, river discharge controls on algal productivity and the production of nutrients for subsurface microbes to clog the pore-space, and anthropogenic conditions superimposed on these. I describe these controlling factors below. Some of these controlling factors are shown in Figure 3.1 and they include channel topography, water table fluctuations, unsaturated zone formation, and a lower riverbed permeability layer overlying the aquifer sediments.

DOC Formation and Supply from Algae

DOC can be supplied to the hyporheic zone by transport from surface waters, where it is initially fixed from atmospheric carbon by photosynthetic algae and plankton, with benthic algal blooms being particularly effective at supplying DOC to subsurface microbes [*Cole*, 1982; *Findlay et al.*, 1993; *Jones et al.*, 1995; *Wetzel et al.*, 1995]. Senescing algae release photosynthates directly into the water column as DOC (sometimes within hours after decay), providing a labile carbon substrate for heterotrophic metabolism Decaying algal cells also produce DOC and particulate organic carbon (POC), which serve as bioavailable, but less labile substrates for growth and heterotrophic metabolism. Although algal exudates may increase DOC in the hyporheic zone to concentrations in the range of 25 100 mg/L [*ElBishlawi and Jaffe*, 2015; *Mann and Wetzel*, 1995; *Wyatt et al.*, 2012], the rate of DOC supply to microbial communities may be much higher, since microbial utilization of DOC may occur as rapidly as DOC is supplied [*Cole*, 1982], and processing of DOC in losing rivers is estimated to be 35g /m^2/day [*von Gunten et al.*, 1994]. Unsurprisingly, growth rates of heterotrophic bacteria in the hyporheic zone increase with increasing Chl-α content of infiltrating water [*White et al.*, 1991].

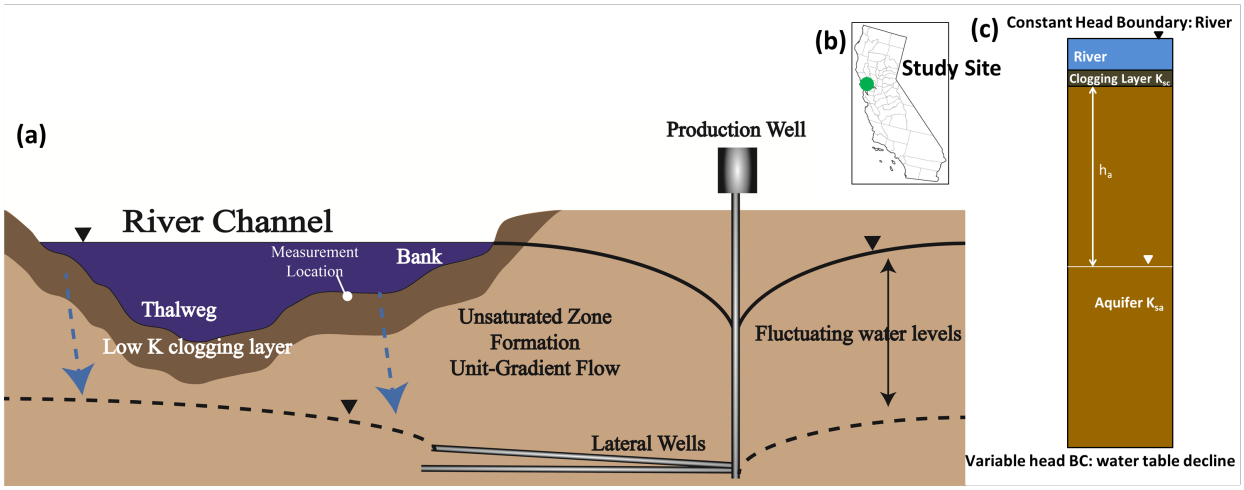

Figure 3.1: (a) Conceptual, two-dimensional diagram of a river and key aspects that govern infiltration, based on the Wohler RBF site in CA. The figure illustrates aspects such as riverbed clogging layer (low conductivity layer), aquifer layer, fluctuating water table, unsaturated zone formation (disconnection), location of unit-gradient (UG) flow, RBF well location, and lateral pumping wells. (b) Location map of the Wohler RBF site in California, whose data inspired this study (Lat: 38.5, Long: -122.9). (c) One-dimensional profile of the layered sediments at a general location within the river cross section where the flow path is dominantly vertical and where disconnection occurs. Note: This figure is not to scale. Lateral wells are located sufficiently below the river that all flow paths are dominantly vertical from the river, even those in the unsaturated zone.

Microbial Bioclogging

Microbes in the hyporheic zone are well known to generate bioclogging of sediments [*Yarwood et al.*, 2006; *Thullner*, 2010; *Rosenzweig et al.*, 2014], and leading to reductions in permeability (K) and porosity (ϕ) [*Thullner et al.*, 2002a, b, 2004; *Brovelli et al.*, 2009]. The implications of bioclogging for microbial population dynamics at the river-scale, however, are complicated by feedbacks introduced because bioclogging limits the rate of infiltration that sustains microbial growth. The consequences of such feedbacks include large changes in total infiltration flux, unsaturated zone development, microbial gas production of CO_2 and N_2, long-term K and ϕ dynamics, total hyporheic zone nutrient influx, and cumulative contaminant degradation from upstream to downstream [*Larned et al.*, 2015].

Infiltration Conditions Affecting Substrate Delivery

In losing rivers feeding low water tables, an unsaturated zone can develop causing the flow to become disconnected concurrently with maximum infiltration rates which has implications for transport of substrates for AR and DN [*Brunner et al.*, 2011; *Cook*, 2015]. As bioclogging occurs in losing rivers, a spatial variability factor is introduced and the vertical and horizontal flow components may converge, develop preferential flow paths [*Rubol et al.*, 2014; *Batlle-Aguilar et al.*, 2015] and show unique controls and feedbacks on infiltration [*Newcomer et al.*, 2016]. Bioclogging may not occur spatially evenly across all sediment types and porosity sizes, and little information is available on the functional relevance of bed and suspended particles on subsurface flowpaths and transformations [*Garcia-ruiz et al.*, 1998; *Nogaro et al.*, 2010]. Rates of AR and DN vary with respect to location in the watershed and local and regional groundwater flows which can contribute to dominantly vertical flow-paths with very high resident time distributions (RTDs) [*Ranalli and Macalady*, 2010].

Water-table fluctuations associated with anthropogenic pumping can induce oscillations between conditions of gaining losing and disconnection/re-connection. Where connection-disconnection oscillations occur, fluctuations will also be induced in the subsurface redox conditions, changing the relative dominance of anaerobic versus aerobic microbial processes [*Wyatt et al.*, 2012]. Consequently, the seasonal trajectories of infiltration, aquifer storage, bio-geochemical cycling and biogenic gas production arise as a function of wet season and dry season conditions and their interaction with anthropogenic groundwater extraction. This complexity challenges a simple assessment of river health and ecosystem function [*Harvey and Gooseff*, 2015; *Larned et al.*, 2015] and means that standard models which do not address the temporal variation in hyporheic conditions fail to reproduce observations [*Cuthbert et al.*, 2010]. Models that address physical and biological processes in the hyporheic zone are needed to facilitate improved prediction of river function [*Nogaro et al.*, 2010]. Such models must be formulated based on an inter-disciplinary approach which addresses hydrological and biological feedbacks, dynamic behavior of hydraulic parameters, and an exploration of how wet and dry season climatic variability and management decisions (in the form of pumping) influence the behavior of the river system.

Mediterranean Climates

During wet winter conditions, river flows are elevated [*Cayan et al.*, 1999], increasing the rate of scour of riverbeds and enhancing overall sediment fluxes out of the catchment leaving behind clean, well-sorted gravel beds [*Andrews and Antweiler*, 2012]. By scouring the bed, populations of sediment-living grazers are suppressed, enabling increased algal growth in the river water column and benthic habitat [*Power et al.*, 2013, 2015] and ultimately enhancing dissolved organic carbon (DOC) concentrations in the hyporheic pore-space, as

algal biomass decays [*Wyatt et al.*, 2012]. Even one scouring bankfull discharge event, may have large regional effects on the dynamics of benthic ecosystems such as algae growth, grazer consumption, and subsurface bioclogging [*Power*, 1992; *Piggott et al.*, 2015]. Episodic sediment fluxes entrained by large disturbances in other locations around the world point to the influence that large scale, top-down effects can have on local scale geomorphologic features [*Aalto et al.*, 2003; *Kondrashov*, 2005], as well as cascading effects on food-webs that feed subsurface micro-organisms [*Power*, 1992; *Power et al.*, 2008, 2009]. Conversely, following relatively dry winters, lack of any scouring floods may increase the percentage of fines within sediment, skewing the sediments towards lower conductivity and porosity values from poorly sorted packing arrangements, may allow a 3-4 level food chain to develop that releases grazers from predator consumption, and allow grazer control of algae growth. DOC concentrations in this scenario are hypothesized to be much lower than in years with strong winter floods.

The summer dry season following wet winters represents a period in which Mediterranean rivers often transition from being gaining to losing rivers [*Pryet et al.*, 2015], particularly as groundwater levels decline [*Lavers et al.*, 2015]. As drying progresses, losing rivers can further transition from being connected to the groundwater through a continuously saturated zone, to being disconnected with the underlying aquifer [*Su et al.*, 2007; *Treese et al.*, 2009; *Lamontagne et al.*, 2013; *McCallum et al.*, 2013]. Disconnected rivers and aquifers develop large unsaturated zones allowing maximum infiltration in this state [*Brunner et al.*, 2009]. Gaining rivers are typically found in temperate regions that remain fully connected even during pumping [*Schubert*, 2002, 2006]. Combined effects of Mediterranean climate controls on DOC and temporal summer infiltration patterns represent the main drivers of nutrient supply for subsurface biogeochemical transformations. Bio-geochemical cycling after water enters subsurface sediment then hinges on the accurate representations on microbial guilds that then provide additional functional services to this cycle [*Bouskill et al.*, 2012].

Sediments

Despite the positive associations between algal production in rivers and subsurface respiration, there remains tremendous heterogeneity in the ability of rivers to process nutrients and contaminants. River-aquifer flow conditions and overall sediment structure may help explain these differences. Microbial AR and DN are primarily limited by the rate of DOC, DO and Nitrate supply, suggesting that the spatial and temporal pattern and directionality of flow (as mediated by transitions between gaining and losing conditions, changes in permeability and porosity due to bioclogging, and initial conditions of sediment and geomorphic characteristics) could regulate growth rates [*Battin et al.*, 2016].

Mediterranean climates, for example, have wet winters that lead to strong flows with the potential to overturn bed sediments from bankfull events. Effects of river velocity variations

and shear stress on sediment particle deposition when low flows and spates occur are varied [*Leonardson*, 2010]. For example, non-linear effects on riverbed grain-size distributions occur when certain configurations of low-velocity (i.e. siltation [*Schaap et al.*, 2001]) and high-velocity (i.e. turbulent impaction [*Cunningham et al.*, 1987]) both lead to decreased conductivity. Large storm events can increase the conductivity of riverbeds [*Mutiti and Levy*, 2010], while post-flood/post-scour siltation can lead to net decreased conductivity [*Wu and Huang*, 2000; *Chen et al.*, 2013a]. Losing versus gaining rivers also have dichotomous effects on conductivity [*Chen et al.*, 2013b]. Conductivity of riverbed sediments is highly dependent on the median grain size and sorting characteristics [*Boadu*, 2000; *Shepherd*, 1989] which may allow certain sediment packing arrangements to have similar porosity values yet order of magnitude different conductivities [*Sneider*, 1987]. The complexity associated with sediment texture and sorting, porosity, and conductivity have been reported (Figure 3.2) [*Beard and Weyl*, 1973; *Sneider*, 1987; *Slatt*, 2006].

Sediment properties and local geomorphology are known to exert a strong control on surface water groundwater interactions, RR, RTDs, of nutrients, and O_2 consumption [*Findlay*, 1995]. Current thinking suggests that high permeability sediments cannot contribute to DN because of short RTDs which inhibit development of anaerobic conditions [*Ranalli and Macalady*, 2010]. Discrepancies exist, however, concerning gravelly rivers that show almost complete removal of O_2 from surface water [*Findlay*, 1995]. Initial sediment properties have been found to exert a strong control on these interactions, yet mean sediment grain size alone cannot account for the wide variability O_2 removal rates from field data [*Findlay*, 1995; *Dodds et al.*, 1996]. A possible explanation for data inconsistency concerning AR and DN rates within a watershed may be explained by the time-variable nature of these reactions as microbes grow during their life-cycle. Accounting for microbial feedbacks on infiltration rates and sediment characteristics may help resolve this discrepancy through better understanding of how RR and RTDs may change over time and across scales within a watershed.

Study Goals

This study aims to assess the temporal trajectory of bioclogging and related feedbacks in a Mediterranean climate environment controlled by initial sediment conditions and DOC delivery within the riverbed. I hypothesize that the initial sediment characteristics, specifically conductivity (K) and porosity (ϕ) corresponding to the conditions at the end of the wet season, and beginning of the dry summer growing season exert a major control on total bioclogging and C, and N, consumption. During the wet season, sediments are scoured and deposited, allowing algal and phytoplankton populations in the water column to establish and provide exudate and detrital sources of nutrients and DOC to subsurface heterotrophs. For example, wet years with intense winter floods scour riverbeds sediments, shift rivers towards more gravelly, well-sorted sediments and allow algae to flourish. The timing of the

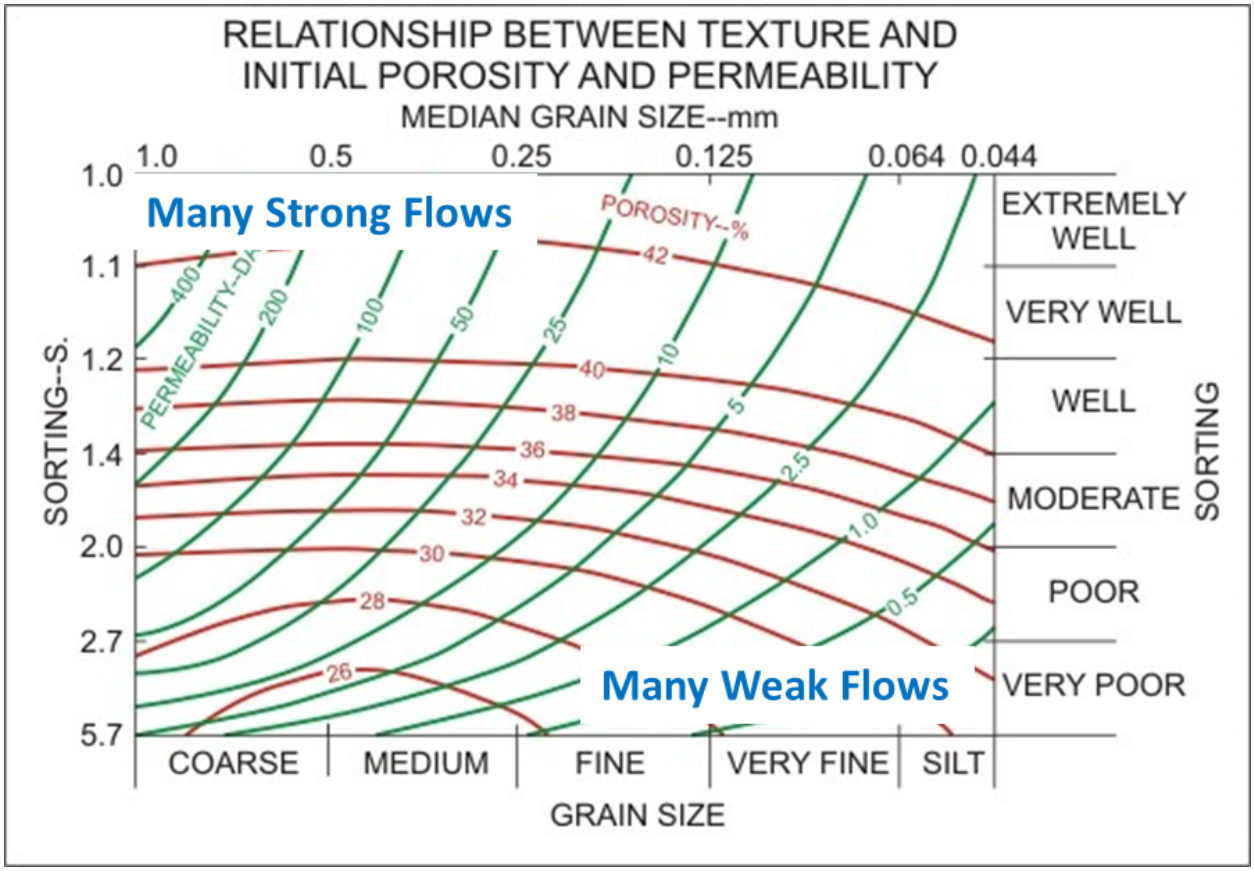

Figure 3.2: Relations among grain size, sorting, porosity (red lines), and permeability (green lines). Data is from [*Beard and Weyl*, 1973] and the figure is reproduced by [*Sneider*, 1987]. A permeability of 5 darcies can have porosities ranging from 0.26-0.42 where porosity is dependent on the level of sorting. A sediment porosity of 0.30 can have permeabilities ranging over 3 orders of magnitude.

scour is important for ecological succession of algae and subsequent clogging during algal senescence [*Power*, 1992; *Power et al.*, 2008]. If rivers do not scour, ecological succession is suppressed through grazer proliferation, and so is the availability of carbon as a substrate. The combination of these factors is required in assigning river boundary conditions in subsurface models of flow and transport.

This work provides insights into how coupled biological and physical processes at river beds influence two critical ecosystem services: net primary productivity for the river and denitrification from hyporheic zone contributions. The goal of this study is therefore to assess the trajectories of: Seasonal denitrification, heterotrophic respiration, and net primary

productivity (NPP). In a model that is cognizant of the biological-physical feedbacks in the river bed, that explores different ICs in terms of DOC/POC availability and sediment conditions, and which accounts also for variability in substrate aerobic conditions induced in response to anthropogenic pumping, total C and N budget can be improved by quantifying the subsurface component to these budgets.

To address these limitations, I used 1D and 2D numerical hydro-biogeochemical models with K and ϕ represented as time-variable parameters representative of antecedent winter river flow conditions. I used scenarios of initial parameter conditions to represent the influence of wet-year and dry-year end-members to simulate feedback mechanisms of biomass growth, infiltration, gas production, and carbon cycling. I analyzed these feedback mechanisms within the framework of a seasonally dry semi-arid river periodically undergoing disconnection, and prone to prolonged periods of drought. I stochastically simulate water levels using pumping data from our field site. This paper addresses three main questions: 1) Given wet/dry end-member scenarios, how does infiltration and total carbon cycling change? 2) Do initial riverbed conditions dependent on wet/dry end-members enhance or limit gas production (CO_2, N_2)? 3) How will introducing fluctuations in the water table including topographic variability influence overall trajectories of biological growth, total infiltration fluxes, gas production, and carbon cycling? These problems were investigated along the Russian River CA which provided a test bed for the combination of these effects. Within the numerical code MIN3P, I implemented the river geometry, disconnection, pumping fluctuations, and bioclogging processes to test how water level fluctuations and wet/dry end-members influenced initial parameter conditions govern the trajectory of bioclogging and gas production.

3.2 Study Site

The Wohler Riverbank Filtration site operated by the Sonoma County Water Agency (SCWA) maintains 6 collector wells along the Russian River, providing 600,000 people annually with drinking water (Figure 3.3). The Russian River drains approximately 3,850 km^2 in Northern California, with an annual average discharge of approximately 2.0 km^3 that varies with winter precipitation. A major variable of interest at the Russian river site is infiltration because the river and aquifer are conjunctively used for drinking water and for maintaining riparian vegetation and streamflow habitat. Dominant process controlling infiltration includes pumping which contributes to unsaturated zone development beneath the river; a temporary dam raises hydraulic heads and increases infiltration; bioclogging reduces K and ϕ and reduces infiltration. Each year algal and cyanobacterial growth cause river quality concerns. During its life cycle, algae die and exude dissolved organic carbon (DOC) for subsurface heterotrophic bacteria that clog the subsurface pore space. Surface

periphyton algae growth (*sp. Spyrogyra* summer, *Cladophora* spring) is shown in Figure 3.3b. Decaying algae is then processed by surface microorganisms (grazers) that allow quick transfer of carbon to a particulate and dissolved phase providing a substrate for subsurface micro-organisms. Field samples of subsurface microbial biomass across the river and along the river flow direction are shown in Figure 3.4a. Subsurface biomass is concentrated in the north and west side of the river which is closest to the production wells. Methods used to obtain the field data are fully described in a previous study [*Ulrich et al.*, 2015].

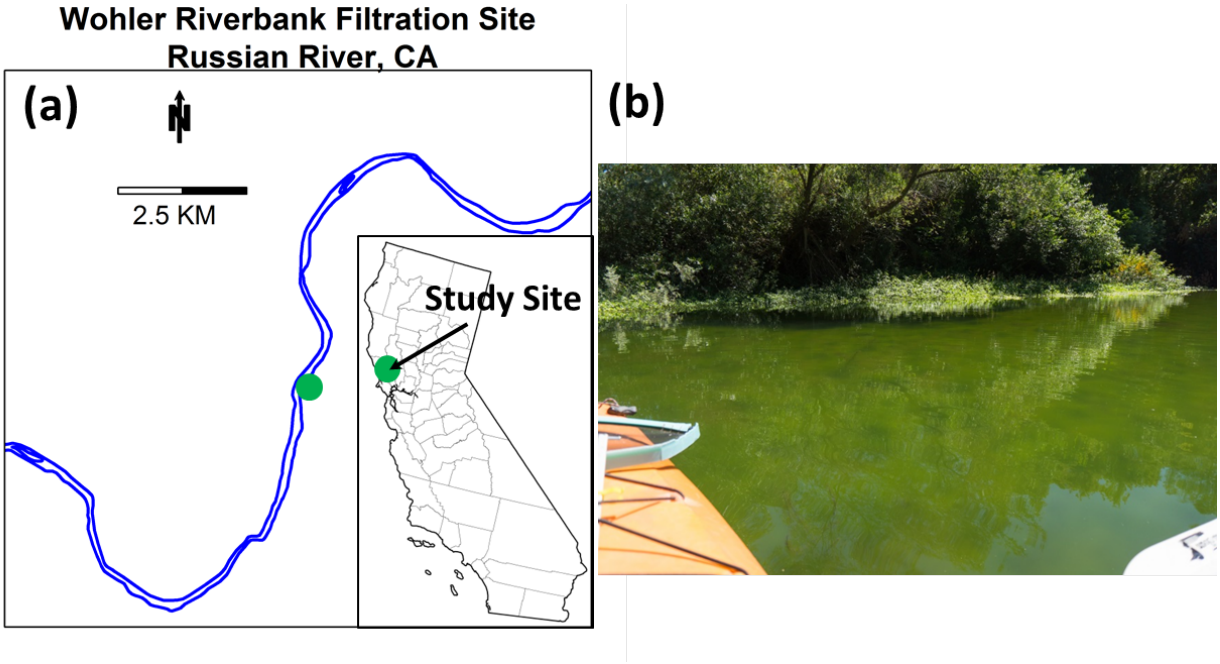

Figure 3.3: (a) Location of the Wohler Study Site along the Russian River, CA. Wohler is located approximately 10 km upstream of the USGS Guerneville Station #11467000. (b) Algal growth during the summer near the collector wells.

The Russian river is conceptualized as a river undergoing periodic connection and disconnection. Field data of ground water levels from a nearby observation well and river levels from the inflatable dam show the water table decline and the periodic and growing water table fluctuations in response to pumping (Figure 3.4b). As the river periodically transitions from gaining to losing, the potential for overlapping zones of aerobic (river losing) and anaerobic waters (river gaining) can trigger unique microbial responses. The pumping time series is later used to reconstruct stochastic water level simulations.

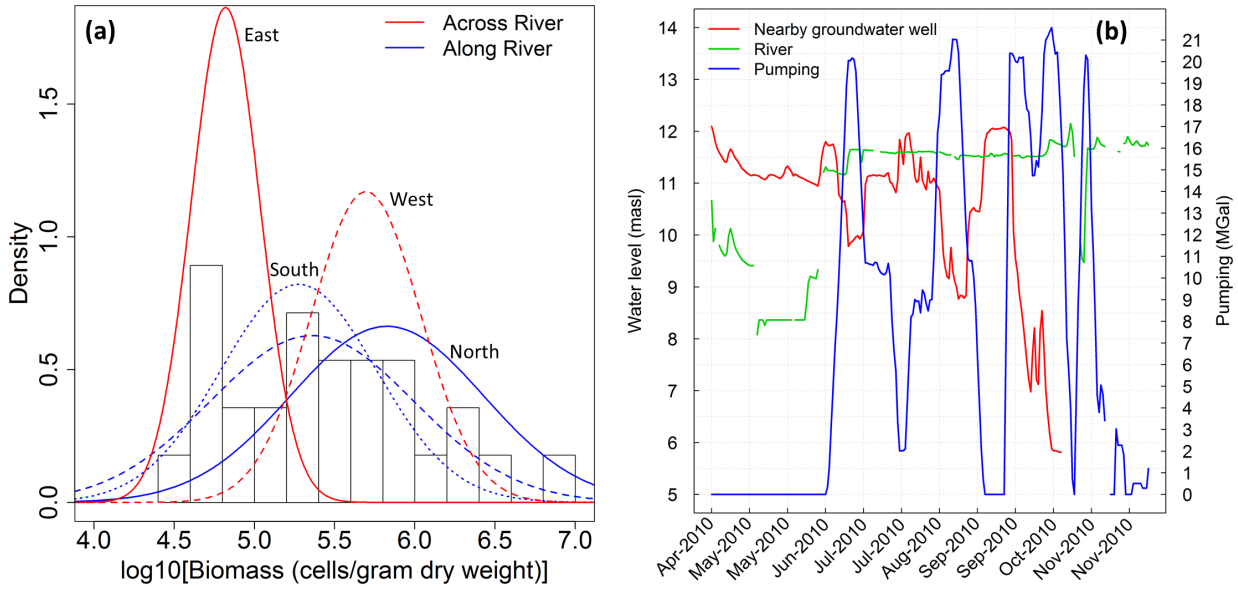

Figure 3.4: (a) Biomass spatial distribution across the river and along the river in the direction of flow from north to south. (b) Subsurface and river water levels, and pumping in 2010. The oscillating groundwater levels are in phase (but opposite) to pumping. The river water level remains constant during the summer because of a downstream inflatable dam.

3.3 Methods

In this study I compare infiltration, nutrient, and microbial gas production feedbacks across multiple scenarios of climate derived wet-year/dry-year El Niño Southern Oscillation (ENSO) end-members. Models of a river undergoing periodic connection-disconnection are achieved with stochastic water table fluctuations that are derived from dominant frequencies of pumping field data. Effects from the water table fluctuations are assessed with a variety of initial parameter conditions representing end-member dry-year/wet-year scenarios as well as comparisons across fluctuating and non-fluctuating cases. I compare the modeled seepage to field seepage data and I simulate water table fluctuation effects on biogeochemical cycling.

Field Seepage

Seepage from May-November 2012 was estimated at the Wohler site from distributed temperature sensors (DTS) at multiple spatial and vertical locations. Sensors were placed at the riverbed, 20cm, 50cm, and 80 cm below the riverbed. I used the Matlab code VFLUX

which implements analytical solutions from *Hatch et al.* [2006], and *Keery et al.* [2007], to the 1D heat convection-conduction equation [*Stallman*, 1965; *Gordon et al.*, 2012]. Ranges of parameters used in VFLUX are given here and were determined from a previous analysis [*Ulrich et al.*, 2015]: thermal conductivity = 0.0052 [W m^{-2} K^{-1}] (0.0024-0.0095 cal (s cm C)$^{-1}$), thermal dispersivity = 0.001-0.05 [m], specific heat capacity of the sediment = 0.0031 [J cm^{-3} K^{-1}] (0.2-0.55 cal (cm^3 C)$^{-1}$), and specific heat capacity of the fluid = 0.0153 [J cm^{-3} K^{-1}] (1 cal (cm^3 C)$^{-1}$).

Classifying the Winter-Spring End-Members

To account for the effects of winter and spring river flow conditions in the modeling framework, grain size distributions (GSD) and peak annual river flow were used to classify the ENSO end-members by informing the initial parameter conditions (K and ϕ). GSDs for sands, pebbles, and gravels between years were classified as El Niño (EN) or La Niña (LN) based on the Multi-variate ENSO Index (MEI) scale [*Wolter and Timlin*, 1993] (Figure 3.5a). Bed sediment GSDs are shown for the USGS Guerneville Station #11467000 which is a few km downstream of the Wohler site. During EN years (MEI > +0.3), gravels contributed to a much larger fraction of the sample compared with LN years (MEI < -0.3) (p=0.1). During LN years, coarse sands (which fill the matrix of gravels and reduce porosity) were significantly larger compared with EN years (p=0.03). The general pattern of GSD based on flow regime can be interpreted as such: larger porosites and more uniform GSD during EN years, and smaller porosities with more non-uniform GSD during LN years.

Annual peak river discharge values for each water year were extracted from the USGS Guerneville station and classified as EN or LN based on the same scale as described above. Return intervals were calculated by ranking the data such that the largest Q has rank 1. The return interval is then the total number of years in the dataset/rank. Cumulative density functions (CDFs) for the return intervals for the specified peak flow were calculated from a Gumbel exceedance probability distribution Figure 3.5b.

$$F\left(x:\mu,\beta\right)=\exp\left(-\exp\left(-\left(\frac{x-\mu}{\beta}\right)\right)\right) \tag{3.1}$$

Where x is the peak flow, μ is a location parameters corresponding to the peak (also referred to as mode), β is the scale parameter associated with the width of the Gumbel CDF and is given as:

$$\beta=\frac{\sqrt{6}\sigma}{\pi} \tag{3.2}$$

Where σ is the standard deviation of the discharge data. The first theoretical moment about the origin:

$$E[x] = \mu + \gamma\beta \tag{3.3}$$

Where γ is the EulerMascheroni constant $\approx$0.5772. The method of moments was used to rearrange equation 3.3:

$$\mu = -\gamma\beta + mean\,(discharge) \tag{3.4}$$

Equation 3.4 was substituted into Equation 3.1 leaving no unknown parameters.

Output from the Gumbel analysis is shown in Figure 3.5b. In general, EN years show slightly larger peak fluxes predictions than LN years for return intervals >1.5 years while LN years show slightly larger peak fluxes for return intervals < 1.5 years. However, overlapping confidence intervals on the fits suggest that we cannot reject the hypothesis that the EN and LN years follow the same relationship between return interval and flow rate. A similar classification of higher peak flows for EN years versus LN years was also found for the Salinas River, CA [*Gray et al.*, 2015]. While the Figures in 3.5a and 3.5a, can be considered as part of our results, I present them here in the methods because I use these data and classifications for our model development.

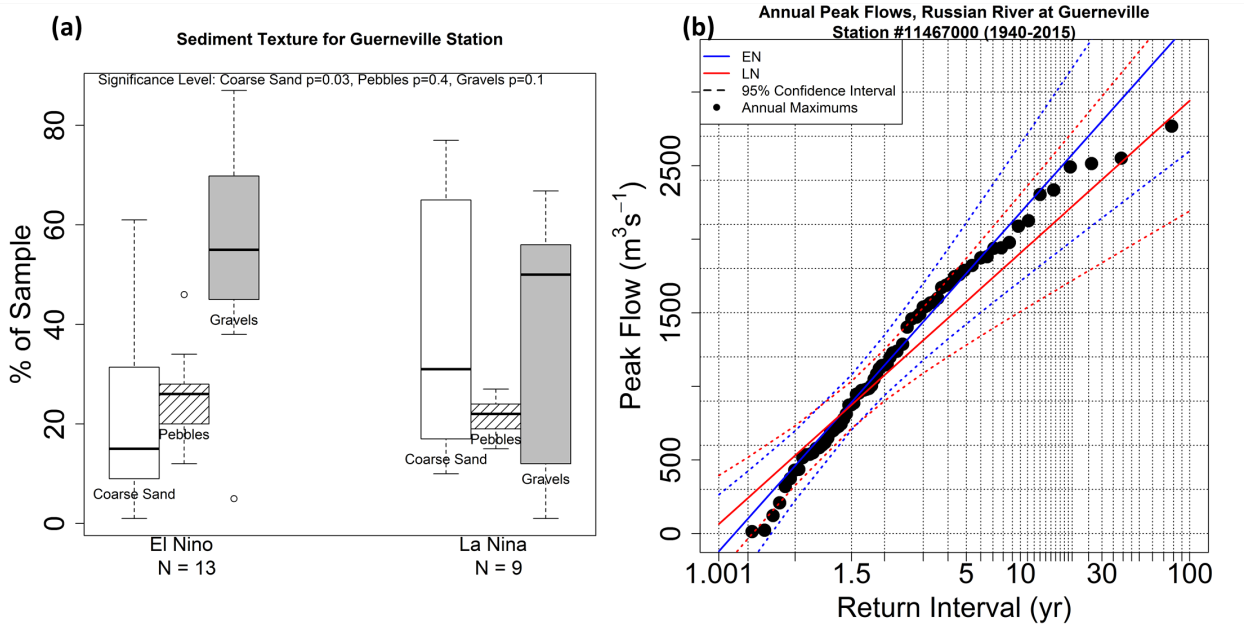

Figure 3.5: (a) Bed sediment texture classified by EN and LN years from the USGS Guerneville Station (b) Annual peak flow classified by EN or LN.

The GSD and peak flow data obtained from the USGS station provided the overall conceptual framework for the ENSO end-member classification scheme. I classify the effects of ENSO on sediment parameters riverbed conductivity (Kc) and riverbed porosity (ϕ) in the following way based on the graphical relationship between Kc and ϕ presented in Figure 3.2:

Wet-winter wet-spring: Higher than average river flows contribute to enhanced sediment scour, higher porosities, spring spates allows well-sorted sediments, and higher conductivities and porosities. High Kc-High ϕ.

Wet-winter dry-spring: Higher than average river flows contribute to enhanced sediment scour, and larger grain sizes, while dry spring contribute to fine sediment deposition decreasing the sorting. Somewhat higher than average river flow, yet the total number of storms still encourage scour and some sediment sorting. High conductivities remain, but sediments become poorly sorted and this lowers porosity. In coarse sediments, sorting impacts porosity even while maintaining conductivity. High Kc-Low ϕ.

Dry-winter wet-spring: Somewhat lower than average river flow, but a greater number of total storms than a typical strong LN year. Overall GSD sediments are shifted to sands instead of gravels. The frequent small storms keep sandy sediments well-sorted which allow porosities to remain high while conductivities are low because of the shift in overall GSD. Low Kc-High ϕ.

Dry-winter dry-spring: Lower than average river flow contributes to reduced total sediment scour, lower porosities from sediment deposition, poorly sorted sediments, and lower conductivities. Low Kc-Low ϕ.

Model Development

1D and 2D models of the Russian River were developed using the MIN3P reactive transport code [*Mayer et al.*, 2002]. MIN3P is a finite volume numerical code for variably saturated subsurface flow and multi-component reactive transport. An unstructured mesh representing the river topography used in numerical simulations is shown in Figure 3.6 as well as model assumptions for ENSO effects on riverbed parameters.

Model cross sections for the 2D and 1D models are shown in Figure 3.7. The model setup included a riverbed clogging layer and an aquifer layer. The riverbed layer represents sediments that are distinctly different from aquifer sediments as they are prone to scour and microbial clogging. Reactive transport conditions for bioclogging included microbial aerobic respiration (AR), and microbial denitrification (DN). Since most groundwater/vadose zone codes do not include growth and decay model for algal biomass in the surface water column, the carbon substrate (DOC) is specified via a transport flux across the boundary conditions. Dissolved oxygen (DO) is treated similarly. DOC is assumed to be the limiting substrate. The reactive transport model accounts for intra-aqueous reactions of biomass growth using

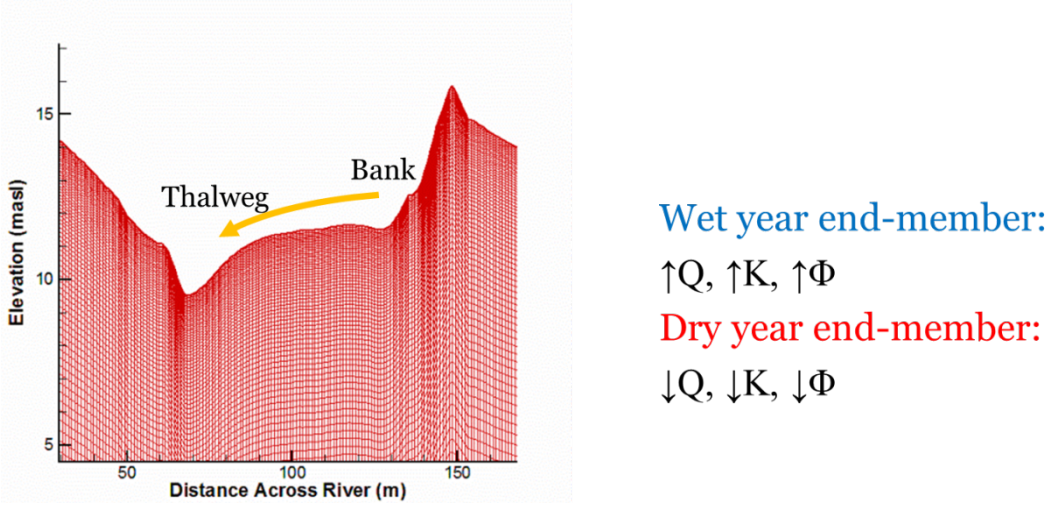

Figure 3.6: Assumptions for the wet year and dry year end-members are shown. Variations across the river spatial gradient are assumed homogenous for each case.

Monod kinetics. Aquatic organic matter with a generalized formula representing dissolved organic carbon was represented by the ratio C_1:H_2:O_1 [*Matsunaga et al.*, 1993]. DOC concentration was specified at 20-40 mg/L in the river water based on previous reports of algal contributions to DOC. Few studies have reported the contribution of algae to DOC in riverine settings, but current estimates suggest that carbon exudation from algae can raise DOC levels upwards of 35 mg/L stimulated by water table variations where lower water tables contribute to higher DOC value [*Wyatt et al.*, 2012]. Other studies have found similarly high concentrations of DOC in subsurface strata ranging between 50-100 mg/L [*Mann and Wetzel*, 1995] and 25 mg/L [*ElBishlawi and Jaffe*, 2015]. River topography was included in the 2D model.

A novel implementation of a bioclogging feedback mechanism was implemented in the MIN3P code. Bioclogging was simulated in MIN3P and simultaneously allowed for sequential parameter updates of the riverbed hydraulic conductivity Kc and the porosity ϕ. As the biomass grows, the physical pore space declines because of biomass growth which reduces Kc and ϕ. The bioclogging Colonies constitutive model relating biomass growth to permeability reduction was implemented in MIN3P with published parameters to simulate the feedback between biomass growth and parameter updates at each time step [*Thullner et al.*, 2002a, b]. Biomass accumulation was represented in the MIN3P model as a volume fraction of biomass occupying the pore space. At each time step, the new porosity (minus biomass) and the hydraulic conductivity was updated with the Colonies model which assumes an aggregated form of clogging preferentially in the pore-throats [*Thullner*, 2010]. Equations for

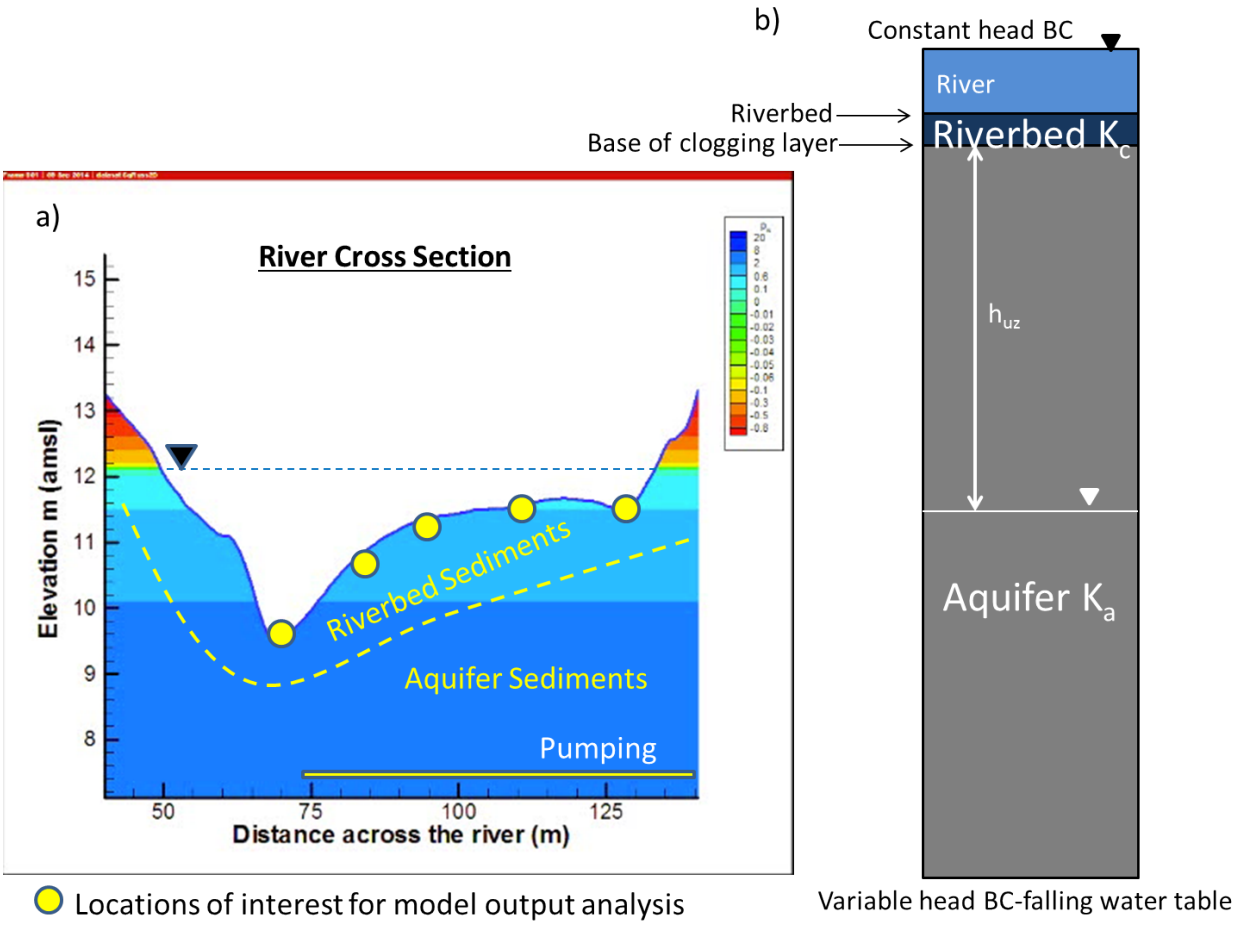

Figure 3.7: (a) Setup of the MIN3P model for the 2D cross-section. Note the large vertical exaggeration. Locations of interest are shown as the yellow dots. (b) Setup of the 1D MIN3P model. In both the 1D and 2D models, riverbed sediment with different porosities and conductivities overlie the aquifer sediments.

this procedure can be found in Chapter 2 Equations 2.6-2.8.

Modeling frameworks exist for microbial species across many different terminal electron accepting processes (TEAPs) in the redox sequence [*Thullner et al.*, 2007]. Using reactant terms, inhibition terms, and Monod kinetics, microbial growth can be specified as a function of the concentration of nutrient substrates and the concentration of microbial mass already in the system [*Murphy and Ginn*, 2000]. This method assumes a single step approach when partitioning organic carbon to dissolved inorganic carbon and biomass in the following

reaction for aerobic respiration shown in Equation 3.5:

$$3\,[CH_2O] + 2\,[O_2] \rightarrow 2\,[CO_3]^{-2} + 4\,[H]^{+} + Biomass \tag{3.5}$$

Organic carbon is assumed to be either in dissolved or particulate form. Carbon is the oxidized species and oxygen is the reduced-electron acceptor. Biomass growth through the oxidation of organic carbon through aerobes is expressed as the biomass term in Equation 3.5 and is represented by a ratio of C:H:O of 1:2:1. Carbonate thereafter undergoes a transformation to CO_2(g).

Biomass growth through the anaerobic degradation of organic carbon and nitrate by anaerobes is considered through the following equation where nitrogen is the electron acceptor (reduced species) and carbon is oxidized shown in Equation 3.6:

$$[CH_2O] + 0.8\,[NO_3]^{-1} \rightarrow [CO_3]^{-2} + 0.4N_2 + 1.2\,[H]^{+} + 0.4\,[H_2O] + Biomass \tag{3.6}$$

Parameter variation, gas production, feedbacks, and total water fluxes were measured and assessed across 100 stochastic water level simulations , 252 parameters sets, and 3 water level type groups. Two sets of models were run: 1) 1D models for their simplicity and to compare gas production across the 100 x 252 x 3 simulations. Once a subset of parameters were identified that produced seepage that best fit the field seepage data and represented the ENSO end-members, those groups of parameter combinations were used for the 2D modeling experiments.

1D Model: A 25 m long model was discretized with 0.1m spacing and two sediment layers representing the clogging layer and aquifer layer (Figure 3.7b). A constant head of 1m and DOC/DO concentration boundary condition of 40 and 11 mg/L respectively was specified on the top of the riverbed, and a variable head boundary condition was specified on the bottom with a flux concentration boundary. The variable head boundary condition on the bottom was populated with water table fluctuations from pumping induced disconnection. DOC concentrations were chosen based on previous studies suggesting carbon exhudation from algae growth can produce DOC subsurface concentrations ranging from 30-100 mg/L. Models were run for 1000 days.

2D Model: River topography was obtained from a GPS survey in 2012 and was used to create the deformed mesh for the 2D model (Figure 3.7a). Mesh discretization ranged from 0.1 m distance between nodes at the riverbed to 1 m at distances several km away from the pumping well. The left and bottom of the domain were specified as no flow boundary conditions representing bedrock. The upper boundary conditions were specified as a constant head to represent the river (the constant head is dependent on the location within the river), and constant concentration to represent the influx of substrates. The right far-field condition was specified as a constant head boundary representing the regional aquifer water table.

Pumping was introduced as several sink nodes that extend laterally underneath the river to represent the configuration of the pumping well that pumps evenly across many lateral pumps.

Bootstrapping the Pumping Periodogram

Stochastic water level fluctuations were implemented to represent natural and human based effects on regional and local water levels. Introducing stochastic water level fluctuations not only perturbs the model with drought and human based effects, but also introduces feedbacks in subsurface regions that experience periods of overlap between aerobic/anaerobic and wet/dry periods. Fourier series can adequately represent these fluctuations as a function of superimposed sin/cos curves that represent different dominant modes of pumping. The water level fluctuations are represented in the form:

$$y = -At + Bsin\left(\frac{2\pi t}{f_1}\right) + Csin\left(\frac{2\pi t}{f_2}\right) + Dsin\left(\frac{2\pi t}{f_3}\right) + ... \tag{3.7}$$

Where y is the water level at time t, A, B, C, D are coefficients, and f_1, f_2, f_3, are periods (days/cycle). The coefficient A represents the seasonal water table drop trend and can be conceptualized as fast or slow given climatic conditions for a particular year.

A time series block bootstrapping approach was implemented to estimate the parameters of the Fourier series (B, C, D, f_1, f_2, f_3) from the Wohler pumping time series from 2007-2015 [*Plant*, 2012] (Figure 3.8b). The block bootstrapping approach preserves the integrity of the correlation structure of the time series data. This method involves resampling blocks of data instead of sampling individual datapoints to calculate the periodogram of the given time series. The blocks of data were sampled randomly as well as the time span of each block sample. From each time-block, a periodogram was constructed and the dominant frequencies and amplitudes were extracted. The simulation was run 100 times to obtain 100 blocks of time series data, a periodogram was calculated for each block (representing the range of periodgrams in Figure 3.8a), and the dominant frequencies and amplitudes greater than a given threshold were extracted. From this I obtained 100 sample periods for peak 1 (f_1) and 100 sample periods for peak 2 (f_2) allowing calculation of a mean and standard deviation for these parameters from the probability density functions (pdfs) (Figure 3.8c,d). I excluded the seasonal frequency domain because I implement a trend on the stochastic fluctuations to represent the summer regional decline.

Generating the Water Level Fluctuations

From each of the peak frequency pdfs, 100 samples were randomly drawn from each pdf to use in Equation 3.7. Dominant frequencies ranged between a 15-30 day cycles. Water

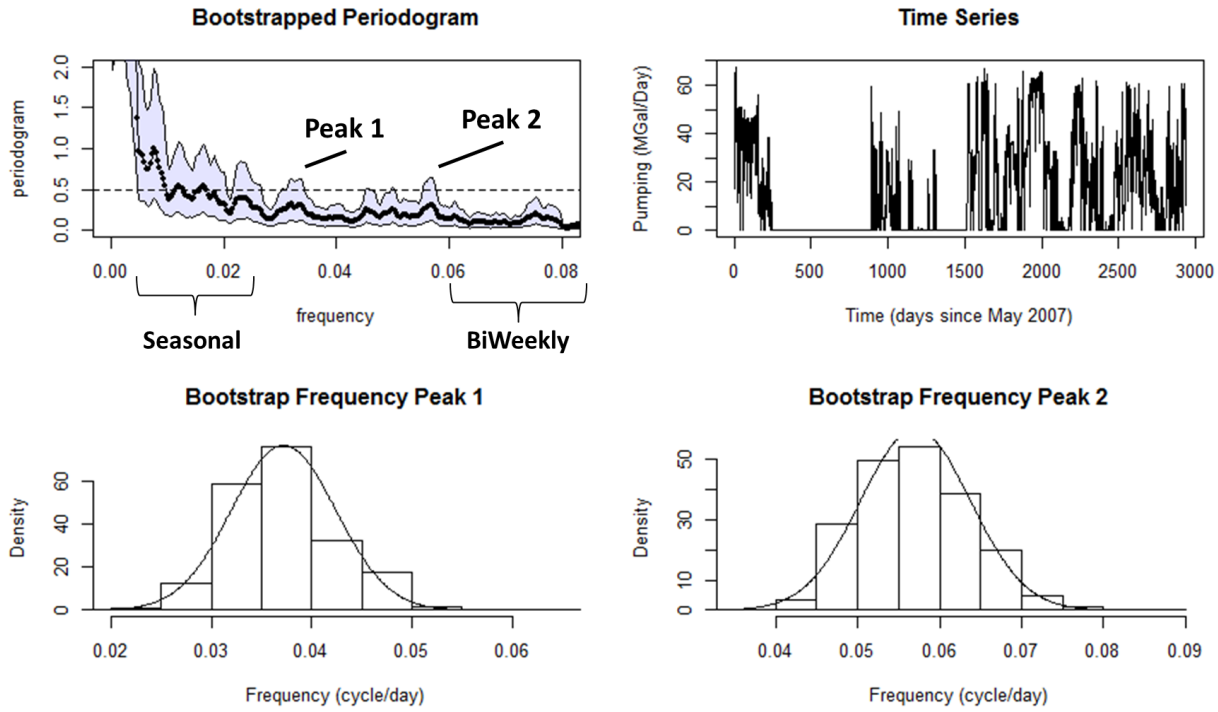

Figure 3.8: Block bootstrapped time series used to create the sampled periodograms. (a) For each periodogram, frequencies for the peaks in-between the seasonal and biweekly groups exceeding the threshold were extracted. (b) The pumping time series from 2007-2015. Each extracted frequency was used to estimate the pdf of values for (c) peak 1 and (d) peak 2. For example, the pdf for peak 1 is used to sample an f_1 value for use in Equation 3.7

levels were reconstructed as a function of the dominant frequencies superimposed on fast or slow regional water level drops to simulate drought and human based forcings. Fast and slow water regional water table drops (coefficient A) were sampled from a uniform distribution (100 samples of water table decline rates). Three types of long/term seasonal cycles were tested: 1) Case A: A water table that includes high frequency fluctuations and rises and falls seasonally in a triangular pattern, 2) Case B: A water table that drops and never recovers the original position with no water table fluctuations, and 3) Case C: A water table that rises and falls seasonally in a triangular pattern with no short term fluctuations. Example simulations with different frequencies and an overall trend are shown in Figure 3.9. These three types of simulations allow us to test how shorter term fluctuations from human induced pumping can affect the long-term stress of drought that overall can drop regional water tables.

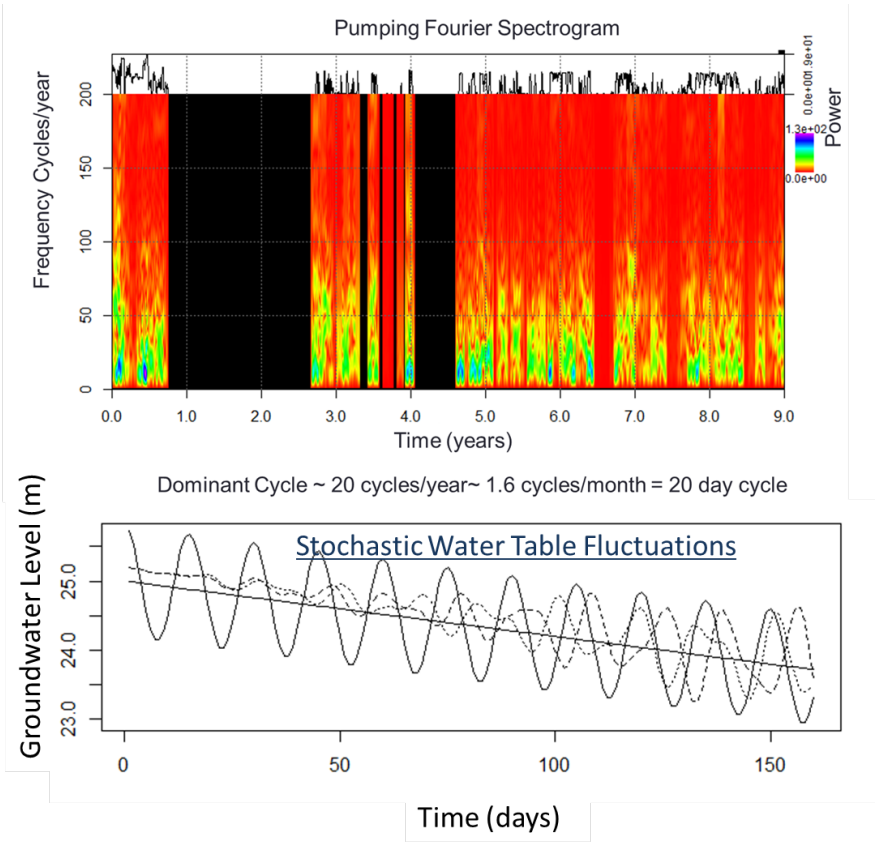

Figure 3.9: Water table decline over time with superimposed fluctuations. Water table can drop fast or slow, with large and small fluctuations superimposed.

Assessing the Feedbacks

Total infiltration fluxes, biomass growth, carbon consumption from aerobic respiration and microbial denitrification, and CO_2 and N_2 gas production were extracted from all 1D models and compared across the different ENSO end-member groups. I implemented the ENSO effects through variations in the initial values for Kc and ϕ with the end-member assumptions as described above. Five locations of interest along the riverbed representing a gradient of depths are the focus of the 2D models for assessment of preferential flow and larger scale feedbacks (Figure 3.7a).

3.4 Results & Discussion

Results are compared between the three different water table simulations: 1) Long-term drought representing a water table that drops and never recovers the original position, 2) An average neutral ENSO period where the water table rises and falls seasonally in a triangular pattern and includes shorter term fluctuations, and 3) A water table that rises and falls seasonally in a triangular pattern without short term fluctuations (this helps to isolate the effects of the fluctuations of redox-controlled memory effects in sediment strata).

Field Seepage Results

Field seepage estimated from DTS probes is shown in Figure 3.10. The grey lines show the range of values from the different thermal parameter combinations. The blue line represents an average with a 20-day moving window. Seepage generally increases and decreases representing the effect of the river initially undergoing disconnection followed by seepage declines from bioclogging. At the beginning of the summer (Time 0 in May), the infiltration is around 0, and shows that the river may be gaining in May and in November. In early May, pumping is not yet a dominant factor for infiltration at the site, and previous winter discharge may have provided enough bank storage that local water levels are higher than the river allowing the aquifer to discharge into the river. As the river undergoes disconnection, shown by the increasing trend in infiltration, nutrient fluxes are also enhanced leading to greater substrate delivery for microbes in the hyporheic zone. Approximately 100 days after fluxes increase, infiltration flux begins to decrease again from bioclogging feedbacks that clog pore-spaces and limit vertical infiltration. Large fluctuations in the seepage time series are assumed to be a function of pumping on/off cycles.

MIN3P Results Without Pumping Fluctuations

Modeled seepage is shown in Figure 3.11 as a function of many parameter groups with pumping fluctuations turned off. Larger aquifer (Ka) and riverbed (Kc) conductivities generally produce larger infiltration fluxes. Larger riverbed conductivities also lead to greater infiltration declines as biomass clogs the pore space. The larger infiltration fluxes with higher initial conductivities enhance the nutrient fluxes and leader to quicker bioclogging and infiltration decline compared to smaller conductivities. Smaller initial riverbed conductivities and smaller porosities generally show infiltration declines later as small nutrient fluxes limit substrates for biomass growth.

Bioclogging from aerobic respiration (AR) is shown in Figure 3.12 with the same parameter groups as in Figure 3.11. When initial Kc is large (green-lines), biomass clogs the pore space much earlier in time because of fast initial nutrient delivery for aerobic growth.

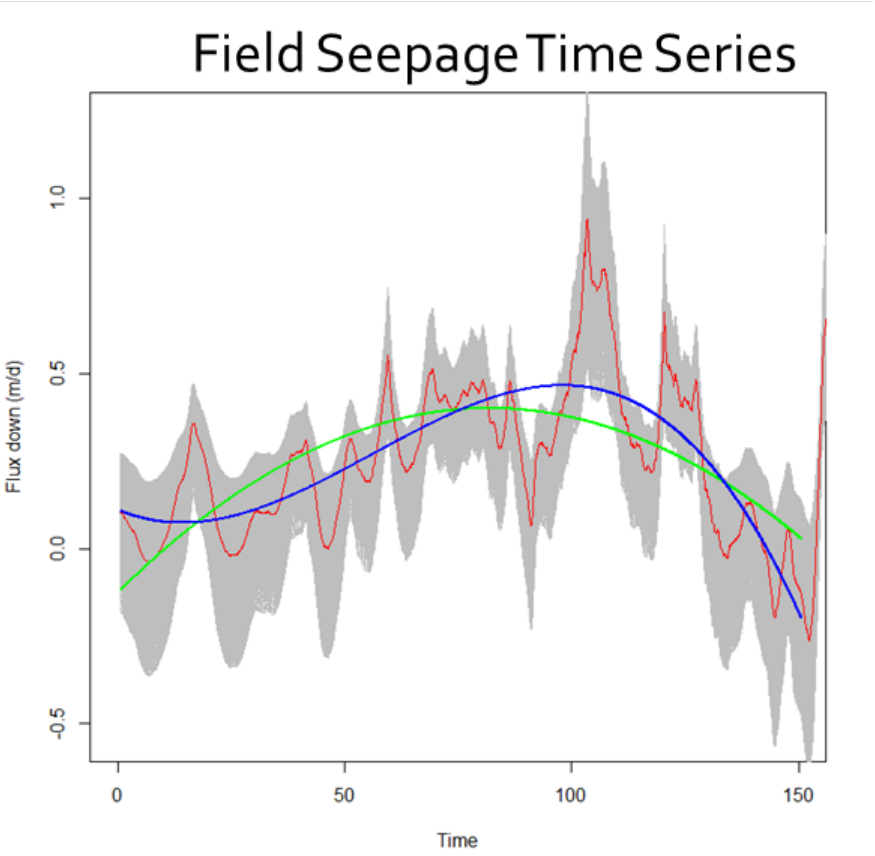

Figure 3.10: Field seepage data estimated from distributed temperature sensing probes. Day 0 occurs on May 30, 2012.

However, fast initial delivery of nutrient from high Kc initiates a feedback after sediments become clogged. This feedback limits nutrient delivery, and bioclogging from AR declines mid-way through the simulation because of nutrient limitations as infiltration declines (Figure 3.11). Bioclogging from AR in low Kc sediments (brown-lines, Figure 3.12) is limited because low Kc sediments do not sufficiently supply enough substrate to clog the range of porosities tested. The riverbed porosity value (ϕ) shows an apparent control on the timing of fully clogged sediments. When riverbed porosities are small (ϕ =0.17), full clogging begins around day 100, whereas when ϕ =0.29, full clogging occurs around day 250. The timing of fully clogged and non-fully clogged sediments is important and this determines how long nutrients are delivered to deeper sediment before infiltration declines and shuts-off transport. The implications of the timing of fully clogged sediments become important for anaerobic

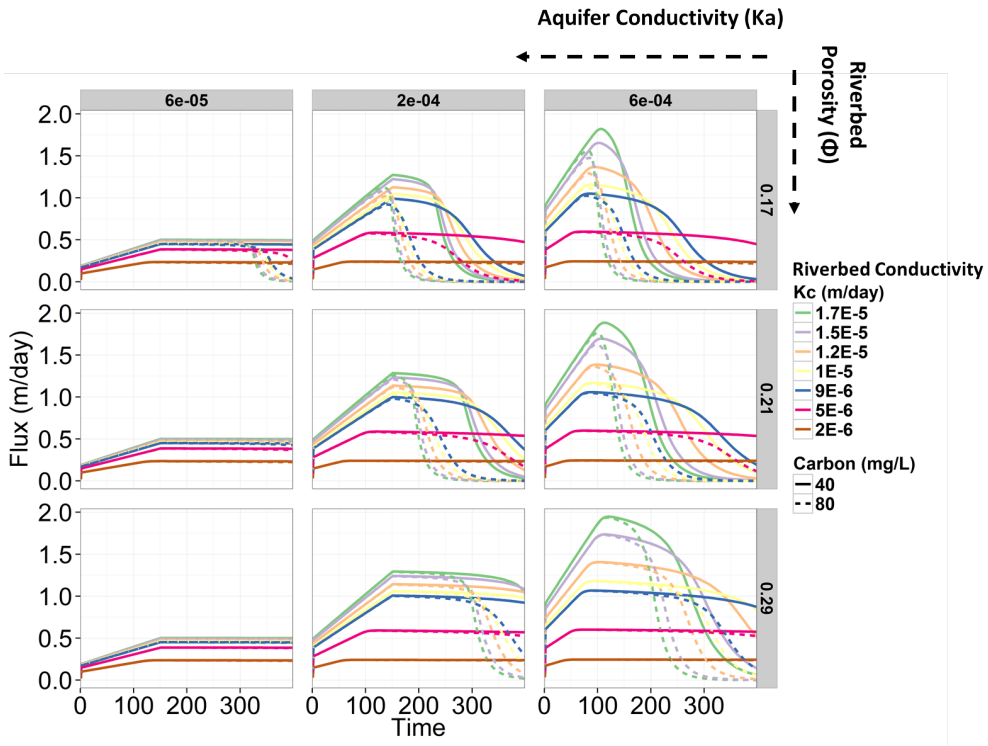

Figure 3.11: Infiltration fluxes over time for different combinations of parameters riverbed (Kc) and aquifer conductivities (Ka) and riverbed porosity. Aquifer conductivities are shown in the columns and riverbed porosities are shown in the rows, and riverbed conductivities are shown with different colors. Different incoming carbon concentration from the river water is shown as the dashed and solid lines.

reactions that rely on full O_2 consumption from AR and sufficient delivery of remaining DOC and Nitrate for DN to occur. Reaction rates for DN are also much slower than AR reactions and thus they need more time overall to consume similar amounts of DOC relative to AR. In low Kc riverbed sediments, Kc limits infiltration and nutrient fluxes which limits growth rates (based on Monod reaction terms) and biomass only grows enough to clog 50% of the pore space. Even though these types of sediments limit AR-based bioclogging, this configuration actually stimulates DN relative to higher Kc sediments that fully clog and limit bioclogging from DN.

Infiltration fluxes across the spatial gradient of the 2D model are shown in Figure 3.13. Infiltration varies between the model simulations depending on the initial riverbed sediment conditions (i.e. high porosity-high conductivity (high ϕ-high Kc) or low porosity-low conductivity (low ϕ-low Kc)). It is interesting to note that the initial sediment parameter

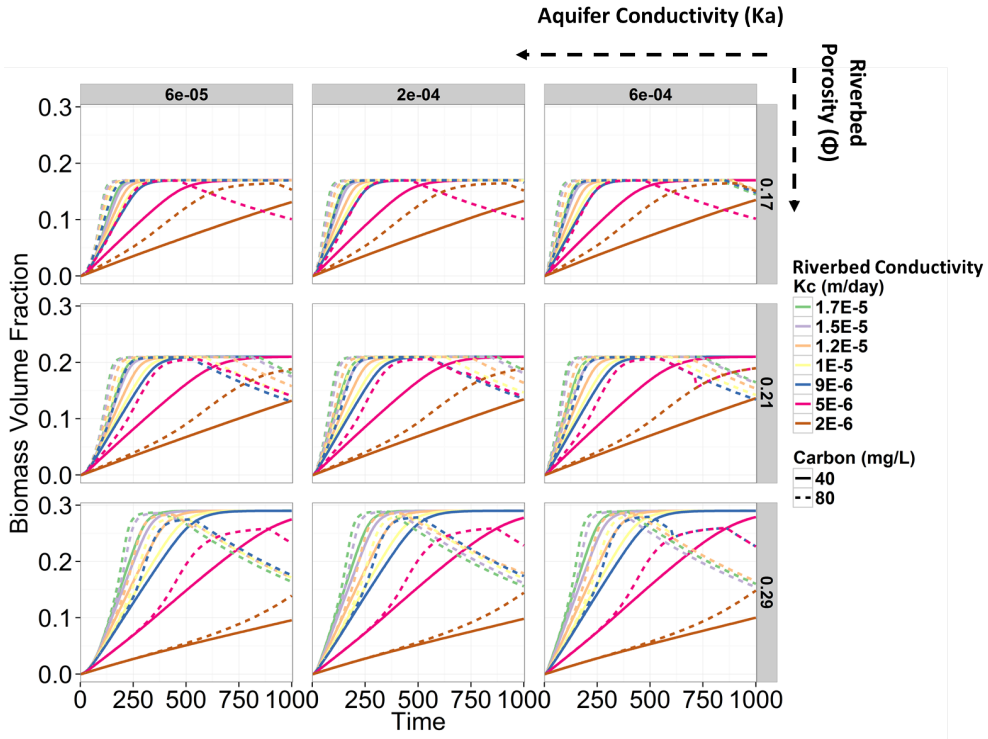

Figure 3.12: Biomass volume fraction from Aerobic Respiration (AR). Biomass volume fraction can be understood as the amount of space within the bulk sediment that is occupied by biomass. When riverbed porosityϕ =0.17, biomass grows until it reaches the maximum volume fraction which is equal to the porosity. When biomass reaches a volume fraction of 0.17, then the pore-space is completely full.

values determine whether or not the system will undergo disconnection. The strength of losing-connected or losing-disconnected conditions determines the rate of infiltration fluxes which governs nutrient delivery to the subsurface. The bank is the initial section to undergo disconnection in the low ϕ-low Kc sediment. This is shown by the initial infiltration rise and then bioclogging limitations to flux thereafter. As the water table drops, additional sections of the river begin to undergo disconnection and disconnection transitions from the bank to the thalweg. Hydraulic gradient increases leading to infiltration increases, and enhanced nutrient delivery to those sections allow pulses of additional high DOC and DO to enter the subsurface. Nutrient fluxes and reaction rates are directly proportional to infiltration rates thus the spatially variable infiltration contributes to spatially variable biomass growth and the development of bioclogging hotspots. In the high ϕ-high Kc sediment, infiltration fluxes remain larger overall, and more sustained throughout the simulation relative to the

low ϕ-low Kc case. When infiltration goes to 0, this indicates that sediments have become fully clogged after disconnection was reached.

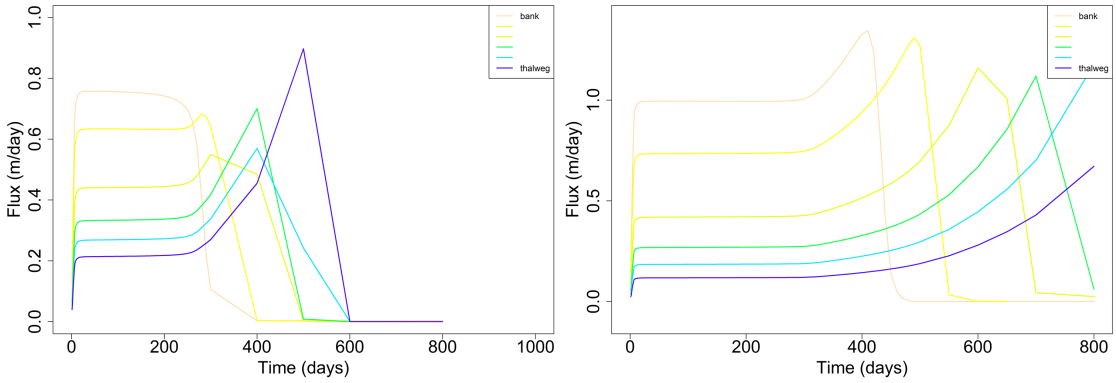

Figure 3.13: Infiltrations fluxes across the spatial gradient from the bank to the thalweg for the low ϕ-low Kc sediment (left) and the high ϕ-high Kc sediment (right).

Pressure head reduction below 0m leads to unsaturated zone growth beneath the riverbed. Pressure head reduction can be caused by drops in the water table due to pumping or from fully clogged sediments that shut off infiltration. In lowϕ-low Kc sediments (Figure 3.14), pressure reduction below 0 and full disconnection in the subsurface occurs at all locations from the bank to the thalweg, but at different times. The bank disconnects around day 200, while the thalweg disconnects around day 500. Once the unsaturated zone is established, no further pumping can increase infiltration and conductivity (a function of bioclogging) fully determines the rate of infiltration [*Newcomer et al.*, 2016]. In highϕ-high Kc sediments, the bank undergoes disconnection around day 400 which is much later than in lowϕ-low Kc sediments and the thalweg never undergoes disconnection. Because the highϕ-high Kc sediments never undergo disconnection, the infiltration rates are less susceptible to large changes in Kc relative to rivers-aquifers that have experienced disconnection. Hydraulic-gradient changes from declining water tables and temporal changes in Kc are competing factors governing infiltration fluxes. Infiltration fluxes can remain high (even if bioclogging occurs) if the system is always on the verge of disconnecting (shown by the infiltration peaks in Figure 3.13).

Total carbon consumption from AR and DN in the 100 stochastic models without water table fluctuations (Case B) are shown in Figure 3.15. Case B is when the water table drops and never recovers the original position. Carbon consumption from AR and DN is 2-3 times greater for higher porosity riverbed sediments. When comparing total carbon consumption between AR and DN, DN is always 2-3 times greater than AR. With larger initial riverbed Kc values, carbon consumption is greater because larger riverbed Kc sediment allow greater

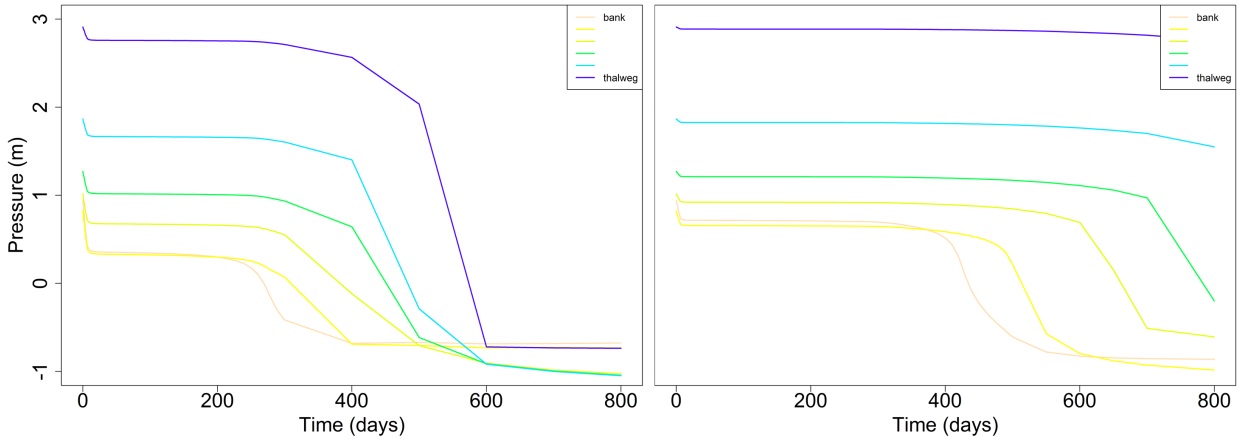

Figure 3.14: Pressure head showing the area of localized disconnection for the bank relative to the thalweg. The lowϕ-low Kc sediment (left) and the highϕ-high Kc sediment (right) are compared.

nutrient fluxes, allow AR to fully consume O_2 and initiate DN reactions in deeper sediments, and do not undergo disconnection. Comparing high Kc values across all porosities indicates that porosity has an even stronger control on carbon consumption because of the timing full bioclogging. Higher porosity sediments facilities longer times for full clogging to occur and allows substantially greater stocks of C and N to arrive at subsurface sediments where redox conditions are sufficient for DN to begin. Carbon consumption is proportional to the reaction rates for the AR and DN components which show that DN and AR carbon consumption and reaction rates are always higher for the highϕ-high K sediment.

MIN3P Results with Fluctuations: Fluctuations Hasten Infiltration Declines

Infiltration fluxes simulated from the MIN3P numerical model (Figure 3.16) reproduce the infiltration fluctuations found in the field data (Figure 3.9). Once the river becomes disconnected, the infiltration rate is only influenced by the water table if it periodically re-connects, shown by the peaks in infiltration after the main peak around day 90. The peak of the infiltration fluxes, indicating full disconnection has been reached is hastened for higher riverbed Kc sediments. In the case of high initial riverbed Kc, the infiltration decline occurs almost 100 days earlier compared to the lower conductivity case. The larger Kc sediments allow much greater nutrient fluxes and reaction rates, and lead to overall greater bioclogging feedback effects compared to lower Kc sediments. Notice that the final infiltration

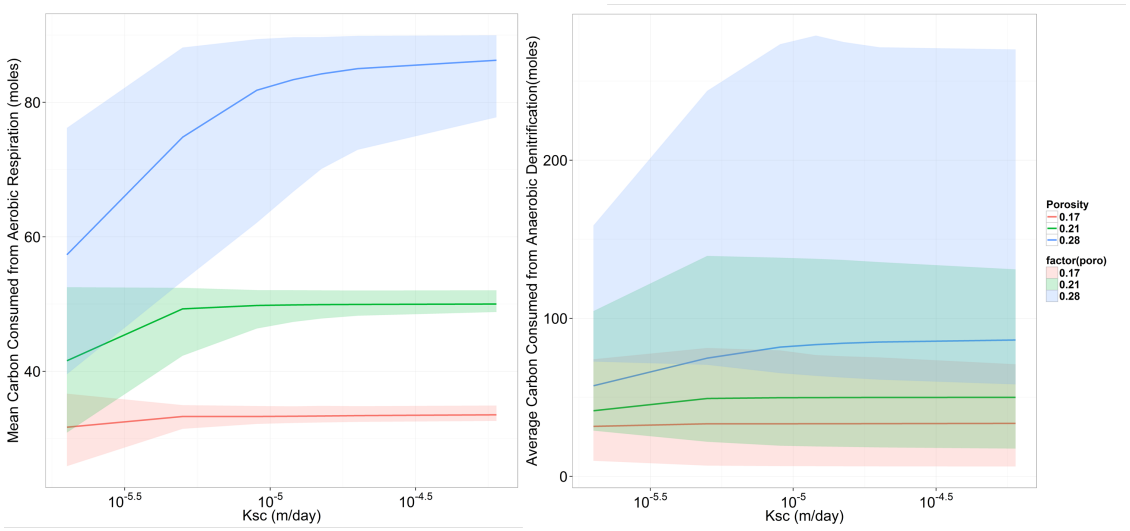

Figure 3.15: Total carbon consumption from the sum of AR and DN across parameter sets for results without water table fluctuations (Case B). Mean consumption is shown by the solid line and the 5% and 95% percentiles are shown by the bounded shaded region across the many water table decline simulations (without fluctuations).

for the higher conductivity sediment is lower compared with the lower conductivity sediment indicating that bioclogging feedback effects are much more pronounced when sediments are initially allowed to clog fast.

Maximum average rates of AR and DN are shown in Figure 3.17 for the different water table fluctuation cases. Case A represents the high-frequency fluctuations. Respiration rates for both AR and DN are greater for highϕ-high Kc sediment cases and are generally greater for the Case A- when the water table is highly fluctuating. Lowϕ-low Kc sediments also show much reduced DN rates compared with the highϕ-high Kc sediment case. Even though DN rates are lower in the lowϕ-low Kc sediments, this does not inhibit growth from anaerobic microbes or their ability to clog pore spaces, only that their growth, on average, was slower over the entire simulation. Respiration rates are proportional to infiltration rates, and increase as infiltration rates increase while undergoing disconnection. Higher respiration rates in general lead to greater gas production over a simulation period. Case B and Case C represent water table simulations that only decline, or simply rise and fall seasonally respectively. These cases lack the high frequency fluctuations from Case A. AR rates for Case B and Case C are always lower than Case A, and this occurs across all porosity values. Fluctuations have the effect of increasing the AR reaction rate across all porosities and conductivities. This occurs because the water table fluctuations allow the infiltration rate

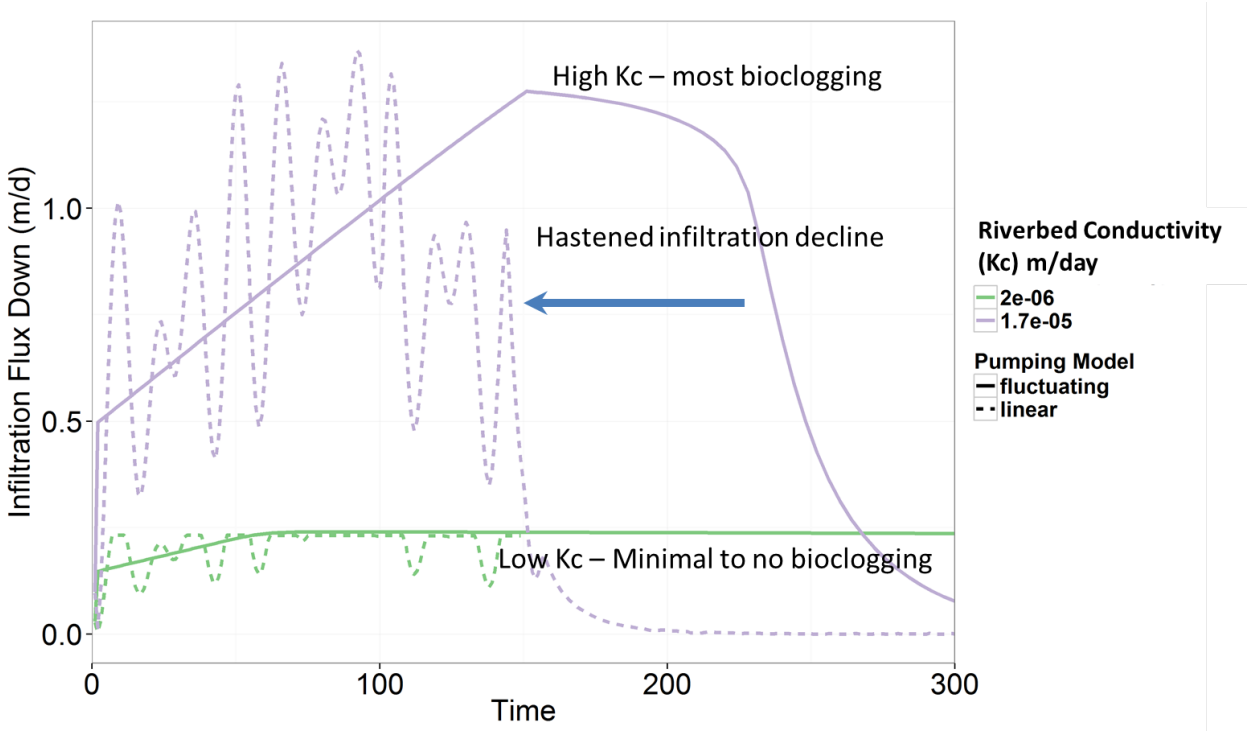

Figure 3.16: Infiltration is shown for the lowest porosity ϕ=0.17 for one water table realization.

to fluctuate about the linear trend (Figure 3.16), which have a great feedback effect on the nutrient bursts that stimulating additional microbial reactions.

Fluctuations Limit Clogging at the Surface

The percent of pore-space filled by AR and DN is shown in Figure 3.18 and 3.19 as a function of porosity, Kc, two different depths, and type of fluctuation model. Aerobic bioclogging increases as the sediment hydraulic conductivity increases. This occurs because of increased nutrient fluxes. AR biomass represents a greater fraction of the pore-space for high-Kc sediment. Highϕ-high Kc sediments also show less overall clogging by AR relative to smaller ϕ counterparts. This is because, the same volume of biomass will occupy different % of the pore-space given different porosities. Anaerobic bioclogging, however, is enhanced in lower conductivity sediments, and is larger in high ϕ sediments. Biomass from DN occupies a smaller % of the pore-space relative to AR, however shows an opposite trend with Kc compared to AR biomass. DN clogs a significantly smaller percentage of the pore space in

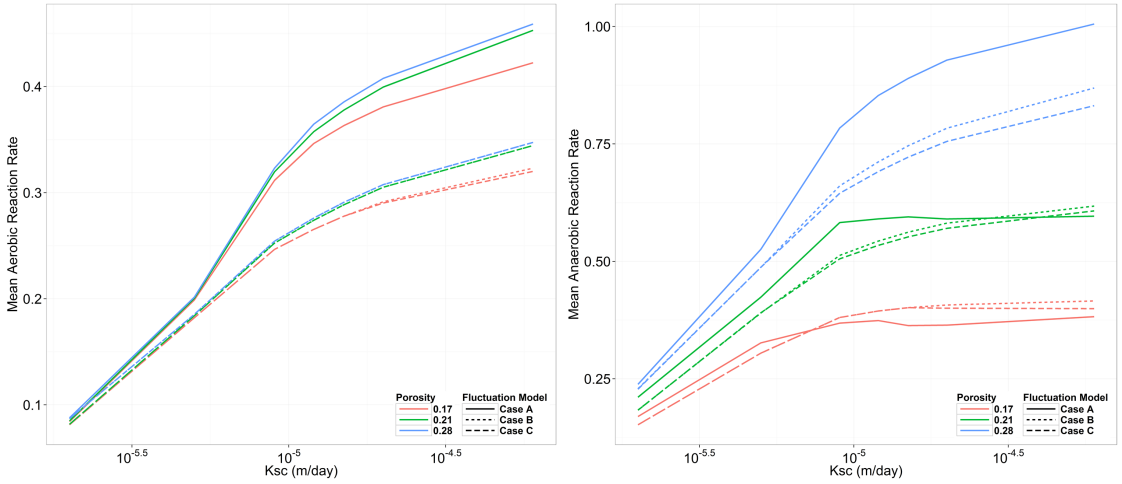

Figure 3.17: Mean growth rates for AR and DN across the different water table fluctuation models and porosity/conductivity values.

high-Kc sediments and decreases as Kc increases. Anaerobic bioclogging is enhanced in those sediments because all O_2 is consumed quickly from aerobic clogging, and infiltration fluxes are not fast enough to move O_2 water downward. Since O_2 is the limiting substrate, DOC is not fully consumed by aerobic respiration and is subsequently consumed by anaerobes in the next sediment layer. Relative biomass as a percentage of the pore space occupied is shown in Figure 3.18. While aerobic microbial production is generally greater in larger conductivity and porosity sediment, the overall percentage of the pore space they occupy is less compared with lower conductivity and porosity sediments. Comparing just one value of conductivity, for example, similar flow rates allow the same nutrient flux and the same biomass growth. However, similar volumes of biomass growth take up a greatly different percentage of the pore space. Since they occupy different relative volumes, this changes the updated values of conductivity predicted by the Colony constitutive model and feeds-back into differences in the flow rate at the next time step. While their initial conductivities may be the same, their initial porosity governs the conductivity update and the clogging update at each time step as the pores clog.

Biomass deeper in the sediment column beneath the river experiences different redox conditions and different trajectories of biomass growth depending on the sediment parameters and on the water table simulation type (Figure 3.19). AR biomass shows enhanced growth in higher conductivity sediments, but biomass in high ϕ sediments occupies lower relative space compared with low ϕ sediments. DN biomass shows increases with Kc for high ϕ sediments, but decreases with Kc for lower ϕ sediments. Cases without water table fluctuations (Case B

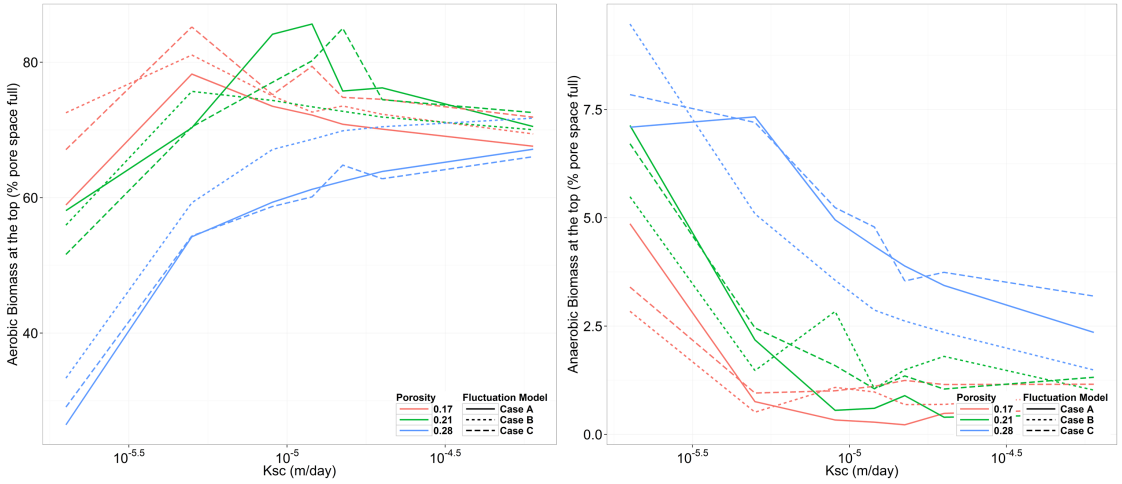

Figure 3.18: Bioclogging histograms at the top of the column where maximum bioclogging from aerobic and anaerobic growth occurs.

and Case C) generally show slightly greater biomass compared to Case A with fluctuations.

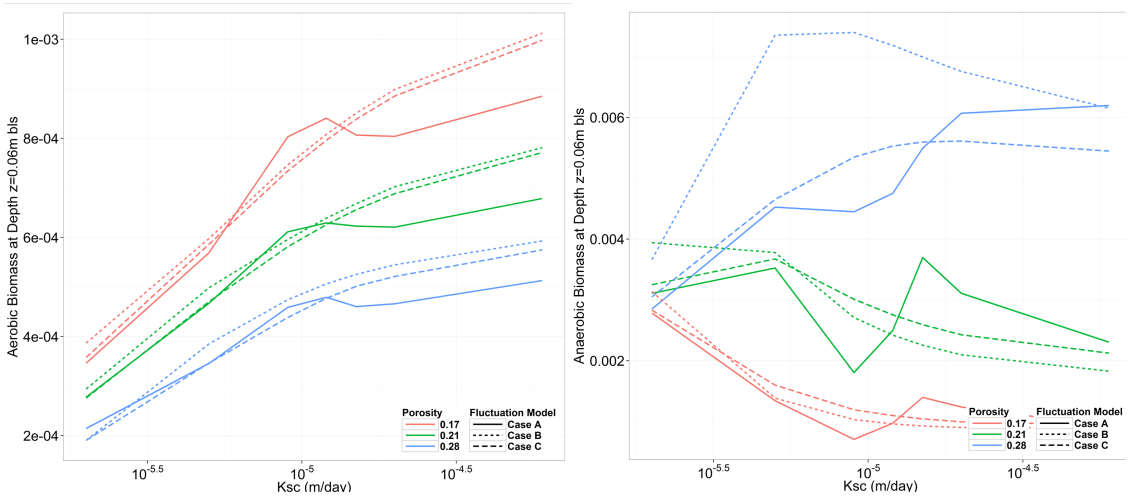

Figure 3.19: Bioclogging from AR and DN comparing cases with and without fluctuations for deeper sediments at 0.06m below the zone of maximum clogging.

Total carbon consumption from AR and DN in the 100 stochastic simulations with water table drops and fluctuations are shown in Figure 3.20. Magnitudes of the total carbon consumption are similar to those without fluctuations; with noticeable differences in the

mean values for DN. Mean values for DN are generally lower compared to the case without fluctuations (Figure 3.15).

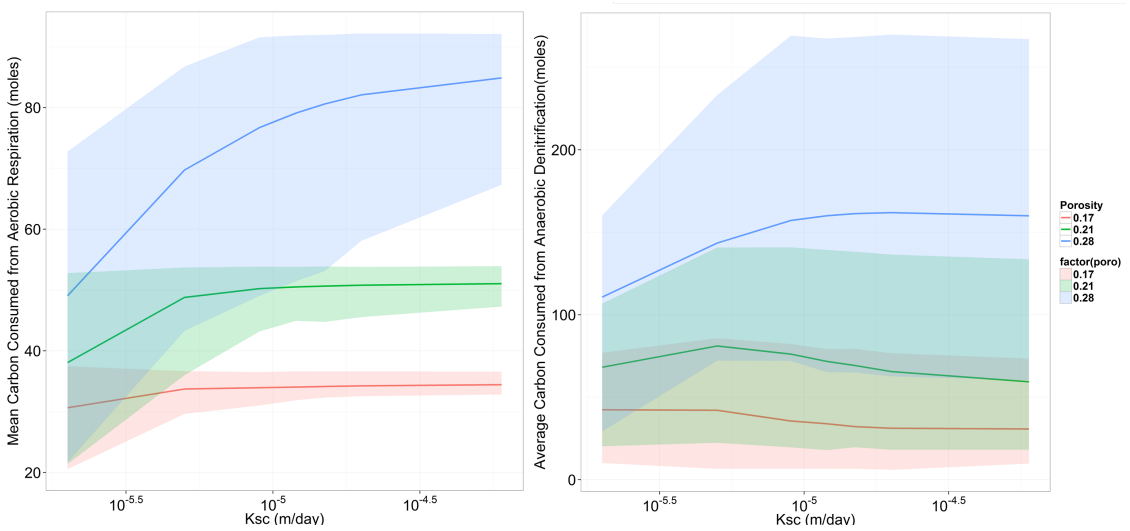

Figure 3.20: Total carbon consumption from the sum of AR and DN across parameter sets for results with water table fluctuations.

Sediment Effects on Gas Production

Gas production of CO_2 and N_2 as a by-product of AR and DN bioclogging varied significantly between the sediment parameter cases. Higher conductivity sediments typically produce 2-3 times the CO_2 relative to the lower conductivity counterpart (Figure 3.21). This occurs for a few reasons. In the lower conductivity sediment, infiltration fluxes are generally lower limiting nutrient fluxes. Limitations to nutrient fluxes also limit the Monod growth rate term. Biomass growth is slower overall, and while biomass can still grow and clog the pore-spaces, total nutrient transformation and carbon consumption over the entire 900 day simulations is 30% relative to the higher conductivity sediments. In the higher conductivity sediment, biomass grows fast, and while infiltration is limited after biomass fully clogs, microbes are still consuming O_2 and DOC to maintain current populations. The growth rate term is maximized when biomass fully occupy the pore space. Infiltration declines cause nutrient limitations to microbial communities and thus biomass clogging begins to decline. This does not indicated that microbes have stopped consuming O_2 and DOC, only that the rate of consumption is smaller than when at fully capacity.

Gas production differences between Case A and Case B water table schemes are shown in Figure 3.21. Wet-year end-member cases with high porosity-well sorted sediments (highϕ-

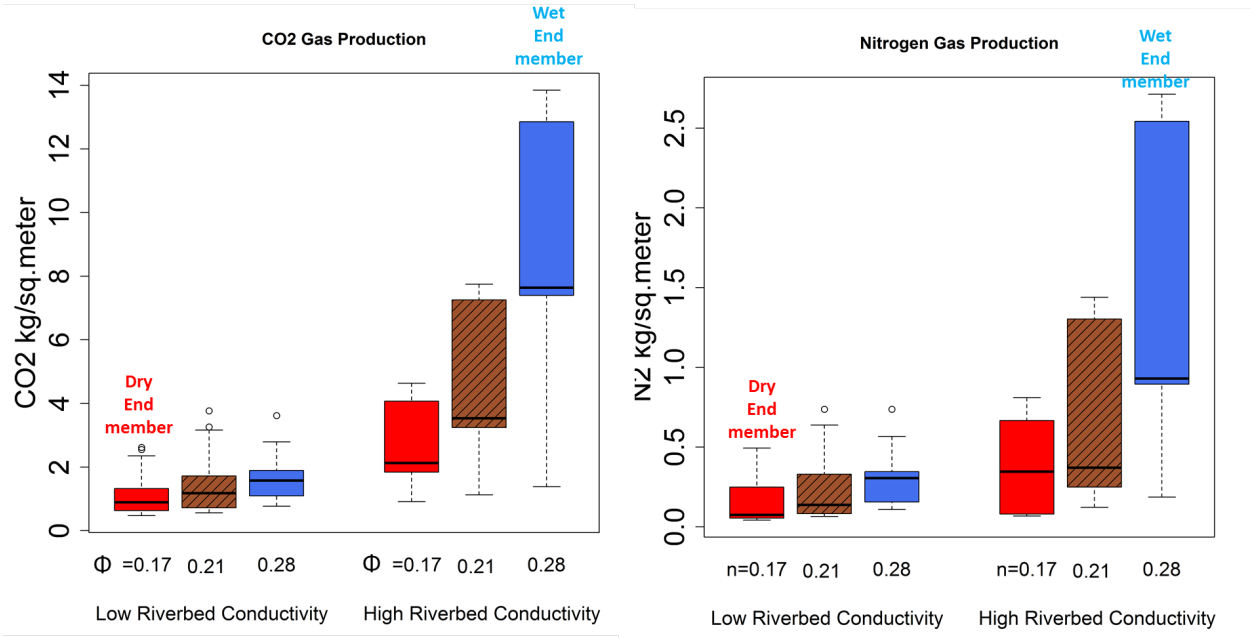

Figure 3.21: CO_2 and N_2 gas production as a function of riverbed Kc and riverbed porosity ϕ.

high Kc) show the most gas production independent of whether the water table was fluctuating or not. Dry-year cases sediments (lowϕ-low Kc) however, show strong pumping fluctuation controls on total biogenic gas production. The differences may emerge from whether the sediment configuration allows disconnection or not. When the sediment configuration allows disconnection to occur (mainly the lowϕ-low Kc cases), any bioclogging and Kc reductions have a strong influence on infiltration. In the dry-year case, when long-term draw-down occurs (case without pumping fluctuations), infiltration and nutrient fluxes are maximized until bioclogging limits it. In those cases, even while the system is fully connected, infiltration is steady and large. When pumping introduces water table fluctuations, infiltration oscillates from high to low which facilitates and deprives substrates to microbes. Substrate deprivation limits total reactions at the surface where AR occurs and in deeper sediments that no longer receive nutrients.

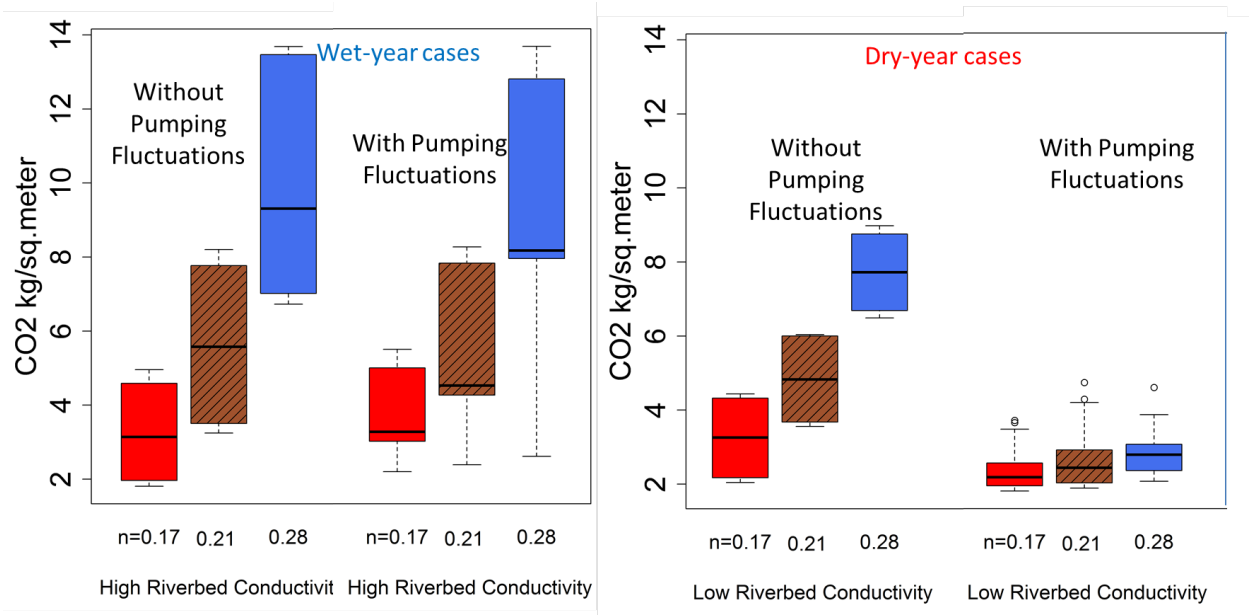

Figure 3.22: Carbon dioxide gas production shown with and without fluctuations for the high K (left) and low K (right) cases.

Sediment Effects on Spatial Gradients of Bioclogging in a 2D Profile

The distribution of aerobic biomass across the spatial gradient from the bank to the thalweg is shown in Figure 3.23. On the bank of the LN end member with lowϕ-low Kc sediment, the pore-spaces become fully clogged on the bank much earlier than the thalweg. In the lowϕ-low Kc riverbed sediments, the bank undergoes disconnection much earlier in time than the thalweg allowing infiltration rates to always be greater on the bank. Greater infiltration rates keep nutrient fluxes, and growth rates high leading to greater overall bioclogging. In the highϕ-high Kc end member the sediments show biomass growth but they do not become fully clogged and much less of the total pore space contains biomass compared to the lowϕ-low Kc sediments. In the highϕ-high Kc end-member case, the subsurface from the bank to the thalweg undergoes the disconnection process, but never shows a fully developed unsaturated zone or full disconnection. However, even though the hydraulic gradient between the river and aquifer is small compared to the lowϕ-low Kc case, the initial conductivities in the highϕ-high Kc are sufficient to maintain higher infiltration rates relative to the lowϕ-low Kc case. With high growth rates in the highϕ-high K case all of the O_2 is consumed facilitating anaerobic biomass growth.

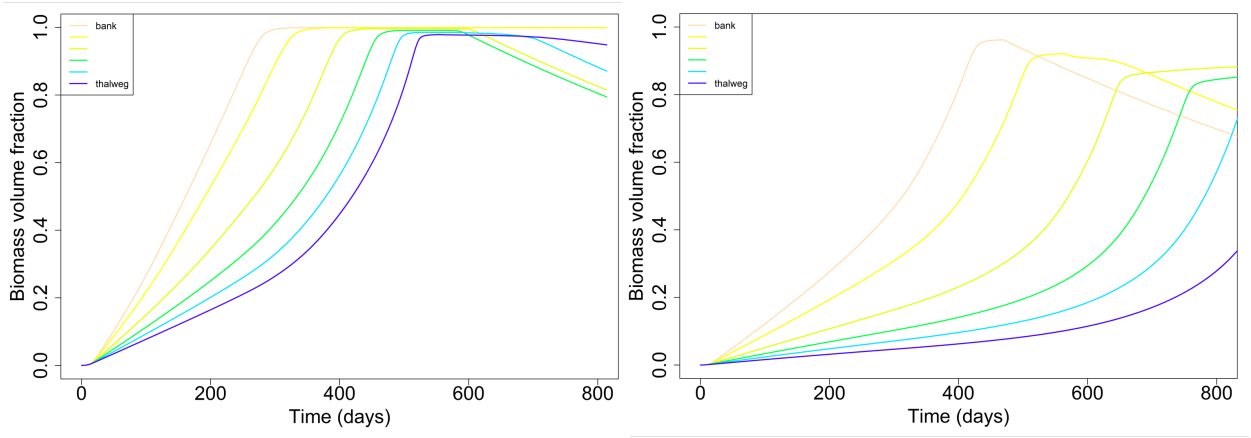

Figure 3.23: Aerobic biomass growth across the spatial gradient for both of the end-member cases. Low ϕ-low Kc sediment (left) and the high ϕ-high Kc sediment (right).

Anaerobic bioclogging is shown in Figure 3.24 across the spatial gradient from the bank to the thalweg. Anaerobes contribute to a much higher percentage of the pore space in the highϕ-high Kc sediment case. This is consistent with the previous figures that show these sediments have the higher infiltration rates, highest growth rates, and fastest consumptions of the limiting substrate O_2. Once O_2 becomes limiting, conditions are favored for anaerobic growth. Disconnection and unsaturated zone development become an important factor here and this is observed in the differences between the bank and thalweg between the two end-member cases. In the lowϕ-low Kc sediment, the bank is the first to disconnection and the show maximum AR bioclogging. All O_2 is consumed and anaerobic bioclogging begins. However, infiltration declines because of bioclogging limitations on conductivity suppress nutrient fluxes such as DOC for subsurface anaerobes. In the thalweg, infiltration fluxes increase because the thalweg begins to undergo disconnection increasing infiltration, growth rates and nutrient fluxes. Initial volume fractions of aerobic and anaerobic biomass accelerated the effect of disconnection in the thalweg that allowed microbes to make full use of incoming nutrient fluxes. In the highϕ-high Kc sediment case, an opposite distribution pattern occurs. Neither the bank nor the thalweg disconnect, but infiltration rates are high because of large conductivities. This allows AR to fully consume all incoming substrates and for bioclogging to occur, but aerobic biomass never clogs 100% of the pore space which allows fluxes to continue to deeper layers stimulating anaerobic clogging.

Modeled aqueous oxygen concentrations are shown in Figure 3.25 ranging from blue (oxic) to red (anoxic). Oxygen concentrations are compared between the lowϕ-low Kc and highϕ-high Kc simulations. The initial porosity has a very strong spatially distributed effect on the subsurface dissolved oxygen concentrations at late and early times. When the riverbed

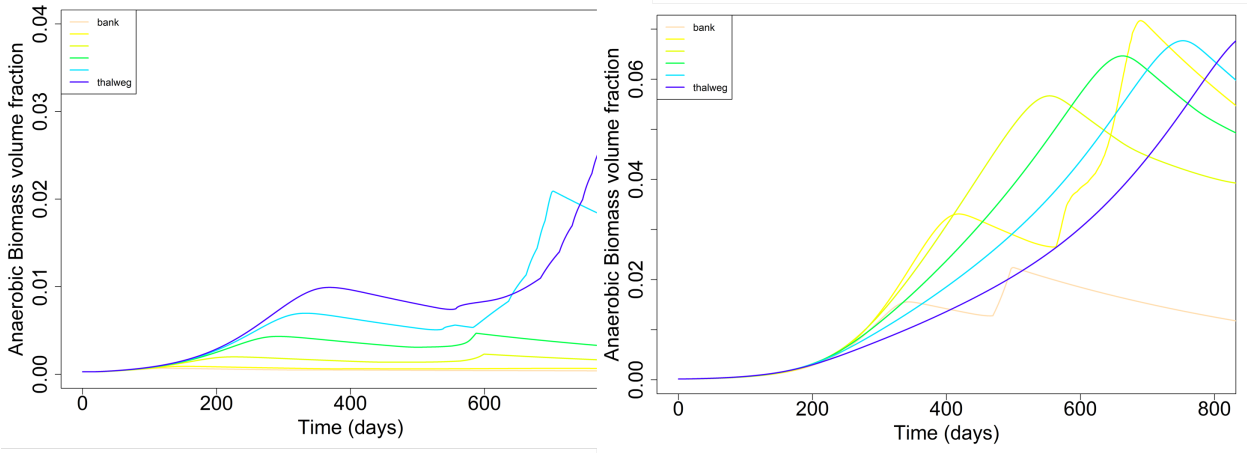

Figure 3.24: Anaerobic biomass growth across the spatial gradient for both of the end-member cases.

sediments have lowϕ-low Kc, oxic zones of incoming water shift as the system undergoes disconnection. The thalweg undergoes disconnection at a later time compared with the bank which undergoes disconnection first. As the region of maximum infiltration shifts from the bank to the thalweg, high O_2 water follows, but AR accelerates and quickly consumes the incoming O_2 after the maximum infiltration is reached. As microbes consume nutrients, O_2 is quickly consumed and the region becomes anaerobic again. When the riverbed sediments have highϕ-high Kc, the entire subsurface is anaerobic and oxygen is completely depleted even though the sediments are not fully clogged. All sediments from the bank to the thalweg are growing at the maximum growth rate, and infiltration increases from any addition hydraulic gradient increases from disconnection will not supply any additional nutrients. Microbes are consuming all O_2 which is the limiting substrate and provided maximum DOC fluxes to anaerobic microbes.

Carbon dioxide gas production follows a similar trend; higher growth rates and fully losing-connected conditions produce a more even distribution of carbon dioxide gas production in the highϕ-high Kc case (Figure 3.26). Interestingly, in the low porosity simulation, biomass growth was concentrated in the zone along the bank where the sediments had undergone disconnection early in the simulation. The bank is the shallowest section of the river and also the first to disconnect from the aquifer, and produces the highest concentration of CO_2 gas. Since bioclogging in the thalweg was quite low during the initial time when the bank was undergoing disconnection, microbial growth rates in the thalweg remained low until the infiltration starts to increase from the transition from connected to disconnected conditions. The growth rates are proportional to the infiltration rate and do not increase

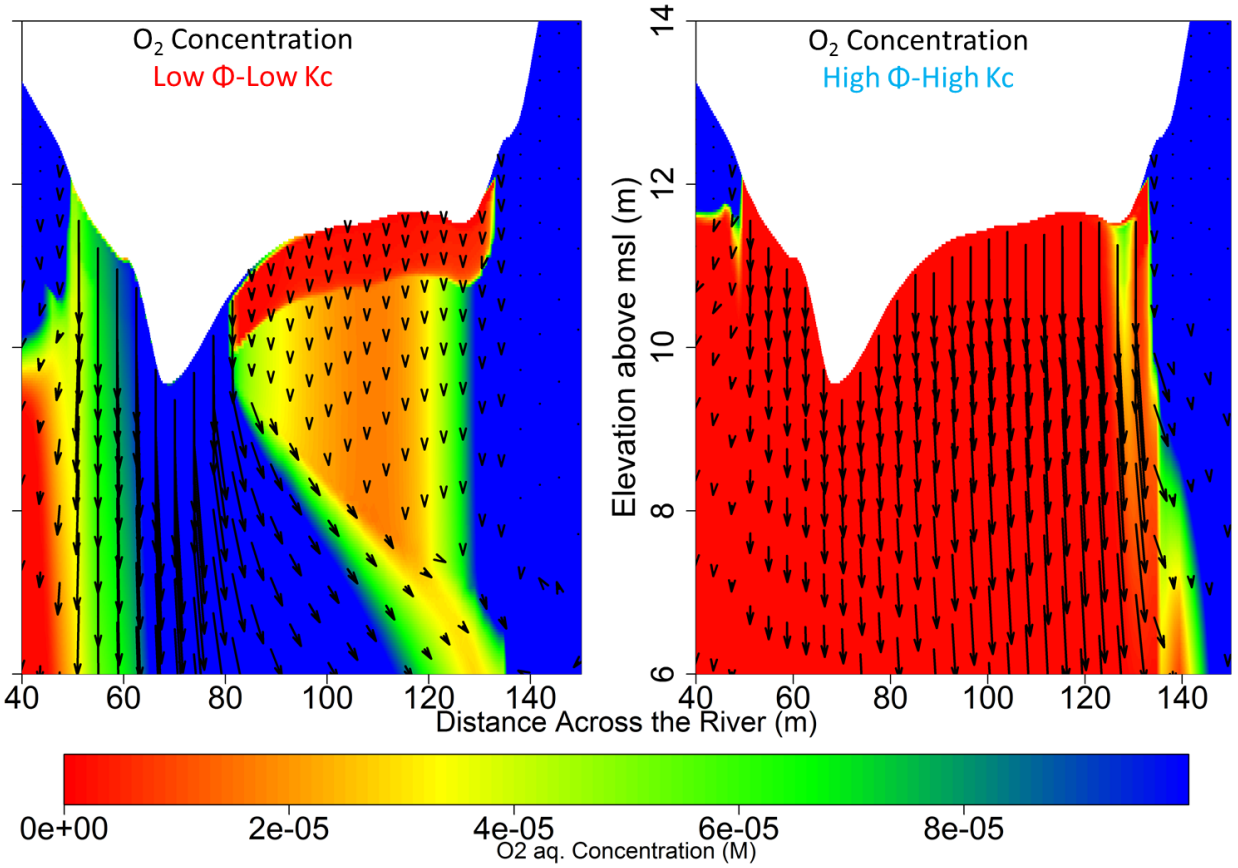

Figure 3.25: Oxygen concentration across the spatial gradient for both of the end-member cases.

until additional sections of the river undergo disconnection. The sudden rise in infiltration allows a larger nutrient flux before growth rates catch up to fully consume the incoming nutrients. After the thalweg is at maximum losing conditions, the growth rate of microbes in the thalweg begins to increase and fully consume incoming nutrients.

3.5 Discussion

Many conceptual models of riverbed bioclogging and river-aquifer interactions are compared in this research: 1) Dry-year end-members with Lowϕ-low Kc sediments versus wet-year end-members with highϕ-high Kc sediments, 2) A river undergoing disconnection and a river remaining connected, and 3) Top-down water table fluctuations that are conceptualized

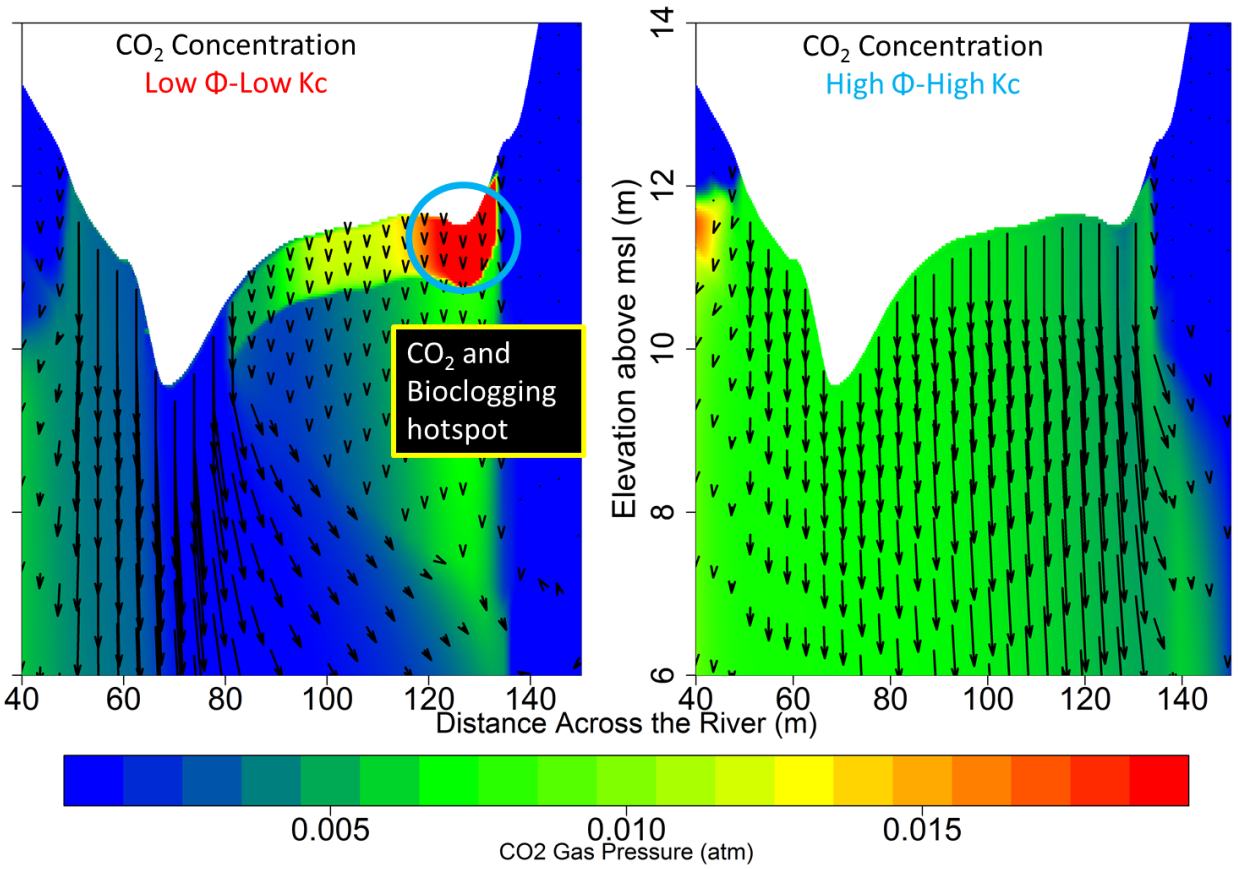

Figure 3.26: Carbon dioxide the spatial gradient for both of the end-member cases.

as a function of climate and anthropogenic causes.

In general, losing rivers representative of river characteristics that have highϕ-high Kc sediments (i.e. wet-year end-member) have larger total infiltration fluxes and overall greater carbon cycling than losing-connected rivers. Rivers showing characteristics of the wet-year end member favor higher infiltration rates, deeper bioclogging, greater C consumption, and greater overall C and N transformations that lead to biogenic gas formation. Rivers showing characteristics of the dry-year end member favor complete river-aquifer disconnection, lower infiltration rates, shallow and quicker bioclogging, less C consumption, and less overall C and N transformations that lead to biogenic gas formation. Connected and disconnected rivers show major differences in biogenic gas production. Under the same pumping rate, rivers remaining connected (highϕ-high Kc) allow nutrient fluxes to continue. In those cases, pumping does not induce disconnection, but rather only when the sediments fully clog the pore space do unsaturated conditions develop in the aquifer. Full bioclogging does not always

imply maximum biogenic gas production and our results show that this result in highly dependent on the connection conditions governing infiltration. In some cases, infiltration is sufficiently reduced such that new bioclogging in deeper layers is inhibited limiting C and N transformations. Organic matter processing rates in highly losing rivers are estimated around 70 mg of organic matter per liter of infiltrating water (35g /m^2/day) [*von Gunten et al.*, 1994].

Sediment effects were shown to significantly affect N2 and CO2 production and total N and C consumption. Lowϕ-low Kc sediments were most prone to becoming fully clogged early on, but highϕ-high Kc were most hospitable for later and deeper bioclogging contributing to greater cumulative N and C consumption. This result is in line with findings from [*Garcia-ruiz et al.*, 1998] who found denitrification occurring in large grain size sediment and in anaerobic microcosms of oxic zones in downstream areas of a catchment. They hypothesized that finer sediments contributed to higher rates of denitrification in downstream sediments, however it is possible that this effect is instead a function of the better sorting at downstream sites leading to greater porosity.

3.6 Conclusion

A numerical investigation was conducted to study the interactions, feedbacks, and dependence of bioclogging, and C and N consumption on initial conditions of the riverbed representing wet-year and dry-year end members in Mediterranean rivers. This work provides insights into how coupled biological and physical processes at river beds influence two critical ecosystem services: 1) denitrification in the subsurface, and 2) net primary productivity in rivers through subsurface aerobic respiration. I quantify the subsurface contribution to river NPP and denitrification driven by sources of C and N from local and upstream sources which is used as a substrate for subsurface growth. Subsurface heterotrophic respiration has played an unknown role in total C and N budgets, and this study attempts to describe, in mechanistic terms, the controlling factors for heterotrophic growth. The role of the hyporheic zone in the C and N cycle, and the conditions under which subsurface microbial growth occurs, I show influences the partitioning of C and N into CO_2 and N_2 which is overall less likely for sequestration through net burial and longer term C removal. The balance between these processes has a major influence on the role of rivers in carbon cycling.

I used a modeling framework that was cognizant of the biological-physical feedbacks in the river bed, that explored different initial conditions in terms of DOC/POC availability and sediment characteristics, and accounted for stochastic variability in substrate aerobic and anaerobic conditions induced through water table fluctuations. I find that the role of a river in mediating these fluxes is not static over time, but instead arises from the interplay of biological and physical processes within the hyporheic zone which together control the

transport of water and N and C substrates to microbiological communities, the size of the community itself which controls the permeability and porosity characteristics of the river bed, and the resulting development and cycling between aerobic and anaerobic conditions in the subsurface. I found that these dynamics leading to N and C consumption and biogenic gas production are strongly mediated by flow conditions prior to the major growing season which supplies DOC to subsurface microbes. This feedback is a response to top-down controls from the Mediterranean climate that controls the wet-season and dry-season river dynamics, that under high flow conditions can reshape the bed, changing ecological conditions that alter water column primary productivity, and changing sediment conditions and thus initial permeability and porosity.

Bibliography

Aalto, R., L. Maurice-Bourgoin, T. Dunne, D. R. Montgomery, C. A. Nittrouer, and J.-L. Guyot (2003), Episodic sediment accumulation on Amazonian flood plains influenced by El Nio/Southern Oscillation, *Nature*, *425*(6957), 493–497, doi:10.1038/nature02002.

Andrews, E. D., and R. C. Antweiler (2012), Sediment Fluxes from California Coastal Rivers: The Influences of Climate, Geology, and Topography, *The Journal of Geology*, *120*(4), 349–366, doi:10.1086/665733.

Baker, M. A., C. N. Dahm, and H. M. Valett (1999), Acetate retention and metabolism in the hyporheic zone of a mountain stream, *Limnology and Oceanography*, *44*(6), 1530–1539, doi:10.4319/lo.1999.44.6.1530.

Batlle-Aguilar, J., Y. Xie, and P. G. Cook (2015), Importance of stream infiltration data for modelling surface watergroundwater interactions, *Journal of Hydrology*, *528*, 683–693, doi:10.1016/j.jhydrol.2015.07.012.

Battin, T. J., K. Besemer, M. M. Bengtsson, A. M. Romani, and A. I. Packmann (2016), The ecology and biogeochemistry of stream biofilms, *Nature Reviews Microbiology*, *14*(4), 251–263, doi:10.1038/nrmicro.2016.15.

Beard, D. C., and P. K. Weyl (1973), Influence of Texture on Porosity and Permeability of Unconsolidated Sand, *AAPG Bulletin*, *57*(2), 349–369.

Boadu, F. K. (2000), Hydraulic Conductivity of Soils from Grain-Size Distribution: New Models, *Journal of Geotechnical and Geoenvironmental Engineering*, *126*(8), 739–746, doi:10.1061/(ASCE)1090-0241(2000)126:8(739).

Bouskill, N. J., J. Tang, W. J. Riley, and E. L. Brodie (2012), Trait-Based Representation of Biological Nitrification: Model Development, Testing, and Predicted Community Composition, *Frontiers in Microbiology*, *3*, doi:10.3389/fmicb.2012.00364.

Brovelli, A., F. Malaguerra, and D. Barry (2009), Bioclogging in porous media: Model development and sensitivity to initial conditions, *Environmental Modelling & Software*, *24*(5), 611–626, doi:10.1016/j.envsoft.2008.10.001.

Brunner, P., P. G. Cook, and C. T. Simmons (2009), Hydrogeologic controls on disconnection between surface water and groundwater, *Water Resources Research*, *45*(1), 1–13, doi:10.1029/2008WR006953.

Brunner, P., P. G. Cook, and C. T. Simmons (2011), Disconnected Surface Water and Groundwater: From Theory to Practice, *Ground Water*, *49*(4), 460–467, doi:10.1111/j.1745-6584.2010.00752.x.

Cayan, D. R., K. T. Redmond, and L. G. Riddle (1999), ENSO and Hydrologic Extremes in the Western United States, *Journal of Climate*, *12*(9), 2881–2893, doi:10.1175/1520-0442(1999)012⟨2881:EAHEIT⟩2.0.CO;2.

Chen, W., C. Huang, M. Chang, P. Chang, and H. Lu (2013a), The impact of floods on infiltration rates in a disconnected stream, *Water Resources Research*, *49*(12), 7887–7899, doi:10.1002/2013WR013762.

Chen, X. H., W. H. Dong, G. X. Ou, Z. W. Wang, and C. Liu (2013b), Opposite distribution pattern of streambed hydraulic conductivity in losing and gaining stream reaches, *Hydrology and Earth System Sciences Discussions*, *10*(2), 1693–1723, doi:10.5194/hessd-10-1693-2013.

Cole, J. J. (1982), Interactions Between Bacteria and Algae in Aquatic Ecosystems, *Annual Review of Ecology and Systematics*, *13*, 291–314.

Cook, P. G. (2015), Quantifying river gain and loss at regional scales, *Journal of Hydrology*, *531*, 749–758, doi:10.1016/j.jhydrol.2015.10.052.

Cunningham, A., C. J. Anderson, and H. Bouwer (1987), Effects of SedimentLaden Flow on Channel Bed Clogging, *Journal of Irrigation and Drainage Engineering*, *113*(1), 106–118, doi:10.1061/(ASCE)0733-9437(1987)113:1(106).

Cuthbert, M., R. Mackay, V. Durand, M.-F. Aller, R. Greswell, and M. Rivett (2010), Impacts of river bed gas on the hydraulic and thermal dynamics of the hyporheic zone, *Advances in Water Resources*, *33*(11), 1347–1358, doi:10.1016/j.advwatres.2010.09.014.

Dodds, W. K., C. A. Randel, and C. C. Edler (1996), Microcosms for Aquifer Research: Application to Colonization of Various Sized Particles by Ground-Water Microorganisms, *Ground Water*, *34*(4), 756–759, doi:10.1111/j.1745-6584.1996.tb02065.x.

ElBishlawi, H., and P. R. Jaffe (2015), Characterization of dissolved organic matter from a restored urban marsh and its role in the mobilization of trace metals, *Chemosphere*, *127*, 144–151, doi:10.1016/j.chemosphere.2014.12.080.

Findlay, S. (1995), Importance of surface-subsurface exchange in stream ecosystems: The hyporheic zone, *Limnology and Oceanography*, *40*(1), 159–164, doi:10.4319/lo.1995.40.1.0159.

Findlay, S., D. Strayer, C. Goumbala, and K. Gould (1993), Metabolism of streamwater dissolved organic carbon in the shallow hyporheic zone, *Limnology and Oceanography*, *38*(7), 1493–1499, doi:10.4319/lo.1993.38.7.1493.

Garcia-ruiz, Pattinson, and Whitton (1998), Denitrification in river sediments: relationship between process rate and properties of water and sediment, *Freshwater Biology*, *39*(3), 467–476, doi:10.1046/j.1365-2427.1998.00295.x.

Gomez-Velez, J. D., J. W. Harvey, M. B. Cardenas, and B. Kiel (2015), Denitrification in the Mississippi River network controlled by flow through river bedforms, *Nature Geoscience*, *8*(12), 941–945, doi:10.1038/ngeo2567.

Gordon, R. P., L. K. Lautz, M. A. Briggs, and J. M. McKenzie (2012), Automated calculation of vertical pore-water flux from field temperature time series using the VFLUX method and computer program, *Journal of Hydrology*, *420-421*, 142–158, doi:10.1016/j.jhydrol.2011.11.053.

Gray, A. B., G. B. Pasternack, E. B. Watson, J. A. Warrick, and M. A. Goi (2015), Effects of antecedent hydrologic conditions, time dependence, and climate cycles on the suspended sediment load of the Salinas River, California, *Journal of Hydrology*, *525*, 632–649, doi:10.1016/j.jhydrol.2015.04.025.

Hall, R. O., J. L. Tank, M. A. Baker, E. J. Rosi-Marshall, and E. R. Hotchkiss (2015), Metabolism, Gas Exchange, and Carbon Spiraling in Rivers, *Ecosystems*, doi:10.1007/s10021-015-9918-1.

Harvey, J., and M. Gooseff (2015), River corridor science: Hydrologic exchange and ecological consequences from bedforms to basins, *Water Resources Research*, *51*(9), 6893–6922, doi:10.1002/2015WR017617.

Harvey, J. W., J. K. Bhlke, M. A. Voytek, D. Scott, and C. R. Tobias (2013), Hyporheic zone denitrification: Controls on effective reaction depth and contribution to whole-stream mass balance: Scaling hyporheic flow controls on stream denitrification, *Water Resources Research*, *49*(10), 6298–6316, doi:10.1002/wrcr.20492.

Hatch, C. E., A. T. Fisher, J. S. Revenaugh, J. Constantz, and C. Ruehl (2006), Quantifying surface watergroundwater interactions using time series analysis of streambed thermal records: Method development, *Water Resources Research*, *42*, doi:10.1029/2005WR004787.

Hotchkiss, E. R., R. O. Hall Jr, R. A. Sponseller, D. Butman, J. Klaminder, H. Laudon, M. Rosvall, and J. Karlsson (2015), Sources of and processes controlling CO2 emissions change with the size of streams and rivers, *Nature Geoscience*, *8*(9), 696–699, doi:10.1038/ngeo2507.

Jones, J. B., Jr., S. G. Fisher, and N. B. Grimm (1995), Vertical Hydrologic Exchange and Ecosystem Metabolism in a Sonoran Desert Stream, *Ecology*, *76*(3), 942–952, doi:10.2307/1939358.

Keery, J., A. Binley, N. Crook, and J. W. N. Smith (2007), Temporal and spatial variability of groundwatersurface water fluxes: Development and application of an analytical method using temperature time series, *Journal of Hydrology*, *336*(12), 1–16, doi:10.1016/j.jhydrol.2006.12.003.

Kondrashov, D. (2005), Oscillatory modes of extended Nile River records (A.D. 6221922), *Geophysical Research Letters*, *32*(10), doi:10.1029/2004GL022156.

Lamontagne, S., A. R. Taylor, P. G. Cook, R. S. Crosbie, R. Brownbill, R. M. Williams, and P. Brunner (2013), Field assessment of surface water - groundwater connectivity in a semi-arid river basin (Murray-Darling, Australia), *Hydrological Processes*, pp. 1561–1672, doi:10.1002/hyp.9691.

Larned, S. T., M. N. Gooseff, A. I. Packman, K. Rugel, and S. M. Wondzell (2015), Groundwatersurface-water interactions: current research directions, *Freshwater Science*, *34*(1), 92–98, doi:10.1086/679491.

Lavers, D. A., D. M. Hannah, and C. Bradley (2015), Connecting large-scale atmospheric circulation, river flow and groundwater levels in a chalk catchment in southern England, *Journal of Hydrology*, *523*, 179–189, doi:10.1016/j.jhydrol.2015.01.060.

Leonardson, R. (2010), Exchange of fine sediments with gravel riverbeds, Ph.D. thesis, University of California, Berkeley.

Mann, C. J., and R. G. Wetzel (1995), Dissolved Organic Carbon and Its Utilization in a Riverine Wetland Ecosystem, *Biogeochemistry*, *31*(2), 99–120.

Matsunaga, T., G. Karametaxas, H. von Gunten, and P. Lichtner (1993), Redox chemistry of iron and manganese minerals in river-recharged aquifers: A model interpretation of a column experiment, *Geochimica et Cosmochimica Acta*, *57*(8), 1691–1704, doi:10.1016/0016-7037(93)90107-8.

Mayer, K. U., E. O. Frind, and D. W. Blowes (2002), Multicomponent reactive transport modeling in variably saturated porous media using a generalized formulation for kinetically controlled reactions, *Water Resources Research*, *38*(9), 13–1–13–21, doi:10.1029/2001WR000862.

McCallum, A. M., M. S. Andersen, B. M. S. Giambastiani, B. F. J. Kelly, and R. Ian Acworth (2013), Riveraquifer interactions in a semi-arid environment stressed by groundwater abstraction, *Hydrological Processes*, *27*(7), 1072–1085, doi:10.1002/hyp.9229.

Murphy, E. M., and T. R. Ginn (2000), Modeling microbial processes in porous media, *Hydrogeology Journal*, *8*(1), 142–158.

Mutiti, S., and J. Levy (2010), Using temperature modeling to investigate the temporal variability of riverbed hydraulic conductivity during storm events, *Journal of Hydrology*, *388*(3-4), 321–334, doi:10.1016/j.jhydrol.2010.05.011.

Newcomer, M. E., S. S. Hubbard, J. H. Fleckenstein, U. Maier, C. Schmidt, M. Thullner, C. Ulrich, N. Flipo, and Y. Rubin (2016), Simulating bioclogging effects on dynamic riverbed permeability and infiltration, *Water Resources Research*, pp. n/a–n/a, doi:10.1002/2015WR018351.

Nogaro, G., T. Datry, F. Mermillod-Blondin, S. Descloux, and B. Montuelle (2010), Influence of streambed sediment clogging on microbial processes in the hyporheic zone, *Freshwater Biology*, *55*(6), 1288–1302, doi:10.1111/j.1365-2427.2009.02352.x.

Peyrard, D., S. Delmotte, S. Sauvage, P. Namour, M. Gerino, P. Vervier, and J. Sanchez-Perez (2011), Longitudinal transformation of nitrogen and carbon in the hyporheic zone of an N-rich stream: A combined modelling and field study, *Physics and Chemistry of the Earth*, *36*(12), 599–611, doi:10.1016/j.pce.2011.05.003.

Piggott, J. J., R. K. Salis, G. Lear, C. R. Townsend, and C. D. Matthaei (2015), Climate warming and agricultural stressors interact to determine stream periphyton community composition, *Global Change Biology*, *21*(1), 206–222, doi:10.1111/gcb.12661.

Plant, R. E. (2012), *Spatial data analysis in ecology and agriculture using R*, CRC Press, Boca Raton.

Power, M., R. Lowe, P. Furey, J. Welter, M. Limm, J. Finlay, C. Bode, S. Chang, M. Goodrich, and J. Sculley (2009), Algal mats and insect emergence in rivers under Mediterranean climates: towards photogrammetric surveillance, *Freshwater Biology*, *54*(10), 2101–2115, doi:10.1111/j.1365-2427.2008.02163.x.

Power, M. E. (1992), Hydrologic and trophic controls of seasonal algal blooms in northern California rivers, *Archiv fr Hydrobiologie*, *125*(4), 385–410.

Power, M. E., M. S. Parker, and W. E. Dietrich (2008), Seasonal reassembly of a river food web: floods, droughts, and impacts of fish, *Ecological Monographs*, *78*(2), 263–282, doi:10.1890/06-0902.1.

Power, M. E., J. R. Holomuzki, and R. L. Lowe (2013), Food webs in Mediterranean rivers, *Hydrobiologia*, *719*(1), 119–136, doi:10.1007/s10750-013-1510-0.

Power, M. E., K. Bouma-Gregson, P. Higgins, and S. M. Carlson (2015), The Thirsty Eel: Summer and Winter Flow Thresholds that Tilt the Eel River of Northwestern California from Salmon-Supporting to Cyanobacterially Degraded States, *Copeia*, *2015*(1), 200–211, doi:10.1643/CE-14-086.

Pryet, A., B. Labarthe, F. Saleh, M. Akopian, and N. Flipo (2015), Reporting of Stream-Aquifer Flow Distribution at the Regional Scale with a Distributed Process-Based Model, *Water Resources Management*, *29*(1), 139–159, doi:10.1007/s11269-014-0832-7.

Ranalli, A. J., and D. L. Macalady (2010), The importance of the riparian zone and in-stream processes in nitrate attenuation in undisturbed and agricultural watersheds A review of the scientific literature, *Journal of Hydrology*, *389*(3-4), 406–415, doi:10.1016/j.jhydrol.2010.05.045.

Rode, M., M. Hartwig, D. Wagenschein, T. Kebede, and D. Borchardt (2015), The Importance of Hyporheic Zone Processes on Ecological Functioning and Solute Transport of Streams and Rivers, in *Ecosystem Services and River Basin Ecohydrology*, edited by L. Chicharo, F. Mller, and N. Fohrer, pp. 57–82, Springer Netherlands, Dordrecht.

Rosenzweig, R., A. Furman, C. Dosoretz, and U. Shavit (2014), Modeling biofilm dynamics and hydraulic properties in variably saturated soils using a channel network model, *Water Resources Research*, *50*(7), 5678–5697, doi:10.1002/2013WR015211.

Rubol, S., A. Freixa, A. Carles-Brangar, D. Fernndez-Garcia, A. M. Roman, and X. Sanchez-Vila (2014), Connecting bacterial colonization to physical and biochemical changes in a sand box infiltration experiment, *Journal of Hydrology*, *517*, 317–327, doi:10.1016/j.jhydrol.2014.05.041.

Schaap, M. G., F. J. Leij, and M. T. van Genuchten (2001), Rosetta: A computer program for estimating soil hydraulic parameters with hierarchical pedotransfer functions, *Journal of Hydrology*, *251*(34), 163–176, doi:10.1016/S0022-1694(01)00466-8.

Schubert, J. (2002), Hydraulic aspects of riverbank filtrationfield studies, *Journal of Hydrology*, *266*(34), 145–161, doi:10.1016/S0022-1694(02)00159-2.

Schubert, J. (2006), Experience with Riverbed Clogging Along the Rhine River, in *Riverbank Filtration Hydrology*, edited by S. A. Hubbs, no. 60 in Nato Science Series: IV: Earth and Environmental Sciences, pp. 221–242, Springer Netherlands.

Shepherd, R. G. (1989), Correlations of Permeability and Grain Size, *Ground Water*, *27*(5), 633–638, doi:10.1111/j.1745-6584.1989.tb00476.x.

Slatt, R. M. (2006), *Stratigraphic reservoir characterization for petroleum geologists, geophysicists, and engineers*, Chapter 5 Figure 5-19, Elsevier, Amsterdam; Oxford.

Sneider, R. (1987), Practical petrophysics for exploration and development, *AAPG Education Department Short Course Notes*, AAPG.

Stallman, R. W. (1965), Steady one-dimensional fluid flow in a semi-infinite porous medium with sinusoidal surface temperature, *Journal of Geophysical Research*, *70*(12), 2821–2827, doi:10.1029/JZ070i012p02821.

Su, G. W., J. Jasperse, D. Seymour, J. Constantz, and Q. Zhou (2007), Analysis of pumping-induced unsaturated regions beneath a perennial river, *Water Resources Research*, *43*(8), doi:10.1029/2006WR005389.

Thullner, M. (2010), Comparison of bioclogging effects in saturated porous media within one- and two-dimensional flow systems, *Ecological Engineering*, *36*(2), 176–196, doi:10.1016/j.ecoleng.2008.12.037.

Thullner, M., J. Zeyer, and W. Kinzelbach (2002a), Influence of Microbial Growth on Hydraulic Properties of Pore Networks, *Transport in Porous Media*, *49*(1), 99–122, doi:10.1023/A:1016030112089.

Thullner, M., L. Mauclaire, M. H. Schroth, W. Kinzelbach, and J. Zeyer (2002b), Interaction between water flow and spatial distribution of microbial growth in a two-dimensional flow field in saturated porous media, *Journal of Contaminant Hydrology*, *58*(34), 169–189, doi:10.1016/S0169-7722(02)00033-5.

Thullner, M., M. H. Schroth, J. Zeyer, and W. Kinzelbach (2004), Modeling of a microbial growth experiment with bioclogging in a two-dimensional saturated porous media flow field, *Journal of Contaminant Hydrology*, *70*(12), 37–62, doi:10.1016/j.jconhyd.2003.08.008.

Thullner, M., P. Regnier, and P. Van Cappellen (2007), Modeling Microbially Induced Carbon Degradation in Redox-Stratified Subsurface Environments: Concepts and Open Questions, *Geomicrobiology Journal*, *24*(3-4), 139–155, doi:10.1080/01490450701459275.

Treese, S., T. Meixner, and J. F. Hogan (2009), Clogging of an Effluent Dominated Semiarid River: A Conceptual Model of Stream-Aquifer Interactions, *JAWRA Journal of the American Water Resources Association*, *45*(4), 1047–1062, doi:10.1111/j.1752-1688.2009.00346.x.

Ulrich, C., S. Hubbard, J. Florsheim, D. O. Rosenberry, S. Borglin, M. Trotta, and D. Seymour (2015), Riverbed Clogging associated with a California Riverbank Filtration System: An assessment of mechanisms and monitoring approaches, *Journal of Hydrology*, *529*(3), 1740–1753, doi:10.1016/j.jhydrol.2015.08.012.

Vico, G., S. E. Thompson, S. Manzoni, A. Molini, J. D. Albertson, J. S. Almeida-Cortez, P. A. Fay, X. Feng, A. J. Guswa, H. Liu, T. G. Wilson, and A. Porporato (2015), Climatic, ecophysiological, and phenological controls on plant ecohydrological strategies in seasonally dry ecosystems, *Ecohydrology*, *8*(4), 660–681, doi:10.1002/eco.1533.

von Gunten, H. R., G. Karametaxas, and R. Keil (1994), Chemical Processes in Infiltrated Riverbed Sediments, *Environmental Science & Technology*, *28*(12), 2087–2093, doi:10.1021/es00061a017.

Wetzel, R. G., P. G. Hatcher, and T. S. Bianchi (1995), Natural photolysis by ultraviolet irradiance of recalcitrant dissolved organic matter to simple substrates for rapid bacterial metabolism, *Limnology and oceanography*, *40*(8), 1369–1380.

White, P. A., J. Kalff, J. B. Rasmussen, and J. M. Gasol (1991), The effect of temperature and algal biomass on bacterial production and specific growth rate in freshwater and marine habitats, *Microbial Ecology*, *21*(1), 99–118, doi:10.1007/BF02539147.

Wolter, K., and M. Timlin (1993), Monitoring ENSO in COADS with a seasonally adjusted principal component index, in *Proc. of the 17th Climate Diagnostics Workshop*, pp. 52–57, NOAA/NMC/CAC, NSSL, Oklahoma Clim. Survey, CIMMS and the School of Meteor., Univ. of Oklahoma, Norman,, OK.

Wu, F.-C., and H.-T. Huang (2000), Hydraulic Resistance Induced by Deposition of Sediment in Porous Medium, *Journal of Hydraulic Engineering*, *126*(7), 547–551, doi: 10.1061/(ASCE)0733-9429(2000)126:7(547).

Wyatt, K. H., M. R. Turetsky, A. R. Rober, D. Giroldo, E. S. Kane, and R. J. Stevenson (2012), Contributions of algae to GPP and DOC production in an Alaskan fen: effects of historical water table manipulations on ecosystem responses to a natural flood, *Oecologia*, *169*(3), 821–832, doi:10.1007/s00442-011-2233-4.

Yarwood, R. R., M. L. Rockhold, M. R. Niemet, J. S. Selker, and P. J. Bottomley (2006), Impact of microbial growth on water flow and solute transport in unsaturated porous media, *Water Resources Research*, *42*(10), n/a–n/a, doi:10.1029/2005WR004550.

Chapter 4

Ecological Controls on Subsurface Iron and Nitrate Dynamics

Abstract: Critical microbial processes that support freshwater biota, regulate biogeochemical cycling, and degrade contaminants occur in the hyporheic zone, where groundwater meets surface water flowing through channels. These ecotones support the supply of services to rivers that are conjunctively used for subsurface storage, drinking water filtration, and riparian habitat. Surface water ecological processes, such as primary productivity are a fundamental top-down prerequisite that supports bottom-up feedbacks from subsurface metabolic processes. Quantifying how coupled hydrological, ecological, and physical processes occur across different modes of flow and spatial scales is a challenge crucial for enhancing our understanding of dominant controls on subsurface biogeochemical transformations. This is especially so in Mediterranean climates where river flow is highly seasonal and in some cases represents a critical top-down driver of hyporheic geomorphological structures. Riverbed bioclogging from microbial growth is one such feedback mechanism that at once drives organic matter decay and carbon cycling while simultaneously clogging the very pore-space supporting its growth. To assess the dynamic feedback geochemistry of riverbed bioclogging and mineral/metal reactions at the groundwater-surface water interface, 1D and 2D MIN3P numerical models were developed that incorporate top-down and bottom-up controls. Dominantly vertical hyporheic flow versus dominantly horizontal flow models were assessed for their ability to transform Carbon and Nitrogen inputs given primary productivity controls on dissolved oxygen. Input chemical and flow boundary conditions were modeled from a U.S. Geological Survey (USGS) National Water Information System (NWIS) water quality dataset. Surface water primary production modeled with depth and temperature in the surface water and resulting dissolved organic carbon (DOC) from algal decay provided the nutrient substrate for subsurface heterotrophic microbial growth and bioclogging. Redox stratified zones were found to be enhanced in downwelling areas of the near subsurface

from complete oxygen consumption and shifted upward as hyporheic water returns to the surface in a fully reduced state. This feedback mechanism accelerated Fe(II) oxidation leading to precipitation of Mackinawite (an Iron Sulfide mineral) when hyporheic water flows into otherwise healthy rivers. Enhanced nitrate consumption in the simulation that included the ecological boundary suggests a dependence of microbial transformations on the seasonal pulse of nutrients. These results help inform our understanding of the role of large-scale, top-down sediment and ecological drivers of subsurface biogeochemistry.

4.1 Introduction

Feedback mechanisms between surface water and groundwater systems are ubiquitous in nature, often occurring at time scales relevant for water resources management decisions. A bio-aware perspective of the role of ecosystems services in benthic habitats in the larger context of river-aquifer interactions would greatly aid water resources management decisions, especially in drought prone areas where surface waters must be conjunctively used for ecological habitat and for drinking water such as from Riverbank Filtration (RBF) systems. Floodplain ecosystems scale from the pore-scale representing individual pore-spaces in the sediment network, hierarchically nested within organized geomorphic structures up through the catchment [*Lowe et al.*, 2006; *Doering et al.*, 2012] (Figure 4.1). Scales of hyporheic fluxes also range from small, lateral flows through dunes, riffles, and gravel bars, up to larger local scale vertical flows categorized as losing (from the river to the aquifer) or gaining (from the aquifer to the river) and are well known to vary across all spatial scales and modes of heterogeneity [*Cook*, 2015; *Larned et al.*, 2015; *Pryet et al.*, 2015]. Scales and feedbacks between ecological habitats within dominant modes of hydrological flow remains a frontier in river-aquifer interaction research [*Lowe et al.*, 2006]. Neglecting hyporheic processing of nutrients has the potential to lead to large errors and major uncertainty in downstream water quality predictions [*Hinkle et al.*, 2001]. Quantification of exchange fluxes (i.e. rates of water and nutrient movement) are vital for preserving these sensitive ecosystems, yet this remains a difficult task as models must contend with many processes, linkages, and parameters to fully describe system feedbacks [*Sophocleous*, 2002].

Important hyporheic zone biogeochemical processes have been known to play a significant role in many landscapes across scales, providing hotspots for global carbon degradation and emissions [*Battin et al.*, 2016] [Battin et al., 2016], yet the quantitative influence on stream water chemistry is still a growing research area [*Findlay*, 1995; *Rode et al.*, 2015]. As a vital ecotone, the hyporheic zone has been established as a critical zone for total river biodiversity [*Marmonier et al.*, 2012]. The hyporheic zone is an active mixing layer characterized by high biogeochemical processing rates, and time variability of organic matter substrates, and physical parameters (i.e. porosity, hydraulic conductivity). Current modeling frameworks

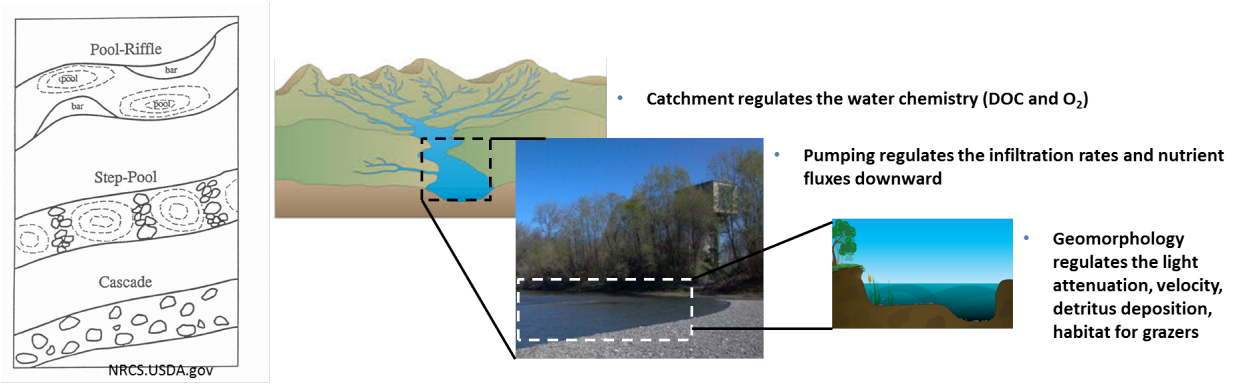

Figure 4.1: Nested spatial scales from the small geomorphic scales up through catchment scales that dominate magnitude and frequency of flows.

ignore the interconnected nature of the river-aquifer interactions that attenuate contaminants, supply nutrients to ecosystems, regulate benthic habitats, control carbon storage, and ultimately govern infiltration rates [*Field et al.*, 2015]. Additionally, the hyporheic zone provides habitat for diverse microbial assemblages that enhance the mass transfer of nutrients and solutes between the surface/subsurface interfaces, regulating these supplies to their subsurface aerobic/anaerobic counterparts. Aerobic and anaerobic contributions to whole-stream metabolism will depend on how surface water ecological processes in space and time are hydrologically linked through physical flows to the subsurface [*Hinkle et al.*, 2001].

Bioclogging through the consumption of Carbon (C) and Nitrogen (N) is one such subsurface process reliant on catchment scale drivers (i.e. discharge, temperature, DOC inputs) that shape river topography, sediment structure, benthic ecology, and chemical constituents [*Harvey and Gooseff*, 2015]. Often dynamically co-related, top-down controls from surface primary productivity in the form of phytoplankton and benthic algae growth [*Wyatt et al.*, 2012], grazer suppression [*Bajracharya et al.*, 2014], and abiotic environmental variables control substrate delivery for subsurface heterotrophic bacteria /fungal growth [*Wetzel et al.*, 1995; *Battin et al.*, 2008; *Hotchkiss et al.*, 2014]. The dominant mode of water flow, either through vertical flows or horizontal exchanges within the hyporheic zone may be a critical control on N and C cycling. Combined with top-down controls on sediment, the dominant direction of water flow may help explain the cumulative controlling effects on reaction rates and residence time distributions (Dahmköhler number) of different rivers, and why some fast flowing sediments become reaction limited over time [*Harvey et al.*, 2013]. Current thinking suggests that waters with the greatest contact time with sediments result in the greatest rates of O_2 removal [*Findlay*, 1995]. However, field data sometimes contradict this explanation as many gravel bedded rivers with very small residence times and contact times

can, in some cases, completely remove all O_2 from surface water [*Findlay*, 1995; *Harvey et al.*, 2013]. Initial sediment properties have been found to exert a strong control on these interactions, yet mean sediment grain size alone cannot account for the wide variability in O_2 removal rates from field data [*Findlay*, 1995; *Dodds et al.*, 1996]. Accounting for top-down controls on ecology, sediments, dominant flow direction, and microbial feedbacks on infiltration rates and sediment parameters may help resolve this discrepancy (Figure 4.2). Figure 4.2 shows a conceptual hypothesis for how flow direction and sediment structure controls reaction and residence timescales along the catchment to local scales. Strong support for DOC removal as a function of discharge along a horizontal hyporheic corridor has been documented [*Kamjunke et al.*, 2016].

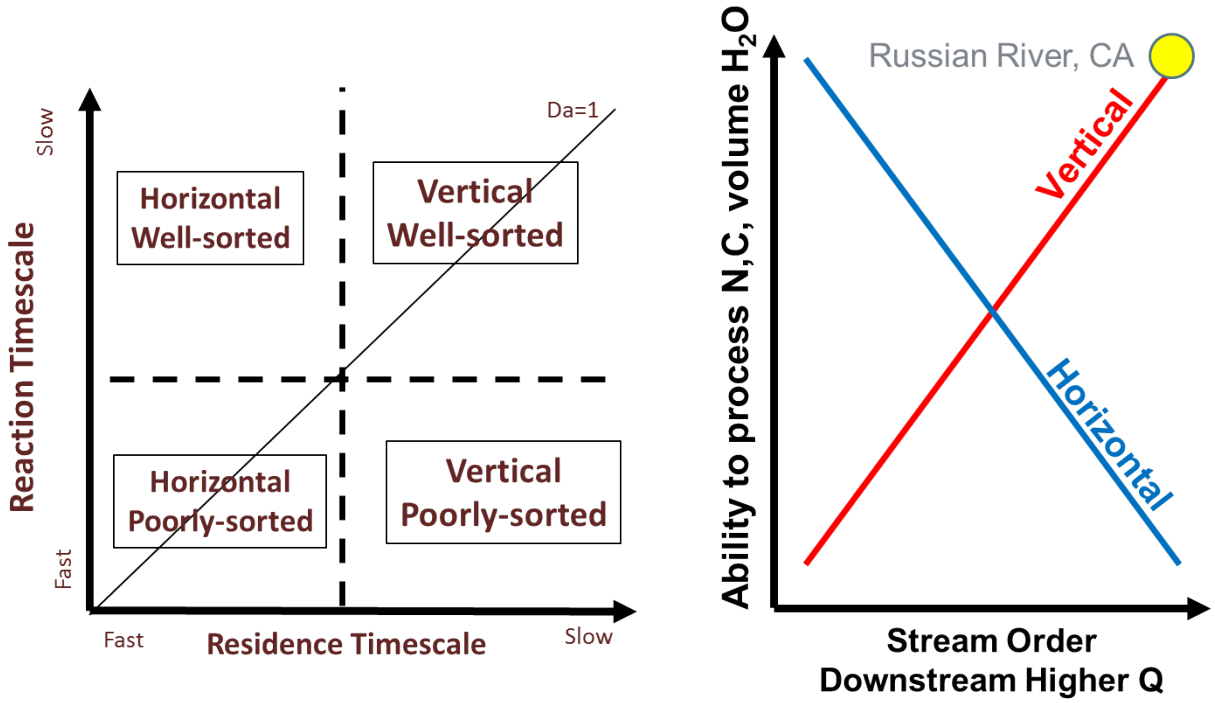

Figure 4.2: Dahmköhler number as a hypothesized function of sediments and flows (left) and the conceptual limitations of a rivers ability to process N,C and total volumes as a function of stream order and dominant direction of flow.

Algal growth in rivers is quantitatively and ecologically linked to subsurface heterotrophic microbial metabolism through carbon substrate provisions and feedbacks in gaining and losing rivers. Major differences in periphyton biomass have been found between dominantly gaining versus losing streams [*Doering et al.*, 2012]. Gaining rivers have been positively asso-

ciated with higher *Chl-α* in periphyton biomass associated with higher photosynthetic rate and correspondingly higher O_2 generation while higher sediment respiration has been detected in losing streams [*Doering et al.*, 2012]. Considerable surface contributions from algal participation have been detected in the carbohydrate pool of subsurface heterotrophic bacteria. This occurs via cell leakage from algal exudates of the senescing algal cells which serve as a dissolved or particulate organic carbon (DOC or POC) growth substrate for bacteria [*Battin and Sengschmitt*, 1999]. Pore-scale feedback mechanisms in turn produce exopolymers that can sufficiently clog pore spaces, and mechanical clogging from cells physically located in pore-throats [*Vandevivere and Baveye*, 1992], regulating the exchange of flow and nutrients that initially sustained microbial growth. Leading to strong redox gradients in the subsurface over small spatial scales (mm to cm), bioclogging may enhance subsequent redox processes including Iron and Sulfate reduction and methanogenesis. In terms of water management through RBF, DOC contributions to riverbed and aquifer sediments are of vital concern because of the link between DOC and Fe/Al mineral enhanced entrainment of pathogens through changes in the sorption capacity of the Fe sediments [*Metge et al.*, 2011]. Iron precipitation when highly reduced groundwater reaches oxygenated surface waters may be an indication of these strong subsurface bioclogging enhanced redox gradients.

Heterogeneity nested within these geomorphological and microbial scale structures can dramatically determine how biomass, fueled from surface algae growth can clog subsurface pore spaces. Vertical variations in growth along subsurface temperature and redox gradients are a source of spatial variability that may enhance preferential flow paths that influence the prevalent microbial community [*Rubol et al.*, 2014]. Subsequent changes occur in pore-scale Ksc (saturated hydraulic conductivity) and (porosity) parameter fields that allow the system to behave as a quasi-transient system [*Brovelli et al.*, 2009]. Discharge flow variations related to inter-annual variability may change the time period over which scour occurs in the river, ultimately influencing initial conditions for biomass growth the following year [*United Nations*, 1989]. Geostatistical analysis of algal growth at the field scale is a necessary next step and numerous methods exist to address this using remote sensing [*Pedretti et al.*, 2011]. Scales and feedbacks between surface and subsurface productivity remain a valuable question for understanding how scales and feedbacks between fluxes and clogging change total nutrient transformations and transport.

To address these questions, I propose the following conceptual model (Figure 4.3) for processes dominating subsurface biogeochemical transformations and redox gradients leading to Fe-precipitation on algae in the Russian River, CA at the Wohler RBF site. The Wohler site makes use of subsurface storage and relies on fast infiltration from rivers that naturally filter river contaminants. Dominantly gaining versus losing flow paths occur depending on pumping rates and length of pumping during the summer season. The site is either dominantly gaining during winter and spring, or dominantly losing during summer and fall. Spring gaining conditions combined with mild winter floods are hypothesized to reset

bed sediments, limit grazer suppression, and discharge nutrients into the river for algae growth. Over time, as winter floods recess, and groundwater discharge wanes, residual deeper groundwater discharges Fe-reduced (Fe(III) $\rightarrow$ Fe(II)) water into the river that precipitates once reaching oxic conditions. Combined with warming water, stress from diatoms, low river discharge during summer, algae die, exude high carbon substrates, and provide nutrients for subsurface heterotrophic reactions. Summer conditions are combined with high pumping rates that lead to large infiltration and nutrient fluxes of substrates in the dominantly vertical direction. Over time, this imposes a negative-feedback where the larger biomass growth rates limit nutrient flow and subsurface reactions. Deep subsurface redox conditions are initiated, and after winter floods, flows Fe(II) rich water back out into the river during the following spring.

Numerical models with varying initial sediment conditions and boundary conditions representing two different dominant types of hyporheic flow (horizontal versus vertical) are tested. Using this modeling framework and conceptual model to guide numerical process development, I model the DO concentration from the surface waters from algal primary productivity to stimulate redox controlled Fe reduction and Fe oxidation at different locations within the subsurface to test flow path delivery of Fe(II) to surface waters and Fe precipitation along the flow path. In the horizontal exchange model, I hypothesize that terminal electron accepting processes (TEAPs) will be distributed longitudinally along the flow path in the hyporheic zone where aerobic respiration (AR), denitrification (DN), iron reduction (IR), and sulfate reduction (SR) will occur delivering Fe(II) to upwelling waters occurring at fast (hourly) time scales. In the dominantly vertical model (losing/gaining), I hypothesize that redox zones will shift upward and downward, releasing Fe(II) from older recharged groundwaters from the previous summer pumping season. I hypothesize that these two fundamentally different types of flow regimes, one dominated by horizontal flows, the other dominated by vertical exchanges will show different responses to microbial respiration and opposing responses when flow paths are clogged.

I introduce a novel numerical feedback mechanism allowing growth of microbes associated with TEAPs to subsequently clog their own pore spaces that originally served as the nutrient pathway for their growth. This feedback clogging mechanism can help explain previously confounding interpretations of field data [*Findlay*, 1995] and opposing responses of microbes in gravels versus silts [*Dodds et al.*, 1996]. I hypothesize that clogging feedbacks in silts will slow the flux of water and nutrients leading to lower O_2 removal rates with higher residence times. In gravels, this feedback will continue unimpeded with low residence times, complete O_2 removal, and growth of anaerobic microcosms. Larger grain sediments therefore are predicted to have the ability to act as better conduits, creating overall more reducing conditions and larger C and N capture zones. Field evidence of Fe precipitation on algae in the riverbed provides support for this hypothesis and methodological framework.

Accounting for bioclogging processes that feedback and influence the delivery of water and

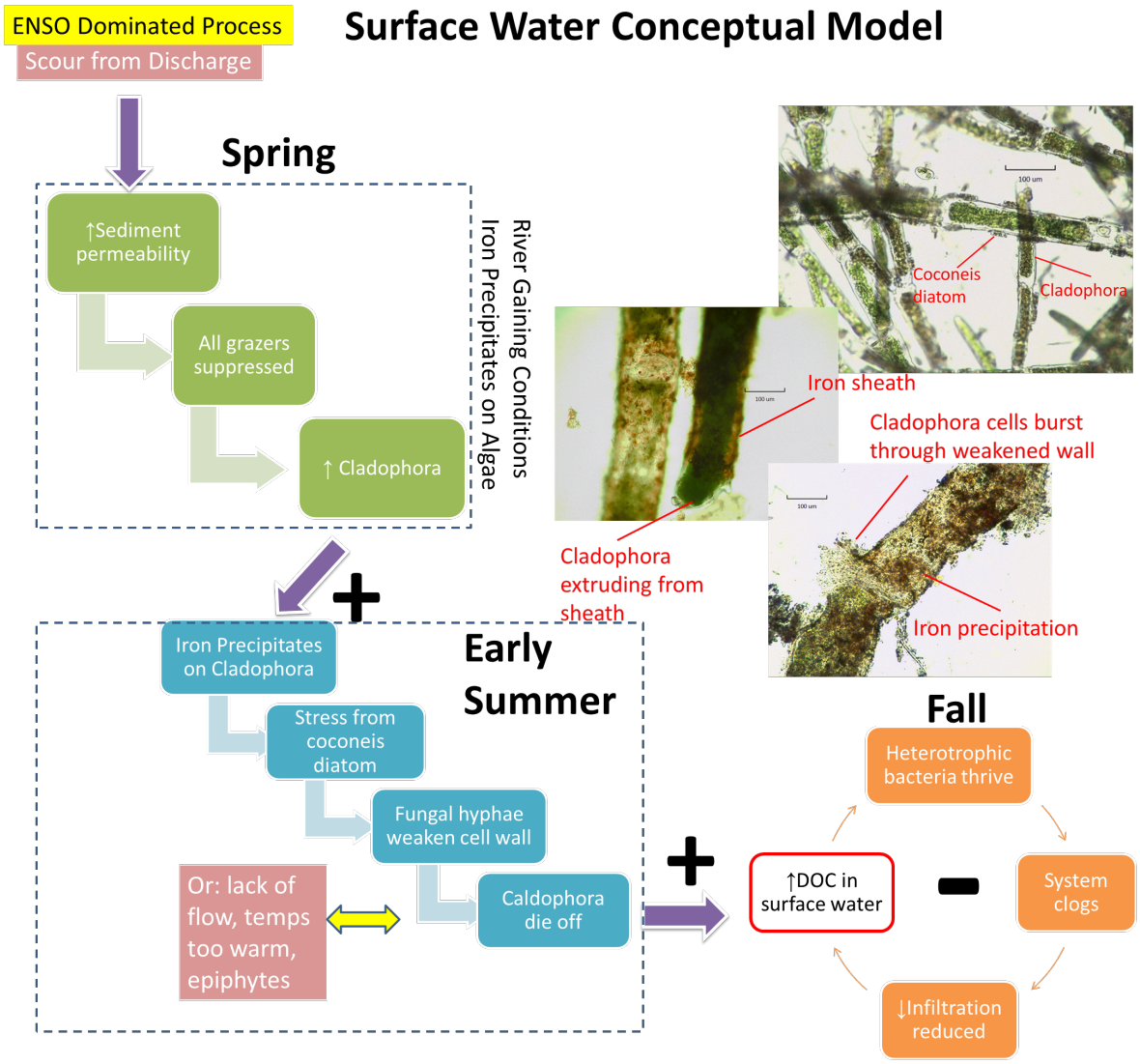

Figure 4.3: Conceptual model for feedbacks in the Russian River from bioclogging, hyporheic, and losing/gaining flows.

nutrients is crucial for better, more accurate C and N budgeting from rivers and hyporheic zones. This is especially pertinent given catchment scale representations of the small scale processes as cumulative observed river discharge and chemistry. The watershed function that produces the observed, downstream, cumulative effects may be representative of the sum of the transformations that occurred along the entirety of the river corridor (Figure 4.4).

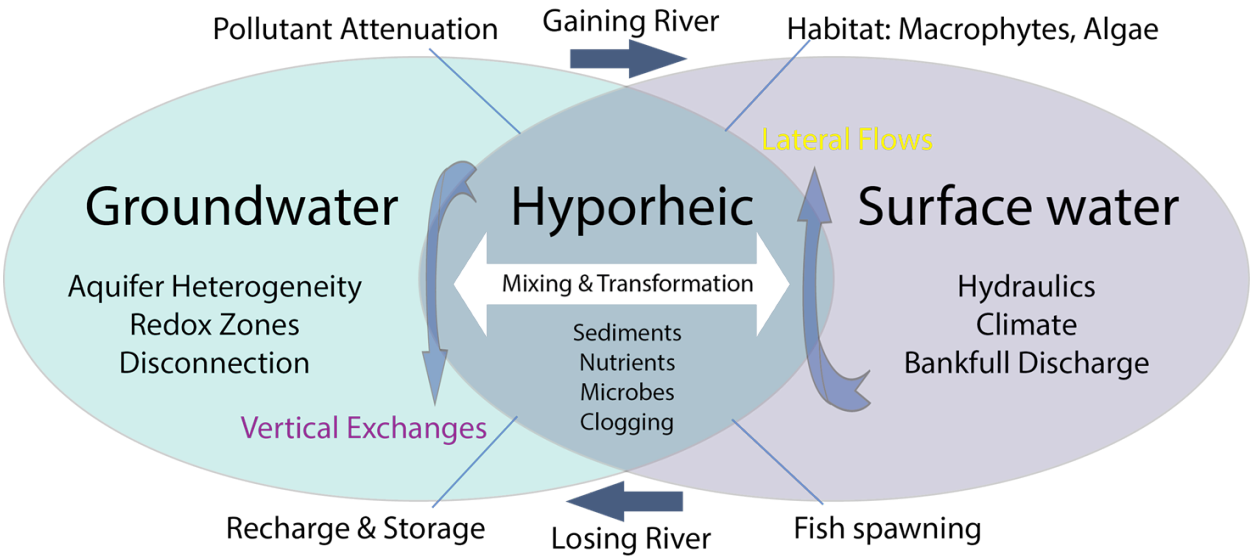

Figure 4.4: Organizing framework of hyporheic flows in the context of surface water and groundwater exchanges.

4.2 Background

Algae growth and river food webs

Benthic algae growth in rivers is governed by hydrological flow regimes, food webs, and nutrients. One species of green algae, *Cladophora spp.* is a mid to late successional filamentous species in fresh water ecosystems and is an adequate food source for many fresh water invertebrates. It is generally an attached benthic alga, but can also be found as a floating mat. *Cladophora spp.*. is found in association with nitrogen fixing cyanobacteria epiphytes. *Cladophora spp.* can survive in nitrogen deficient water because it can utilize the nitrogen fixed and NO3- released by cyanobacteria. *Cladophora spp.* is often found in highly exposed benthic habitats where competition for light exists between *Cladophora spp.* and epiphytes. Temperatures usually predict seasonal growth as die off can occur when temps are ¿ 25 deg. C or when Nitrogen and Phosphorous become limiting [*Dodds and Gudder*, 1992].

Hydrological factors: Water velocities can have both positive and negative effects on algae growth. Rates of photosynthesis generally increase with water velocity as this provides an increased supply of CO_2 availability, and better mixing and transport of nutrients for large attached periphyton that is in competition with neighboring periphyton [*Finlay et al.*, 1999]. *Cladophora spp.* has the ability to withstand shear stress in fast moving environments; however velocities that are too fast limit growth. As individual filaments become more tightly

packed, this can also decrease the photosynthetic rate of *Cladophora spp.* Lower nutrient supplies and higher river temperatures during summer months contribute to summer die-offs [*Dodds and Gudder*, 1992]. Hydrological wetting and drying effects from aquifer water table fluctuations may also affect surface and subsurface algal metabolism. Net effects of altered hydrology on algal primary productivity may depend on water table position as opposing directions of water flow may displace more oxic, favorable conditions for algal metabolism [*Wyatt et al.*, 2012]. Catchment scale hydrological modeling efforts demonstrate that incorporating periphyton effects could help explain, and better predict, upstream and downstream carbon and nitrogen chemistry [*Flipo et al.*, 2004].

Trophic Interactions: Aquatic vegetation and its location within the water column can strongly influence trophic interactions in freshwater communities. Algae initially grow as benthic turfs, but over time may detach and form floating mats. The timing and persistence of turfs versus mats may strongly influence the routing of insect production in river food webs, providing greater refuge for insects from predators with greater accrual of epiphytic diatoms [*Power*, 1990]. Hydrologically mediated disturbance events can maintain inverted trophic pyramids where predators dominate food webs. During succession after gravelmobilizing discharge events, food webs can shift from resource limited such as during algal growth in the absence of predators, and then predator limited during long periods when consumers return [*Power*, 2001].

Carbon Inputs to Subsurface Models from Algal Decay

Benthic algal blooms are known to play a primary role is subsurface microbial metabolism where algal decay typically provide a large source of dissolved organic carbon (DOC) and Particulate Organic Carbon (POC) for microbial utilization in the subsurface [*Cole*, 1982; *Findlay et al.*, 1993; *Jones et al.*, 1995; *Wetzel et al.*, 1995]. When algae senesce, DOC and POC are produced which are substrates for heterotrophic bacterial/fungal growth. Algae release their photosynthate directly into the water column as DOC (sometimes within hours after decay) and their exudates are generally considered more labile for heterotrophic metabolism. Uptake rates by microbes are often equal to the rate of production of DOC [*Cole*, 1982]. Since groundwater models do not include algae growth functions, heterotrophic biomass growth in the subsurface pore space must be modeled as a function of DOC and POC, the delivery of which is included as a model boundary condition (Figure 4.5). Few studies have reported the contribution of algae to DOC in riverine settings, but current estimates suggest that carbon exudation from algae can raise DOC levels upwards of 35 mg/L stimulated by water table variations where lower water tables contribute to higher DOC values [*Wyatt et al.*, 2012]. Other studies have found similarly high concentrations of DOC in subsurface strata ranging between 50-100 mg/L [*Mann and Wetzel*, 1995] and 25 mg/L [*ElBishlawi and Jaffe*, 2015]. Organic matter processing rates in highly losing rivers

are estimated around 70 mg of organic matter per liter of infiltrating water (35g /m2/day) [*von Gunten et al.*, 1994].

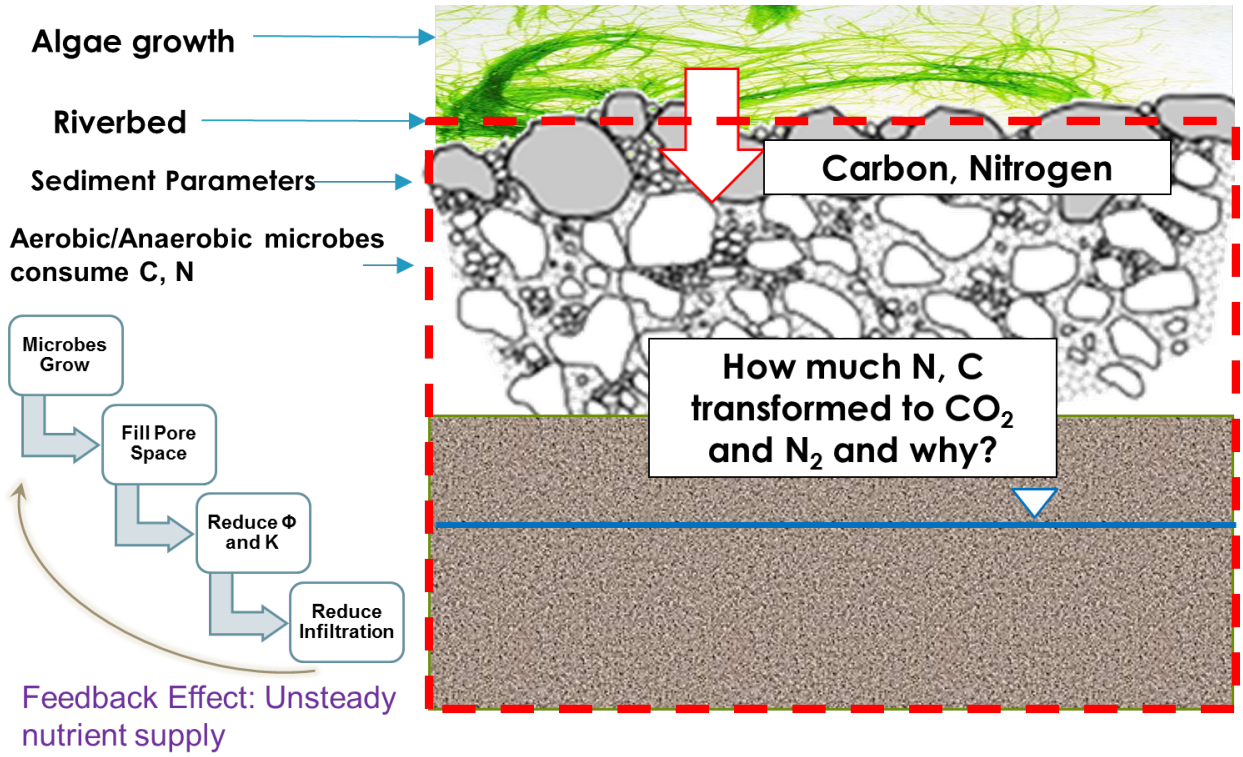

Figure 4.5: Conceptual model of the modeling domain and the dissolved organic carbon concentration boundary condition used in modeling. Algae grow heterogeneously on the surface and provide spatially variable carbon inputs to the subsurface.

Bioclogging in porous media

A large range of processes may contribute to riverbed clogging, including phytoplankton deposition, sedimentation, armoring, mineral precipitation, and physical clogging from microbes that create biofilms or occupy pore throats [*Brunke*, 1999; *Blaschke et al.*, 2003; *Schubert*, 2006; *Rosenberry and Healy*, 2012; *Ulrich et al.*, 2015]. Of these processes, I focus on riverbed clogging by subsurface microbial processes because of the potential for significant decreases in permeability over relatively short time periods (i.e. one summer season). Biofilms are aggregates of eukaryotic and prokaryotic microorganisms, immobilized and embedded in a matrix of extracellular polymeric substances (EPS). Organic macromolecules

including polysaccharides, proteins, lipids, humic substances, and nucleic acids are found in different densities within the EPS matrixthe structure and proportions of these vary significantly among samples [*Wingender et al.*, 1999]. When biomass occupies >5% of the void space, 100-fold decreases in saturated hydraulic conductivity (Ksc) can occur, even more so if clogging occurs in pore throats rather than voids spaces [*Gupta and Swartzendruber*, 1962; *Baveye et al.*, 1998; *Wingender et al.*, 1999]. Even under conditions where the cell density is low, exopolymers produced by the bacteria have the ability to significantly clog the pore spaces [*Vandevivere and Baveye*, 1992].

Dynamic permeability represented as temporal and spatial changes in Ksc and porosity (ϕ) are rarely accounted for in models of hyporheic horizontal flows or vertical exchanges [*Doppler et al.*, 2007; *Genereux et al.*, 2008; *Rosenberry and Healy*, 2012]. Although many models represent microbial growth and decay as a function of nutrient substrates [*Molz et al.*, 1986; *Murphy and Ginn*, 2000; *Thullner et al.*, 2007], most model approaches describing bioclogging are pore-scale models [e.g. *Suchomel et al.* [1998]; *Kim et al.* [2000]; *Dupin et al.* [2001a, b]; *Thullner et al.* [2002a, b]; *Thullner and Baveye* [2008]; *Ezeuko et al.* [2011]; *Rosenzweig et al.* [2014]]. Few of these incorporate scaled-up representations of bioclogging processes [*Kildsgaard and Engesgaard*, 2001; *Thullner et al.*, 2004; *Brovelli et al.*, 2009; *Soleimani et al.*, 2009; *Sams et al.*, 2016] that are required to simulate bioclogging influences on river system behavior. This is quite problematic as most field measurements indicate that riverbed permeability is often dynamic, due to processes such as subsurface bioclogging and sedimentation [*Annan*, 2001; *Blaschke et al.*, 2003; *Doppler et al.*, 2007; *Genereux et al.*, 2008; *Hatch et al.*, 2010; *Engeler et al.*, 2011; *Zhang et al.*, 2011; *Kurtz et al.*, 2012; *Taylor et al.*, 2013], yet most surface-groundwater numerical models assume that it is constant over time [*Doppler et al.*, 2007; *Flipo et al.*, 2014]. Mathematical constitutive models relating clogging to parameter changes have been well-established [*Thullner et al.*, 2002a, b, 2004; *Brovelli et al.*, 2009].

Representing bioclogging feedbacks on sediment parameters in numerical models can help predict total biogeochemical transformation, transport, and the development of aerobic and anaerobic patches in hyporheic zones. Previous studies have shown that biofilms have the potential to create micro-niches where the physicochemical conditions of the incoming water and the biofilm work together to allow diverse microbes of various redox preferences to grow in close vicinity to one another, although at order of magnitude different rates [*Storey et al.*, 1999]. Assuming sediment parameters are time-invariant can pose challenges to correctly predicting infiltration and biogeochemical fluxes, and relying on initial parameter estimates may introduce errors if in fact those parameters are temporally dynamic [*Doppler et al.*, 2007; *Su et al.*, 2004, 2007; *Zhang et al.*, 2011]. Without accounting for temporally dynamic parameters of riverbed sediments, numerical models of these flow regimes may be incorrect, especially at time scales where biomass growth in the pore-space becomes quite an important limit to flow. These limitations necessitate a better understanding of how

dynamic permeability alters seepage trends under the framework of a horizontal and vertical flow dominated river system [*Su et al.*, 2007; *Zhang et al.*, 2011].

Bioclogging from Horizontal Hyporheic Fluxes

Horizontal hyporheic fluxes are known to create persistent nutrient hotspots from the result of microbial activity at upwelling and downwelling sites [*Storey et al.*, 1999]. Heterogeneity (i.e. spatial variability) of the hyporheic zone geomorphic structure (dunes, ripples, bars, meanders Figure 4.1) coupled with heterogeneity of sediment parameters has yet to be examined in the literature, especially with regard to how these structures influence the micro-niches of microbes. Microbes in the subsurface also comprise the base of the interstitial food web and require much more research to fully understand their contributions [*Storey et al.*, 1999]. Downwelling and upwelling zones within hyporheic strata preferentially favor certain reactions depending on the redox potential and O_2 concentration [*Storey et al.*, 1999]. Attention to bioclogging is lacking in river ecosystems, as most of the attention currently is in contaminated rivers were sewage effluence is a primary problem. In average river settings where nutrient concentrations are low, bioclogging feedbacks present a significant source of potential carbon and nitrogen sequestration [*Rockhold et al.*, 2004; *Tang et al.*, 2015; *Battin et al.*, 2016], however relatively little has been done to study coupled hydrogeological and eco-hydrologcal processes within the hyporheic zone [*Rockhold et al.*, 2005; *Flipo et al.*, 2014]. Little research has accounted for the inter-dynamics of invertebrate and microbial communities in response to hydrogeological and environmental factors [*Larned et al.*, 2015] especially in response to anthropogenic alterations (Figure 4.4) [*Harvey and Gooseff*, 2015; *Larned et al.*, 2015; *Piggott et al.*, 2015].

Bioclogging from Vertical Exchanges

Rivers can have order of magnitude larger vertical exchanges to the underlying aquifer relative to horizontal hyporheic flows. In many arid, semi-arid, and Mediterranean climatic around the world, rivers are typically have losing-connected or losing-disconnected with the underlying aquifer [*Su et al.*, 2007; *Treese et al.*, 2009; *Lamontagne et al.*, 2013; *McCallum et al.*, 2013]. Disconnected rivers typically have a large unsaturated zone beneath the river and infiltration fluxes downward are fully maximized in this state (Figure 4.6) [*Newcomer et al.*, 2016; *Brunner et al.*, 2009]. Gaining rivers are typically found in temperate regions that remain fully connected even during pumping [*Schubert*, 2002, 2006]. When fluxes from gaining or losing conditions are large, horizontal fluxes can becomes negligible contributors to overall transformations relative to the large scale flow patterns [*Cardenas*, 2009]. Transient connection regimes (i.e. those that shift from gaining $\rightarrow$ losing $\rightarrow$ gaining) may dominate patterns and processes of biogeochemical cycling especially during low base flow conditions

[*Cardenas*, 2009]. Infiltration patters along river networks can be a function of both the connection status and bioclogging regime, and can vary spatially along the downstream corridor with direction of flow [*Ivkovic*, 2009; *Lamontagne et al.*, 2013]. Assumptions of saturated conditions with constant parameters are typical for river-aquifer studies leading to errors in projected infiltration rates and estimates of nutrient cycling [*Brunner et al.*, 2009; *Lamontagne et al.*, 2013].

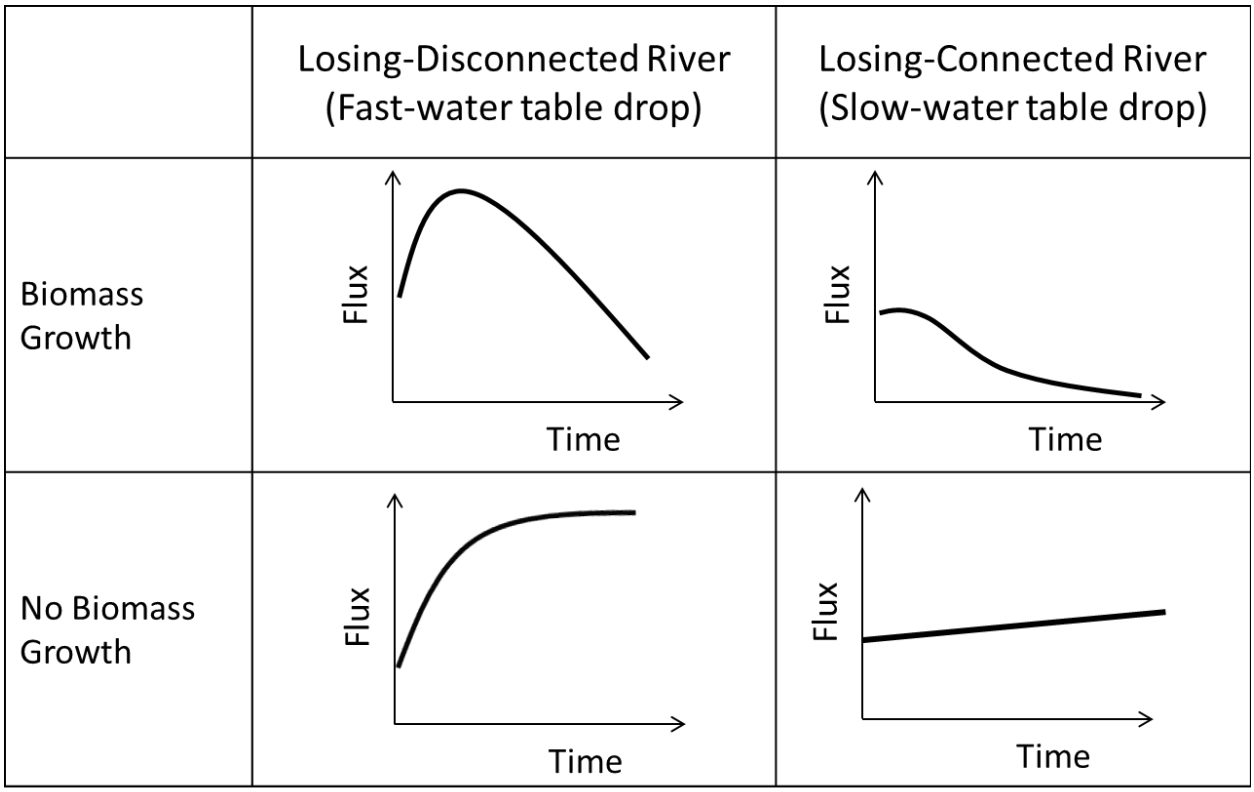

Figure 4.6: Differences in how subsurface biomass growth affects losing connected versus losing disconnected rivers.

Climate Factors

Floods and droughts are important agents of natural disturbance, and dominate connection regimes in rivers. The type of climate regime found in a location can be a strong predictor of the gaining or losing conditions of rivers[*Su et al.*, 2007; *Treese et al.*, 2009; *Lamontagne et al.*, 2013; *McCallum et al.*, 2013]. Relationships between seepage and bioclogging

may also differ widely in gaining versus losing streams, connected versus disconnected states, and type of climate dominating river flow. These factors can drastically change the growth of an unsaturated zone, spatially focused reduction in hydraulic conductivity from bioclogging, and feedbacks between nutrient fluxes and infiltration direction [*Hatch et al.*, 2010]. The role of climate variability introduced from the El NiñoSouthern Oscillation (ENSO) is one such process. Climate variability from ENSO is related to changes in the strength of the Walker Circulation in the Pacific Ocean [*NOAA CPC*, 2015]. Warm phases of ENSO (El Niño -EN) are related to warmer sea-surface temperature and lower pressure anomalies in the Eastern Pacific (near Ecuador and Peru) which reduce the strength of the Walker Circulation and enhance the strength of convective cells across latitudes. Warm phases typically produce greater than average precipitation in California. Opposite effects and reduced precipitation typically occur during cold periods (La Niña -LN) [*NOAA CPC*, 2015]. ENSO and other climatic perturbations, even one scouring bankfull discharge event, may have large regional effects on the dynamics of benthic ecosystems such as algae growth and bioclogging (Figure 4.7) [*Power*, 1992; *Piggott et al.*, 2015].

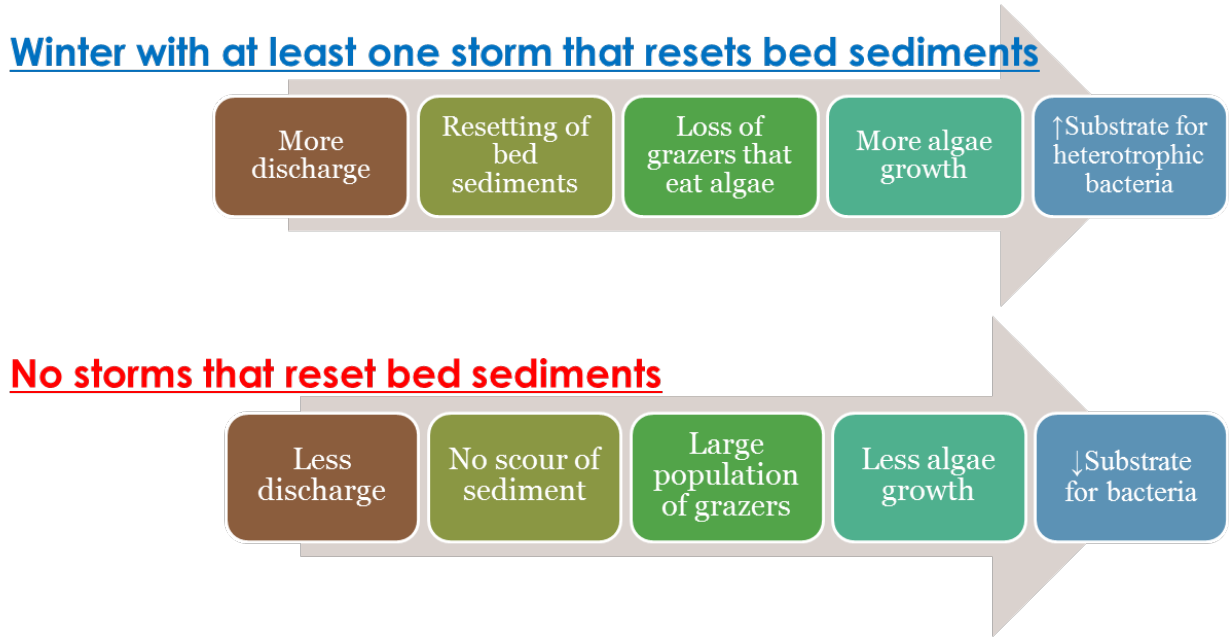

Figure 4.7: A conceptual model of the difference in algae growth based on the occurrence of at least one bankfull discharge event. These processes have been shown to occur in previous studies of algae growth in the Eel and Russian Rivers, CA [*Power*, 1992, 2001; *Power et al.*, 2008].

The semi-arid climate in California is responsible for the characteristic wet winter dry

summer conditions with superimposed 5-7 years oscillations from ENSO extremes. Many studies have closely established the significance of the ENSO signal in precipitation, snowfall accumulation, sediment transport, and streamflow in other locations around the world [*Cayan et al.*, 1999]. California Rivers typically show reduced signals of ENSO and highly depend on latitude. Effects of ENSO on California sediment transportation can range over 5 orders of magnitude in phase with climate fluctuations despite flow management amongst most rivers [*Inman and Jenkins*, 1999; *Andrews and Antweiler*, 2012]. ENSO was found to be a dominant factor in sand suspended sediment discharge with 10x more sediment discharge between EN versus LN years in the Salinas River, CA [*Gray et al.*, 2015]. Episodic sediment flux and deposition events related to ENSO in other locations around the world point to the influence that large scale climate perturbations can have on local scale geomorphologic features [*Aalto et al.*, 2003; *Kondrashov*, 2005].

ENSO effects on Sediments

Climatic perturbations do not always have linear effects on streambed sediments. Discharge flow regimes can have, in many cases, confounding and pronounced effects on sediment particle deposition and resulting infiltration rates, being a non-linear function of stream velocities. At certain velocities, siltation, armoring and straining can dominate the structure of depositing sediments and completely change the riverbed sediment properties (e.g. decreases porosity, less well-graded). Even higher velocities can cause smaller infiltration rates through enhanced capture and impaction, where smaller sediment are impacted into pores through turbulence [*Cunningham et al.*, 1987]. In other cases, streambed infiltration does not increase after scouring flood events because of enhanced post-flood/post-scour siltation [*Chen et al.*, 2013a]. River losing or gaining conditions may also contribute to patterns of sediment variability. Enhanced deposition found in losing rivers leading to lower riverbed conductivity contrasted with enhanced winnowing and higher conductivities in gaining rivers demonstrate that opposite distribution patterns of conductivity are possible depending on dominant flow regime. This also explains the lack of a sediment based clogging layer in many rivers which allows stream sediment conductivity to range several orders of magnitude [*Chen et al.*, 2013b].

ENSO effects on Algae

Algae growth in some rivers, especially those in Mediterranean climates, are dominated by the antecedent flood and scour regimes [*Power*, 1992]. Effects of flood disturbances in rivers can drastically affect sediment conditions for algal and grazer assemblages to grow and proliferate. *Cladophora spp.*, a type of algae, was found to vary consistently as a function of hydrologically mediated food chain effects in a Northern California river [*Power et al.*, 2008].

In the absence of river flooding during droughts, primary consumers dominate, producing a 2-level food chain where algae will not undergo a significant growth cycle [*Power*, 1992]. Flood years however, have the potential to allow unlimited algae growth and senescence by producing conditions ripe for higher level consumers to suppress grazers that consume algae [*Power et al.*, 2008]. Additionally, algal accrual during any given summer can be patchy, varying over substrate types, water depths which limit irradiance, and nutrient loadings [*Power et al.*, 2008]. Non-stationary seasonal drying and wetting cycles from water table fluctuations stimulate nutrient loadings in subsurface waters through "memory effects" following rewetting as water tables rise again. It is unknown how more frequent dry and wet events from water table may change algal productivity [*Wyatt et al.*, 2012].

Different phases of the ENSO cycle can drastically change the river discharge conditions that control river scour and cycles of algae growth. For example, in a Mediterranean river of Northern California, during years where bankfull discharge was reached, larger blooms of algae are possible if bed sediments were mobilized. Whereas years where bankfull discharge was not reached, algae growth was limited. Bankfull discharge can eliminate grazers that consume algae thus creating a cascading effects on the food-web allowing algae to proliferate [*Power*, 1992; *Power et al.*, 2008, 2009]. Pre-flood algal assemblages and percent cover of algae are typically reduced post-flood allowing emerging successional sequences. Floods that displace floating mats and clear epiphytes may enhance algae growth because of lack of food for the dominant grazer (minnows) [*Power and Stewart*, 1987]. Effects of winter hydrological disturbances have been shown to have a strong control on water quality and food-chains through a dependency on the nature of summer flows after winter floods leading to potential growth of harmful cyanobacteria [*Power et al.*, 2015].

Nutrient Cycling: Iron, Nitrogen, and Carbon

The redox ladder in the subsurface defines many oxidizing and reducing conditions of water as it travels through the pathway between sediment grains (Figure 4.8). When water first infiltrates the subsurface from the river, oxic conditions typically prevail and sustain aerobic heterotrophic microbes. As oxygen is depleted, conditions become favorable for denitrifies that consume nitrate and generate nitrogen gas. As water continues to travel, and as different components are consumed, conditions of the water pH and substrates available will support different communities of microorganisms at different depths in the subsurface (Figure 4.8).

Iron Precipitation

Iron is found in many field settings and commonly precipitates out of solution at groundwater seeps when reduced water containing Fe(II) encounters oxic conditions. Iron can also

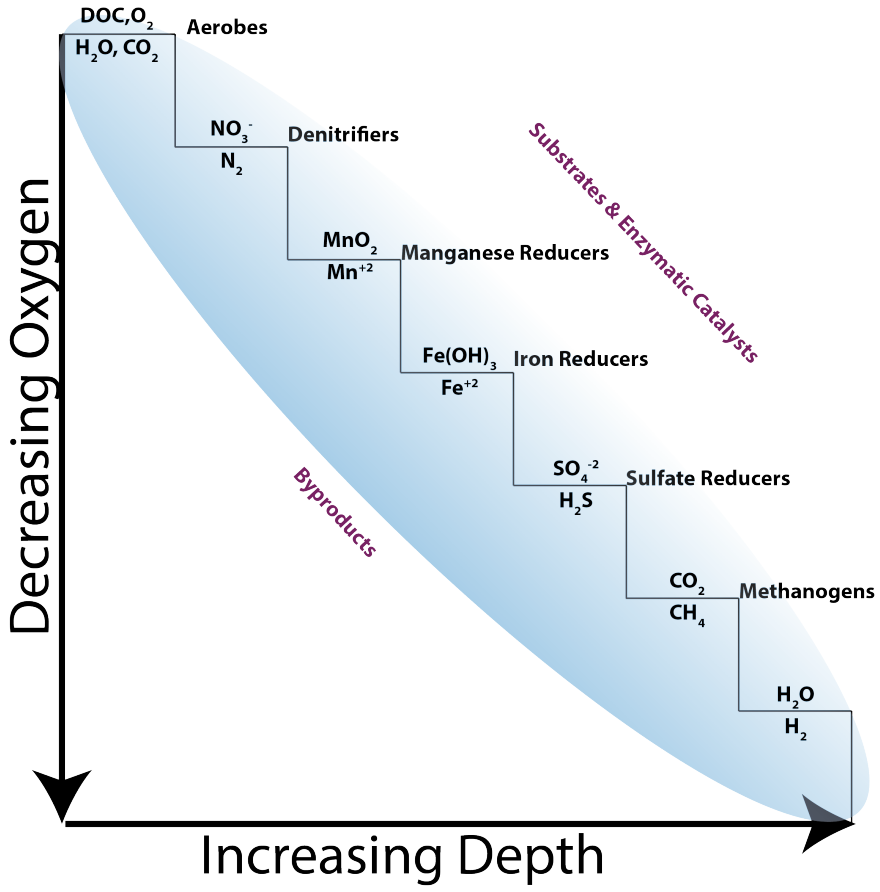

Figure 4.8: Redox ladder found within the subsurface vadose zone and groundwater.

precipitate in low oxygen conditions where Fe(II) reacts with high concentrations of S_2^- to form FeS (Mackinawite). Iron oxidation can occur as a biotic or abiotic reaction depending on oxygen levels, typically Fe(II) oxidation occurring first. When iron bearing groundwater encounters oxygenated zones, iron hydroxides will precipitate abiotically. When O_2 is between 1-3 mg/L and when corresponding levels of pH are between 6-7, bacterial/chemical oxidation of Fe(II) will occur [*Storey et al.*, 1999]. Biotic reactions occur in the presence of Iron oxidizing bacteria (FeOB) which are typically gram-negative and occur around natural groundwater springs [*James and Ferris*, 2004]. Epilithic biofilms that occur on streambed sediments may also create suitable chemolithotrophic micro-niches which can play an important role in subsurface oxygen dynamics and resulting hyporheic-heterotrophic microbial production [*Storey et al.*, 1999]. In cases where mediated by bacteria, Fe can precipitate in many pH environments not just low pH anoxic environments typically found lower on the re-

dox ladder. Enzymatic catalysts can often aid iron precipitation reactions through help from exopolysaccharide production, commonly increasing precipitation rates by up to 4 orders of magnitude higher than inorganic rates alone [*Kasama and Murakami*, 2001]. Lepidocrocite, Ferrihydrite, Goethite, and Mackinawite (FeS) are common Fe minerals that precipitate in different settings (Figure 4.9) [*Larsen and Postma*, 2001].

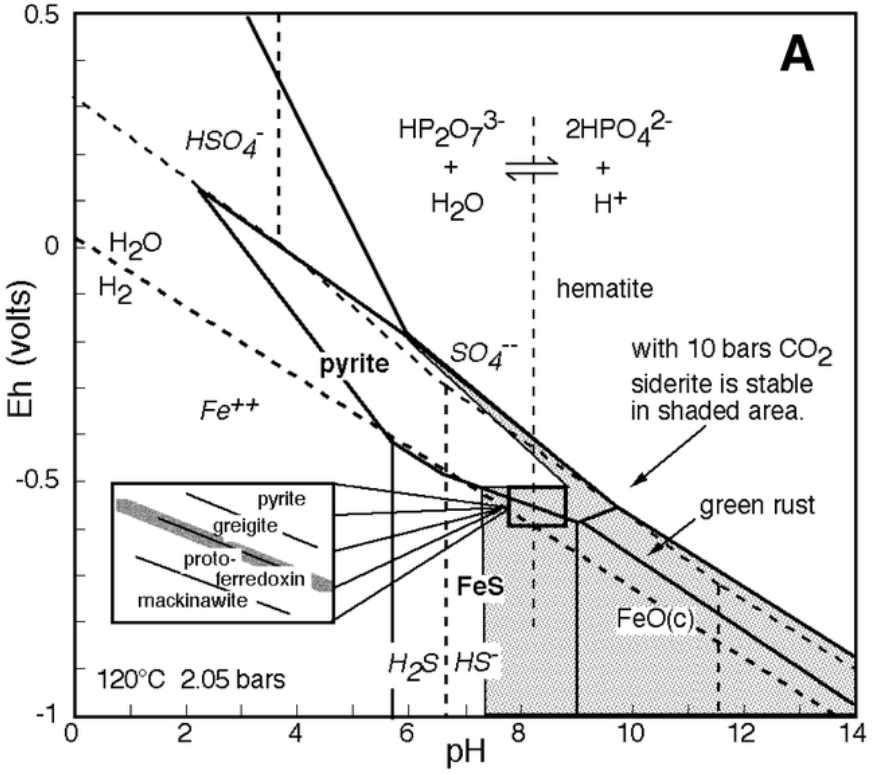

Figure 4.9: Eh-pH diagram of Fe in the aqueous and solid phases. Figure from [*Russell and Hall*, 2006].

Hyporheic zones can facilitate strong and fast redox conditions that create iron curtains in hyporheic zones when reduced groundwater mixes with incoming river water. Oscillations introduced from water table fluctuations or from transient river conditions have been shown to the aid in the formation of this natural reactive barrier because of overlapping reducing and oxidizing conditions at a site, especially when sediments are sandy rather than clayey [*Jung et al.*, 2015]. Strong seasonal variations in Fe in pore waters are strongly associated with seasonal cycles of decomposing organic matter [*Matsunaga et al.*, 1993]. Seasonal variations in the concentration of Fe in a losing river are related to temperature controlled microbiologically mediated decomposition of organic matter. Spikes in Fe dissolution in the

Spring co-occur with larger springtime biological activity [*von Gunten et al.*, 1994]. Seasonally driven springtime, summer and wintertime subsurface redox conditions verify cyclical redox conditions and transitions from oxidizing to reducing on a seasonal basis through field in-situ observations reported in previous studies [*Matsunaga et al.*, 1993; *von Gunten et al.*, 1994]. When DOC and Fe interact in sediments, associated pathogen re-entrainment in sediments may occur which is of particular concern for drinking water sources [*Metge et al.*, 2011].

Nitrogen Cycling

Nitrogen cycling in streams commonly takes place through denitrification (DN), however, little is understood about where this process is most efficient and why some rivers provide better DN services than others [*Gomez-Velez et al.*, 2015]. Nested flow paths in hyporheic zones superimposed in losing versus gaining streams significantly affect transformation of N [*Doering et al.*, 2012]. Denitrification in hyporheic sediment has shown to be a major contributor to stream nitrogen budgets serving as a nitrogen removal buffer [*Findlay*, 1995]. Latitudinal variations from hyporheic flow can increase denitrification and biogeochemical cycling and many modeling efforts show that accounting for subsurface transformation is required to simulate accurate downstream nitrate concentrations [*Peyrard et al.*, 2011]. Many conditions of the stream itself can cause the stream to either be a source or sink of nitrogen, however it is not yet well understood how these factors combine to control this [*Peyrard et al.*, 2011]. Strong hyporheic redox gradients [*Peyrard et al.*, 2011], and decreases in observed total dissolved inorganic nitrogen along a flowline in an aerobic area of the hyporheic zone [*Storey et al.*, 1999], support the idea of functional microbial guilds living co-laterally that respond quickly to shifts in water chemistry or water table oscillations [*Hinkle et al.*, 2001]. These microbial micro-niches allow denitrification to occur across many locations within the hyporheic zone, yet most models only account for denitrification as a transformation rather than an organic activity supporting microbial growth feedbacks.

Nitrogen cycling hinges on the accurate representation of microbial guilds that provide functional services to this cycle and to overall ecosystem productivity [*Bouskill et al.*, 2012]. Simulating microbial guilds and their contributions to physicochemical impacts from pulsed substrate impulses, nitrifier community development was shown to be a function of environmental conditions and a range of spatial and chemical gradients [*Bouskill et al.*, 2012].Trait based modeling studies have explained an emerging need for numerically characterizing the key physiological parameters that contribute toward ecological functions and strategies within certain redox zones [*Cusack et al.*, 2011; *Bouskill et al.*, 2012]. Most modeling schemes neglect this important pore-scale feedback accounting for the growth of microbial mass and biofilms, and filling this gap could provide key information for better and more accurate nitrogen budgets. Accounting for bioclogging from anaerobic denitrification may

help explain why some rivers better support this service than others.

Carbon Cycling

Estimates of groundwater subsidies of CO_2 to rivers is currently unknown and has only been crudely estimated at large and small scales as the residual of stream based metabolism [*Hall et al.*, 2015; *Hotchkiss et al.*, 2015]. Carbon subsidies from groundwater to rivers are thought to be a function of subsurface aerobic respiration (AR) and anaerobic denitrification (DN). Dissolved organic carbon (DOC) has been found to stimulate heterotrophic production of CO_2 from both AR and DN in the hyporheic zone [*Baker et al.*, 1999]. AR and DN are both reliant on DOC as a substrate for CO_2, and in many cases, when DOC is not limiting, this can stimulate anaerobic processes enough so that they dominate heterotrophic metabolism in the hyporheic zone. Conditions where anaerobic processes dominant up through sulfate reduction can become favorable for an iron sulfide mineral (FeS) Mackinawite to precipitate [*Baker et al.*, 1999]. Production of DOC in surface waters has been deterministically linked to temperature and algal effects on bacterial abundance and productivity, showing that growth rates of heterotrophic bacteria increased with increasing Chl-α content of incoming water [*White et al.*, 1991]. Other studies have determined the carbon content of algae based and surface water based on field samples (323 mgC/g sediment) [*von Gunten et al.*, 1994].

Modeling frameworks exist for microbial species across many different TEAPs in the redox sequence [*Thullner et al.*, 2007]. Using reactant terms, inhibition term, and Monod kinetics, microbial growth can be specified as a function of the concentration of nutrient substrates and the concentration of microbial mass already in the system [*Murphy and Ginn*, 2000]. This method assumes a single step approach when partitioning organic carbon to dissolved inorganic carbon and biomass in the following reaction for aerobic respiration shown in Equation 4.1:

$$3\,[CH_2O] + 2\,[O_2] \rightarrow 2\,[CO_3]^{-2} + 4\,[H]^{+} + Biomass \tag{4.1}$$

Where biomass is represented by a ratio of C:H:O of 1:2:1. Organic carbon is assumed to be either in dissolved or particulate form. Carbon is the oxidized species and oxygen is the reduced-electron acceptor. Carbonate then forms carbon dioxide gas after reacting with H+ ions. At different pH levels, the carbonate species may be found in different forms (i.e. bicarbonate). Biomass growth through the anaerobic degradation of organic carbon and nitrate by anaerobes is considered through the following equation where nitrogen is the electron acceptor (reduced species) and carbon is oxidized shown in Equation 4.2:

$$[CH_2O] + 0.8\,[NO_3]^{-1} \rightarrow [CO_3]^{-2} + 0.4N_2 + 1.2\,[H]^{+} + 0.4\,[H_2O] + Biomass \tag{4.2}$$

Dynamics between surface water and groundwater models are rarely included in ecological and hydrological models. Either the model accounts for surface water conditions, or groundwater conditions, rarely linking the two at each time step. A conceptual model for the top-down climatic perturbation of river ecological conditions that supply nutrients to substrate microbes is shown in Figure 4.7. When a winter season has at least one storm that resets bed sediment, conditions are favorable for algae growth which decay and provide substrate for bacteria in the sediment pore space. When a winter does not experience any bed-resetting storms, large populations of grazers continue to consume algae, suppressing the supply of nutrients for subsurface microbes. This hypothesized framework guide the development of the numerical model for both the horizontal and vertical hyporheic flow scenarios.

4.3 Study Site and Data Collection

The Wohler Riverbank Filtration site operated by the Sonoma County Water Agency (SCWA) maintains 6 collector wells along the Russian River, providing 600,000 people annually with drinking water (Figure 4.10). The Russian River drains approximately 3,850 km^2 in Northern California, with an annual average discharge of approximately 2.0 km^2. The SCWA operates the collector wells to make use of subsurface storage, however this method also relies on fast infiltration from rivers to naturally filter river contaminants. Not only used for drinking water, the Russian River provides many ecosystem services including fish corridors, riparian habitat, water storage in groundwater aquifers, and natural filtration of contaminants as water flows through hyporheic zones. A major variable of interest at the Russian river site is infiltration because the river and aquifer are conjunctively used for drinking water and for maintaining riparian vegetation and streamflow habitat. Dominant processes controlling infiltration include pumping which contributes to unsaturated zone development beneath the river (disconnection; a temporary dam raises hydraulic heads and increases infiltration; and bioclogging reduces K and ϕ and reduces infiltration. Each year algal and cyanobacterial growth cause river quality concerns. During its life cycle, algae die and exude dissolved organic carbon (DOC) for subsurface heterotrophic bacteria that clog the subsurface pore space. Surface periphyton algae growth is dominantly *Spyrogyra spp.* (summer), *Cladophora spp.* (spring). Decaying algae is then processed by surface organisms (grazers) that allow quick transfer of carbon to a particulate and dissolved phase providing a substrate for subsurface micro-organisms. Field samples of subsurface microbial biomass were taken in transects across the river and along the river flow shown in Figure 4.10. Subsurface biomass is concentrated in the north and west side of the river which is closest to the production wells. Methods used to obtain the field data are fully described in a previous study [*Ulrich et al.*, 2015].

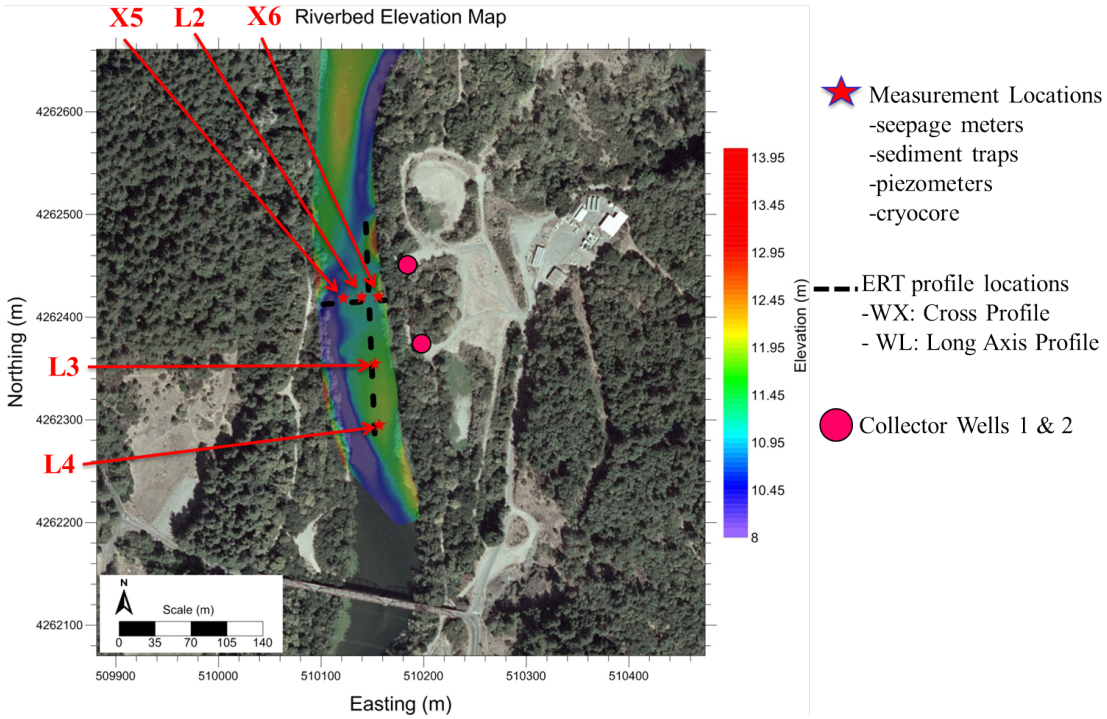

Figure 4.10: Locations of sites L2, L3, L4, X5 and X6.

Phospholipid Fatty Acid Analysis

Cryocores containing sediment and microbial samples were obtained at multiple locations of the field site. The Phospholipid Fatty Acid (PLFA) technique was used to determine the microbial communities and total biomass growing within the first 10 cm of the hyporheic zone with lipid classes grouped into biomass type according to chemical structure. PLFA data was analyzed by date corresponding to each sampling campaign. Total biomass increased from 0.1 μg/g in May to 20 μg/g in November (Figure 4.11). During spring conditions, sulfate reducers, general DMA lipids (anaerobic PLFAs), and gram+ bacteria are much more active relative to other biomass, during late spring/early summer. This is consistent with our hypothesis that spring/early summer conditions allow greater fluxes of reducing conditions from subsurface to surface waters as a function of winter floods that allow the river to transition from losing $\rightarrow$ gaining, supporting anaerobic assemblages. In contrast, during later summer, well after pumping begins, the microbial community dynamics shift, showing an increase in eukaryotic (algal) and fungal PLFA suggesting algal supply of organic matter for subsurface heterotrophic aerobic decomposition. The dynamics of microbial enzymatic activities shown here provides a functional link between dominant flow regime between the

river and aquifer, with the changes in microbial community composition hypothesized to have net effects on C and N storage and CO_2 and N_2 emissions which are the by-product of the microbial reactions. The dynamics of microbial enzymatic activities from PLFA analysis confirms this hypothesis showing that microbial communities are quite sensitive to flow direction within the hyporheic zone.

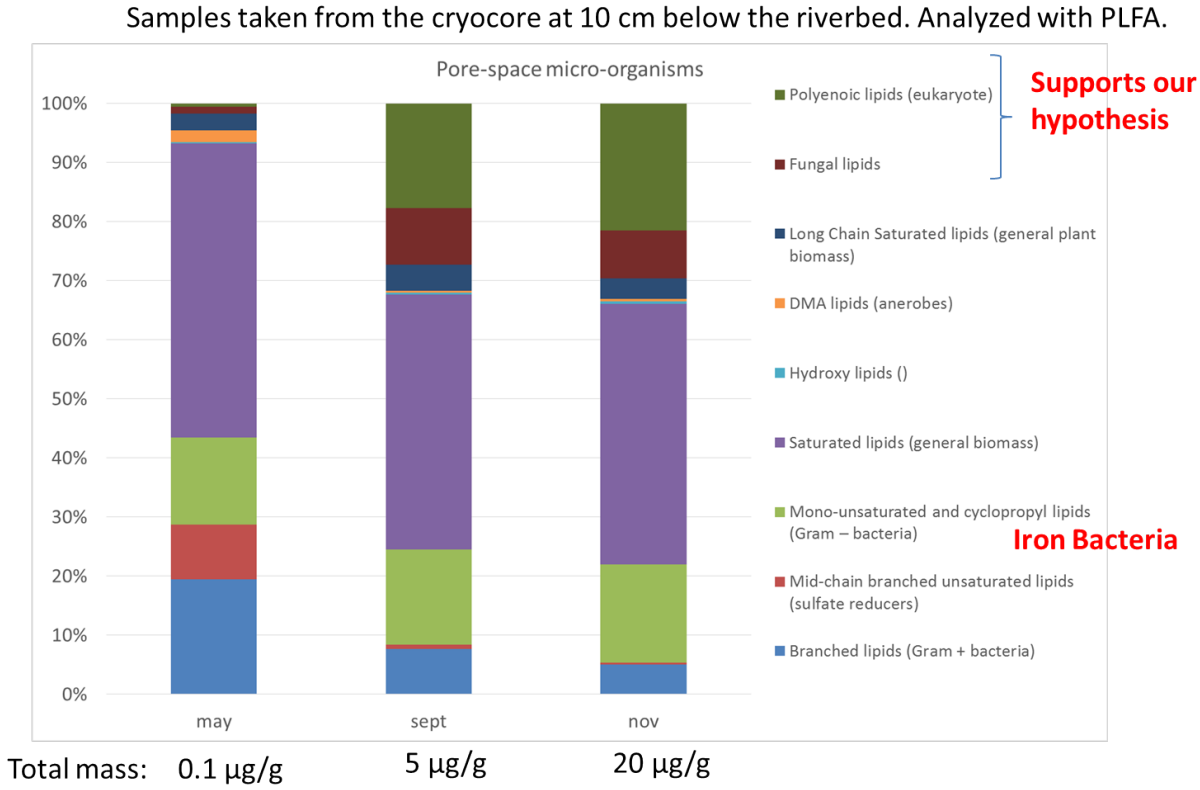

Figure 4.11: PLFA data from the top 10 cm of the riverbed from May-November 2012.

Periphyton Collection and Algal Composition

Algal periphyton samples and other benthic and planktonic organic matter were collected monthly from March 2015-October 2015 to identify dominant species and assemblage dynamics. Many samples from different locations along the riverbank and thalweg were sampled and placed on ice. In the laboratory, samples were placed in vials and preserved in 3% formaldehyde. Samples were obtained, when possible on the gravel bars and in the deeper thalweg to segregate different assemblages based on flow regime. River depths were low

(∼0.5m) from March-July when the temporary dam had not yet been built. Once the dam was installed (July-October), river depths varied from 1.5-2m and samples were obtained by kayak.

Initial Hydraulic Conductivity Predicted from Field GSD

Grain-size distribution curves (GSD) were fit using a logarithmic transformation, and then separated into 2 log-linear models: one for grain sizes >0.85 mm and one for grain sizes <0.85 mm values. Percent distributions corresponding to d10, d20, d50, d60, and d100 were predicted (Figure 4.12). In Figure 4.12, grain size distributions for all sites from 0-5cm from May to November are shown. Generally there are no large shifts in sediment and matrix type (all distributions remain in the fine sand to gravel categories), however a few sites do show shifts. Site L2 shows a noticeable shift towards coarser sediments over the summer with d10 shifting from 0.64mm to 1.04mm. Site L3 shows a fining of sediment from May to September, but then a coarsening from September to November. Site L3 did not show a shift in d10 however. Sites L4 and L2 are quite similar during the month of May and they are located over 100m apart in the North-South direction, however they are located on similar elevations within on the bank. They show divergent trends over the course of the summer. The GSD analysis shows that generally, the main sediment type at all sites is a gravel mixture with a fine to medium sandy matrix. It was noted during field collection of sediments that upon taking the sample, most of the fines were dislodged and floated away. This could bias the GSD toward larger grain diameters. The sediment classification is based on that previously published reports [*Schubert*, 2002].

Initial hydraulic conductivity Ksc (m/s) for the sediments alone were predicted using a formulation of the Kozeny-Carman equation [*Barahona-Palomo et al.*, 2011].

$$K_{sc} = \frac{g}{\nu} C f(\Phi) d_e^2 \tag{4.3}$$

$$C = 8.3x10^{-3}; d_e = d_{10}; f(\Phi) = \left[\frac{\Phi^3}{1-\Phi^2}\right] \tag{4.4}$$

$$\Phi = 0.255\left(1 + 0.83^U\right); U = \left[\frac{d_{60}}{d_{10}}\right] \tag{4.5}$$

Where g is gravitational acceleration [9.8 m/s^2], ν is the kinematic viscosity of the fluid [1.2x10-6 m^2/s], f(ϕ) is a function of porosity ϕ (-), de is an effective grain diameter (m) assumed as d10, and C is defined as a sorting coefficient (-). The values of C, and de, and the type of relationship, f(ϕ), depend on the formulation adopted. In these equations, d10 is the grain size diameter (m) corresponding to the diameter at which 10% of the sample by weight

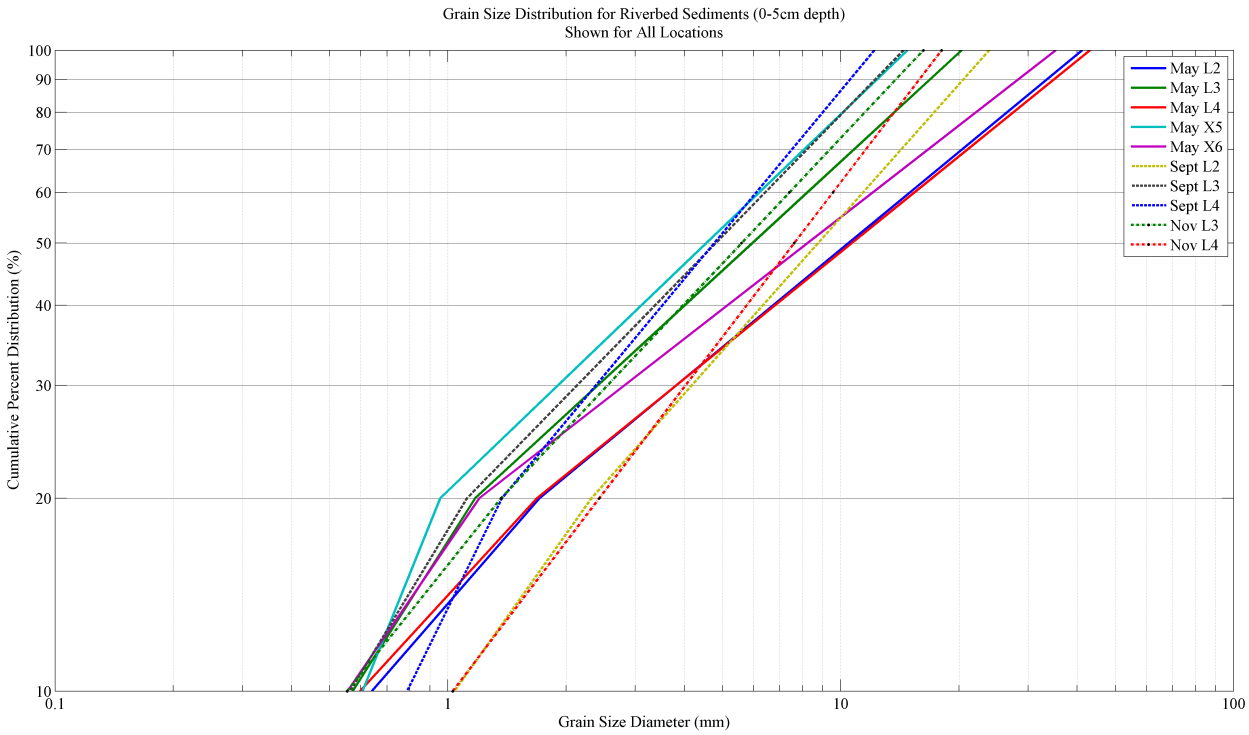

Figure 4.12: Predicted grain size diameters for d10, d20, d50, d60, and d100 for all sites for surficial riverbed sediments.

corresponds. Ksc provides the hydraulic conductivity in m/sec. Hydraulic conductivity as a function of depth, time, and sediment deposition only decreased over the course of the summer at site L3 from 72.3 m/day to 64.2 m/day while the hydraulic conductivity increased slightly at sites L2 and L4. A histogram of all the hydraulic conductivities from all sites and depths is shown in Figure 4.13. The values greater than 150 m/day are found at sites L2 and L4 within the surficial sediments during September and November. Initial hydraulic parameters were also obtained from numerous other studies conducted at the Russian River site (i.e. [*Su et al.*, 2004; *Zhang et al.*, 2011]).

Water Quality Parameters

Water quality parameters of dissolved oxygen and temperature, and the hydrodynamic flow variable of discharge were obtained from two USGS gauging stations near the Wohler site [*USGS*, 2016]. Figure 4.14 shows cumulative discharge from all years from the Guerneville station colored by strength of the MEI index. The Guerneville station (#11467000) is

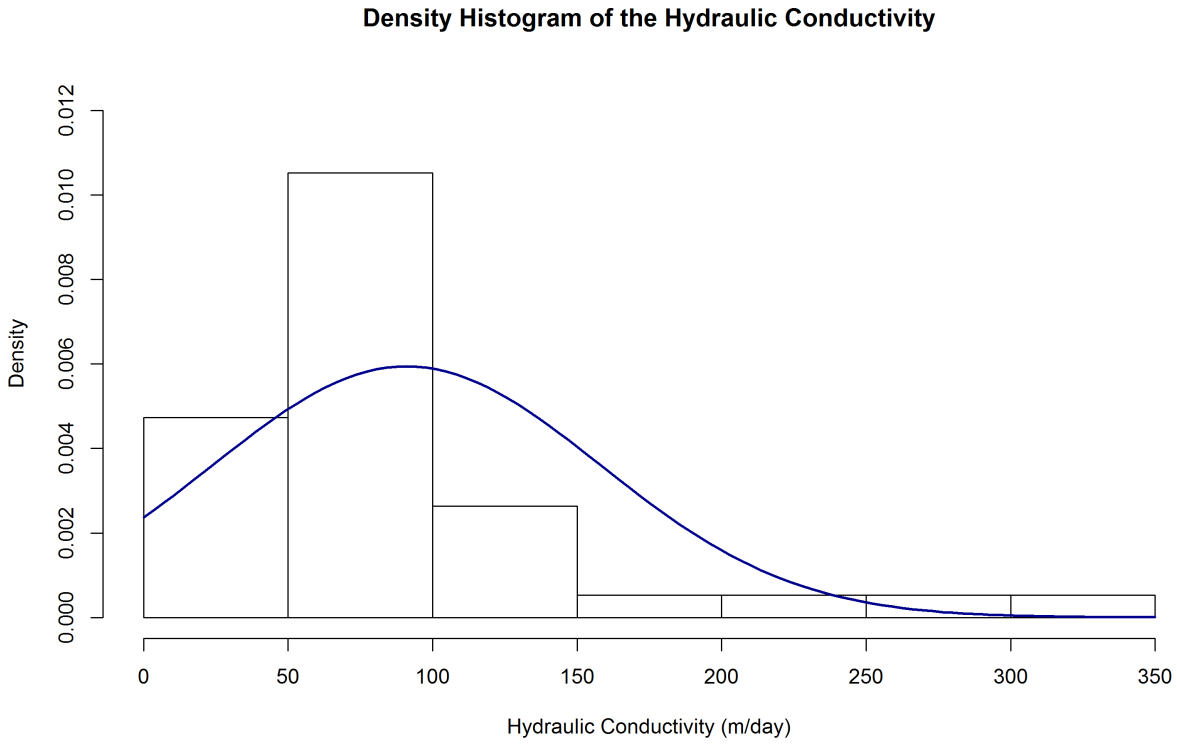

Figure 4.13: Histogram of the hydraulic conductivities for all sites and all depths. It should be noted that these hydraulic conductivity values are only representative of the clean sediments (i.e. sediments where all of the biological material was removed to represent only the effect of sedimentation on hydraulic conductivity). Clean sediments were required for the sieving procedure.

located approximately 4 miles downstream of the Wohler Collector Well site. The USGS Windsor station (#11465390) is approximately 2 miles upstream. Cumulative discharge for the Guerneville station is not a clear function of the MEI index. While the two end-members of the MEI index scale with discharge, many years with neutral ENSO conditions show variable trends in terms of total discharge. Mean daily discharge data displayed for the summer and fall of 2009 shown in Chapter 1 Figure 2.5 demonstrate a marked difference in discharge between the Guerneville and Windsor sites. Guerneville consistently registers approximately half of the discharge compared with Windsor located upstream, except during peak flow periods. The difference in total discharge between the two stations is assumed to be a function of pumping/diversions and overall losing conditions over the entire riverbed.

Average discharge and water temperature are shown for the entire period of record (Figure 4.15).

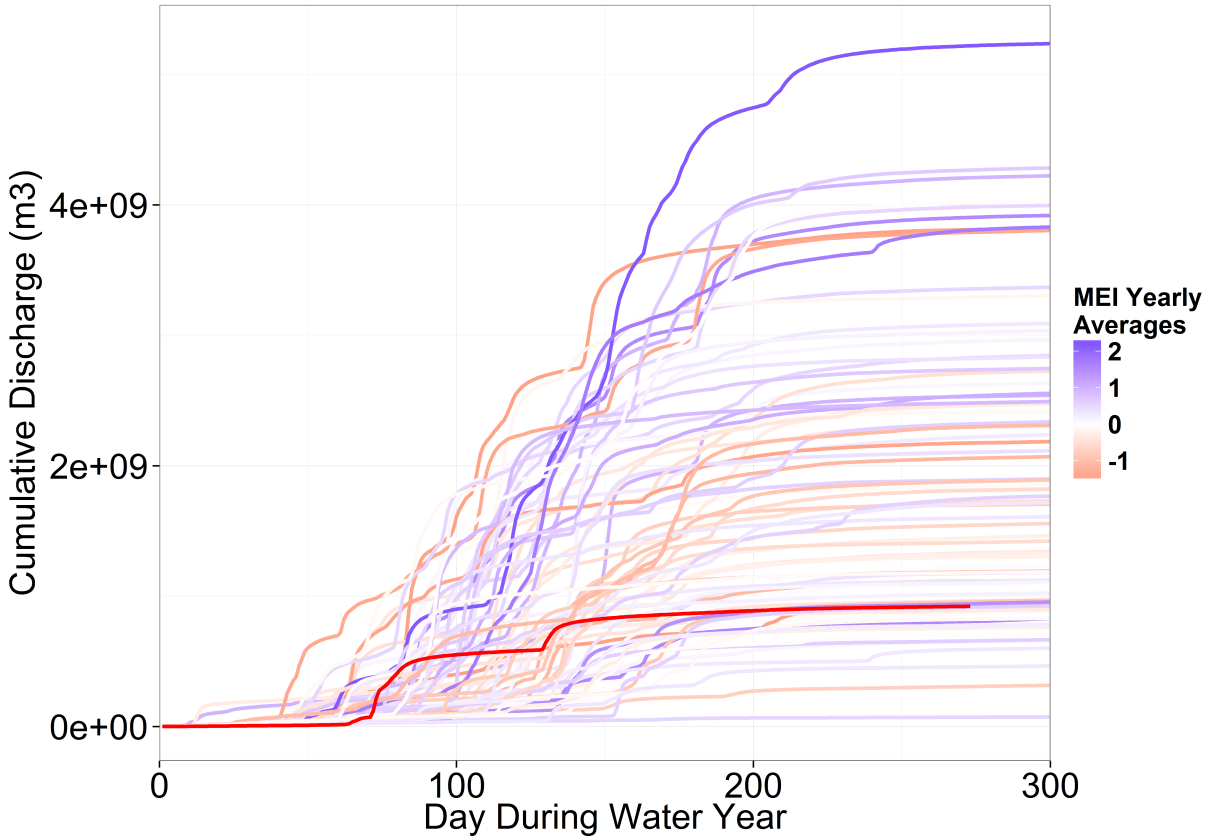

Figure 4.14: Relative locations of the USGS gauging stations, the Wohler Site collector wells and the inflatable dam.

4.4 Methods

We simulate the effect of surface water benthic primary productivity on redox conditions within the subsurface. Contributions of dissolved oxygen (DO) as a function of primary productivity and dissolved organic carbon (DOC) assumed from algal decay are used as the substrates for subsurface bioclogging. Redox conditions contributing to aerobic and anaerobic biomass growth, plus precipitation of iron minerals are examined in two types of contrasting settings: 1) A horizontal hyporheic flow scenario where flow is quickly moving in

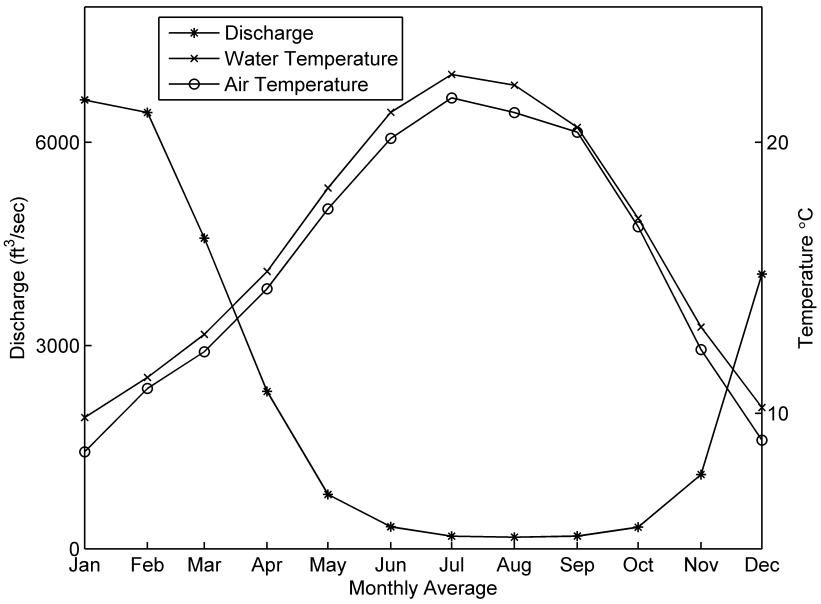

Figure 4.15: Monthly averages of discharge, water temperature, and air temperature from the Guerneville station.

and out of the riverbed, 2) A dominantly vertical hyporheic flow scenario where river gaining and losing conditions are considered. Both scenarios represent different scales of interest and contrasting dominant directions of flow.

Horizontal Hyporheic Flow Scenario

A novel implementation of a bioclogging feedback mechanism was implemented in the MIN3P code. MIN3P is a finite volume numerical code for variably saturated subsurface flow and multi-component reactive transport. Bioclogging was simulated in reactive transport code MIN3P and simultaneously allowed for sequential parameter updates of the riverbed hydraulic conductivity Ksc and the porosity ϕ [*Mayer et al.*, 2002]. As the biomass grows, the physical pore space declines because of biomass growth which reduces K and ϕ. The bioclogging Colonies constitutive model relating biomass growth to permeability reduction was implemented in MIN3P with published parameters to simulate the feedback between biomass growth and parameter updates at each time step [*Thullner et al.*, 2002a, b]. Previous studies have shown the Colonies and Biofilm constitutive models are both representative of field scale scenarios, and thus we only use the Colonies model for the rest of this analysis

[*Newcomer et al.*, 2016]. Biomass accumulation was represented in the MIN3P model as a volume fraction of biomass occupying the pore space. At each time step, the new porosity (minus biomass) and the hydraulic conductivity was updated with the Colonies model which assumes an aggregated form of clogging preferentially in the pore-throats [*Thullner*, 2010].

A 2D model of a generic horizontal hyporheic flow scenario was developed using the MIN3P reactive transport code to simulate dominantly small-scale vertical and horizontal hyporheic fluxes [*Mayer et al.*, 2002]. Reactive transport conditions for bioclogging included microbial aerobic respiration (AR), and microbial denitrification (DN). Substrates include dissolved organic carbon (DOC), Nitrate (NO_3^-) and dissolved oxygen (DO), with DOC and NO_3^- assumed as the limiting substrates. DOC is assumed to come from local algal decay (neglecting algal-grazer interactions) and upstream detrital processes. The reactive transport model accounts for intra-aqueous reactions of biomass growth using Monod kinetics. Aquatic organic matter with a generalized formula representing dissolved organic carbon is represented by the ratio C_1:H_2:O_1 [*Matsunaga et al.*, 1993].

A 1m x 1m long model was discretized with 0.01m spacing and a uniform, homogenous sediment structure. A spatially variable head boundary condition following the model specified below was imposed on the top to simulate hyporheic fluxes [*Elliott and Brooks*, 1997a, b]. The Elliot and Brooks head boundary is shown here:

If H/d $\leq$ 0.34:

$$h_m = 0.28\frac{U^2}{2g}\left(\frac{H/d}{0.34}\right)^{3/8} \tag{4.6}$$

If H/d $\geq$ 0.34:

$$h_m = 0.28\frac{U^2}{2g}\left(\frac{H/d}{0.34}\right)^{3/2} \tag{4.7}$$

A no-flow boundary was used as the bottom of the flow domain, and flux boundaries used on the sides. A mixed concentration boundary was used at the top to allow a concentration boundary when flow enters and a flux boundary when flow exits the domain. Models were run for 600 days using two different nutrient cases: Case 1: A *time-invariant* DO and temperature boundary representing river ecology that is at maximum production year round. This represents a generic modeling approach where the nutrient boundary conditions are constant and do not represent surface ecological effects. Case 2: A *time-variant* DO and temperature boundary based on seasonal patterns of primary productivity. Redox conditions, carbon and nitrate consumption, bioclogging, and Fe(II) precipitation were measured and assessed.

Vertical Hyporheic Flow Scenario

A 1D model of a dominantly losing-gaining river system of the Russian River was developed in MIN3P. A 25 m long model was discretized with 0.1m spacing and two sediment layers representing the clogging layer and aquifer layer. A constant head boundary of 1m imposed at the top and a fluctuating head boundary imposed on the bottom. A mixed DOC/DO boundary condition of 40 and 11 mg/L respectively was specified on the top of the riverbed which allowed a concentration boundary when flow moved into the domain while imposing a flux boundary when flow moved out of the domain. The variable head boundary condition on the bottom was populated with water table fluctuations from pumping induced disconnection to allow for transitional gaining and losing conditions. The methodology for the development of the stochastic water table boundary conditions is discussed at length in Chapter 3. DOC concentrations were chosen based on previous studies suggesting carbon exudation from algae growth can produce DOC subsurface concentrations ranging from 25-100 mg/L [*Mann and Wetzel*, 1995; *Wyatt et al.*, 2012; *ElBishlawi and Jaffe*, 2015]. Models were run for 1000 days. Redox conditions, carbon and nitrate consumption, bioclogging volume fraction, and Fe(II) precipitation were measured and assessed across 100 stochastic water level simulations, 2 parameters sets for low-porosity (ϕ=0.17) and high-porosity (ϕ=0.37) cases representing the initial conditions of the riverbed sediments, parameter updates to porosity and hydraulic conductivity from bioclogging, and 2 water level type groups to represent a simply losing river and a river that transitions from losing $\rightarrow$ gaining. One-dimensional models were chosen for their simplicity and to ensure computational efficiency for simulating Fe precipitation across the 100 x 2 x 2 simulations.

The two water level groups were chosen to represent effects of climate and human-based top down controls. In case 1, a losing river that always remains losing can represent a long-term water table drop (for example from a drought). The river and aquifer undergo disconnection in this case. In case 2, a transitioning losing $\rightarrow$ gaining river scenario with losing conditions for 100 days during the summer and gaining conditions thereafter on a yearly cycle can represent the effects of human controls on water tables. Initial head boundaries and rates of water table decline were randomly sampled from a uniform distribution.

Modeling Primary Productivity

Surface water primary productivity was modeled to create a transient dissolved oxygen (DO) boundary condition for the subsurface horizontal hyporheic modeling framework[*Ginot and Herv*, 1994]. Modeled DO was supplied as a transient boundary to the MIN3P numerical model for horizontal hyporheic flow to simulate river ecological drivers on subsurface metabolism. Primary production rate is directly related to O_2 production rate because 2 atoms of O are produced for each atom of C assimilated. DO in surface water results

from diffusion from the atmosphere, production by algae, loss by algal cell respiration, and consumption by heterotrophic bacteria in the surface water according to Equation 4.8:

$$\frac{dX}{dt} = D\left(X_s - X\right) + P - R - HX \tag{4.8}$$

In Equation 4.8, D is a diffusion constant, Xs is the DO at saturation, X is the current DO concentration, P is the primary productivity, R is the respiration rate, and H rate of heterotrophic consumption of DO. All represented in terms of Oxygen and converted to Carbon. The coefficient for H for heterotrophic consumption was modeled dependent on temperature. Primary productivity (P) was a function of light as photosynthetically active radiation (PAR), and depth represented by the Smith photosynthetic model:

$$P(z) = \frac{P_{max}}{kz} ln \left(\frac{L_s + \sqrt{\left(\frac{P_{max}}{\alpha}\right)^2 + L_s^2}}{L(z) + \sqrt{\left(\frac{P_{max}}{\alpha}\right)^2 + L(z)^2}} \right) \tag{4.9}$$

The Smith photosynthetic model is expressed in the closed form expression of Equation 4.9 [*Ginot and Herv*, 1994]. Pmax was modeled as a linear function of temperature. Light as a function of depth represented by the Beer-Lambert law is already incorporated into Equation 4.9. Light reaching the surface of the water (Ls) was modeled as a function of hourly radiation, day of year, and latitude. Equation 4.8 was solved at 15 minute intervals using a 4th order Runge-Kutta numerical scheme and calibrated using observed O_2 concentrations at 15 minute intervals obtained from the USGS Guerneville Station.

Chemistry Boundary & Initial Conditions

Cyclical O_2 boundary conditions modeled from Equations 4.8 and 4.9 were imposed on the horizontal hyporheic flow simulations to represent DO changes as a function of algae growth and heterotrophic consumption calibrated from field data. The modeled O_2 data was used as the time-variant boundary condition for the MIN3P models. Time variable temperature conditions were also imposed on the model surface to coincide with the time-variant DO boundary. The decay of benthic organic matter was assumed to produce the DOC and POC substrate for the model boundary conditions for subsurface AR and DN to occur.

Inorganic Fe(II) precipitation was modeled in subsurface sediments and at the boundary where the subsurface meets the surface waters with a starting neutral pH of 7. No clear evidence for Iron bacteria, such as *Gallionella spp.* exists so only inorganic precipitation is considered. Ferrihydrite $Fe(OH)_3$, Goethite (FeOOH), and Mackinawite (FeS) were given initial volume fractions within the sediment. Decomposing organic matter occurred via

aerobic respiration and anaerobic denitrification according to the two pathways shown in Equation 4.1 and Equation 4.2. The rates of the reactions in Equation 4.1 and Equation 4.2 are known to have a significant effect on the dissolution and precipitation of Fe minerals [*Matsunaga et al.*, 1993].

4.5 Results

Taxonomic Classification

Figure 4.16: (left) March samples, (right) May samples.

Algae samples collected monthly are described below. In March, the river was low flow, with shallow clear water, with many dense healthy algae patches of *Cladophora spp.* Algae was fully attached to benthic substrata, healthy, showing a few colonizing diatoms (epiphyte *Coconeis spp.*) and no evidence of aquatic hypohomycetes or iron precipitation (Figure 4.16). March samples were more highly branched, cleaner, slender and with fewer diatoms (Figure 4.17). By May, river water became more stagnant, all healthy algae had disappeared, with only remnants of dead algae leftover. All samples were completely covered in the visible iron sheath and weakened cells are shown bursting through the cell wall. May samples were nearly brown/black in the field, densely covered in diatoms, and many surrounded by aquatic hypohomycetes. Observations between these months March 2015 May 2015 indicate that within 30 days, grazers can completely consume the entire substrate of algae on the riverbed, or a change in dominant hyporheic flow shifted the nutrient balance.

Samples from June show a much more varied structure and assemblage (Figure 4.18). In June, the river remained shallow because the temporary dam had not gone up yet. Some live

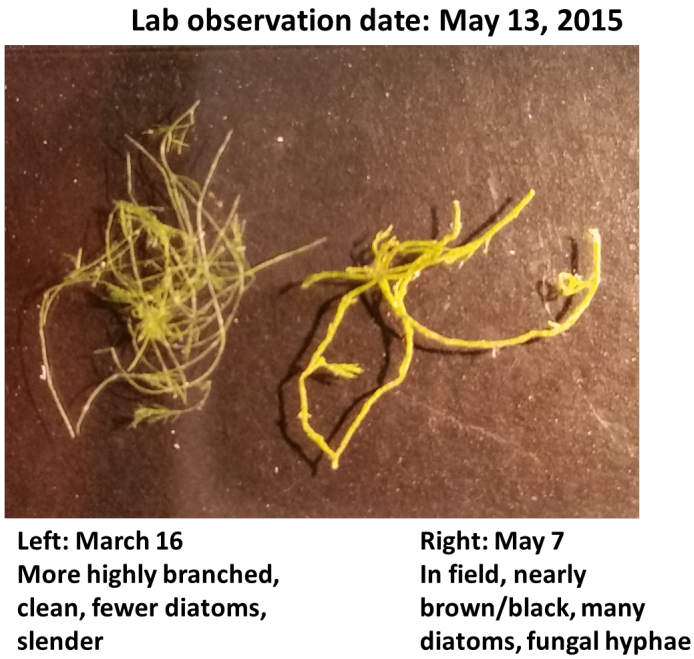

Figure 4.17: Unscaled images of algae in March versus May.

algae were found in the deeper thalweg section. New algal branches were clean of *Coconeis spp.* diatoms, old branches were highly colonized indicating *Coconeis spp.* was in midsuccession. Many algal cells are half full indicating decay. In the deeper thalweg, *Rhoicospehnia spp.* was observed on algal strands which is an indicator for poor-quality streams, and may also indicate Nitrogen limitations. *Encyonema spp.* frustules were observed, some covered in a mucilaginous sheath which is a polymer the diatom uses to recycle its own waste. The mucus may also be a possible contributor to clogging in the subsurface from *Encyonema spp.* deposition and decay. *Cymbella spp.* were also observed growing at the end of mucilaginous stalks attached to algae strands. *Cymbella spp.* are siliceous frustules that occasionally attach to algae with stalks to capture nutrients away from the boundary layer of the algae strand. *Fragilaria spp.* were found as epiphytic colonies on algal strands, also covered with *Coconeis spp.* The shallow bank shows microorganism excrement, with no evidence of any healthy algae observed in the shallow section. Species found on the shallow bank include the cyanobacteria *Anabaena spp.*, *Gomphonema spp.* which are also sensitive to nutrient conditions, yet other species of *Gomphonema* are pollution-tolerant [*Piggott et al.*, 2015]. Other diatoms including *Synedra capitata* and *Synedra pulchella*, *Melosira spp.* diatoms, the most common species of which grows in benthic habitats of eutrophic streams and lakes. Larger

sheaths surrounding the algae indicate either diatoms in girdle view or iron precipitation covering the algal cells. Brown irregular freckles on the algae are likely iron precipitates. The myriad of species found may indicate that there is a 3-4 level food chain because grazers may be suppressed and allow benthic growth and diversity. In phototrophic benthic communities, biofilms of many diatom species can form filamentous microcolonies that aid in bacterial growth [*Battin et al.*, 2016].

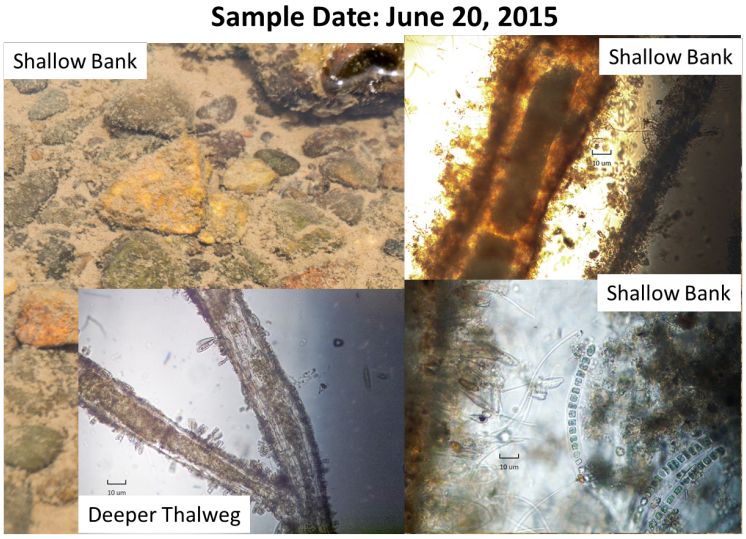

Figure 4.18: Algae samples from June.

In July, the temporary dam had been raised and the water at the Wohler site was ∼2m deep. The temporary dam structure shown in Figure 4.19 was constructed with a fish passage. Water was murky green-brown, no observed healthy algae, and a large amount of decaying organic matter was found on the bottom. The algae species was likely *Spyrogyra spp.* shown by the helical chloroplast structure (Figure 4.19). Algae had highly branched strands, some completely void of cell contents, thickened with surrounding brown mucus keeping strands highly packed. Red/brown striated strands are likely algal filament under flocculation, covered with epiphytes, and precipitates of the mineral Lepidokrite [*Larsen and Postma*, 2001].

August observations show bright full *Spyrogyra spp.* algal blooms (Figure 4.20). Algae samples were bright green, thin, wispy, bloomed between July and August and completely covered the entirety of the gravel bank with high density at ∼1m depth. In, the deeper sections (∼2m depth) *Spyrogyra spp.* was absent; however the entire water column was a murky brownish dark green color. Small floating mats were observed at many different locations.

Figure 4.19: Field samples from July.

Samples for August were obtained for the gravel bar, the bank, and the floating mat (Figure 4.21). Gravel bar algae of the *Spyrogyra spp.* were clean of any epiphytes, bright green, no branching, long and thin with very distinct cell walls showing chloroplasts, some of which were empty but most of them were completely full. A species of *Fragilaria spp.* a freshwater planktonic species was observed. This indicates the bloom was recent growth and very healthy.

Floating mat observations from August (Figure 4.22) showed a significantly large cyanobacteria community of *Anabaena cyanobacteria spp.*, *Oscillatoria spp.*, *Tolypothrix spp.* which showed the cap and some branching. Species of algae include: *Spyrogyra spp.*, *Zygnema spp.* with the two star shaped chloroplasts, many oblate diatom species, and long-spindly clear cells that moved through the slide, which can possibly be interpreted as a fungus. Many reddish- brown blobs of tightly packed cells similar to the ones from the bank were also observed. Bank observations of *Spyrogyra spp.* and *Cladophora spp.* algae were generally darker green than the gravel bar sample and included brown mucilaginous sheaths clumping cells together. Many of the chloroplast cells *Spyrogyra spp.* were empty and some were full, and no epiphytes were found on the stalks. *Anabaena cyanobacteria spp.* with heterocys-

Figure 4.20: *Spyrogyra spp.* bloom in August. Small floating mats are shown in the inset.

tic nitrogen-fixing cells were observed both on the bank and in the floating mats. Other cyanobacteria observed included *Oscillatoria spp.*, a long, un-branching filamentous bacteria that conducts photosynthesis, and possibly some broken hormogonia fragments of *Oscillatoria spp.*, and possibly *Microcystis spp.*, a brown highly clumped species indicated by tightly packed brown/green groups of cells. Other diatoms including *Navicula spp.* diatoms, *Synedra pulchella*, *Gomphonema spp.* stalks with attached to other species, unidentified pennate diatoms, *Chaetoceros decipiens spp.* characterized by the setae, which lie in place within the cells. A remnant of a dinoflagellate species is possibly observed, however the remnant makes identification difficult. Worm-like micro-organisms traveled through the slides during microscopic observation.

By September, observations from the field show that most of the algae had died and began to detach and float away. On the gravel bar, some healthy *Spyrogyra spp.* was observed in a few healthy patches but most was dead. Microscopic observations show very clean, algal strands with no diatoms. The river was very murky-green, and no *Spyrogyra spp.* algae was found on the bank. A few thick floating mats were observed. Laboratory observations of the floating mat show possibly a *Microcystis spp.*, with brown highly clumped species indicated by tightly packed brown/green groups of cells, no observations of *Oscillatoria spp.*, or *Anabaena spp.*, and a red brown furry, hair/frond like structure with needle tip ends, with attached ends which could possibly indicate the cyanobacteria *Rivularia spp.*

October samples were collected after the temporary dam had been removed and shallower flows returned. Much of the bank and gravel bar became exposed after the dam was removed,

Figure 4.21: Species found within the gravel bar from August.

and siltation on the gravel bar and bank was quite apparent (Figure 4.23). Algae on the gravel bar and bank began to dry out and decay. In the extremely shallow water sections (5-10cm), many new algal mats formed that were highly productive, producing nodules of gas that were stuck below the thin film of the algal mats. When the bubbles were compressed, gas was released. The algae were also quite sensitive and would dissolve into particulate when gently touched.

Dissolved Oxygen

Modeled dissolved oxygen is shown in Figure 4.24. Results indicate that the overall seasonal trend of DO is well reproduced based on parameter selection and modeled primary productivity, respiration, and heterotrophic consumption. Excursions from the modeled results are likely due to unique feedbacks between invertebrates and algae based on climate, and discharge conditions of the previous winter and spring that either reset algae conditions or allow invertebrates to thrive. In the Russian River, heterotrophic consumption of DO in the surface water is greater than DO production by primary productivity causing DO levels to be highest in winter and lowest in summer. This indicates that while algae blooms in the summer produce high levels of DO, consumption by other microbes quickly removes DO from the water column.

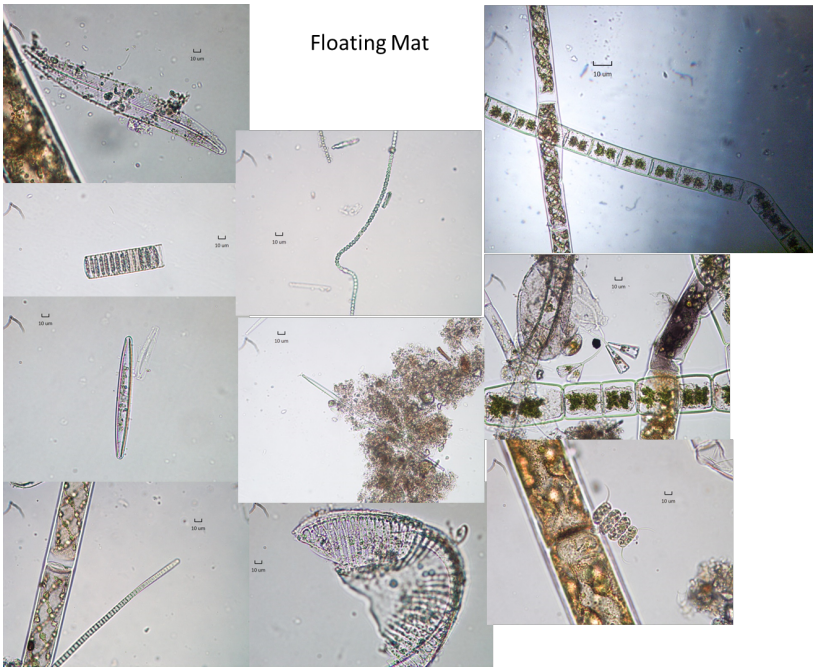

Figure 4.22: Species found within the floating mat from August.

Vertical Hyporheic Flow Scenario Case Study of the Russian River

Case 1: Losing River Undergoing Disconnection

Infiltration fluxes are shown in Figure 4.25. As the water table drops, and the river and aquifer undergo disconnection, infiltration is maximized. In the ϕ=0.17 case, infiltration rises and declines as bioclogging occurs and the conductivity change becomes more dominant relative to the gradient (Figure 2.8). In the ϕ=0.37 case, infiltration fluxes rise, but do not decline until much later in time because conductivity declines are not are strong relative to the gradient change. A lengthy theoretical analysis of the conditions required for a river to undergo disconnection is discussed at length in Chapter 2.

The changes in infiltration can be understood through pressure variations in the subsurface and the development of disconnection between the river and aquifer (Figure 4.26). In the ϕ=0.37 case, the river and aquifer never undergo disconnection. In those cases, river infiltration into the subsurface is dominantly vertical and always maximized, but since the porosity and conductivity conditions do not fulfill the disconnection criteria (Chapter 2), the unsaturated zone never develops. In the ϕ=0.17 case, infiltration is also maximized as

Figure 4.23: Sediments and surficial algae growth after the dam was lowered. Left: Sedimentation on the gravel bar now exposed. Left middle: gas bubble formation on the thin film of algae. Right middle: Newly exposed bank with decaying macrophytes and algae. Right: Algal mat when pulled away from the sediments.

the river-aquifer begin to undergo disconnection, but those infiltration gains quickly become susceptible to conductivity changes once full disconnection is reached and infiltration drops. In Figure 4.26, the pressure at the bottom of the clogging layer (Elevation=9m) for the ϕ=0.37 case does not approach 0. Pressure is required to reach the air-entry value before unsaturated conditions develop. Pressure does approach and surpass the air-entry value for the ϕ=0.17 case because the pressure at the base of the clogging layer is a function of both the unsaturated zone development from disconnection and from clogging induced pressure reduction.

The spatial distribution of anaerobic biomass from DN is shown in Figure 4.26 and confirms the higher production of DN biomass in the ϕ=0.37 case. Anaerobic biomass grows when oxygen concentrations are low allowing the redox potential to favor denitrifier growth. In low porosity sediments, anaerobic biomass occupies a much smaller volume of the pore-space relative to the high porosity case, however the spatial distribution is also much more varied with depth. In the ϕ=0.37 case, anaerobes occupy 3 orders of magnitude more space at the very top layer where river water infiltrates sediments, and another peak is shown around elevation=7m. In the low-porosity case, many peaks and valleys occur in the preferred habitat of anaerobic microbes. The peak in anaerobic biomass growth occurs around elevation=6m for the low-porosity sediment case.

Carbon production from aerobic respiration (AR) and anaerobic denitrification (DN) are shown in Figure 4.27. Carbon production in the form of carbon dioxide gas is produced by both AN and DN as a byproduct. In the ϕ=0.17 case, C production from AN is greater than

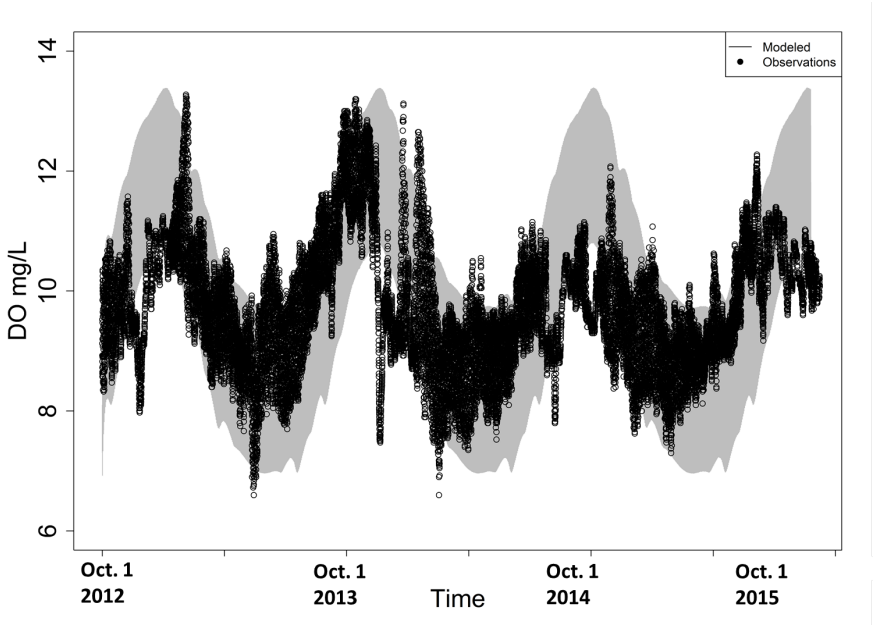

Figure 4.24: Modeled and observed dissolved oxygen concentrations at the Guerneville station.

from DN indicating that AN processes dominate microbial functions in the soil column. In the ϕ=0.37 case, C production from DN is similar to, and slightly larger than from AN. This indicates that anaerobic processes are much more stimulated within this column of sediment. Biomass growth, clogging, and disconnection can help explain this result. In smaller porosity sediment, biomass growth from AR can grow enough to fully clog the sediment pore-spaces, while at the same time, smaller porosity sediments also fulfill the criteria for disconnection in losing rivers. In losing rivers that undergo disconnection, once full disconnection is reached the infiltration rate is only a function of the sediment parameters governing hydraulic conductivity. Once disconnection is reached conductivity fully determines the infiltration rate, and infiltration slows dramatically (Figure 4.25). Slowing infiltration limits nutrient fluxes to deeper sediments where DN is most likely to take place (after all O_2 is consumed from AR). Contrast this behavior with the ϕ=0.37 case where infiltration never slows, but bioclogging continues without impeding flow. For high porosity sediments, disconnection is never initiated and the hydraulic gradient is always stronger than the conductivity decline (Chapter 2) allowing infiltration rates to remain high coincident with nutrient fluxes. Deeper DN reactions receive large fluxes of nutrients that support biological growth.

The concentration of protons (H+ ions) which are directly related to pH values are shown in Figure 4.28. H+ ion concentrations are greater and more spatially varied for the ϕ=0.17

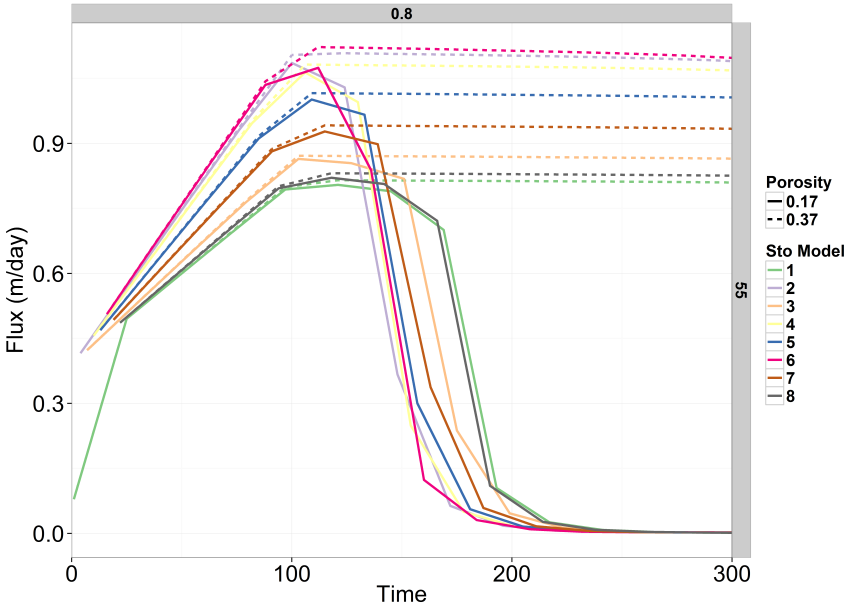

Figure 4.25: River infiltration to the aquifer shown over time for the high porosity and low porosity cases. The different *Sto* models are stochastic variations in the rate of the water table drop (some fast, some slow).

sediment compared with the high porosity case indicating more acidic conditions. H+ ions remain lower in the ϕ=0.37 sediment which is slightly less acidic than the lower porosity case and is more spatially consistent through the entire vertical profile. The lower porosity sediments typically have more acidic conditions in the top layers and less acidic conditions in the bottom of the domain. We can draw a few conclusions from Figure 28 that are consistent with previous interpretations. In ϕ=0.37 sediment, larger porosity values plus lack of disconnection leads to greater transport and more uniform spatially homogeneous biomass growth and pH changes. In ϕ=0.17 sediment, smaller porosity values cause full clogging to occur simultaneously with disconnection allowing different pH zones to develop. Concentration profiles of Nitrate along the vertical spatial gradient are also shown in Figure 4.28. In the low-porosity sediment, Nitrate is fully consumed by DN reactions. Since infiltration is close to 0 near the end of the simulation, mixing in the subsurface does not occur and high concentrations remain in deeper segments.

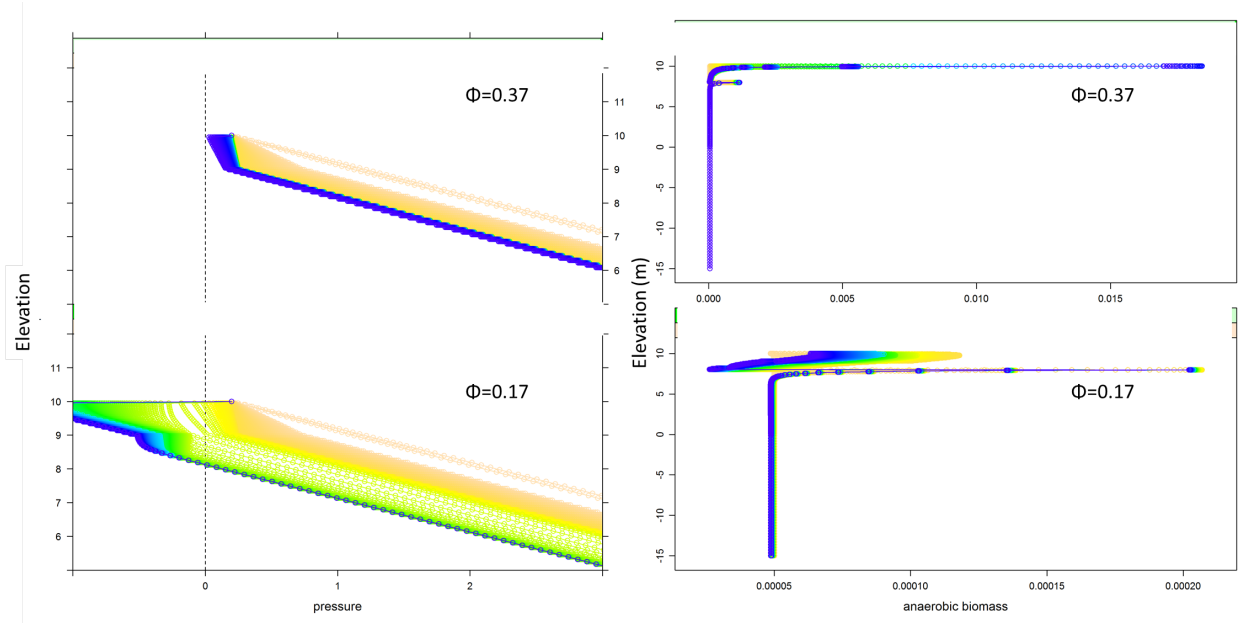

Figure 4.26: Pressure head (m) with depth (left) beneath the riverbed (elevation=10m) and differences based on porosity. The dashed line indicates atmospheric pressure assumed as 0m. When the pressure goes below 0, the river and aquifer begin to disconnect. Yellow colors represent early times, and blues/purples represent late times. Anaerobic biomass growth with depth (right) beneath the subsurface. Low porosity sediments are on the bottom (ϕ=0.17), and high porosity sediments are on the top (ϕ=0.37). Yellow colors represent early times, and blues/purples represent late times.

Case 2: Transitional River Losing→Gaining→Losing→Gaining

In the transitional river losing→gaining scenarios, carbon production from AR and DN is similar to that from the long-term drought case when porosities are small. However, carbon production from AR and DN in the losing→gaining scenario is less than half that produced by the long-term drought case when porosities are large (Figure 4.29). This occurs for a few reasons. In the long-term drought case, the high porosity sediment experience large infiltration rates indefinitely (as long as the river does not dry out). The ϕ=0.37 sediments do not undergo disconnection nor do they fully clog the pore space. In a losing-gaining scenario, water table rises decrease the infiltration rate and thus decrease the direction and magnitude of nutrient fluxes. This behavior limits the amount of biological growth that can occur in shallow and deeper sediments. Water tables from the losing→gaining demonstrate a strong control on the ability of subsurface anaerobic microbes to grow, but do not demonstrate this

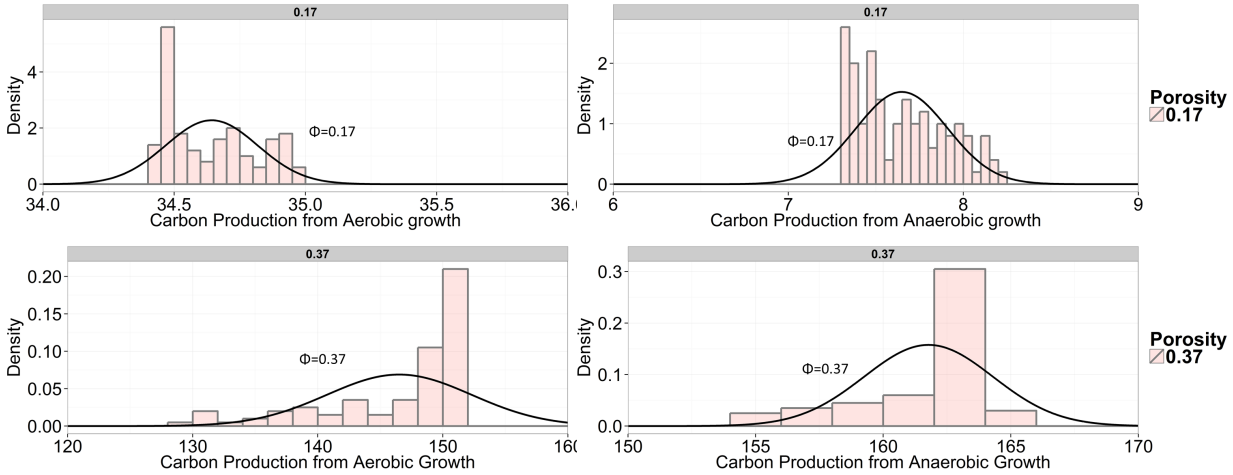

Figure 4.27: Carbon production from aerobic growth (left) and anaerobic growth (right). Low porosity sediments are on the top (ϕ=0.17), and high porosity sediments are on the bottom (ϕ=0.37).

	Mackinawite Formation ϕ=0.17	Mackinawite Formation ϕ=0.37
Long-term Drought	1.4E-5	4E-6
Losing-Gaining	1.0E-5	4E-6

Table 4.1: Total volume fraction of Mackinawite formation compared between the cases.

same control on aerobic microbes.

Precipitation of the FeS mineral (Mackinawite) was enhanced in lower porosity sediments for both cases of the long-term water table drop and the losing→gaining scenario (Table 4.1). In both the long-term drought scenario and the losing-gaining scenario, Mackinawite did not form for the ϕ=0.37 case. In order for Mackinawite to form, conditions have to be sufficiently favorable for both Fe reduction and sulfate reduction allowing free Fe ions to combine with free Sulfur ions. These redox reactions are lower on the redox ladder (Figure 4.8) and occur predominantly is sediment where all oxygen is consumed. In ϕ=0.17 sediments, all oxygen is consumed from AR and bioclogging from AR fully clogs the pore space and reduces infiltration (Figure 4.25). In deeper sediment, so no oxygen is incoming to deeper sediments, additional redox reactions occur that stimulate iron and sulfate reduction. After sulfate reduction occurs, Mackinawite is allowed to form. In higher porosity sediment, or in cases where the direction of infiltration switches, these redox processes do not occur.

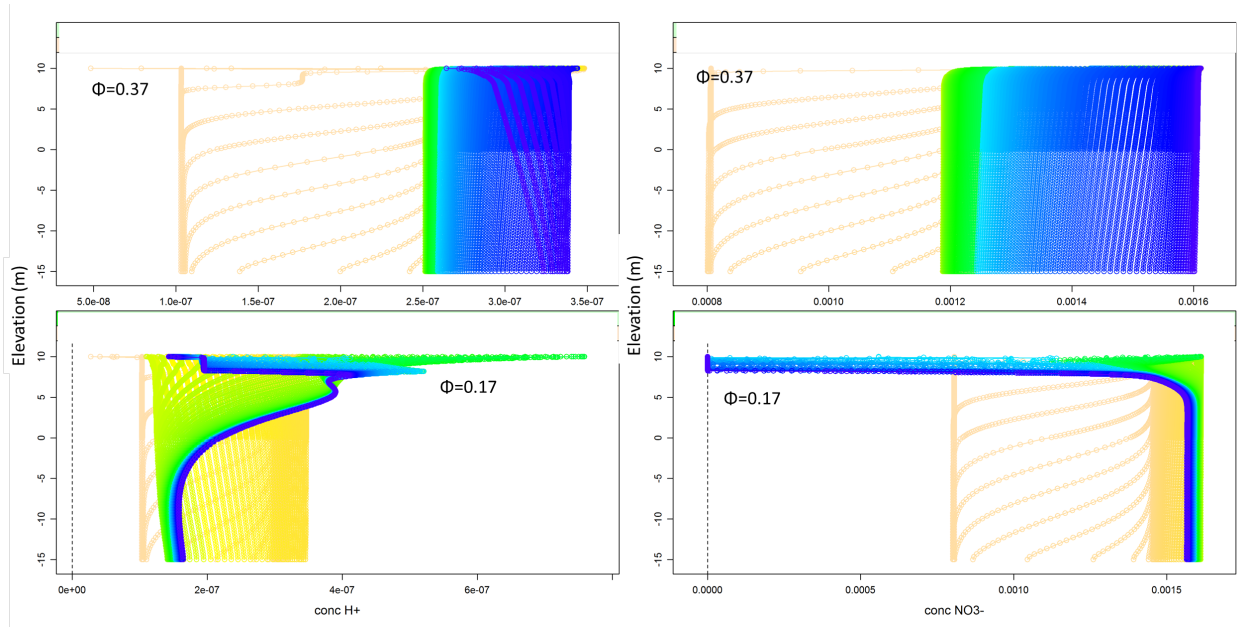

Figure 4.28: Concentration of H+ ions (left). Greater concentration of H+ indicates a more acidic pH value (pH<7 acidic). Yellow colors represent early times, and blues/purples represent late times. Concentration profiles of nitrate (right) along the vertical gradient compared between the low porosity and high porosity sediment. Yellow colors represent early times, and blues/purples represent late times.

Horizontal Hyporheic Case Study

The generic nutrient boundary condition represents a case where primary productivity may be high year round. This may occur in warmer rivers, or in climates that are closer to the equator. The case study that includes the surface ecology represents a river that has a highly seasonal effect on surface photosynthesis. This occurs in Mediterranean or more Temperature climates around the world. Oxygen subsurface concentrations are shown in Figure 4.30. Oxygen is initially highest in the downwelling areas and lowest in upwelling zones. Oxidation of organic matter led to a very quick spatial change in the redox potential, occurring over 2 cm in below the riverbed. The quick reduction in oxygen concentration close to the riverbed surface sets the stage for immediate dissolution of Fe oxides at very short depths within the riverbed (i.e. over spatial scales of cm). Oxygen was completely consumed within the first 2cm of the sediment subsurface from AR allowing DN to quickly consume incoming nitrate within the same spatial zones as AR. This is similar to previous findings where O_2 profiles decreased by a factor of 10 within the first few mm of riverbed

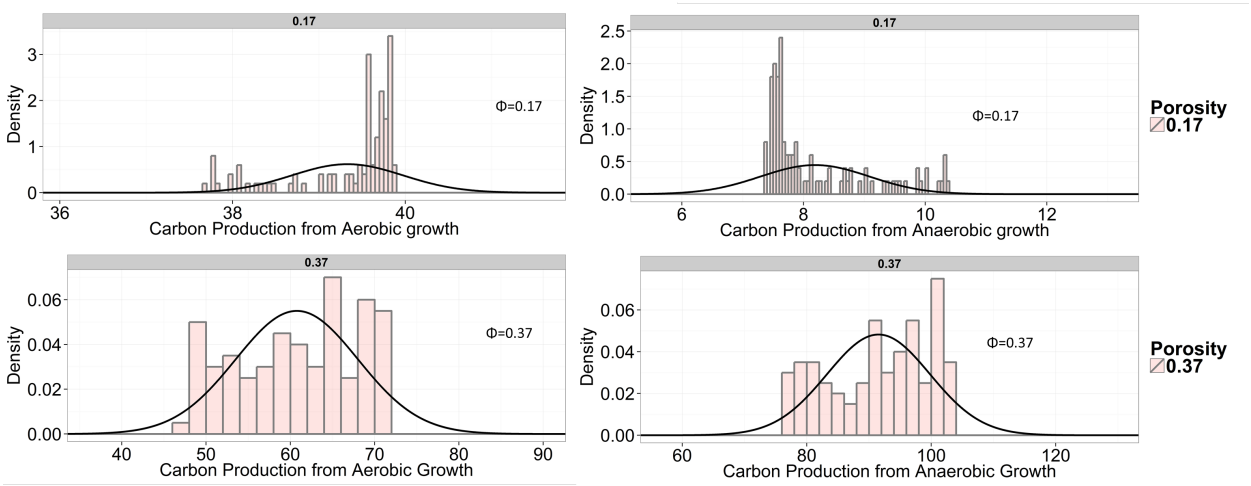

Figure 4.29: Carbon production from aerobic growth (left) and anaerobic growth (right). Low porosity sediments are on the top (ϕ=0.17), and high porosity sediments are on the bottom (ϕ=0.37). This case represents the losing→gaining scenario.

sediment [von Gunten et al., 1994]. Over time as bioclogging occurs, the infiltrating water and nutrients allow the clogging to occur along two fingers of flow that are not directly in the path of the largest flux (Figure 4.30, right). This is similar to previous published findings showing a spatial distribution of biomass growth along the edge of the largest fluxes [Thullner et al., 2002b, 2004]. Spatial distribution of infiltration fluxes are also shown by the vertical arrows in Figure 4.30. Downwelling areas also show the greatest drop in infiltration over time, almost reaching 0 as biomass clogs the pore space. Upwelling areas do not produce substantial bioclogging because most nutrients are fully consumed by the time the water upwells.

Biomass from AR and DN is shown in Figure 4.31 with the generic nutrient case on the left and the ecological boundary case on the right. Neither AR biomass nor DN biomass clogs the locations of upwelling water and preferentially clogs downwelling locations. Areas of downwelling water were almost completely clogged by the combined aerobic and anaerobic biomass and grow in close proximity to each other. The redox gradient within the first few cm of the sediment profile are very strong allowing redox processes across the entire redox ladder to take place quickly and over small spatial gradients. Biological clogging from AR and DN sequentially filled the pore spaces as the reactions marched forward and time. Oxidation of organic matter led to a very quick spatial change in the redox potential, occurring close to the riverbed surface allowing aerobic and anaerobic biomass formation along the vertical spatial gradient. Aerobic biomass growth for the ecological boundary cases shows similar

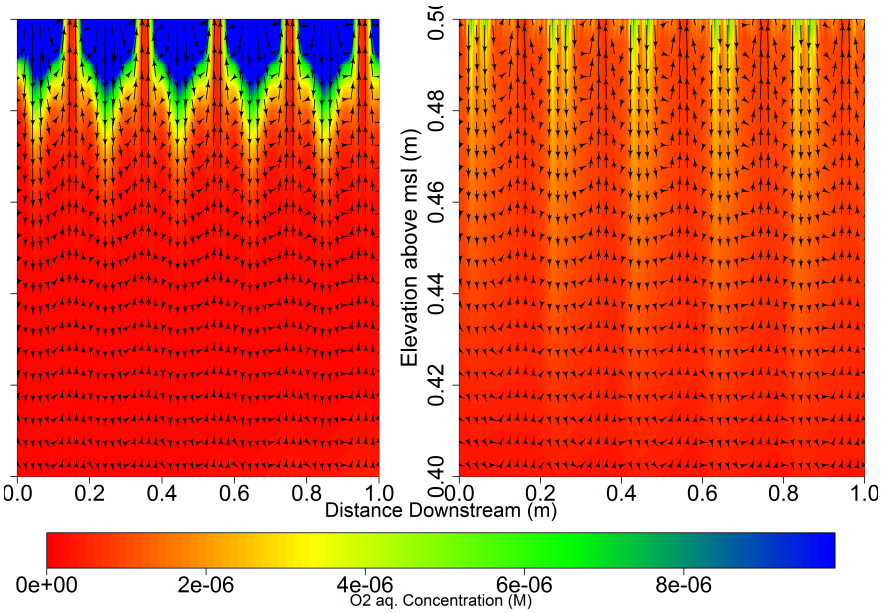

Figure 4.30: Aqueous O_2 concentration at the beginning of the simulation (left) and the end of the simulation (right). O_2 is consumed within the first few centimeters of the soil profile.

spatial trends as the generic case, however anaerobic growth shows substantially greater volume fractions and depths of clogging compared with the generic case. Mackinawite (not shown) produces identical spatial trends as the generic case.

Dissolution of Ferrihydrite occurred in the subsurface providing Fe(II) ions for Mackinawite (FeS) formation. Fe(II) ions and Sulfate also enter the subsurface through background concentrations found in the river water. Mackinawite forms when the redox sequence reaches a pH and electrical potential sufficient for sulfate reduction to bisulfide (HS). Bisulfide reacts with Fe(II) ions to form Mackinawite. Interestingly, this occurred in the downwelling rather than upwelling sections (Figure 4.32). Mackinawite formation in the downwelling zones could indicate that river water concentrations of sulfate and Fe(II) representing background river conditions are sufficient for Mackinawite precipitation because of the higher transition from oxic to anoxic conditions in the subsurface. Dissolution of Ferrihydrite may not be necessary for Mackinawite to form.

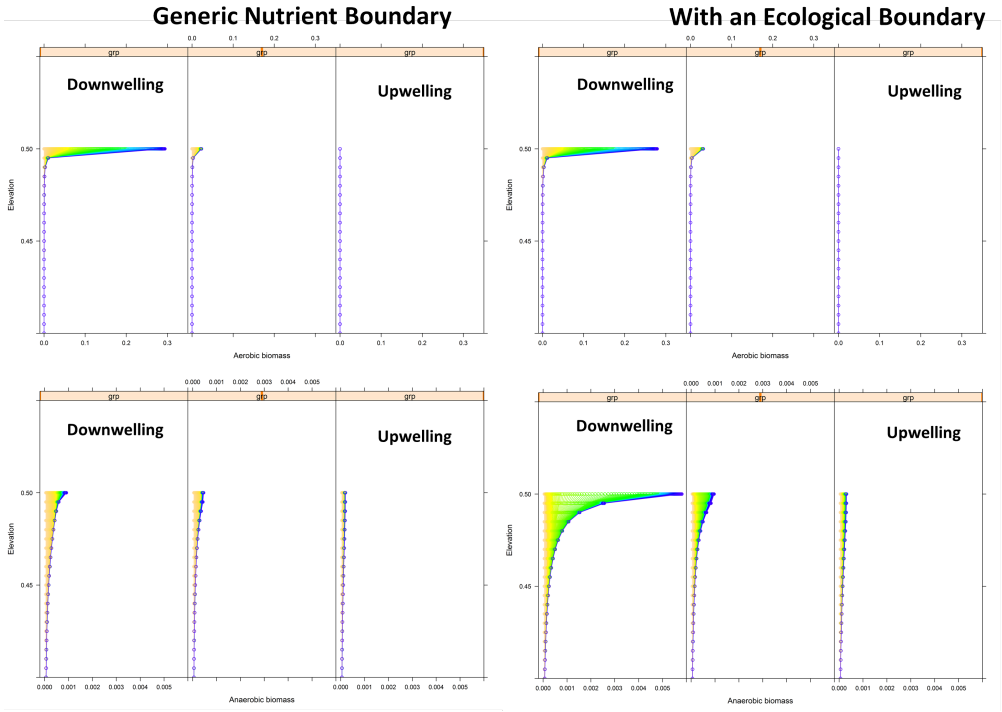

Figure 4.31: AR and DN biomass growth over time in downwelling and upwelling zones. Colors represent initial times (yellow) and late times (blue).

4.6 Discussion

Bioclogging in the Subsurface

Bioclogging occurs in both the horizontal and vertical hyporheic flow models as a function of AR and DN, however the spatial distributions and bio-induced feedbacks significantly vary between the cases. Bioclogging results show that anaerobic denitrification, iron reduction, and sulfate reduction occurred along a flowline in the first few cm of the hyporheic zone within the vicinity of aerobic conditions confirming the idea suggested by [*Storey et al.*, 1999] that microbes can co-occur along close redox gradients (Figure 4.31). Metabolic activities of aerobes and anaerobes grew within sequential numerical layers suggesting that the physicochemical properties of the bulk water movement were able to support many different microbiomes even along small flow paths in the hyporheic zone. The matrix of the pore-space allows colonies of aerobes and anaerobes to grow sequentially along the flow path, (spatial scales of approximately 10 mm) which supports field evidence of this occurrence from the PLFA data (Figure 4.11). Moles of aerobic and anaerobic biomass formed are shown

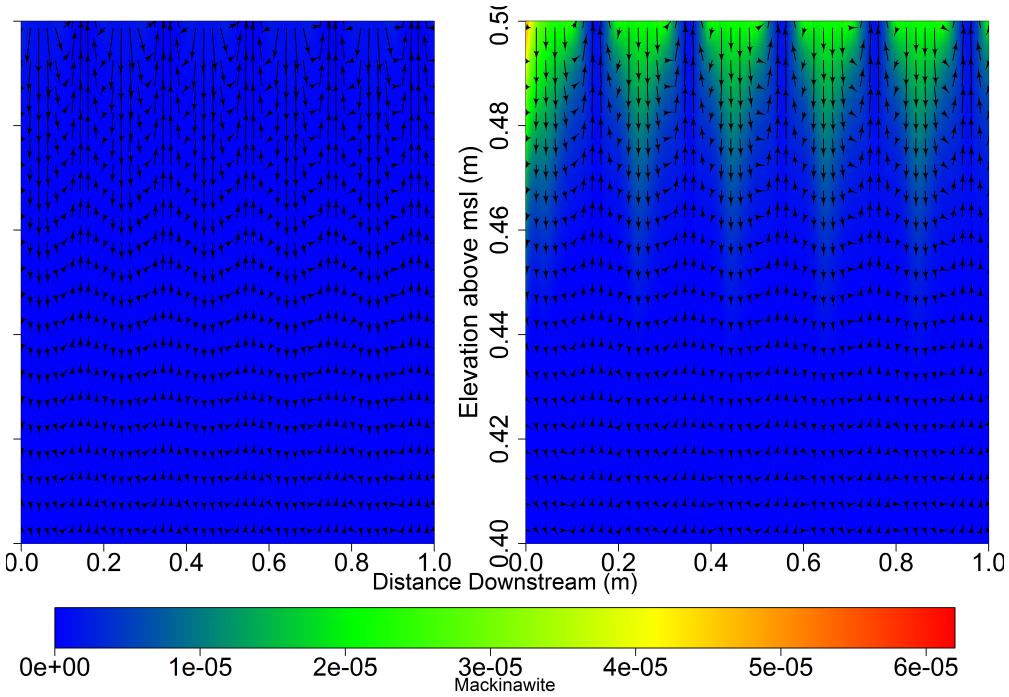

Figure 4.32: Mackinawite volume fraction shown at the start of the simulation (left) and at the end of the simulation (right).

	Moles Aerobic Biomass Formed	Moles Anaerobic Biomass Formed
Generic Boundary	25.6	2.01
Ecological Boundary	25.5	2.85

Table 4.2: Aerobic and anaerobic biomass formed

in Table 4.2 between the generic boundary and the ecological boundary. Moles of aerobic biomass do not show noticeable differences between the two models, however, 30% more moles of anaerobic biomass formed for the model that includes the ecological boundary. This finding suggests that rivers with seasonally dynamic ecological productivity over the course of the year have a greater ability to favor anaerobic microbes that transform nitrate relative to a river that always shows maximum productivity.

Rivers that undergo long-persistent water table drops, indicative of drought conditions were compared with those that are losing for part of the year and gaining in other parts of the year. Long persistent water table drops allow greater infiltration rates for both high and

low porosity sediments, however the effect on biomass grows highly depends on whether the river and aquifer undergo disconnection or not. When the river undergoes disconnection, this allows bioclogging feedbacks to have a substantially larger impact on the following subsurface geochemical reactions. For example, when the river undergoes disconnection (ϕ=0.17), only 30% of the total carbon is consumed from AR and DN relative to the case where the river remains connected (ϕ=0.37). Anaerobic consumption of carbon is also heavily suppressed when rivers are allowed to disconnect. This same feedback mechanism occurs in the case where the river is allowed to transition from losing→gaining. However, the major different in the case of the long-term drought versus the losing→gaining case is in total carbon consumption from anaerobic growth in completely connected sediments (ϕ=0.37). Losing→gaining conditions in high porosity sediments that do not undergo disconnection show half of the total carbon consumption from AR and DN relative to the losing only case. This indicates that water tables that shift from losing to gaining at various times of the year have a strong control on microbial processes because of the shifting redox gradients. When rivers are gaining, low O_2 water moves into the river and halts all substrate transport to microbes and microbial lysis begins.

Influence of Clogging Feedbacks on Geochemistry

Clogging occurred as a function of AR and DN that sequentially filled the sediment pore-spaces. This feedback mechanism, that allows biomass to grow and feedback into the model to allow parameter updates at each time step demonstrated to be a significant control on subsurface transformations. Ecological boundaries in these simulations were imposed as constraints on temperature and O_2 concentration. Without the bioclogging feedback mechanism, maximum nutrient boundary conditions would provide unconstrained nutrient fluxes to subsurface microbes, and microbes would be allowed to continuously process nutrients without any limitations to their growth. When comparing the maximum productivity (generic) simulation to the simulation with a seasonal ecological boundary, major differences are observed in the total moles of nitrate consumed by subsurface microbes. Approximately 50% more nitrate was consumed when a seasonally dynamic ecological boundary was imposed (Table 4.3). Mackinawite precipitation however, was virtually indistinguishable between the two simulations. The reason for this could be the relatively slow dissolution and precipitation of iron minerals relative to aerobic and anaerobic reactions or the similar incoming Fe(II) and Sulfate conditions between the models. Fe(II) and Sulfate were not included in the ecological boundary controls and thus, these concentrations were the same between the two cases. When rivers have contrasting periods of productivity and surface heterotrophic conditions, this stimulates, and then suppresses subsurface microbes. Nutrient pulses stimulate growth then decay which prevents bioclogging from fully clogging the pore space. Pulses are able to go deeper and stimulate additional anaerobic clogging in the layers that were previously

	Moles Carbon Formed	Moles Nitrate Formed	Moles Mackinawite Formed
Generic Boundary	406.0	26.0	2.9
Ecological Boundary	402.0	50.7	2.9

Table 4.3: Total moles of carbon and nitrate consumed, and Mackinawite formation.

nutrient barren. Our findings may help explain why some rivers are better at denitrification than others [*Gomez-Velez et al.*, 2015].

In losing-rivers undergoing disconnection with long-term water table drops, carbon consumption from aerobic and anaerobic processes were 4x and 20x larger in the ϕ=0.37 case compared with the ϕ=0.17 case (Figure 4.27). This finding has important implications for well-sorted gravel bedded rivers compared with poorly-sorted riverbed sediments. High porosity sediments are able to processes much more carbon and nitrogen for a few reasons: 1) Given the same water table drops, these rivers are not susceptible to disconnection and stay completely saturated through the sediment column (Figure 4.26). In these rivers the column is always on the verge of disconnection and so infiltration rates can remain high indefinitely (Figure 4.25). Additionally the high porosity sediments never become fully clogged compared to the low-porosity sediment that clogs and decrease infiltration to 0 after disconnection is reached. Additionally in the high-porosity sediment, conditions become favorable for greater anaerobic metabolism. Our findings show that high porosity sediments, even with faster travel times through the pore-space are much better at processing nutrients given each dominant flow regime. These results have important implications for classifying rivers in terms of their transformation potential, which can be represented by the Dahmköhler number and is a major area for future work.

4.7 Conclusions

In this study, I systematically investigated how permeability dynamics induced through bioclogging affected the exchange of flows and nutrients between a river and its underlying aquifer. These model processes were assessed as a function of the connection status of the river, bioclogging, and ecological boundary conditions imposed through primary productivity. This work has many important implications for understanding the coupled biological, ecological and physical flow processes occurring at hyporheic interfaces. Future work will require better understanding of how subsurface microbes influence net primary productivity in rivers and how feedback effects from clogging change this contribution. These results may

also help elucidate why some types of rivers and geomorphological conditions are better at aerobic respiration and denitrification than others. For practical water management, this work helps assess how bioclogging feedbacks affect total infiltration, recharge, and downstream water quality. Scaling up this research to larger, catchment scale models to assess bioclogging effects on cumulative river observations of water quality and discharge is a major area for new research. Models that assume sediment parameters are constant through space and time may produce results with significant errors when scale up to the catchment. Future work that incorporates small scale processes in larger catchment scale models will be a frontier in numerical and hydrological research.

Bibliography

Aalto, R., L. Maurice-Bourgoin, T. Dunne, D. R. Montgomery, C. A. Nittrouer, and J.-L. Guyot (2003), Episodic sediment accumulation on Amazonian flood plains influenced by El Nio/Southern Oscillation, *Nature*, *425*(6957), 493–497, doi:10.1038/nature02002.

Andrews, E. D., and R. C. Antweiler (2012), Sediment Fluxes from California Coastal Rivers: The Influences of Climate, Geology, and Topography, *The Journal of Geology*, *120*(4), 349–366, doi:10.1086/665733.

Annan, J. D. (2001), Modelling under uncertainty: Monte Carlo methods for temporally varying parameters, *Ecological Modelling*, *136*(23), 297–302, doi:10.1016/S0304-3800(00)00413-0.

Bajracharya, B. M., C. Lu, and O. A. Cirpka (2014), Modeling substrate-bacteria-grazer interactions coupled to substrate transport in groundwater, *Water Resources Research*, *50*(5), 4149–4162, doi:10.1002/2013WR015173.

Baker, M. A., C. N. Dahm, and H. M. Valett (1999), Acetate retention and metabolism in the hyporheic zone of a mountain stream, *Limnology and Oceanography*, *44*(6), 1530–1539, doi:10.4319/lo.1999.44.6.1530.

Barahona-Palomo, M., M. Riva, X. Sanchez-Vila, E. Vazquez-Sune, and A. Guadagnini (2011), Quantitative comparison of impeller-flowmeter and particle-size-distribution techniques for the characterization of hydraulic conductivity variability, *Hydrogeology Journal*, *19*(3), 603–612, doi:10.1007/s10040-011-0706-5.

Battin, T., and D. Sengschmitt (1999), Linking Sediment Biofilms, Hydrodynamics, and River Bed Clogging: Evidence from a Large River, *Microbial Ecology*, *37*(3), 185–196, doi:10.1007/s002489900142.

Battin, T. J., L. A. Kaplan, S. Findlay, C. S. Hopkinson, E. Marti, A. I. Packman, J. D. Newbold, and F. Sabater (2008), Biophysical controls on organic carbon fluxes in fluvial networks, *Nature Geoscience*, *1*(2), 95–100, doi:10.1038/ngeo101.

Battin, T. J., K. Besemer, M. M. Bengtsson, A. M. Romani, and A. I. Packmann (2016), The ecology and biogeochemistry of stream biofilms, *Nature Reviews Microbiology*, *14*(4), 251–263, doi:10.1038/nrmicro.2016.15.

Baveye, P., P. Vandevivere, B. L. Hoyle, P. C. DeLeo, and D. S. de Lozada (1998), Environmental Impact and Mechanisms of the Biological Clogging of Saturated Soils and Aquifer Materials, *Critical Reviews in Environmental Science and Technology*, *28*(2), 123–191, doi:10.1080/10643389891254197.

Blaschke, A. P., K.-H. Steiner, R. Schmalfuss, D. Gutknecht, and D. Sengschmitt (2003), Clogging Processes in Hyporheic Interstices of an Impounded River, the Danube at Vienna, Austria, *International Review of Hydrobiology*, *88*(3-4), 397–413, doi:10.1002/iroh.200390034.

Bouskill, N. J., J. Tang, W. J. Riley, and E. L. Brodie (2012), Trait-Based Representation of Biological Nitrification: Model Development, Testing, and Predicted Community Composition, *Frontiers in Microbiology*, *3*, doi:10.3389/fmicb.2012.00364.

Brovelli, A., F. Malaguerra, and D. Barry (2009), Bioclogging in porous media: Model development and sensitivity to initial conditions, *Environmental Modelling & Software*, *24*(5), 611–626, doi:10.1016/j.envsoft.2008.10.001.

Brunke, M. (1999), Colmation and Depth Filtration within Streambeds: Retention of Particles in Hyporheic Interstices, *International Review of Hydrobiology*, *84*(2), 99–117, doi:10.1002/iroh.199900014.

Brunner, P., P. G. Cook, and C. T. Simmons (2009), Hydrogeologic controls on disconnection between surface water and groundwater, *Water Resources Research*, *45*(1), 1–13, doi:10.1029/2008WR006953.

Cardenas, M. B. (2009), Stream-aquifer interactions and hyporheic exchange in gaining and losing sinuous streams, *Water Resources Research*, *45*(6), n/a–n/a, doi:10.1029/2008WR007651.

Cayan, D. R., K. T. Redmond, and L. G. Riddle (1999), ENSO and Hydrologic Extremes in the Western United States, *Journal of Climate*, *12*(9), 2881–2893, doi:10.1175/1520-0442(1999)012⟨2881:EAHEIT⟩2.0.CO;2.

Chen, W., C. Huang, M. Chang, P. Chang, and H. Lu (2013a), The impact of floods on infiltration rates in a disconnected stream, *Water Resources Research*, *49*(12), 7887–7899, doi:10.1002/2013WR013762.

Chen, X. H., W. H. Dong, G. X. Ou, Z. W. Wang, and C. Liu (2013b), Opposite distribution pattern of streambed hydraulic conductivity in losing and gaining stream reaches, *Hydrology and Earth System Sciences Discussions*, *10*(2), 1693–1723, doi: 10.5194/hessd-10-1693-2013.

Cole, J. J. (1982), Interactions Between Bacteria and Algae in Aquatic Ecosystems, *Annual Review of Ecology and Systematics*, *13*, 291–314.

Cook, P. G. (2015), Quantifying river gain and loss at regional scales, *Journal of Hydrology*, *531*, 749–758, doi:10.1016/j.jhydrol.2015.10.052.

Cunningham, A., C. J. Anderson, and H. Bouwer (1987), Effects of SedimentLaden Flow on Channel Bed Clogging, *Journal of Irrigation and Drainage Engineering*, *113*(1), 106–118, doi:10.1061/(ASCE)0733-9437(1987)113:1(106).

Cusack, D. F., W. L. Silver, M. S. Torn, S. D. Burton, and M. K. Firestone (2011), Changes in microbial community characteristics and soil organic matter with nitrogen additions in two tropical forests, *Ecology*, *92*(3), 621–632, doi:10.1890/10-0459.1.

Dodds, W. K., and D. A. Gudder (1992), The Ecology of Cladophora, *Journal of Phycology*, *28*(4), 415–427, doi:10.1111/j.0022-3646.1992.00415.x.

Dodds, W. K., C. A. Randel, and C. C. Edler (1996), Microcosms for Aquifer Research: Application to Colonization of Various Sized Particles by Ground-Water Microorganisms, *Ground Water*, *34*(4), 756–759, doi:10.1111/j.1745-6584.1996.tb02065.x.

Doering, M., U. Uehlinger, and K. Tockner (2012), Vertical hydrological exchange, and ecosystem properties and processes at two spatial scales along a floodplain river (Tagliamento, Italy), *Freshwater Science*, *32*(1), 12–25, doi:10.1899/12-013.1.

Doppler, T., H.-J. H. Franssen, H.-P. Kaiser, U. Kuhlman, and F. Stauffer (2007), Field evidence of a dynamic leakage coefficient for modelling riveraquifer interactions, *Journal of Hydrology*, *347*(12), 177–187, doi:10.1016/j.jhydrol.2007.09.017.

Dupin, H. J., P. K. Kitanidis, and P. L. McCarty (2001a), Simulations of two-dimensional modeling of biomass aggregate growth in network models, *Water Resources Research*, *37*(12), 2981–2994, doi:10.1029/2001WR000310.

Dupin, H. J., P. K. Kitanidis, and P. L. McCarty (2001b), Pore-scale modeling of biological clogging due to aggregate expansion: A material mechanics approach, *Water Resources Research*, *37*(12), 2965–2979, doi:10.1029/2001WR000306.

ElBishlawi, H., and P. R. Jaffe (2015), Characterization of dissolved organic matter from a restored urban marsh and its role in the mobilization of trace metals, *Chemosphere*, *127*, 144–151, doi:10.1016/j.chemosphere.2014.12.080.

Elliott, A. H., and N. H. Brooks (1997a), Transfer of nonsorbing solutes to a streambed with bed forms: Laboratory experiments, *Water Resources Research*, *33*(1), 137–151, doi:10.1029/96WR02783.

Elliott, A. H., and N. H. Brooks (1997b), Transfer of nonsorbing solutes to a streambed with bed forms: Theory, *Water Resources Research*, *33*(1), 123–136, doi:10.1029/96WR02784.

Engeler, I., H. Hendricks Franssen, R. Mller, and F. Stauffer (2011), The importance of coupled modelling of variably saturated groundwater flow-heat transport for assessing riveraquifer interactions, *Journal of Hydrology*, *397*(34), 295–305, doi:10.1016/j.jhydrol.2010.12.007.

Ezeuko, C., A. Sen, A. Grigoryan, and I. Gates (2011), Pore-network modeling of biofilm evolution in porous media, *Biotechnology and Bioengineering*, *108*(10), 2413–2423, doi:10.1002/bit.23183.

Field, J. P., D. D. Breshears, D. J. Law, J. C. Villegas, L. Lpez-Hoffman, P. D. Brooks, J. Chorover, G. A. Barron-Gafford, R. E. Gallery, M. E. Litvak, R. A. Lybrand, J. C. McIntosh, T. Meixner, G.-Y. Niu, S. A. Papuga, J. D. Pelletier, C. R. Rasmussen, and P. A. Troch (2015), Critical Zone Services: Expanding Context, Constraints, and Currency beyond Ecosystem Services, *Vadose Zone Journal*, *14*(1), 0, doi:10.2136/vzj2014.10.0142.

Findlay, S. (1995), Importance of surface-subsurface exchange in stream ecosystems: The hyporheic zone, *Limnology and Oceanography*, *40*(1), 159–164, doi:10.4319/lo.1995.40.1.0159.

Findlay, S., D. Strayer, C. Goumbala, and K. Gould (1993), Metabolism of streamwater dissolved organic carbon in the shallow hyporheic zone, *Limnology and Oceanography*, *38*(7), 1493–1499, doi:10.4319/lo.1993.38.7.1493.

Finlay, J. C., M. E. Power, and G. Cabana (1999), Effects of water velocity on algal carbon isotope ratios: Implications for river food web studies, *Limnology and Oceanography*, *44*(5), 1198–1203, doi:10.4319/lo.1999.44.5.1198.

Flipo, N., S. Even, M. Poulin, M.-H. Tusseau-Vuillemin, T. Ameziane, and A. Dauta (2004), Biogeochemical modelling at the river scale: plankton and periphyton dynamics, *Ecological Modelling*, *176*(3-4), 333–347, doi:10.1016/j.ecolmodel.2004.01.012.

Flipo, N., A. Mouhri, B. Labarthe, and S. Biancamaria (2014), Continental hydrosystem modelling: the concept of nested streamaquifer interfaces, *Hydrology and Earth System Sciences Discussions*, *11*(1), 451–500, doi:10.5194/hessd-11-451-2014.

Genereux, D. P., S. Leahy, H. Mitasova, C. D. Kennedy, and D. R. Corbett (2008), Spatial and temporal variability of streambed hydraulic conductivity in West Bear Creek, North Carolina, USA, *Journal of Hydrology*, *358*(34), 332–353, doi:10.1016/j.jhydrol.2008.06.017.

Ginot, V., and J.-C. Herv (1994), Estimating the parameters of dissolved oxygen dynamics in shallow ponds, *Ecological Modelling*, *73*(3-4), 169–187, doi:10.1016/0304-3800(94)90061-2.

Gomez-Velez, J. D., J. W. Harvey, M. B. Cardenas, and B. Kiel (2015), Denitrification in the Mississippi River network controlled by flow through river bedforms, *Nature Geoscience*, *8*(12), 941–945, doi:10.1038/ngeo2567.

Gray, A. B., G. B. Pasternack, E. B. Watson, J. A. Warrick, and M. A. Goi (2015), Effects of antecedent hydrologic conditions, time dependence, and climate cycles on the suspended sediment load of the Salinas River, California, *Journal of Hydrology*, *525*, 632–649, doi:10.1016/j.jhydrol.2015.04.025.

Gupta, R. P., and D. Swartzendruber (1962), Flow-Associated Reduction in the Hydraulic Conductivity of Quartz Sand, *Soil Science Society of America Journal*, *26*(1), 6, doi:10.2136/sssaj1962.03615995002600010003x.

Hall, R. O., J. L. Tank, M. A. Baker, E. J. Rosi-Marshall, and E. R. Hotchkiss (2015), Metabolism, Gas Exchange, and Carbon Spiraling in Rivers, *Ecosystems*, doi:10.1007/s10021-015-9918-1.

Harvey, J., and M. Gooseff (2015), River corridor science: Hydrologic exchange and ecological consequences from bedforms to basins, *Water Resources Research*, *51*(9), 6893–6922, doi:10.1002/2015WR017617.

Harvey, J. W., J. K. Bhlke, M. A. Voytek, D. Scott, and C. R. Tobias (2013), Hyporheic zone denitrification: Controls on effective reaction depth and contribution to whole-stream mass balance: Scaling hyporheic flow controls on stream denitrification, *Water Resources Research*, *49*(10), 6298–6316, doi:10.1002/wrcr.20492.

Hatch, C. E., A. T. Fisher, C. R. Ruehl, and G. Stemler (2010), Spatial and temporal variations in streambed hydraulic conductivity quantified with time-series thermal methods, *Journal of Hydrology*, *389*(34), 276–288, doi:10.1016/j.jhydrol.2010.05.046.

Hinkle, S., J. Duff, F. Triska, A. Laenen, E. Gates, K. Bencala, D. Wentz, and S. Silva (2001), Linking hyporheic flow and nitrogen cycling near the Willamette River a large river in Oregon, USA, *Journal of Hydrology*, *244*(3-4), 157–180, doi:10.1016/S0022-1694(01)00335-3.

Hotchkiss, E. R., R. O. Hall, M. A. Baker, E. J. Rosi-Marshall, and J. L. Tank (2014), Modeling priming effects on microbial consumption of dissolved organic carbon in rivers: PRIMING OF RIVER DOC CONSUMPTION, *Journal of Geophysical Research: Biogeosciences*, *119*(5), 982–995, doi:10.1002/2013JG002599.

Hotchkiss, E. R., R. O. Hall Jr, R. A. Sponseller, D. Butman, J. Klaminder, H. Laudon, M. Rosvall, and J. Karlsson (2015), Sources of and processes controlling CO2 emissions change with the size of streams and rivers, *Nature Geoscience*, *8*(9), 696–699, doi:10.1038/ngeo2507.

Inman, D. L., and S. A. Jenkins (1999), Climate Change and the Episodicity of Sediment Flux of Small California Rivers, *The Journal of Geology*, *107*(3), 251–270, doi:10.1086/314346.

Ivkovic, K. M. (2009), A topdown approach to characterise aquiferriver interaction processes, *Journal of Hydrology*, *365*(3-4), 145–155, doi:10.1016/j.jhydrol.2008.11.021.

James, R., and F. Ferris (2004), Evidence for microbial-mediated iron oxidation at a neutrophilic groundwater spring, *Chemical Geology*, *212*(3-4), 301–311, doi:10.1016/j.chemgeo.2004.08.020.

Jones, J. B., Jr., S. G. Fisher, and N. B. Grimm (1995), Vertical Hydrologic Exchange and Ecosystem Metabolism in a Sonoran Desert Stream, *Ecology*, *76*(3), 942–952, doi:10.2307/1939358.

Jung, H. B., Y. Zheng, M. W. Rahman, M. M. Rahman, and K. M. Ahmed (2015), Redox zonation and oscillation in the hyporheic zone of the Ganges-Brahmaputra-Meghna Delta: Implications for the fate of groundwater arsenic during discharge, *Applied Geochemistry*, *63*, 647–660, doi:10.1016/j.apgeochem.2015.09.001.

Kamjunke, N., M. R. Oosterwoud, P. Herzsprung, and J. Tittel (2016), Bacterial production and their role in the removal of dissolved organic matter from tributaries of drinking water reservoirs, *Science of The Total Environment*, *548-549*, 51–59, doi:10.1016/j.scitotenv.2016.01.017.

Kasama, T., and T. Murakami (2001), The effect of microorganisms on Fe precipitation rates at neutral pH, *Chemical Geology*, *180*(1-4), 117–128, doi:10.1016/S0009-2541(01)00309-6.

Kildsgaard, J., and P. Engesgaard (2001), Numerical analysis of biological clogging in two-dimensional sand box experiments, *Journal of Contaminant Hydrology*, *50*(3-4), 261–285, doi:10.1016/S0169-7722(01)00109-7.

Kim, D.-S., S. Thomas, and H. S. Fogler (2000), Effects of pH and Trace Minerals on Long-Term Starvation of Leuconostoc mesenteroides, *Applied and Environmental Microbiology*, *66*(3), 976–981, doi:10.1128/AEM.66.3.976-981.2000.

Kondrashov, D. (2005), Oscillatory modes of extended Nile River records (A.D. 6221922), *Geophysical Research Letters*, *32*(10), doi:10.1029/2004GL022156.

Kurtz, W., H.-J. Hendricks Franssen, and H. Vereecken (2012), Identification of time-variant river bed properties with the ensemble Kalman filter, *Water Resources Research*, *48*(10), n/a–n/a, doi:10.1029/2011WR011743.

Lamontagne, S., A. R. Taylor, P. G. Cook, R. S. Crosbie, R. Brownbill, R. M. Williams, and P. Brunner (2013), Field assessment of surface water - groundwater connectivity in a semi-arid river basin (Murray-Darling, Australia), *Hydrological Processes*, pp. 1561–1672, doi:10.1002/hyp.9691.

Larned, S. T., M. N. Gooseff, A. I. Packman, K. Rugel, and S. M. Wondzell (2015), Groundwatersurface-water interactions: current research directions, *Freshwater Science*, *34*(1), 92–98, doi:10.1086/679491.

Larsen, O., and D. Postma (2001), Kinetics of reductive bulk dissolution of lepidocrocite, ferrihydrite, and goethite, *Geochimica et Cosmochimica Acta*, *65*(9), 1367–1379, doi:10.1016/S0016-7037(00)00623-2.

Lowe, W. H., G. E. Likens, and M. E. Power (2006), Linking Scales in Stream Ecology, *BioScience*, *56*(7), 591–597, doi:10.1641/0006-3568(2006)56[591:LSISE]2.0.CO;2.

Mann, C. J., and R. G. Wetzel (1995), Dissolved Organic Carbon and Its Utilization in a Riverine Wetland Ecosystem, *Biogeochemistry*, *31*(2), 99–120.

Marmonier, P., G. Archambaud, N. Belaidi, N. Bougon, P. Breil, E. Chauvet, C. Claret, J. Cornut, T. Datry, M.-J. Dole-Olivier, B. Dumont, N. Flipo, A. Foulquier, M. Grino, A. Guilpart, F. Julien, C. Maazouzi, D. Martin, F. Mermillod-Blondin, B. Montuelle, P. Namour, S. Navel, D. Ombredane, T. Pelte, C. Piscart, M. Pusch, S. Stroffek, A. Robertson, J.-M. Sanchez-Prez, S. Sauvage, A. Taleb, M. Wantzen, and P. Vervier (2012), The role of organisms in hyporheic processes: gaps in current knowledge, needs for future research and applications, *Annales de Limnologie - International Journal of Limnology*, *48*(3), 253–266, doi:10.1051/limn/2012009.

Matsunaga, T., G. Karametaxas, H. von Gunten, and P. Lichtner (1993), Redox chemistry of iron and manganese minerals in river-recharged aquifers: A model interpretation of a column experiment, *Geochimica et Cosmochimica Acta*, *57*(8), 1691–1704, doi:10.1016/0016-7037(93)90107-8.

Mayer, K. U., E. O. Frind, and D. W. Blowes (2002), Multicomponent reactive transport modeling in variably saturated porous media using a generalized formulation for kinetically controlled reactions, *Water Resources Research*, *38*(9), 13–1–13–21, doi:10.1029/2001WR000862.

McCallum, A. M., M. S. Andersen, B. M. S. Giambastiani, B. F. J. Kelly, and R. Ian Acworth (2013), Riveraquifer interactions in a semi-arid environment stressed by groundwater abstraction, *Hydrological Processes*, *27*(7), 1072–1085, doi:10.1002/hyp.9229.

Metge, D. W., R. W. Harvey, G. R. Aiken, R. Anders, G. Lincoln, J. Jasperse, and M. C. Hill (2011), Effects of Sediment-Associated Extractable Metals, Degree of Sediment Grain Sorting, and Dissolved Organic Carbon upon *Cryptosporidium parvum* Removal and Transport within Riverbank Filtration Sediments, Sonoma County, California, *Environmental Science & Technology*, *45*(13), 5587–5595, doi:10.1021/es200544p.

Molz, F. J., M. A. Widdowson, and L. D. Benefield (1986), Simulation of Microbial Growth Dynamics Coupled to Nutrient and Oxygen Transport in Porous Media, *Water Resources Research*, *22*(8), 1207–1216, doi:10.1029/WR022i008p01207.

Murphy, E. M., and T. R. Ginn (2000), Modeling microbial processes in porous media, *Hydrogeology Journal*, *8*(1), 142–158.

Newcomer, M. E., S. S. Hubbard, J. H. Fleckenstein, U. Maier, C. Schmidt, M. Thullner, C. Ulrich, N. Flipo, and Y. Rubin (2016), Simulating bioclogging effects on dynamic riverbed permeability and infiltration, *Water Resources Research*, pp. n/a–n/a, doi:10.1002/2015WR018351.

NOAA CPC (2015), El Nio Southern Oscillation.

Pedretti, D., D. Fernndez-Garcia, X. Sanchez-Vila, M. Barahona-Palomo, and D. Bolster (2011), Combining physical-based models and satellite images for the spatio-temporal assessment of soil infiltration capacity, *Stochastic Environmental Research and Risk Assessment*, *25*(8), 1065–1075, doi:10.1007/s00477-011-0486-4.

Peyrard, D., S. Delmotte, S. Sauvage, P. Namour, M. Gerino, P. Vervier, and J. Sanchez-Perez (2011), Longitudinal transformation of nitrogen and carbon in the hyporheic zone of an N-rich stream: A combined modelling and field study, *Physics and Chemistry of the Earth*, *36*(12), 599–611, doi:10.1016/j.pce.2011.05.003.

Piggott, J. J., R. K. Salis, G. Lear, C. R. Townsend, and C. D. Matthaei (2015), Climate warming and agricultural stressors interact to determine stream periphyton community composition, *Global Change Biology*, *21*(1), 206–222, doi:10.1111/gcb.12661.

Power, M. (2001), Controls on food webs in gravel-bedded rivers: The importance of the gravel-bed habitat to trophic dynamics, in *Gravel-bed Rivers V*, edited by M. Mosley, pp. 405–421, New Zealand Hydrological Society, Wellington.

Power, M., R. Lowe, P. Furey, J. Welter, M. Limm, J. Finlay, C. Bode, S. Chang, M. Goodrich, and J. Sculley (2009), Algal mats and insect emergence in rivers under Mediterranean climates: towards photogrammetric surveillance, *Freshwater Biology*, *54*(10), 2101–2115, doi:10.1111/j.1365-2427.2008.02163.x.

Power, M. E. (1990), Benthic Turfs vs Floating Mats of Algae in River Food Webs, *Oikos*, *58*(1), 67–79, doi:10.2307/3565362.

Power, M. E. (1992), Hydrologic and trophic controls of seasonal algal blooms in northern California rivers, *Archiv fr Hydrobiologie*, *125*(4), 385–410.

Power, M. E., and A. J. Stewart (1987), Disturbance and Recovery of an Algal Assemblage Following Flooding in an Oklahoma Stream, *American Midland Naturalist*, *117*(2), 333–345, doi:10.2307/2425975.

Power, M. E., M. S. Parker, and W. E. Dietrich (2008), Seasonal reassembly of a river food web: floods, droughts, and impacts of fish, *Ecological Monographs*, *78*(2), 263–282, doi:10.1890/06-0902.1.

Power, M. E., K. Bouma-Gregson, P. Higgins, and S. M. Carlson (2015), The Thirsty Eel: Summer and Winter Flow Thresholds that Tilt the Eel River of Northwestern California from Salmon-Supporting to Cyanobacterially Degraded States, *Copeia*, *2015*(1), 200–211, doi:10.1643/CE-14-086.

Pryet, A., B. Labarthe, F. Saleh, M. Akopian, and N. Flipo (2015), Reporting of Stream-Aquifer Flow Distribution at the Regional Scale with a Distributed Process-Based Model, *Water Resources Management*, *29*(1), 139–159, doi:10.1007/s11269-014-0832-7.

Rockhold, M. L., R. R. Yarwood, and J. S. Selker (2004), Coupled Microbial and Transport Processes in Soils, *Vadose Zone Journal*, *3*(2), 368, doi:10.2136/vzj2004.0368.

Rockhold, M. L., R. R. Yarwood, M. R. Niemet, P. J. Bottomley, and J. S. Selker (2005), Experimental Observations and Numerical Modeling of Coupled Microbial and Transport Processes in Variably Saturated Sand, *Vadose Zone Journal*, *4*(2), 407, doi:10.2136/vzj2004.0087.

Rode, M., M. Hartwig, D. Wagenschein, T. Kebede, and D. Borchardt (2015), The Importance of Hyporheic Zone Processes on Ecological Functioning and Solute Transport of Streams and Rivers, in *Ecosystem Services and River Basin Ecohydrology*, edited by L. Chicharo, F. Mller, and N. Fohrer, pp. 57–82, Springer Netherlands, Dordrecht.

Rosenberry, D. O., and R. W. Healy (2012), Influence of a thin veneer of low-hydraulic-conductivity sediment on modelled exchange between river water and groundwater in response to induced infiltration, *Hydrological Processes*, *26*(4), 544–557, doi:10.1002/hyp.8153.

Rosenzweig, R., A. Furman, C. Dosoretz, and U. Shavit (2014), Modeling biofilm dynamics and hydraulic properties in variably saturated soils using a channel network model, *Water Resources Research*, *50*(7), 5678–5697, doi:10.1002/2013WR015211.

Rubol, S., A. Freixa, A. Carles-Brangar, D. Fernndez-Garcia, A. M. Roman, and X. Sanchez-Vila (2014), Connecting bacterial colonization to physical and biochemical changes in a sand box infiltration experiment, *Journal of Hydrology*, *517*, 317–327, doi:10.1016/j.jhydrol.2014.05.041.

Russell, M. J., and A. J. Hall (2006), The onset and early evolution of life, in *Memoir 198: Evolution of Early Earth's Atmosphere, Hydrosphere, and Biosphere - Constraints from Ore Deposits*, vol. 198, pp. 1–32, Geological Society of America.

Sams, R., J. Garca, P. Molle, and N. Forquet (2016), Modelling bioclogging in variably saturated porous media and the interactions between surface/subsurface flows: Application to Constructed Wetlands, *Journal of Environmental Management*, *165*, 271–279, doi:10.1016/j.jenvman.2015.09.045.

Schubert, J. (2002), Hydraulic aspects of riverbank filtrationfield studies, *Journal of Hydrology*, *266*(34), 145–161, doi:10.1016/S0022-1694(02)00159-2.

Schubert, J. (2006), Experience with Riverbed Clogging Along the Rhine River, in *Riverbank Filtration Hydrology*, edited by S. A. Hubbs, no. 60 in Nato Science Series: IV: Earth and Environmental Sciences, pp. 221–242, Springer Netherlands.

Soleimani, S., P. J. Van Geel, O. B. Isgor, and M. B. Mostafa (2009), Modeling of biological clogging in unsaturated porous media, *Journal of Contaminant Hydrology*, *106*(12), 39–50, doi:10.1016/j.jconhyd.2008.12.007.

Sophocleous, M. (2002), Interactions between groundwater and surface water: the state of the science, *Hydrogeology Journal*, *10*(1), 52–67, doi:10.1007/s10040-001-0170-8.

Storey, R. G., R. R. Fulthorpe, and D. D. Williams (1999), Perspectives and predictions on the microbial ecology of the hyporheic zone, *Freshwater Biology*, *41*(1), 119–130, doi: 10.1046/j.1365-2427.1999.00377.x.

Su, G. W., J. Jasperse, D. Seymour, and J. Constantz (2004), Estimation of Hydraulic Conductivity in an Alluvial System Using Temperatures, *Ground Water*, *42*(6), 890–901, doi:10.1111/j.1745-6584.2004.t01-7-.x.

Su, G. W., J. Jasperse, D. Seymour, J. Constantz, and Q. Zhou (2007), Analysis of pumping-induced unsaturated regions beneath a perennial river, *Water Resources Research*, *43*(8), doi:10.1029/2006WR005389.

Suchomel, B. J., B. M. Chen, and M. B. Allen III (1998), Network Model of Flow, Transport and Biofilm Effects in Porous Media, *Transport in Porous Media*, *30*(1), 1–23, doi:10. 1023/A:1006560705680.

Tang, Y., A. J. Valocchi, and C. J. Werth (2015), A hybrid pore-scale and continuum-scale model for solute diffusion, reaction, and biofilm development in porous media, *Water Resources Research*, *51*(3), 1846–1859, doi:10.1002/2014WR016322.

Taylor, R. G., B. Scanlon, P. Dll, M. Rodell, R. van Beek, Y. Wada, L. Longuevergne, M. Leblanc, J. S. Famiglietti, M. Edmunds, L. Konikow, T. R. Green, J. Chen, M. Taniguchi, M. F. P. Bierkens, A. MacDonald, Y. Fan, R. M. Maxwell, Y. Yechieli, J. J. Gurdak, D. M. Allen, M. Shamsudduha, K. Hiscock, P. J.-F. Yeh, I. Holman, and H. Treidel (2013), Ground water and climate change, *Nature Climate Change*, *3*(4), 322–329, doi:10.1038/nclimate1744.

Thullner, M. (2010), Comparison of bioclogging effects in saturated porous media within one- and two-dimensional flow systems, *Ecological Engineering*, *36*(2), 176–196, doi:10. 1016/j.ecoleng.2008.12.037.

Thullner, M., and P. Baveye (2008), Computational pore network modeling of the influence of biofilm permeability on bioclogging in porous media, *Biotechnology and Bioengineering*, *99*(6), 1337–1351, doi:10.1002/bit.21708.

Thullner, M., J. Zeyer, and W. Kinzelbach (2002a), Influence of Microbial Growth on Hydraulic Properties of Pore Networks, *Transport in Porous Media*, *49*(1), 99–122, doi: 10.1023/A:1016030112089.

Thullner, M., L. Mauclaire, M. H. Schroth, W. Kinzelbach, and J. Zeyer (2002b), Interaction between water flow and spatial distribution of microbial growth in a two-dimensional flow field in saturated porous media, *Journal of Contaminant Hydrology*, *58*(34), 169–189, doi:10.1016/S0169-7722(02)00033-5.

Thullner, M., M. H. Schroth, J. Zeyer, and W. Kinzelbach (2004), Modeling of a microbial growth experiment with bioclogging in a two-dimensional saturated porous media flow field, *Journal of Contaminant Hydrology*, *70*(12), 37–62, doi:10.1016/j.jconhyd.2003.08.008.

Thullner, M., P. Regnier, and P. Van Cappellen (2007), Modeling Microbially Induced Carbon Degradation in Redox-Stratified Subsurface Environments: Concepts and Open Questions, *Geomicrobiology Journal*, *24*(3-4), 139–155, doi:10.1080/01490450701459275.

Treese, S., T. Meixner, and J. F. Hogan (2009), Clogging of an Effluent Dominated Semiarid River: A Conceptual Model of Stream-Aquifer Interactions, *JAWRA Journal of the American Water Resources Association*, *45*(4), 1047–1062, doi:10.1111/j.1752-1688.2009.00346.x.

Ulrich, C., S. Hubbard, J. Florsheim, D. O. Rosenberry, S. Borglin, M. Trotta, and D. Seymour (2015), Riverbed Clogging associated with a California Riverbank Filtration System: An assessment of mechanisms and monitoring approaches, *Journal of Hydrology*, *529*(3), 1740–1753, doi:10.1016/j.jhydrol.2015.08.012.

United Nations (1989), Arid zone forestry: A guide for field technicians, *Tech. Rep. 20*, Food and Agricultural Organization of the United Nations-Forestry Department, Via delle Terme di Caracalla, Rome, Italy.

USGS (2016), USGS NWIS Station Mapper.

Vandevivere, P., and P. Baveye (1992), Effect of bacterial extracellular polymers on the saturated hydraulic conductivity of sand columns., *Applied and Environmental Microbiology*, *58*(5), 1690–1698.

von Gunten, H. R., G. Karametaxas, and R. Keil (1994), Chemical Processes in Infiltrated Riverbed Sediments, *Environmental Science & Technology*, *28*(12), 2087–2093, doi:10.1021/es00061a017.

Wetzel, R. G., P. G. Hatcher, and T. S. Bianchi (1995), Natural photolysis by ultraviolet irradiance of recalcitrant dissolved organic matter to simple substrates for rapid bacterial metabolism, *Limnology and oceanography*, *40*(8), 1369–1380.

White, P. A., J. Kalff, J. B. Rasmussen, and J. M. Gasol (1991), The effect of temperature and algal biomass on bacterial production and specific growth rate in freshwater and marine habitats, *Microbial Ecology*, *21*(1), 99–118, doi:10.1007/BF02539147.

Wingender, J., T. R. Neu, and H.-C. Flemming (1999), What are Bacterial Extracellular Polymeric Substances?, in *Microbial Extracellular Polymeric Substances*, edited by J. Wingender, T. R. Neu, and H.-C. Flemming, p. 258, Springer-Verlag, Berlin Heidelberg.

Wyatt, K. H., M. R. Turetsky, A. R. Rober, D. Giroldo, E. S. Kane, and R. J. Stevenson (2012), Contributions of algae to GPP and DOC production in an Alaskan fen: effects of historical water table manipulations on ecosystem responses to a natural flood, *Oecologia*, *169*(3), 821–832, doi:10.1007/s00442-011-2233-4.

Zhang, Y., S. Hubbard, and S. Finsterle (2011), Factors governing sustainable groundwater pumping near a river, *Ground Water*, *49*(3), 432–444.